CANADIAN CLIMATE CENTRE

REPORT NO. 88-1 CCRN18

SURFACE FLUXES AND STRESSES IN GENERAL CIRCULATION MODELS

by

S.J. Lambert
and
G.J. Boer

ATMOSPHERIC ENVIRONMENT SERVICE

DOWNSVIEW, ONTARIO

1988

THIS REPORT HAS RECEIVED ONLY LIMITED CIRCULATION BECAUSE OF THE SPECIAL NATURE OF THE PROJECT. HOWEVER, REFERENCE IS PERMITTED IF THE WORDS "UNPUBLISHED MANUSCRIPT" ARE MADE PART OF THE BIBLIOGRAPHIC ENTRY, IN ACCORDANCE WITH ACCEPTED PRACTICE.

OTHER CANADIAN CLIMATE CENTRE (CCC)
SCIENTIFIC SERIES INCLUDE:

1. CS series - CCC Climatological Study
2. CLI series - CCC Climatological Memoranda
3. CDS/DS series - CCC Climatic Data Summary
   - CCC Documentation Sheet

For further information on climatological publications contact the

Climatological Services Division
Atmospheric Environment Service
4905 Dufferin Street
Downsview, Ontario M3H 5T4

Surface Fluxes and Stresses in General Circulation Models

by

S.J.Lambert and G.J.Boer
Canadian Climate Centre
Downsview, Ontario

A publication of the Canadian Climate Program

Abstract

The coupling of atmospheric general circulation models (AGCMs) to oceanic general circulation models (OGCMs) requires that each behaves appropriately in the uncoupled mode. The lower boundary conditions for uncoupled AGCMs are particularly simple over the oceans and consist of the specified climatological sea surface temperatures. AGCMs develop fluxes of energy, momentum and moisture in response to these specified boundary values and their their internal dynamics and parameterized physics.

The atmosphere-ocean fluxes of energy and momentum developed in a collection of twelve AGCMs are obtained and compared to climatological estimates of these terms. For the snapshot provided by this particular collection of models, the fluxes developed in the AGCMs are qualitatively similar to the climatological estimates but there may be quantitative differences of considerable magnitude for some models as well as scatter among them. Both the observation-based estimates and the model generated values of these basic climatological quantities deserve attention.

Résumé

L'accouplement d'un modèle de circulation générale de l'atmosphère (MCGA) avec un modèle de l'océan (MCGO) exige que chacun se comporte correctement sans couplage. La condition limite inférieure pour un MCGA non couplé est particulièrement simple au-dessus des océans: elle consiste en la spécification des valeurs climatologiques de la température de la mer. Un MCGA développe alors des flux de chaleur, d'humidité et de quantité de mouvement en réponse aux conditions limites imposées, en plus de la dynamique interne et des autres effets physiques.

Les échanges d'énergie et de quantité de mouvement entre l'atmosphère et l'océan tels qu'obtenus par douze MCGA différents sont comparés entre eux et avec les valeurs climatologiques estimées de ces termes. Les flux générés par ces MCGA sont qualitativement similaires aux estimés climatologiques, quoique qu'il existe une dispersion entre eux et que certains modèles montrent des différences quantitatives notables. Tant les valeurs calculées par les MGCA que les estimés climatologiques basés sur les observations méritent attention.

1. Introduction

The atmosphere and the ocean communicate across their common surface by means of fluxes of moisture, momentum, sensible heat and radiation. Atmospheric general circulation models require ocean surface temperatures as lower boundary conditions and produce values of interfacial fluxes based on radiative calculations and boundary layer and other parameterizations in conjunction with model dynamics. Ocean models, on the other hand, are typically formulated with the interfacial fluxes as upper boundary conditions and respond to atmospheric forcing and internal dynamics by developing surface temperature distributions which feed back on the atmospheric model. It is clear that the successful coupling of atmospheric and oceanic models, as envisioned in Streams II and III of the World Climate Research Programme, requires that realistic stresses and fluxes be developed in the coupled system.

Atmospheric general circulation models which are not coupled to ocean models use observed climatological ocean surface temperatures as lower boundary conditions. The atmospheric model responds to these prescribed sea surface temperatures by developing interfacial fluxes which are consistent with them and with model dynamics and physics. The prescription of these sea surface temperatures acts to constrain the atmospheric model in the sense that the climatologically appropriate ocean surface temperatures are maintained even if this is inconsistent with the resulting fluxes of energy, momentum and moisture developed by the model. Since there is no feedback between the ocean and the atmospheric model in this circumstance, the values of these interfacial fluxes are less critical in uncoupled atmospheric

models than is the case when the atmospheric model is coupled to an ocean model. At least partially for this reason, the surface fluxes of energy, momentum and moisture have not been extensively studied in uncoupled atmospheric general circulation models.

A variety of atmospheric general circulation models which are not coupled to ocean models have been developed in the meteorological community for application to forecasting and climatological questions. Many of these models will form the atmospheric component of future coupled models. A useful step in the development of such coupled models is the study and comparison, in as much as possible, of the interfacial fluxes developed in the uncoupled atmospheric models with climatological values of these quantities. Such studies indicate the ability of the uncoupled atmospheric model to simulate atmosphere/ocean fluxes correctly and hence their suitability for coupling to ocean models of various kinds. Such studies may also provide some insight into deficiencies in boundary layer and other parameterizations in atmospheric models.

In order to address this question, an intercomparison study of atmosphere/ocean fluxes developed in non-coupled atmospheric general circulation models has been undertaken. The results of the study are described in what follows.

2. Approach

A request for information on interfacial fluxes developed in their non-coupled atmospheric general circulation models was answered by twelve

modelling groups from around the world. Averaged data for January and July or the December-February and June-August seasons for precipitation, evaporation (or latent heat flux), sensible heat flux, the two components of the surface stress and the net radiative flux across the surface were collected. The origin and characteristics of the models from which data were supplied are summarized in Table 1.

In order to deal with the data in a uniform way and to permit calculations of intermodel statistics, the data are interpolated to a standard 4 x 5 degree grid for subsequent processing and display. This may introduce some interpolation error into the values presented but this should generally be small.

Model quantities are compared with climatological estimates of atmosphere/ocean fluxes based on observations. These climatological quantities, which will be referred to as "climatological estimates", are themselves imperfectly known. Observations over the oceans are by no means uniformly distributed in space or time nor are they always obtained under optimum conditions. Interfacial fluxes are not directly measured primary meteorological quantities but are obtained from empirical formulae and so are themselves subject to a considerable measure of uncertainty as to their values. The climatological estimates of Esbensen and Kushnir (1981) for energy flux components, of Han and Lee (1981) for surface stresses and Möller (1951) for precipitation are compared with model generated quantities.

The geographic distribution and zonally averaged values of the energy flux, surface stress components and moisture flux over the oceans are displayed for the models and are compared with the climatological estimates of these quantities.

As is usual with intercomparisons of these kinds, it is difficult to provide a quantitative measure of the agreement or lack thereof between the various model values and the climatological estimate. Some summary information as to the model results may be given in terms of the "across-model" average and standard deviation.

It must be remembered that an intercomparison of this kind represents a "snapshot" of the situation at a particular time and that it is the nature of general circulation moidels to evolve and improve. Several, and perhaps most, of the models in the study will have undergone modifications - some in response to the desire to couple the AGCM to an ocean model and some in terms of improved numerics, resolution and/or parameterizations of physical processes.

The "general" results, especially those obtained by averaging over the results of all the models, do not represent either the best or the worst case as it existed at the time of the study but gives, rather, some indication of the situation for models in general at that time. The results for individual models are also given.

3. Measures of difference between model values and climatological estimates

The difficulty in obtaining a useful measure of difference between model values and climatological estimates resides in several features of the intercomparison. Firstly, a single climatological estimate of the various quantities is considered. As mentioned above, these climatological flux and stress estimates suffer from a number of difficulties and there is no estimate of their uncertainty. Esbensen and Kushnir (1981) and Han and Lee (1981) discuss methods of obtaining these estimates in detail. Presumably, the estimates of these climatological quantities are relatively stable in the sense that, over much of the oceans, they are based on an appreciable number of independent observations of the basic meteorological variables.

The difference between the climatological estimate and the simulated value of a quantity can be calculated and displayed for individual models or for the model average. One possibility is to measure the difference in terms of the intermodel standard deviation and this is done here. If the difference, measured in units of intermodel standard deviation, is small this does not imply that the model values of some flux quantity are, in fact, the same as the climatological estimate however since an alternative explanation is that the scatter among model values is large. The result is of interest only if the difference is large. In that case, there is some evidence that, on average, the model produced flux differs from the climatological estimate. This may imply that the model(s) are generally biased in

a particular direction compared to the climatological estimate or alternatively that the climatological estimate is questionable. Other information is required to make a choice between these possibilities.

The difference between the model mean $\bar{X}$ and the climatological estimate X_o measured in units of intermodel standard deviation σ may be written as

$$T = \frac{|\bar{X} - X_o|}{\sigma}$$

where the T-ratio resembles the usual t-statistic. The comparison is made either by plotting the limits $X \pm \sigma$ or the T-ratio. A statistical test of the difference between the model values and the climatological estimate of the quantity is not intended. What is desired is simply some measure of the difference which might indicate when and where there is reason to believe that the model generated and climatological estimate of the interfacial fluxes differ in an important way.

4. Results for zonally averaged values over the oceans

Atmosphere/ocean fluxes are presented both in terms of global distributions and as zonally averaged values over the oceanic regions of the globe. The zonally averaged values of the interfacial quantities are a condensed representation of the information. The averaged values given are obtained as

$$[X] = \int_0^{2\pi} \beta X d\lambda \; / \; \int_0^{2\pi} \beta d\lambda$$

where $\beta = 1$ over the oceans and 0 elsewhere. The area involved in the averaging varies with the cosine of the latitude and with the percentage of the latitude band which is ocean. This ocean fraction varies relatively uniformly from a minimum near 70 N to a maximum near 60 S.

a. **The energy balance at the surface**

The net zonally averaged energy balance at the ocean surface is displayed in Figure 1. This quantity is the sum of the net radiative, latent and sensible heat fluxes at the surface. The climatological estimate from Esbensen and Kushnir (1981) is indicated on the diagram by the dark line while light lines are $[\bar{X}] \pm \sigma_{[\bar{X}]}$ for the model values. The model mean value $[\bar{X}]$ is not shown explicitly on the diagram but is exactly half way between the two light lines. The sign of the energy balance term is that appropriate to the ocean, i.e. positive values mean that the ocean is gaining energy while negative values indicate the ocean is losing energy.

The model results capture the general nature of the energy balance which is characterized by transfer of energy to the oceans in summer and loss of energy from the oceans in winter. There is considerable scatter among the various model values as indicated by the width of the $[\bar{X}] \pm \sigma_{[\bar{X}]}$ "tube". Nevertheless, for the December-February season, the climatological estimate is almost everywhere within the tube so that the climatological

estimate is fairly close to the average model value. For the June-August season, the width of the tube is somewhat less and, for some latitudes, the climatological estimate falls outside of it.

The net energy transfer across the surface is composed of radiative, latent and sensible heat fluxes. These components are shown separately in Figures (2-4) in the same fashion as for the net energy balance. The net radiative flux is seen to be largely into the ocean and to be a major component of the net heat flux. It is a rather smoothly varying quantity with latitude. The $\pm\sigma$ tube is relatively narrow and encloses the climatological estimate for the most part although the model values seem to be systematically larger than the climatological estimate in the summer hemispheres. There is a notable difference at northern summer middle latitudes which is reflected also in the net energy balance of Figure 1.

Radiation calculations and the treatment of clouds may differ considerably among models. In particular, some AGCMs specify a zonally averaged cloud distribution while others calculate cloud amounts interactively. The nature of the cloud parameterization and assigned cloud optical properties may also vary.

Latent and sensible heat fluxes are generally from the ocean to the atmosphere. They are the path by which the radiative energy falling on the oceans reaches the atmosphere either locally or at a distance after transport by the oceans. The latent heat flux serves the dual role of transferring water substance and energy between ocean and atmosphere. It is seen to be responsible for the major part of the ocean to atmosphere transfer of energy.

The latent heat flux has a relatively smooth distribution with latitude and season. The $\pm\sigma$ tube in this case is relatively broad, indicating considerable variation among model values for this quantity. The climatological estimate falls within the tube for the most part except for the high latitude northern winter values. There is a tendency for the model value to be somewhat smaller than the climatological estimate, especially for the winter hemisphere.

The sensible heat flux displays a marked seasonal variation with largest fluxes from the ocean to the atmosphere in the winter hemisphere. Some relatively small values of transfer from atmosphere to ocean are seen in the summer hemispheres. Once again the $\pm\sigma$ tube is relatively broad and encloses the climatological estimate for the most part with the exception of a region at southern winter latitudes. Model values tend to be larger than the climatological estimate.

In summary, the energy fluxes simulated by the models capture the general features displayed by the climatological estimates. Nevertheless, the standard deviation of the model values about the mean is relatively large, indicating considerable variation between model estimates of these quantities. The tube of width $\pm\sigma$ which is drawn on the figures is typically of the order of 50 Wm^{-2}. The accuracy in the energy flux, averaged over an ocean basin, which is required for the successful coupling of atmospheric and oceanic models might be on the order of 10 Wm^{-2} based on the results of the CAGE study (Bretherton et al., 1982) for which it was estimated that fluxes across the ocean surface need to be known to this accuracy if the

implied ocean transports are to be reliably inferred. Models differ among themselves by values which are larger than this amount. This does not imply that all models fail to satisfy this criterion, rather that some of them do.

b. Surface stress

The zonally averaged components of the surface stress over the oceans are displayed in Figures (5-6) in the same fashion as for the energy budget terms. Surface stresses are taken to be positive for westerly and for northerly winds. Climatological estimates are taken from Han and Lee (1981).

Once again, the models capture the general features of the distribution of this parameter. For the Southern Hemisphere there is evidence that model values are typically weak compared to the climatological estimate, especially for southern summer, while for the northern winter the reverse would appear to be the case. These features presumably reflect the "traditional" general circulation model deficiencies of excessive zonality and excessively deep Aleutian and Icelandic lows in the northern winter and too weak circumpolar troughs in the Southern Hemisphere especially in summer.

Zonally averaged values in tropical regions display comparatively little scatter and the $\pm\sigma$ tube generally encloses the climatological estimate. However, the lack of variability in the tropical region may imply an increased sensitivity to the absolute value of the stress for the purposes of coupled modelling. There is some suggestion that model values are generally somewhat weaker than the climatological estimate in this region.

Meridional stresses are weaker than zonal values. The general features of the model results and the climatological estimates are similiar although there is apparently a not inconsiderable variation between model values. Once again the climatological estimates tend to be larger than the average of the model values.

c. Surface moisture flux

The zonally averaged net flux of moisture across the ocean/atmosphere interface is measured by the precipitation minus the evaporation and is displayed in Figure 7. Reliable climatological estimates of these quantities are notoriously difficult to obtain. The values displayed here are based on the precipitation rates of Möller (1951) together with evaporation rates based on the latent heat flux of Esbensen and Kushnir.

Moisture fluxes are also difficult to simulate. The general features of the moisture budget are certainly reproduced although there is an apparent excess of precipitation in tropical regions associated with the intertropical convergence zone and an excess of evaporation at subtropical latitudes associated with the subtropical high pressure zones. At more poleward latitudes precipitation again exceeds evaporation in general in association with the mid-latitude storm tracks.

It is notable that the climatological estimate falls outside of the $\pm\sigma$ tube over much of the region. For the winter hemispheres and the tropical region, the model values are typically more positive than the climatological estimate. This reflects the generally larger precipitation rates in the

simulations as shown in Figure 8, although Figure 4 indicates also a tendency for simulated evaporation to be low compared to the climatological estimate.

The summer hemisphere also exhibits a characteristic pattern with the climatological estimate indicating a larger excess of evaporation over precipitation in the subtropics and a larger excess of precipitation over evaporation at higher latitudes than the models. There would appear to be a general mismatch between the climatological estimates and simulated values of this quantity. It is not clear to what extent the climatological estimates are at fault in this case.

d. Individual model values

Figures (1-8) are an attempt to give information on the general correspondence between model and climatological zonally averaged values of atmosphere-ocean fluxes. The net energy balance at the surface, the net moisture balance and the two components of the stress are also given for the individual models in Figures (41-56) of Appendix I.

5. Global distributions of flux quantities

In this section the global distributions of the various flux quantities as obtained by the participating modelling groups listed in Table 1 are displayed together with the climatological estimates of the interfacial quantities.

The climatological estimate of the flux quantity is compared with the average of the simulated values for all models. The intermodel standard deviation $\pm\sigma$ is also presented as an indication of the spread among model values. Values of the ratio

$$T = \frac{|\bar{X} - X_o|}{\sigma_{\bar{X}}}$$

are given and indicate the $\pm\sigma_{\bar{X}}$ "envelope" about the model mean. Values of $T > 1$ indicate that the climatological estimate and the model average of the quantity differ by more than the intermodal standard deviation. This is analogous to the climatological estimate falling outside the $\pm\sigma_{[\bar{X}]}$ "tube" of the previous section.

a. The energy balance at the surface

The climatological estimate of the net energy balance at the ocean surface from Esbensen and Kushnir is given in Figure 9 and the corresponding average of model values of this quantity are given in Figure 10. The value of the T-ratio is given in Figure 11 and the model standard deviation in Figure 12.

As was the case for the zonally averaged values of this quantity, there is a general correspondence between the climatological estimate and model mean although regions of difference can be seen. Generally there are differences associated with the regions of large rates of heat interchange between the ocean and the atmosphere such as the Gulf Stream and Kuroshio.

This may be due in part to the relatively small scale of these current systems in comparison with the model resolution. Additionally, there appear to be broad differences in the net energy balance over regions of the Southern Hemisphere.

As measured by the T-ratio, differences are seen to be concentrated over the Southern Hemisphere oceans in both seasons and over a mid-latitude band in Northern Hemisphere summer. The intermodel standard deviation indicates that there are rather large intermodel differences in the northern winter. The T-ratio is relatively small there not because of particularly good agreement of the means but because the intermodel spread is comparatively large. The T-ratio together with the intermodel standard deviation indicates that there is considerable variation among model simulated values of the net energy flux across the surface and that the mean model value differs from the climatological estimate over several areas of the ocean.

The components of the net energy balance at the surface are also presented. The corresponding diagrams for the net radiation at the surface are given in Figures (13-16). The radiation balance at the surface is a relatively "smooth" field compared to the net energy balance term and reflects the broad geometric features of incoming solar radiation over the oceans. Nevertheless there are also broad regions in which the model mean of this quantity differs from the climatological estimate. As noted previously, the models differ in their treatment of clouds and radiation. Some of the consequences of this are apparent in the plot of the T-ratio. The patterns of

large T-ratio are associated, for instance, with regions of low level cloud, particularly in the summer hemisphere. The parameterization of cloud is an area of particular difficulty in general circulation modelling.

The latent heat flux is the next largest term in the surface energy balance. Figures (17-20) display the various statistics for this quantity. Once again the general features of the climatological estimate of this quantity are seen also in the mean of the model values. The ratio indicates that there is a comparatively small amount of the sea surface for which the means differ by more than the intermodel standard deviation. This can be taken to indicate that if the climatological estimate and the several model values for this term are considered together, the climatological estimate would not be considered to be so different from the model values that it could be selected out a priori. This is not a particularly strong statement when the model values differ considerably among themselves as indicated by the standard deviation of Fig. 20.

The sensible heat flux is the smallest component of the surface energy balance with the largest values occurring over the Gulf Stream and Kuroshio regions in northern winter. Figures (21-24) indicate that the general features of this field are simulated by the models but that the intermodel standard deviation is fairly large. The ratio indicates that the climatological estimate falls outside the $\pm\sigma$ envelope for a fairly large proportion of the ocean surface. This is particularly the case for the more tropical latitudes.

In summary, the general features of the net oceanic surface energy balance and its components as developed in the general circulation models correspond to the climatological estimate. There is nevertheless considerable variation in the model estimates giving rise to relatively large intermodel variances. Differences between model and climatological estimates of the quantities are generally largest in localized regions of large fluxes such as the Gulf Stream and Kuroshio regions in winter. These also tend to be regions of largest intermodel variance.

b. Surface stress

Figures (25-28) give information for the east-west or u-component of the surface stress while the corresponding values for the north-south or v-component are given in Figures (29-32). For the u-component of the stress, the model values are generally somewhat smaller than the climatological estimate. This is especially clear in the Southern Hemisphere circumpolar trough and to a lesser degree in the tropical easterly belt. In the Northern Hemisphere winter, the stresses associated with the mid-latitude westerlies are locally weak while those associated with the more poleward easterlies are strong compared to the climatological estimate. The zonally averaged result of Fig. 5 would seem to contradict this situation in that the model mean is locally larger than the climatological estimate in the centre of the westerlies. The climatological peak is rather broader than that for the models, however, and this is the consequence of the fact that the maximum stresses are not all found at the same latitude so that the

maximum is spread out when zonally averaging. The "traditional" model bias of too deep Aleutian and Icelandic lows and generally large zonal flows and stresses are seen in many of the individual cases that are averaged to give the mean for the models in this season. It is also interesting to note that the model values of stress on the coast of Antarctica in southern winter are generally large. The Han and Lee results are, of course, confined to oceanic values.

The T-values indicate a general difference between the climatological and model stresses in the southern band of westerlies. There are additional regions in the tropics and subtropics where differences are large in terms of intermodel standard deviations. The intermodel standard deviations show that some of the largest model differences occur at the Antarctic coast in summer. Over the rest of the oceans, the patterns are relatively broad indicating differences in the general level of the stresses rather than locally large differences.

The v-component of the stress is rather weaker than the u-component and the model and climatological values agree in their general features. Once again the model average appears to be comparatively weak. Intermodel standard deviations are relatively low over the oceans and the climatological estimate falls outside the $\pm\sigma$ envelope for an appreciable proportion of the ocean as indicated by the T-ratio.

c. Surface moisture flux

Figures (33-36) give the corresponding diagrams for the net water budget at the surface. As mentioned above, this quantity is not well known from observations. Nevertheless, the general agreement between the two fields is reasonable, albeit the magnitude of the climatological estimate is generally larger than the modelled value. Intermodel standard deviations have largest values in the tropical region in association with the variability of the model tropical precipitation band.

The diagrams for precipitation are given in Figures (37-40). The model precipitation values tend to be larger than those of this particular climatological estimate. Intermodel standard deviations are comparatively large in the tropics indicating that the models do not agree as to the amount and distribution of precipitation in this region. Evaporation, the other component of the moisture budget, is synonymous with the latent heat flux of the previous section.

d. Individual model values

Individual model values of the energy budget at the surface and its components, the two components of the surface stress and the moisture budget at the surface are given in Figures (57-158) of Appendix II. These are the basic data from which the model mean and standard deviations are constructed and show in detail the behaviour of the individual models.

6. Concluding remarks

The fluxes of energy, momentum and moisture across the ocean surface for winter and summer as developed in twelve uncoupled general circulation models are displayed both as zonal averages and as geographical distributions. In addition, some basic statistics are calculated namely the across-model average and the intermodel standard deviation. The model average is compared to climatological estimates of the various quantities while a measure of the difference between the various model values is given by the standard deviation. A measure of the difference between the model average and the climatological estimate measured in units of intermodel standard deviation is given by the T-value.

For the snapshot provided by this particular collection of model results, it is clear that non-coupled atmospheric general circulation models develop atmosphere-ocean fluxes of energy, momentum, and moisture which are qualitatively similar to the climatological estimates. There are, nevertheless, quantitative differences of considerable magnitude for some of the models and considerable variation between different model values. These differences highlight both the existence of systematic model error in these quantities and the lack of definitive observation-based knowledge of these primary climatological quantities. Both of these areas deserve attention so that the development of coupled atmosphere-ocean models may continue to proceed successfully.

Acknowledgment

The authors wish to thank J. Cantin for typing this report and Lynda Smith for revisions. Thanks also to those who took the time and effort to contribute to this study.

References

Esbensen, S.K. and Y. Kushnir, 1981: The heat budget of the global ocean: an atlas based on estimates from surface marine observations, Report No. 29, Climatic Research Institute, Oregon State University, Corvallis.

Han, Y.-J. and S.-W. Lee, 1981: A new analysis of monthly mean wind stress over the global ocean, Report No. 26, Climatic Research Institute, Oregon State University, Corvallis, 148 pp.

Möller, F., 1951: Vierteljahrskarten des Niederschlags für die ganze Erde. Petermanns Geogr. Mittiel., Justus Perthes, Gotha, pp. 1-7.

Bretherton, F.P., D.M. Burridge, J. Crease, F. M. Dobson, E.B. Kraus and T.H. Vonder Haar, 1982: Report of the JSC/CCCO CAGE Experiment, A feasibility study. World Climate Programme Series Report WCP-22, 99pp.

Table 1

Table 1. The models for which flux data were received. The column labeled "grid" gives the format in which the data were received.

Model	Grid	Mode	Numerics	Simulation Period	Season
AUSTRALIA (BMRC)	Lat.-Long. 3.0° x 3.0°	Perpet.	Spectral R21	Avg. over last 150 days of 200 day integration	JAN/JUL
CANADA (CCC)	Gaussian* 64 x 32	Annual Cycle	Spectral T20	5 yr. avg.	DJF/JJA
ECMWF	Lat.-Long. 1.875° x 1.875°	Annual Cycle	Grid Point	Avg. over last 30 days of 50 day integration	JAN/JUN
ENGLAND (UKMO)	Lat. - Long. 2.50° x 3.75°	Annual Cycle	Grid Point	3 yr. avg.	DJF/JJA
FRG (Hamburg U.)	Hemispheric Lat. Long. 2.8125° x 2.8125°	Perpet.	Grid Point	300 day avg.	JAN
FRANCE (CNRM)	Gaussian 32 x 20	Annual Cycle	Spectral T10-13 m=10,n=13	10 yr. avg.	DJF/JJA
JAPAN (MRI)	Lat. - Long. 4° x 5°	Annual Cycle	Grid Point	12 yr. avg.	JAN/JUL
USA (COLAI)	Lat. - Long. 4° x 5°	Annual Cycle	Grid Point	2 yr. avg. Using GLAS GCM	JAN/JUL
USA (GFDL)	Gaussian 48 x 40	Annual Cycle	Spectral R15	9 yr. avg.	JAN/JUL
USA (GISS)	Lat. - Long. 4° x 5°	Annual Cycle	Grid point	2 yr. avg.	DJF/JJA
USA (NCAR)	Gaussian 48 x 40	Perpet.	Spectral R15	Avg. over last 150 days of 270 day integration	JAN/JUL
USA (OSU)	Lat. - Long 4° x 5°	Annual Cycle	Grid Point	10 yr. avg.	JAN/JUL

* fields truncated at T20.

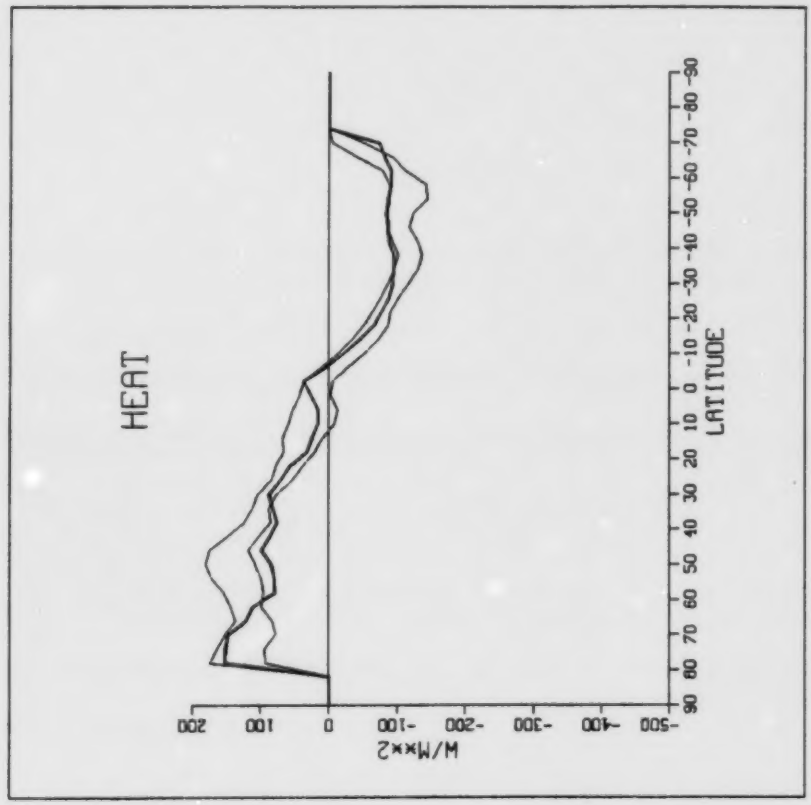
HEAT
W/M**2
200
100
0
-100
-200
-300
-400
-500
LATITUDE
90
80
70
60
50
40
30
20
10
0
-10
-20
-30
-40
-50
-60
-70
-80
-90

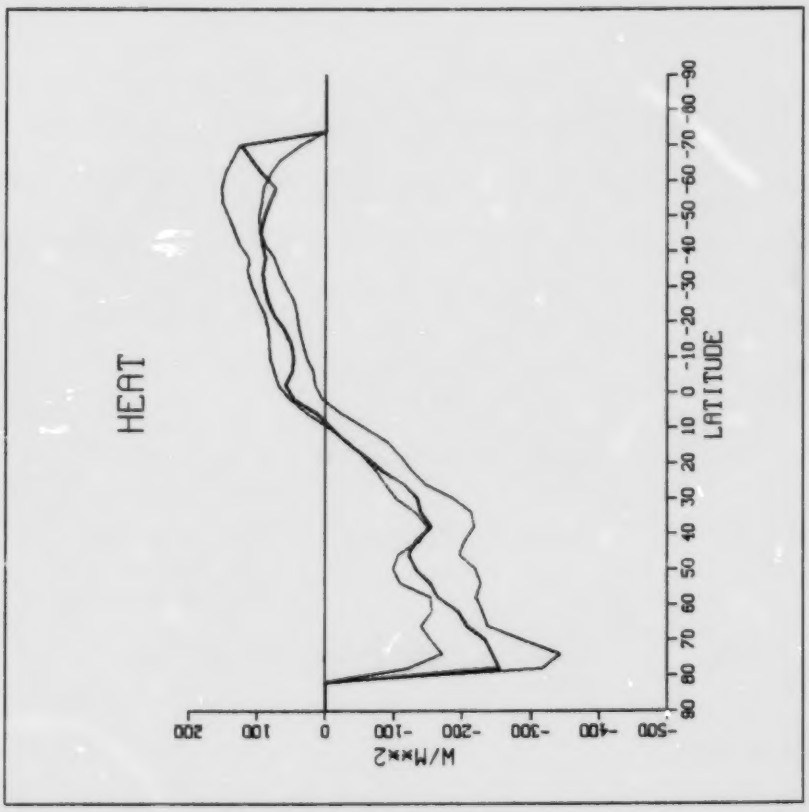
HEAT
W/M**2
200
100
0
-100
-200
-300
-400
-500
LATITUDE
90
80
70
60
50
40
30
20
10
0
-10
-20
-30
-40
-50
-60
-70
-80
-90

Figure 1

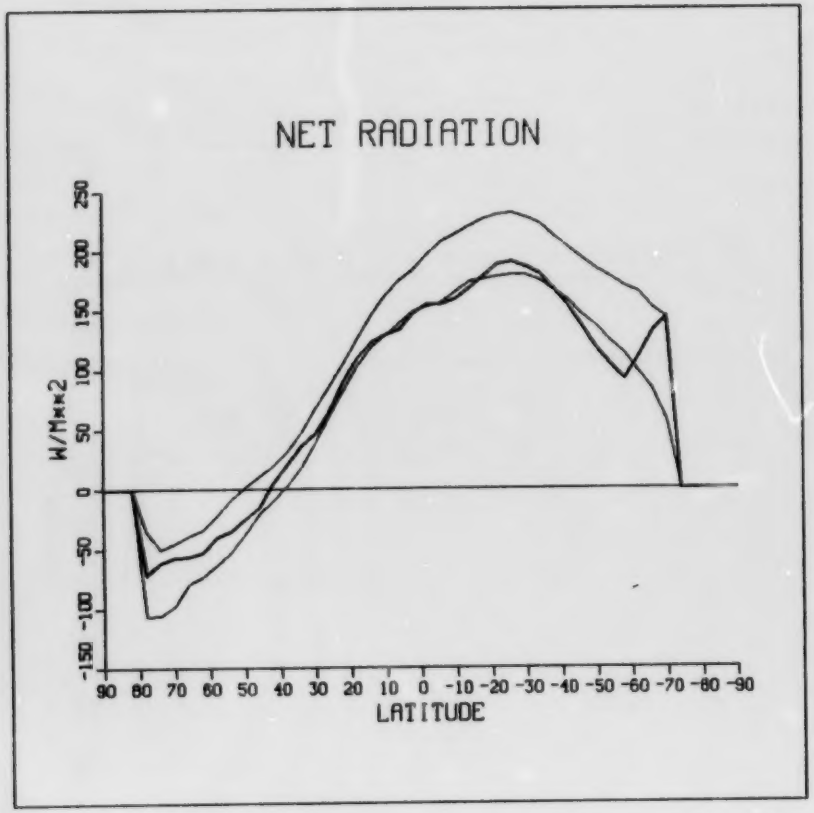
NET RADIATION
W/M**2
250
200
150
100
50
0
-50
-100
-150
90 80 70 60 50 40 30 20 10 0 -10 -20 -30 -40 -50 -60 -70 -80 -90
LATITUDE

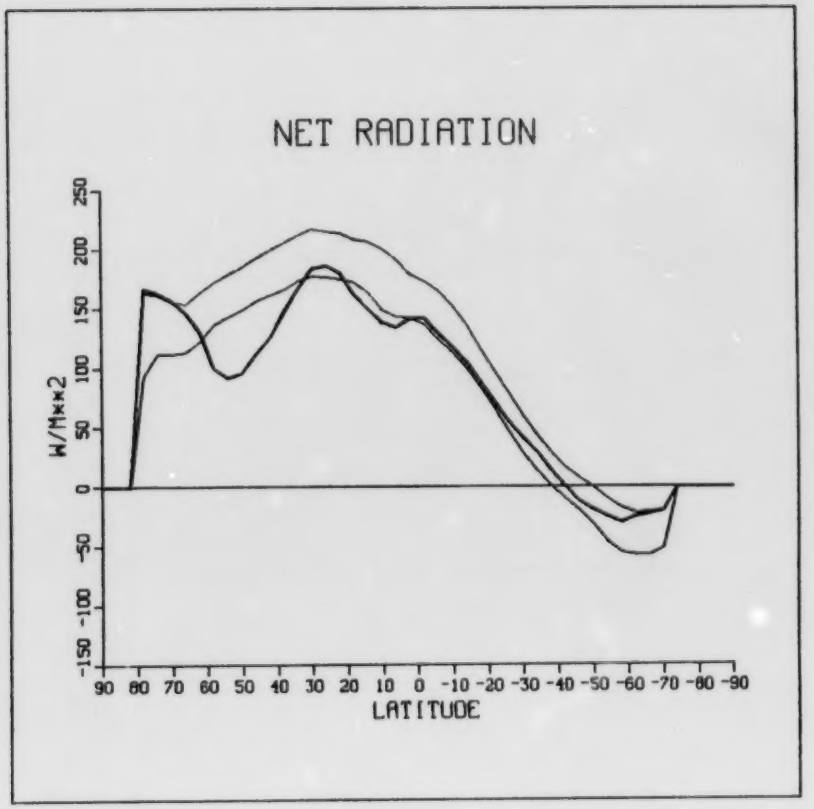
NET RADIATION
W/M**2
250
200
150
100
50
0
-50
-100
-150
90 80 70 60 50 40 30 20 10 0 -10 -20 -30 -40 -50 -60 -70 -80 -90
LATITUDE

Figure 2

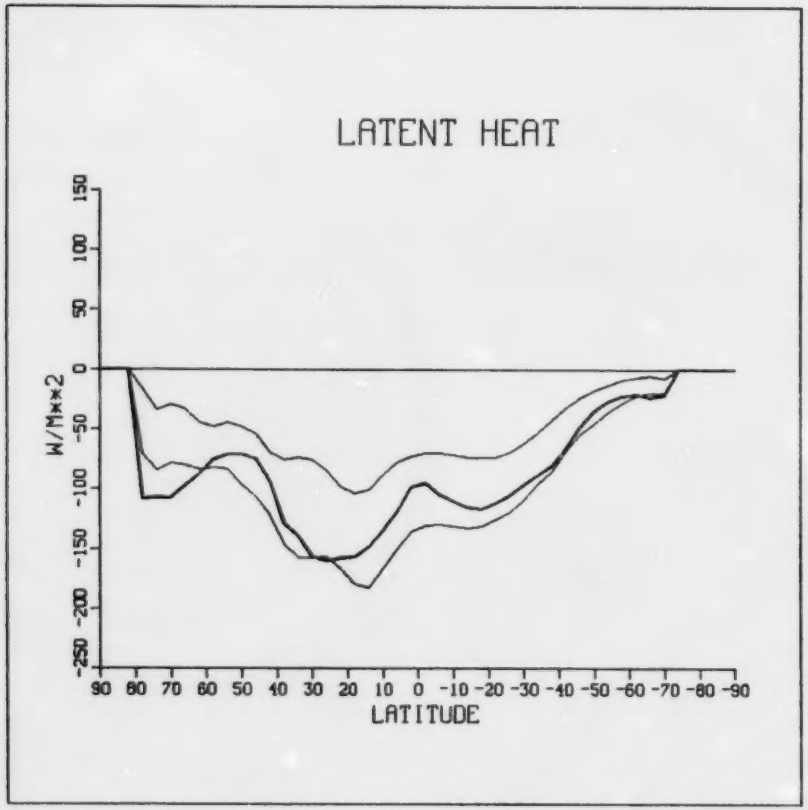
LATENT HEAT
W/M**2
150
100
50
0
-50
-100
-150
-200
-250
90 80 70 60 50 40 30 20 10 0 -10 -20 -30 -40 -50 -60 -70 -80 -90
LATITUDE

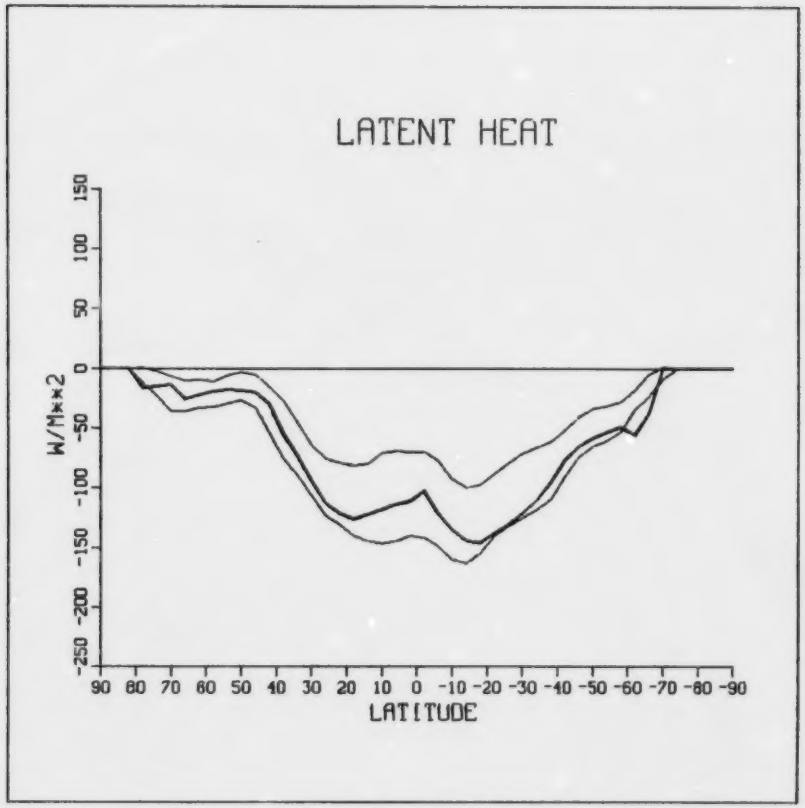
LATENT HEAT
W/M**2
150
100
50
0
-50
-100
-150
-200
-250
90 80 70 60 50 40 30 20 10 0 -10 -20 -30 -40 -50 -60 -70 -80 -90
LATITUDE

Figure 3

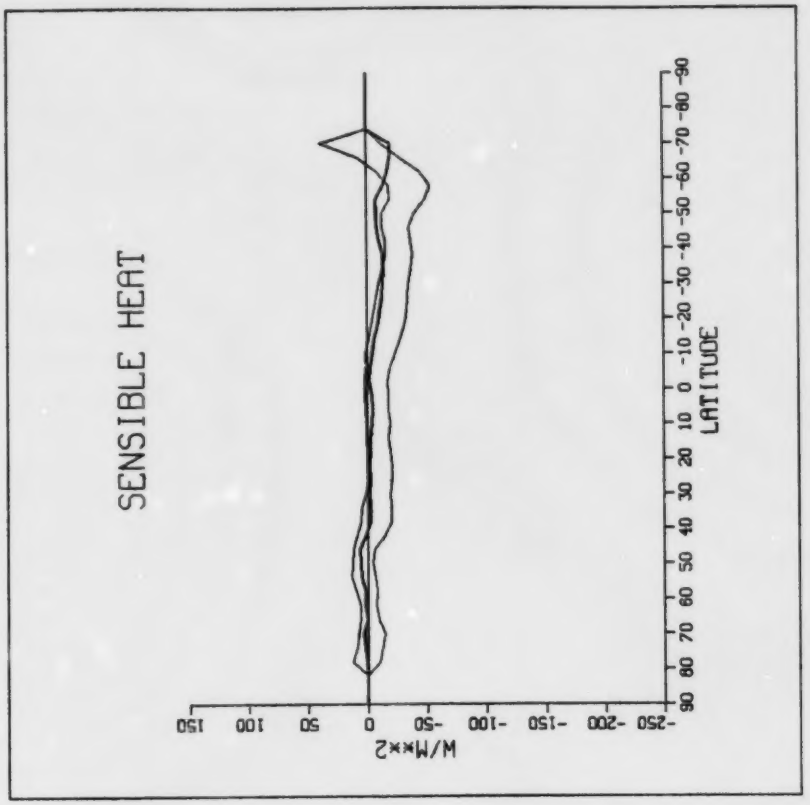
SENSIBLE HEAT
W/M**2
150 100 50 0 -50 -100 -150 -200 -250
LATITUDE
90 80 70 60 50 40 30 20 10 0 -10 -20 -30 -40 -50 -60 -70 -80 -90

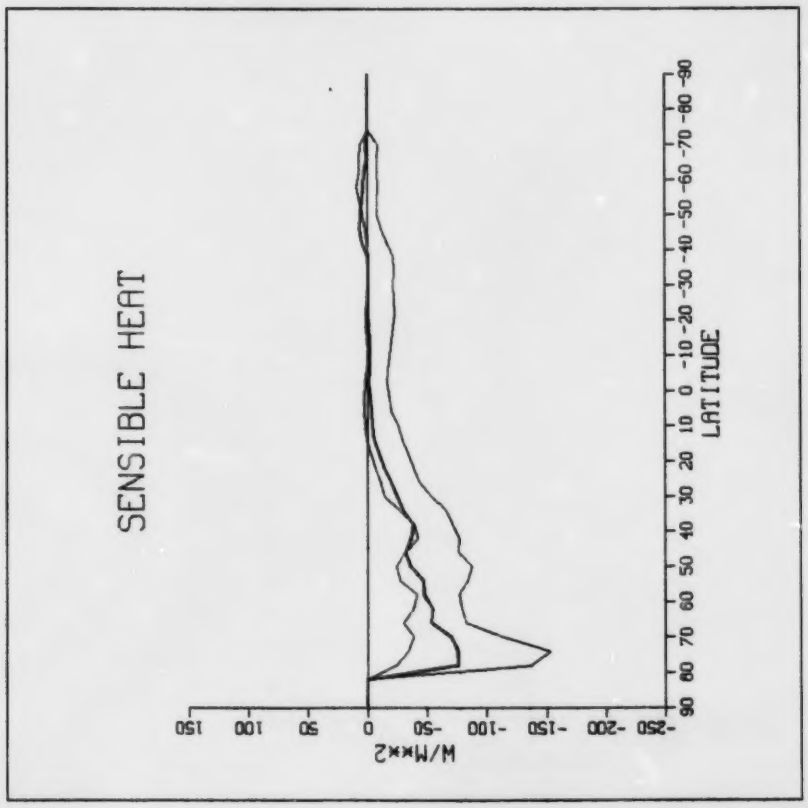
SENSIBLE HEAT
W/M**2
150 100 50 0 -50 -100 -150 -200 -250
LATITUDE
90 80 70 60 50 40 30 20 10 0 -10 -20 -30 -40 -50 -60 -70 -80 -90

Figure 4

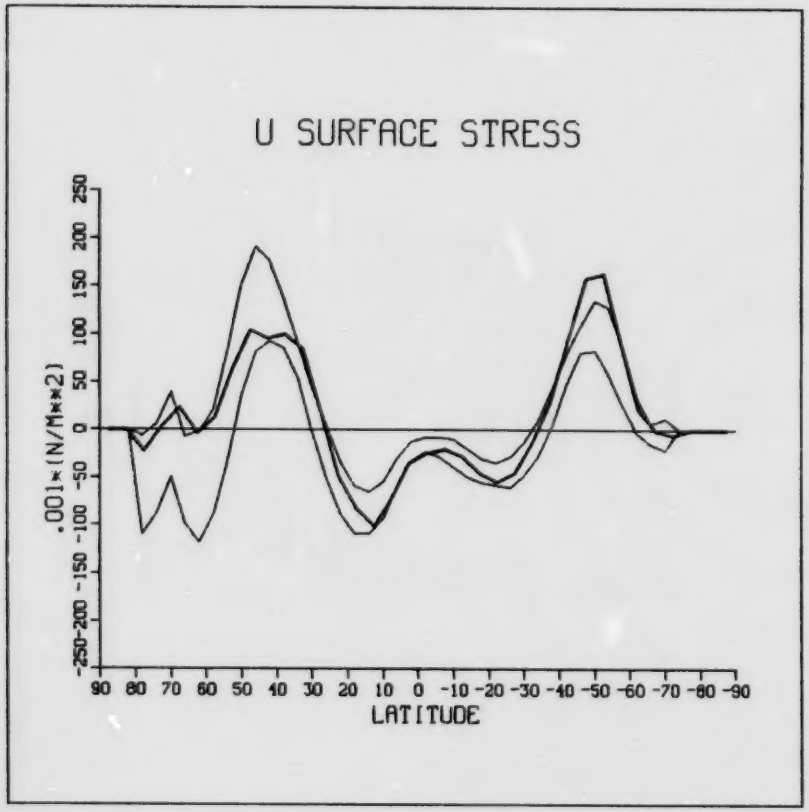
U SURFACE STRESS
.001*(N/M**2)
250
200
150
100
50
0
-50
-100
-150
-200
-250
90 80 70 60 50 40 30 20 10 0 -10 -20 -30 -40 -50 -60 -70 -80 -90
LATITUDE

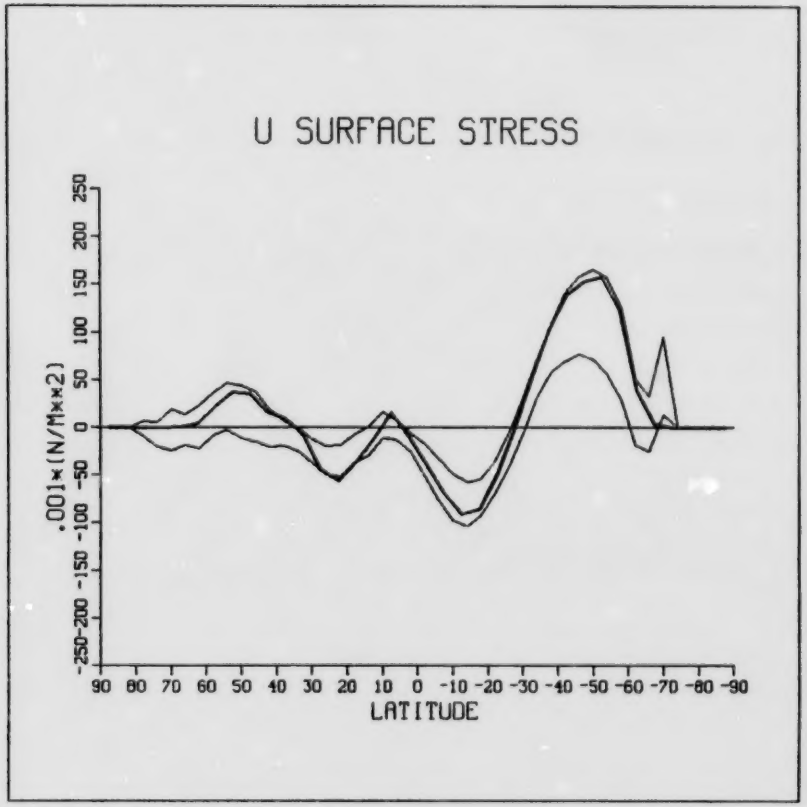
U SURFACE STRESS
.001*(N/M**2)
250
200
150
100
50
0
-50
-100
-150
-200
-250
90 80 70 60 50 40 30 20 10 0 -10 -20 -30 -40 -50 -60 -70 -80 -90
LATITUDE

Figure 5

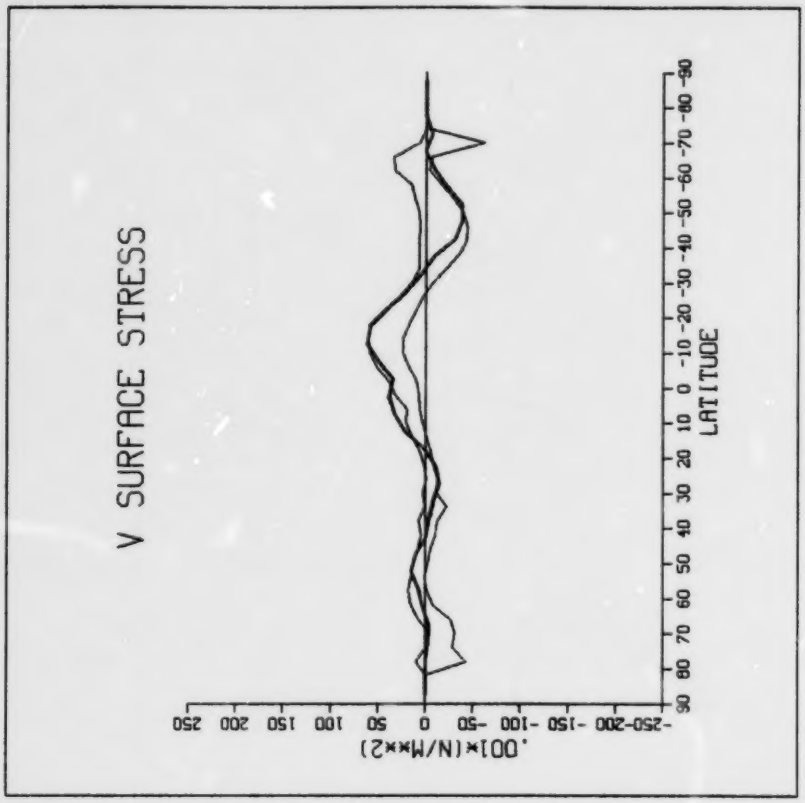
V SURFACE STRESS
.001*(N/M**2)
-250 -200 -150 -100 -50 0 50 100 150 200 250
LATITUDE
90 80 70 60 50 40 30 20 10 0 -10 -20 -30 -40 -50 -60 -70 -80 -90

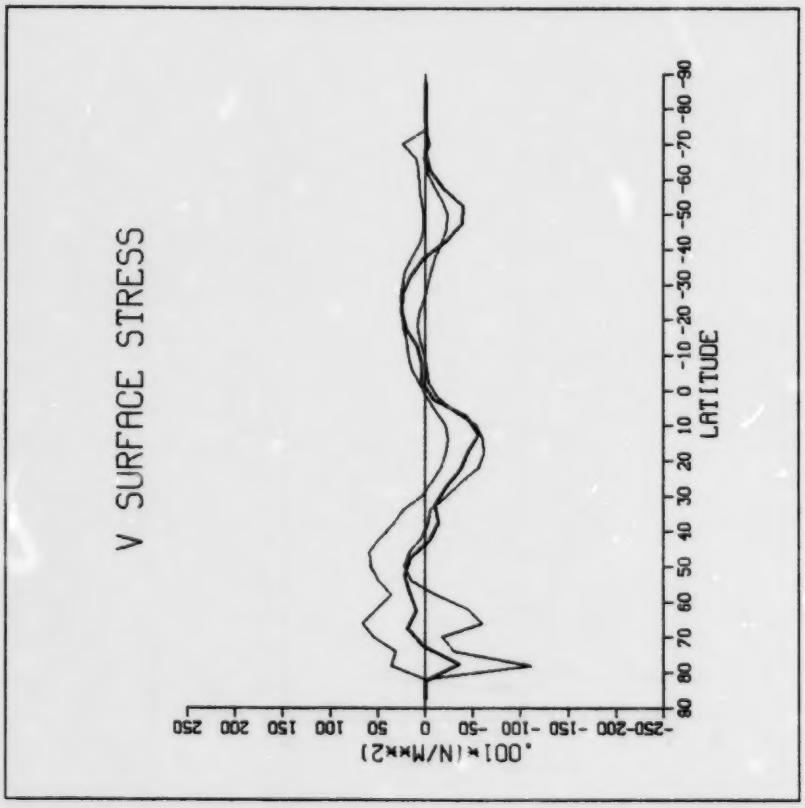
V SURFACE STRESS
.001*(N/M**2)
-250 -200 -150 -100 -50 0 50 100 150 200 250
LATITUDE
90 80 70 60 50 40 30 20 10 0 -10 -20 -30 -40 -50 -60 -70 -80 -90

Figure 6

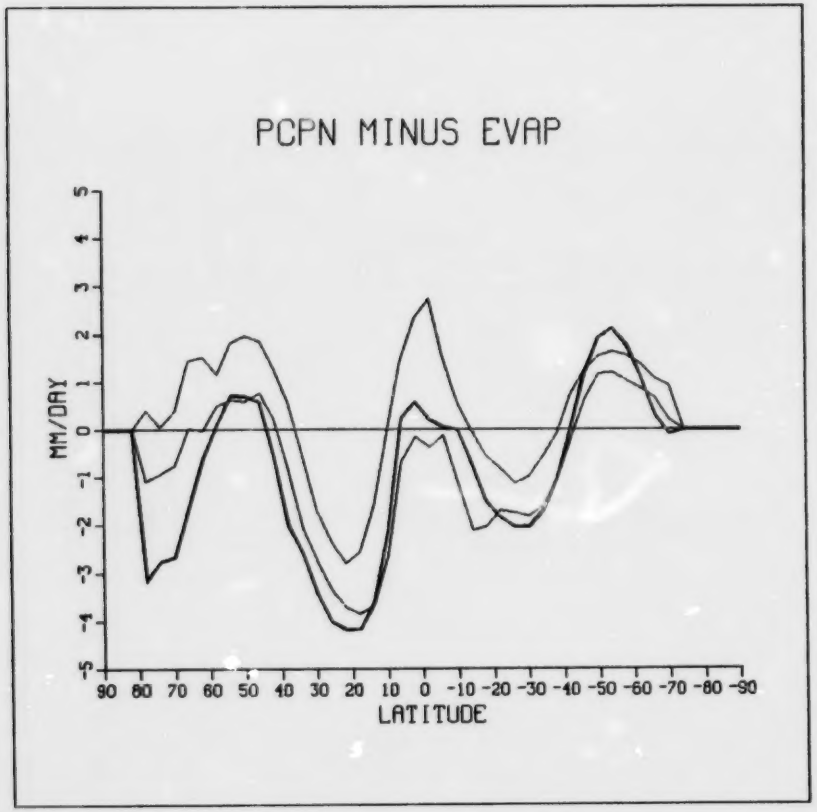
PCPN MINUS EVAP
MM/DAY
5 4 3 2 1 0 -1 -2 -3 -4 -5
90 80 70 60 50 40 30 20 10 0 -10 -20 -30 -40 -50 -60 -70 -80 -90
LATITUDE

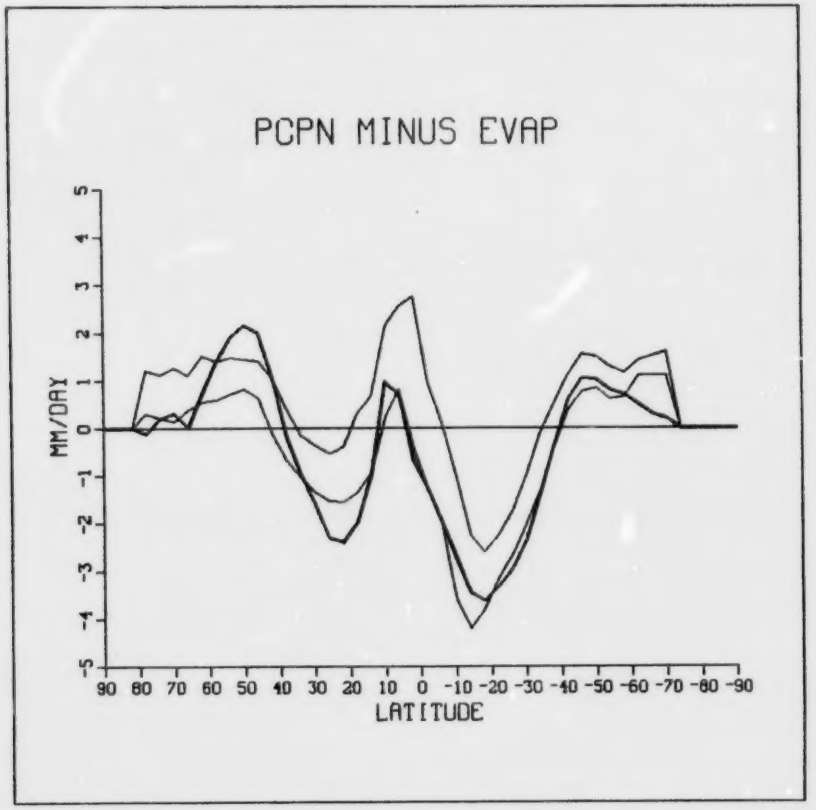
PCPN MINUS EVAP
MM/DAY
5 4 3 2 1 0 -1 -2 -3 -4 -5
90 80 70 60 50 40 30 20 10 0 -10 -20 -30 -40 -50 -60 -70 -80 -90
LATITUDE

Figure 7

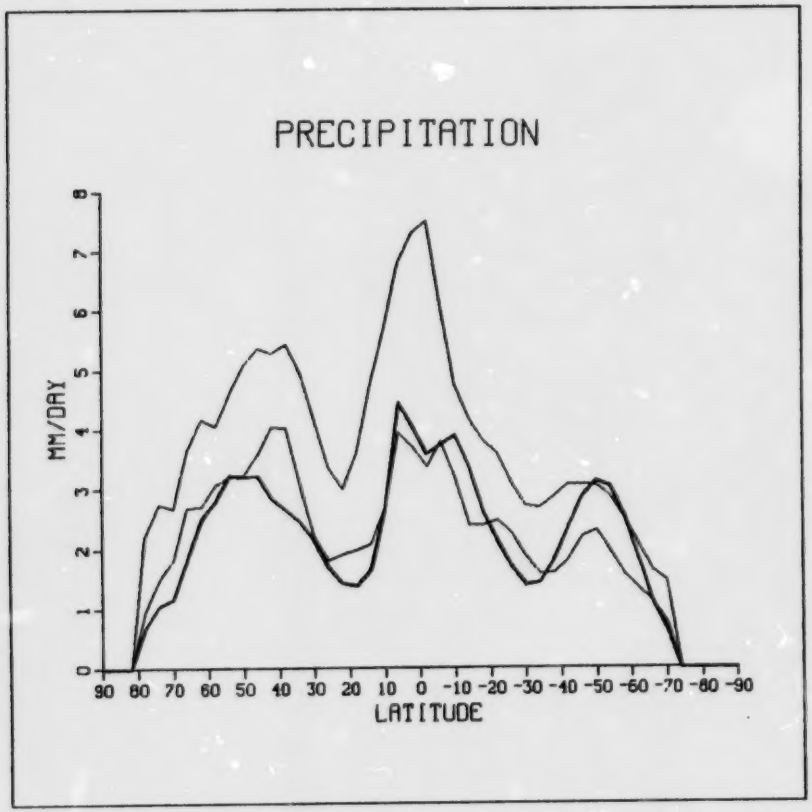
PRECIPITATION
MM/DAY
0 1 2 3 4 5 6 7 8
90 80 70 60 50 40 30 20 10 0 -10 -20 -30 -40 -50 -60 -70 -80 -90
LATITUDE

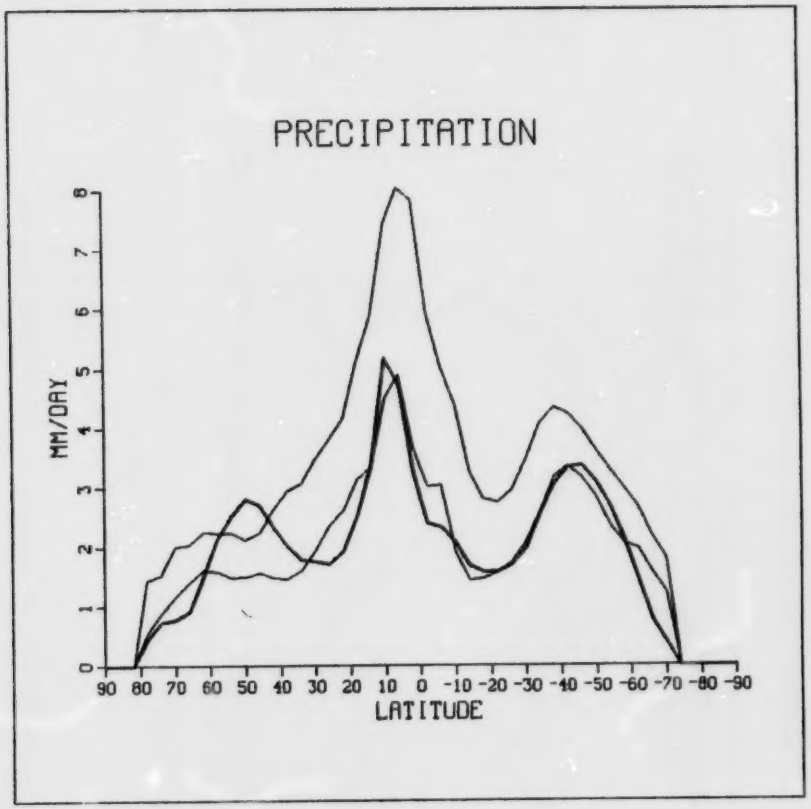
PRECIPITATION
MM/DAY
0 1 2 3 4 5 6 7 8
90 80 70 60 50 40 30 20 10 0 -10 -20 -30 -40 -50 -60 -70 -80 -90
LATITUDE

Figure 8

ESBENSEN AND KUSHNIR JANUARY NET HEAT (W/M**2)

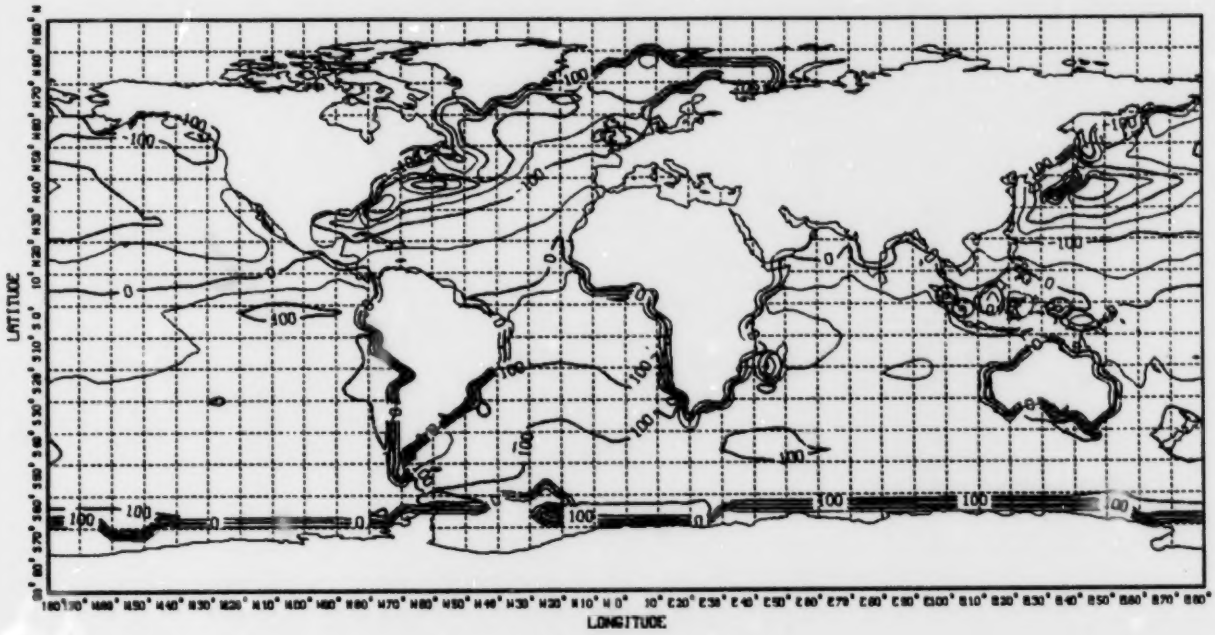

ESBENSEN AND KUSHNIR JULY NET HEAT (W/M**2)

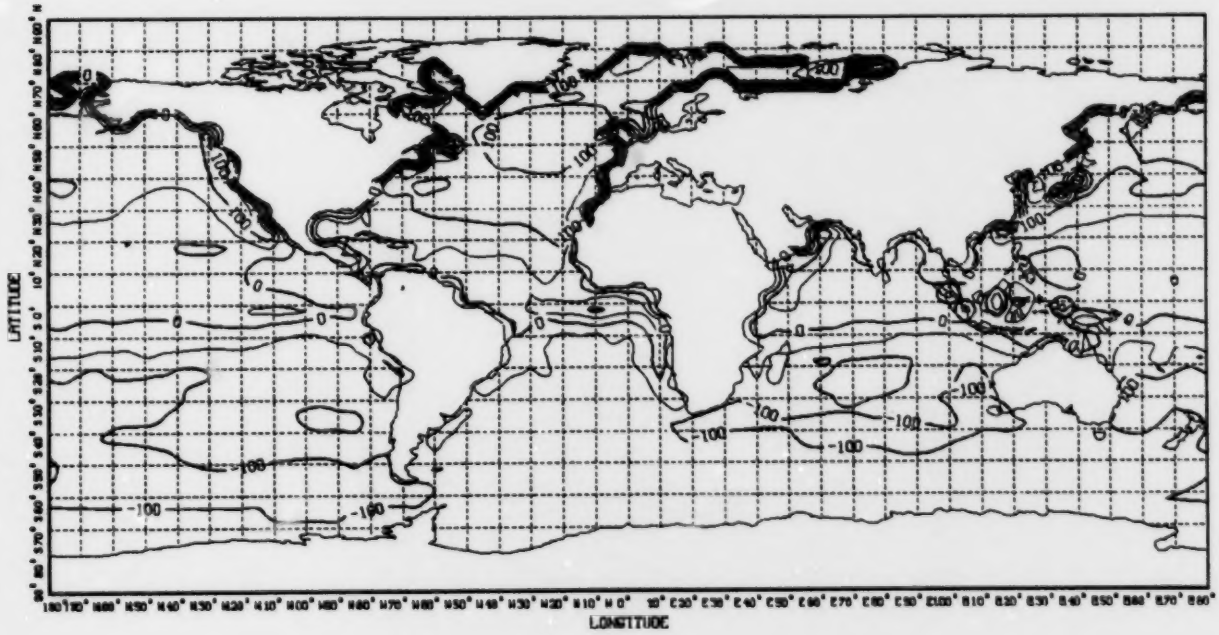

Figure 9

GRAND MEAN JANUARY NET HEAT (W/M××2)

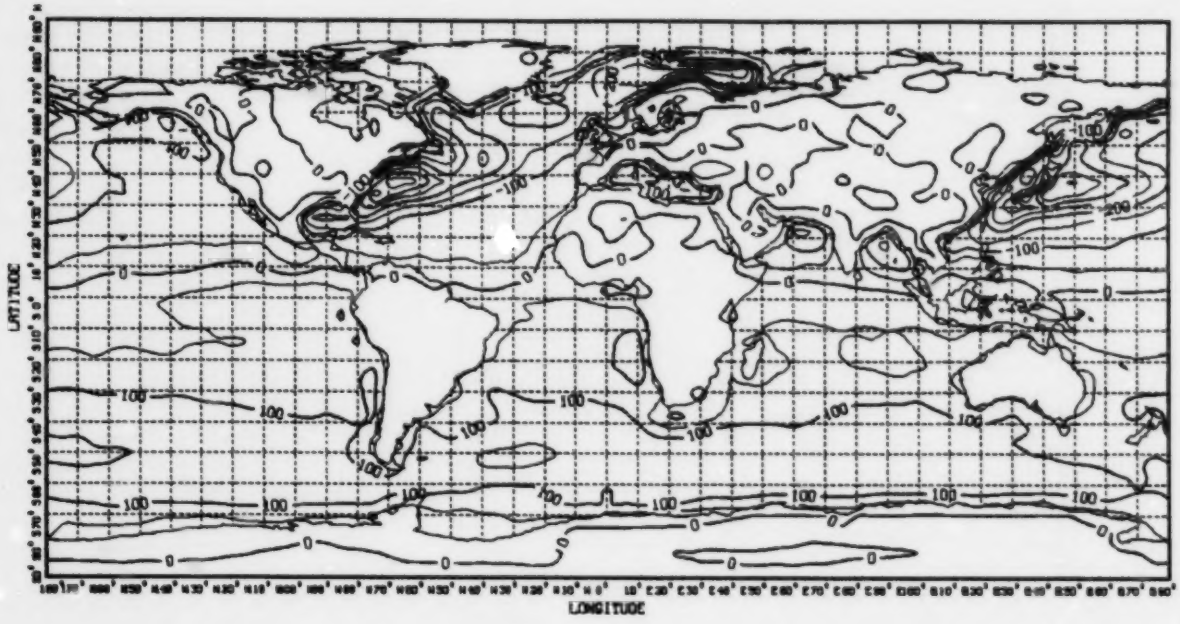

GRAND MEAN JULY NET HEAT (W/M××2)

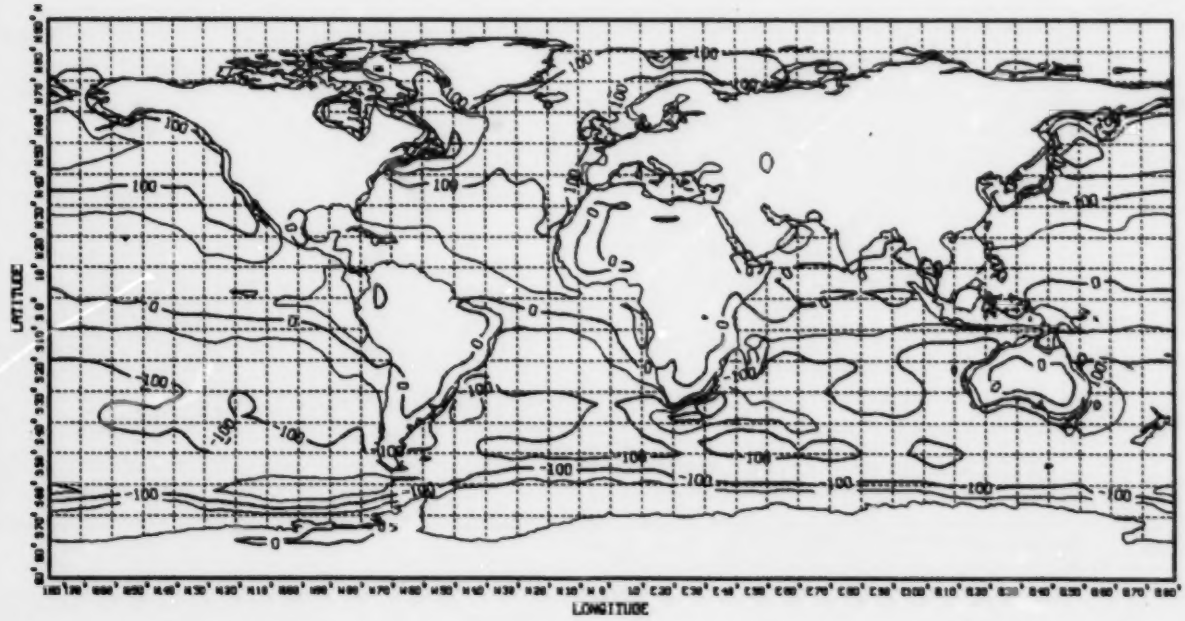

Figure 10

T-STATISTIC JANUARY NET HEAT

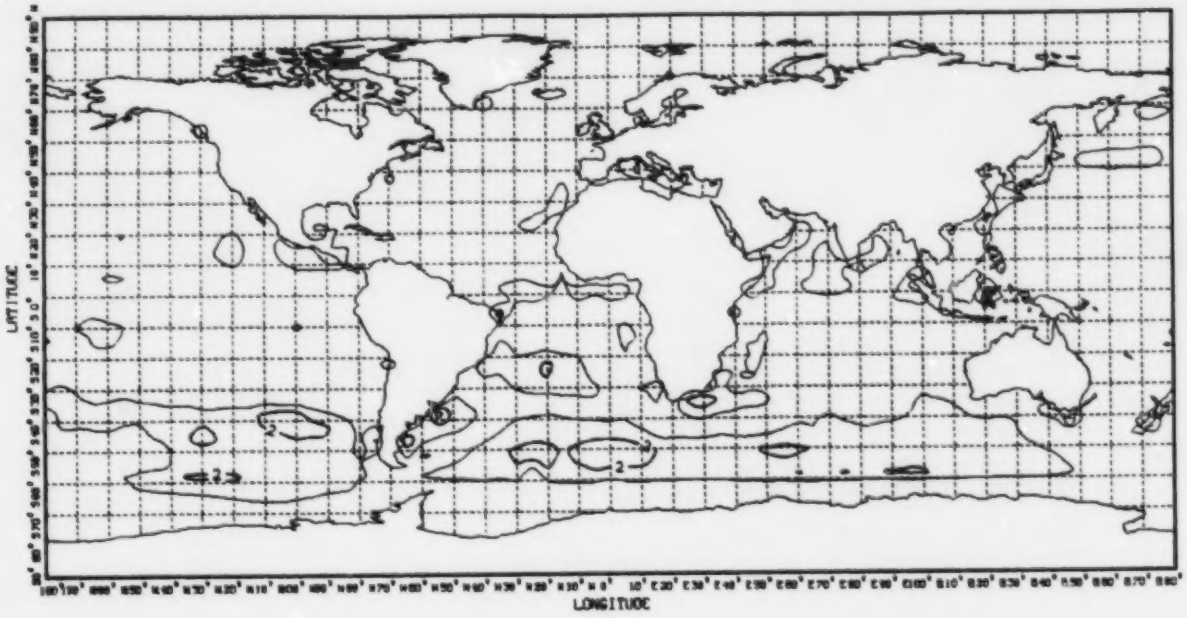

T-STATISTIC JULY NET HEAT

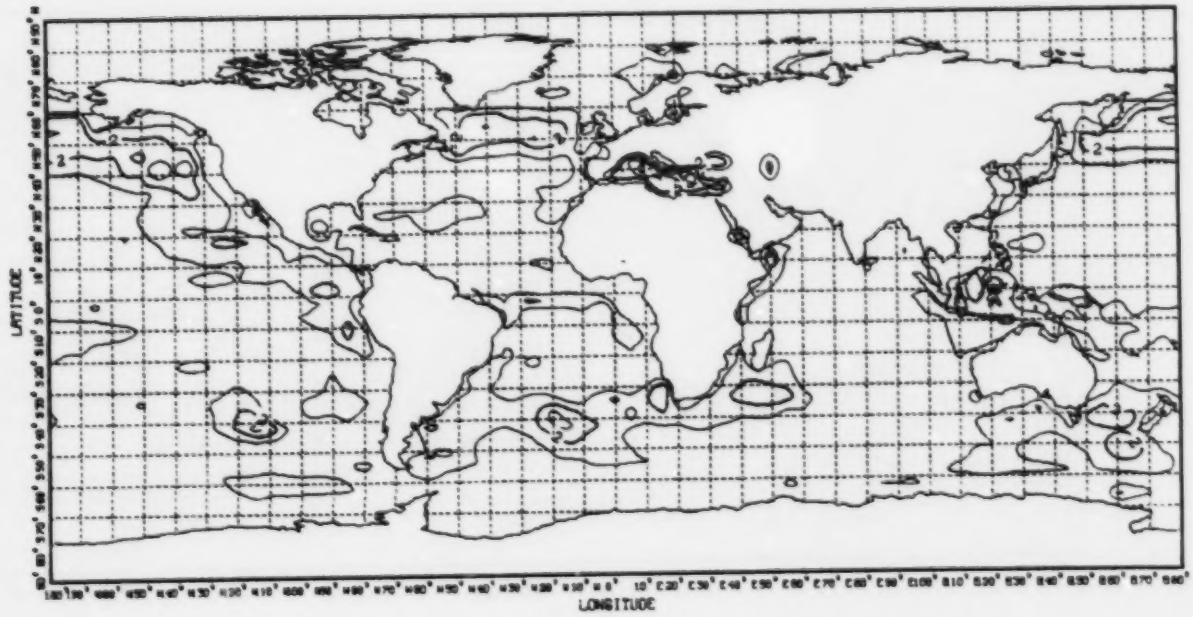

Figure 11

STANDARD DEVIATION JANUARY NET HEAT (W/M**2)

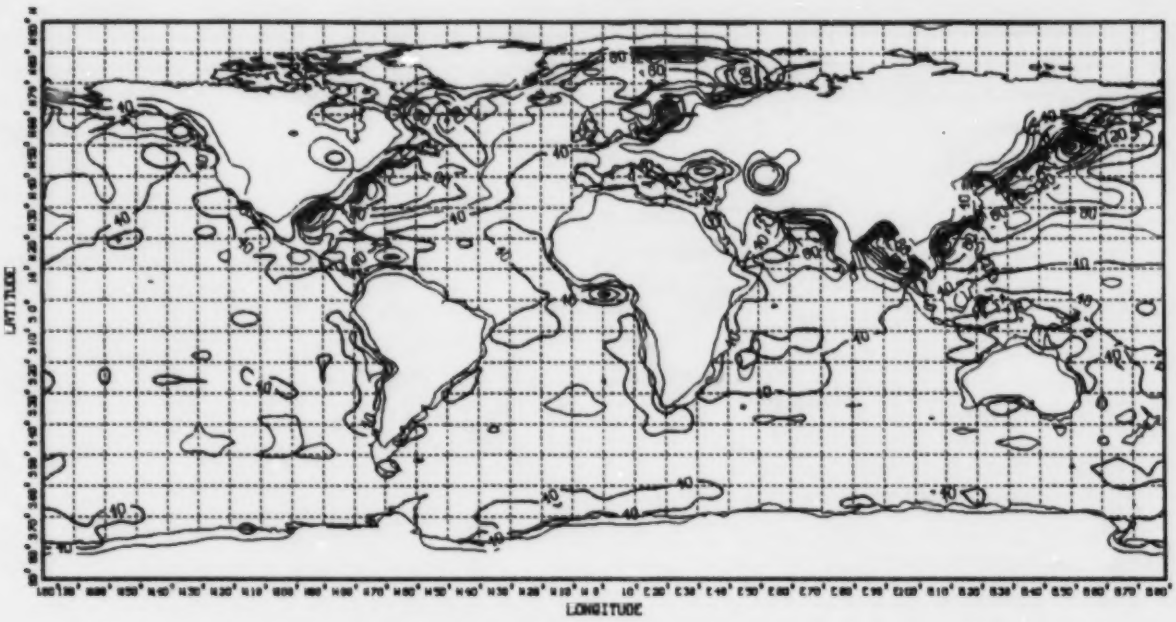

STANDARD DEVIATION JULY NET HEAT (W/M**2)

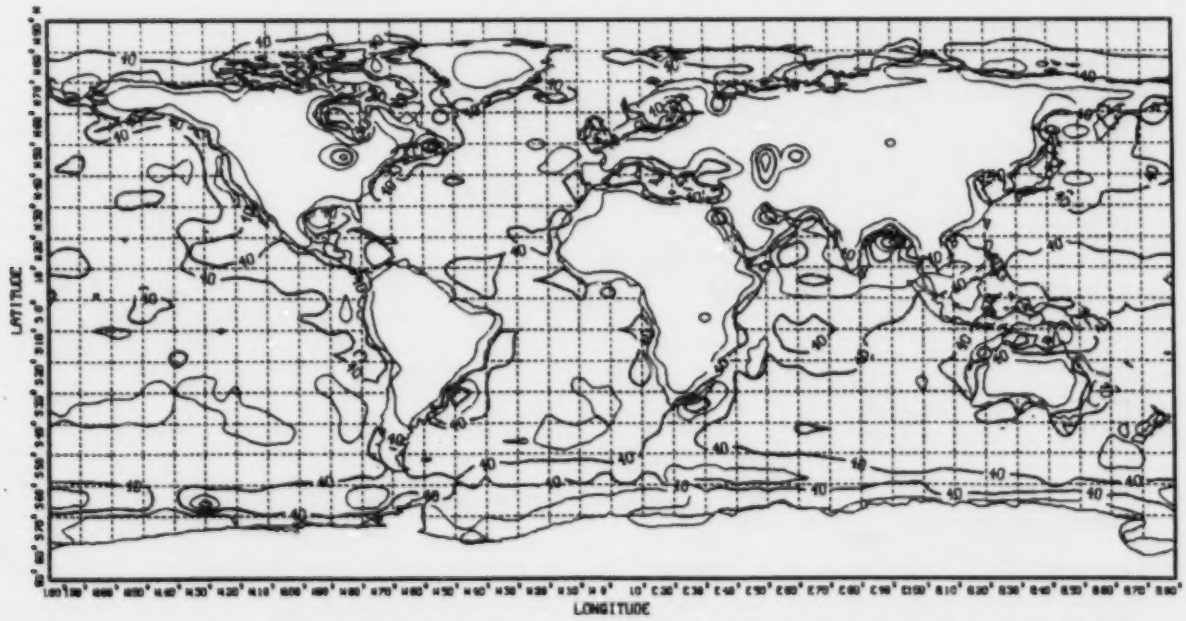

Figure 12

ESBENSEN AND KUSHNIR JANUARY NET RADIATION (W/M**2)

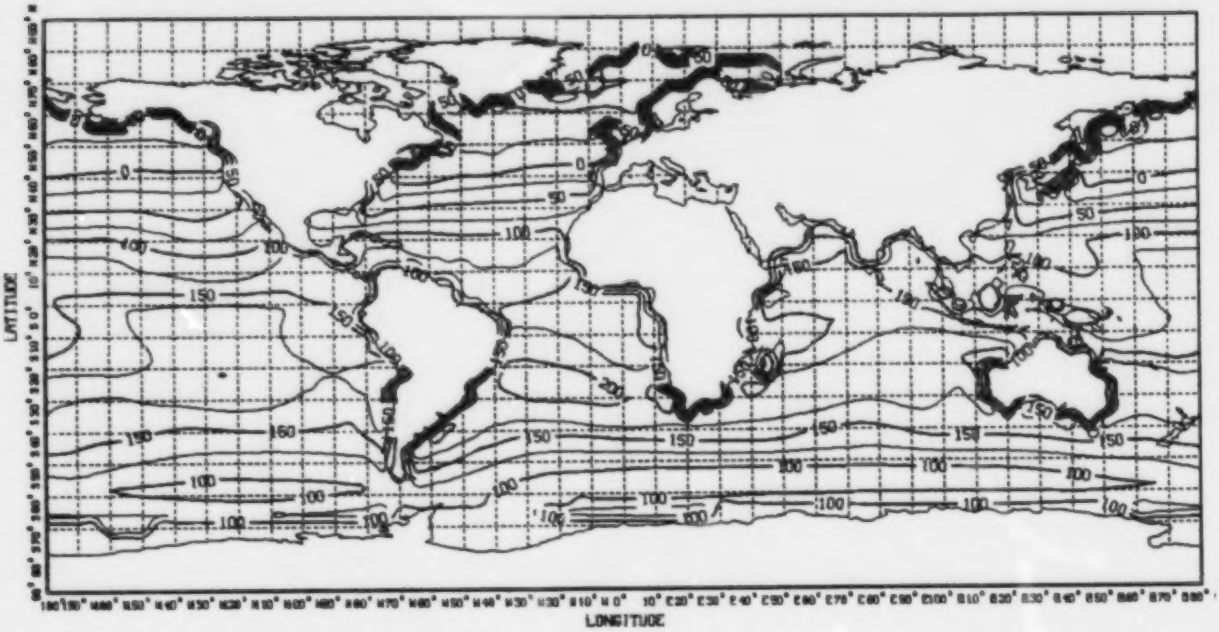

ESBENSEN AND KUSHNIR JULY NET RADIATION (W/M**2)

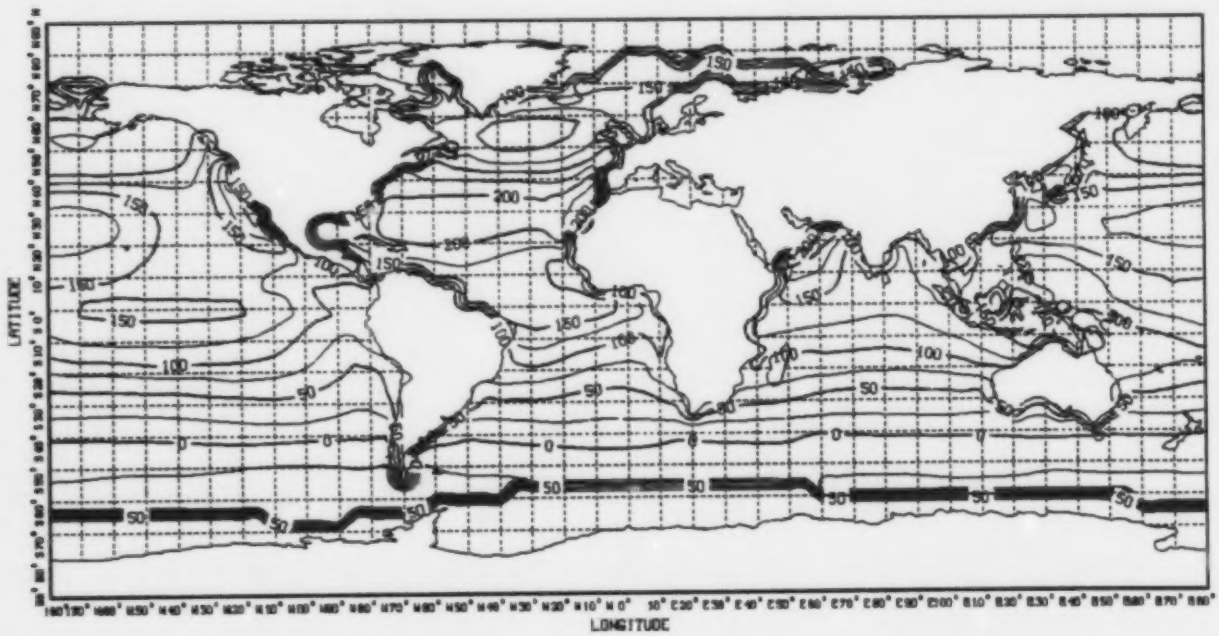

Figure 13

GRAND MEAN JANUARY NET RADIATION (W/M**2)

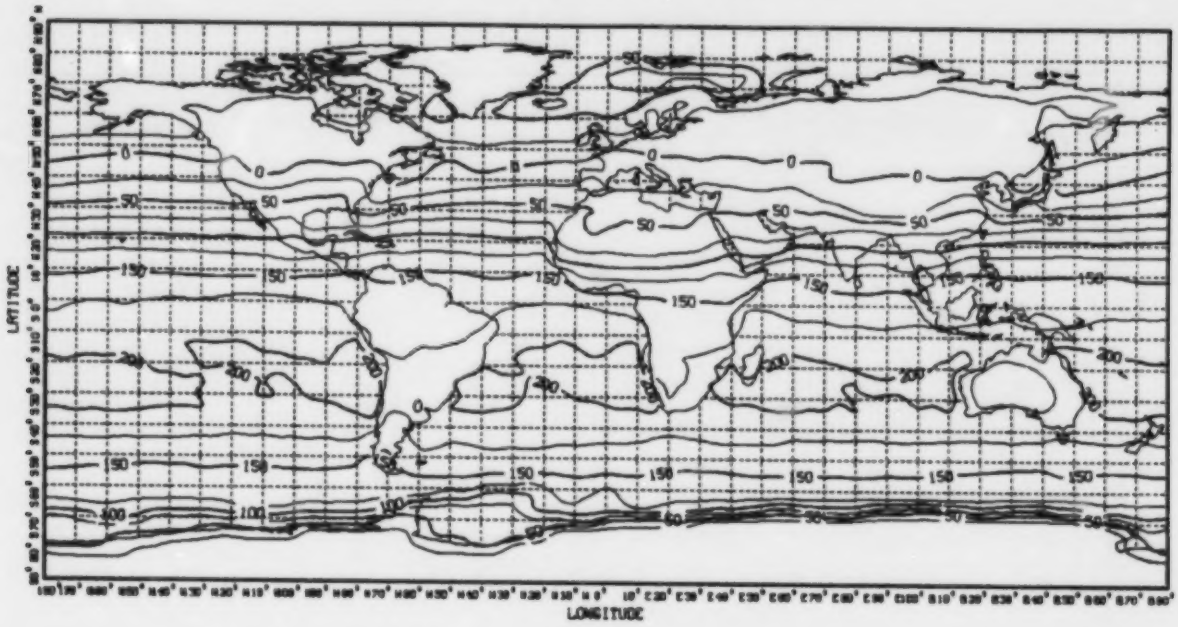

GRAND MEAN JULY NET RADIATION (W/M**2)

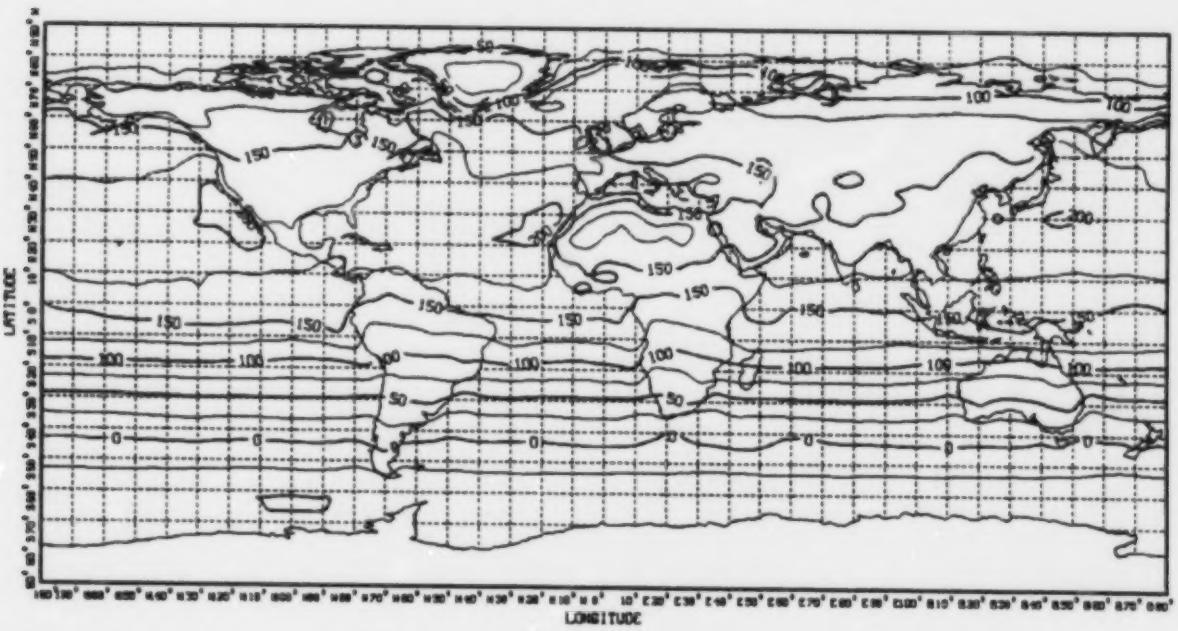

Figure 14

T-STATISTIC JANUARY NET RADIATION

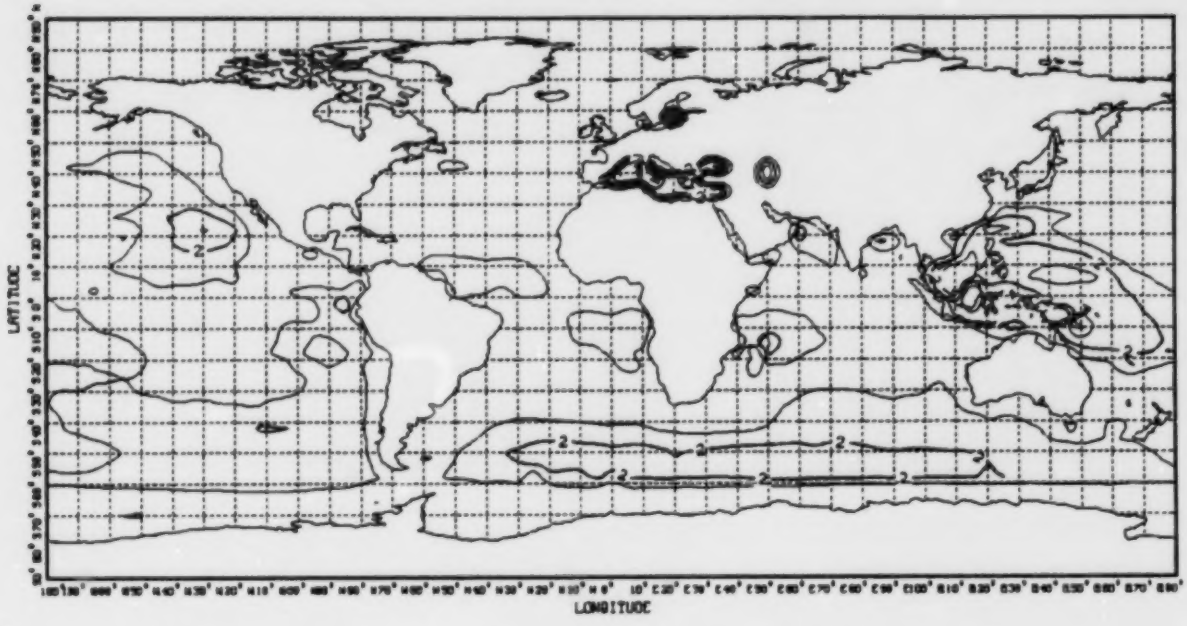

T-STATISTIC JULY NET RADIATION

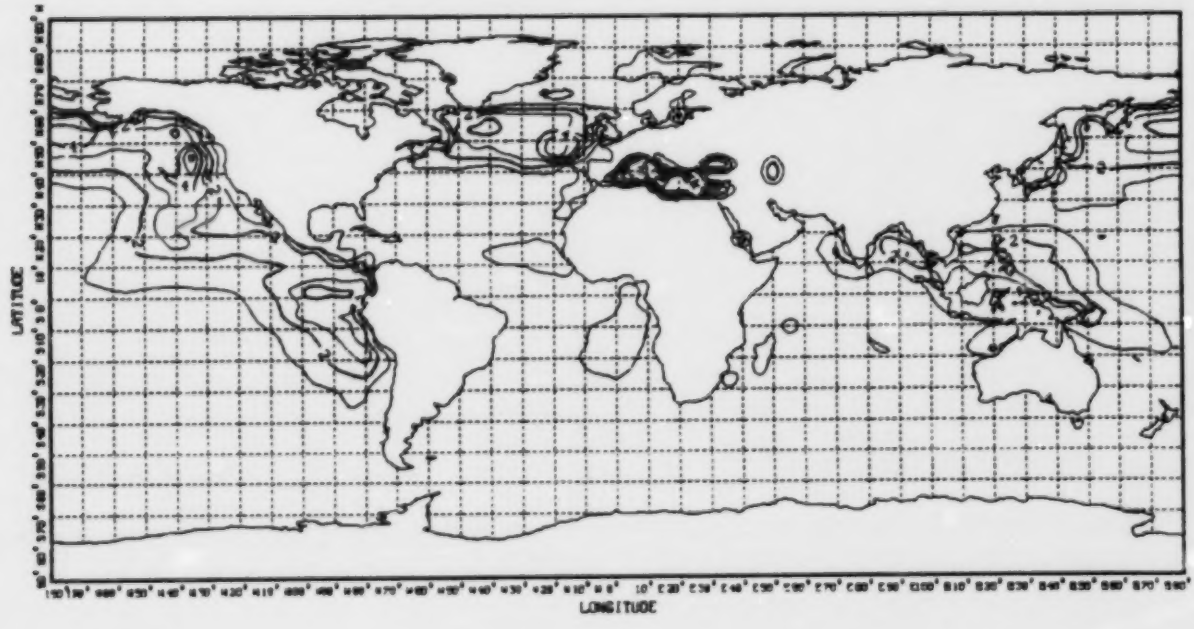

Figure 15

STANDARD DEVIATION JANUARY NET RADIATION (W/M**2)

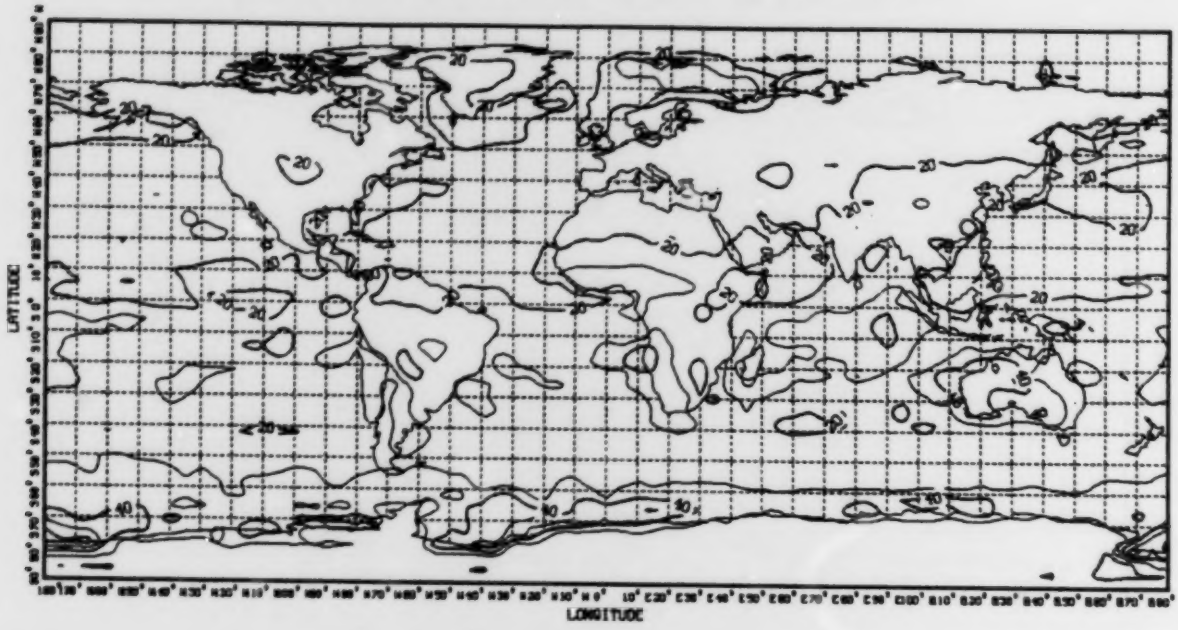

STANDARD DEVIATION JULY NET RADIATION (W/M**2)

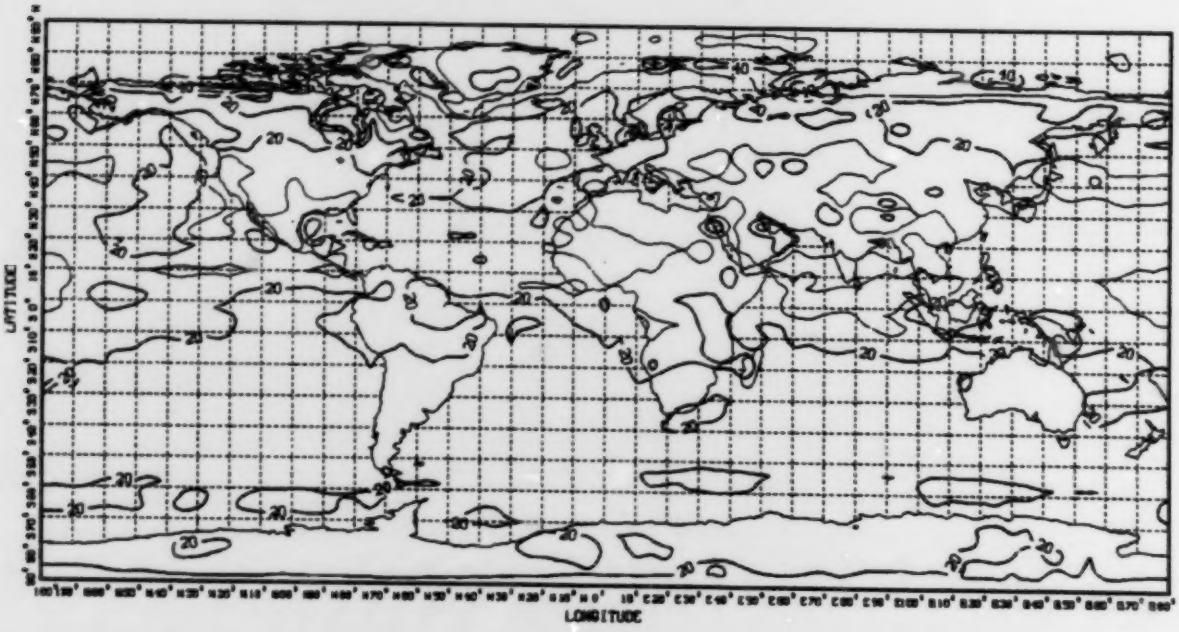

Figure 16

ESBENSEN AND KUSHNIR JANUARY LATENT HEAT (W/M**2)

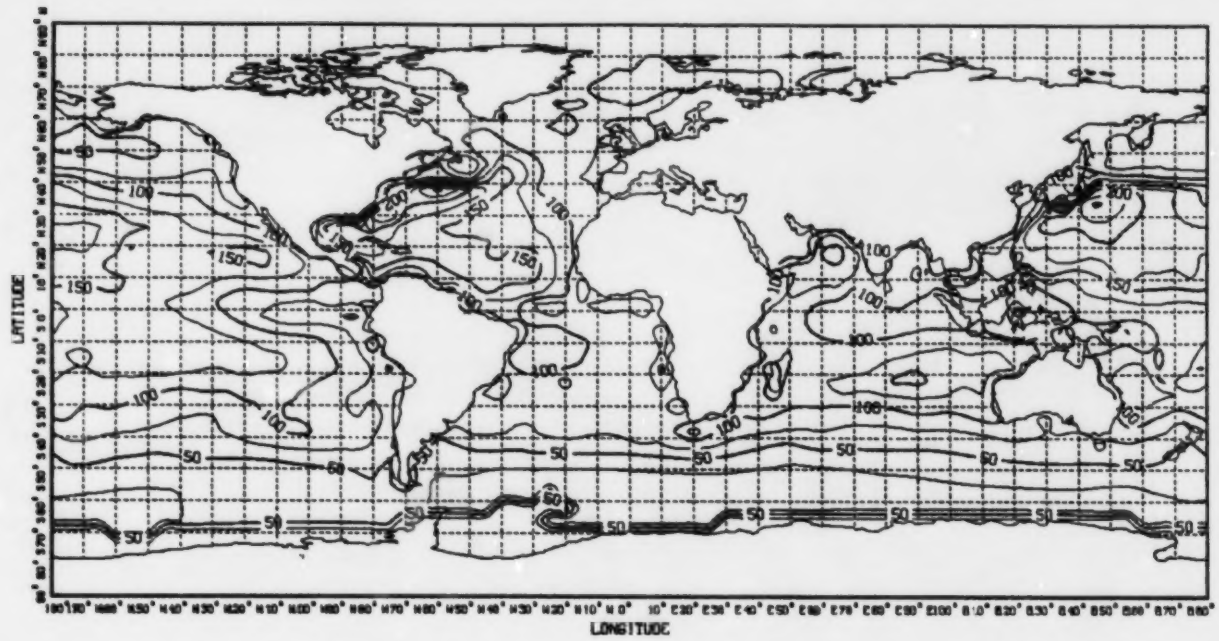

ESBENSEN AND KUSHNIR JULY LATENT HEAT (W/M**2)

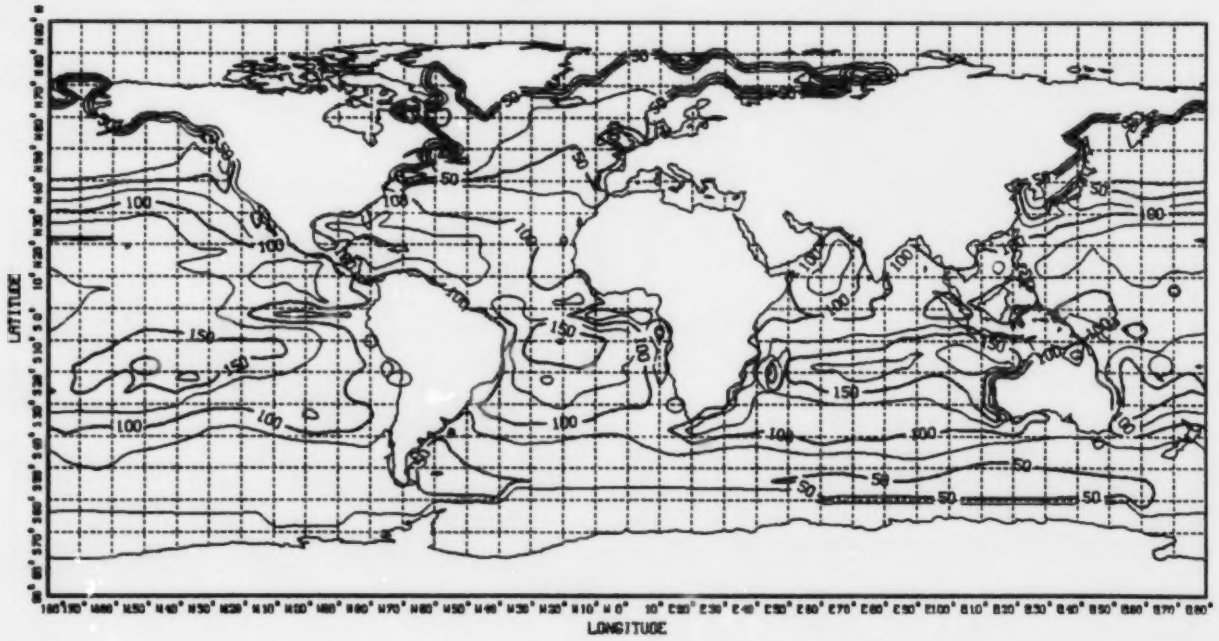

Figure 17

GRAND MEAN JANUARY LATENT HEAT (W/M**2)

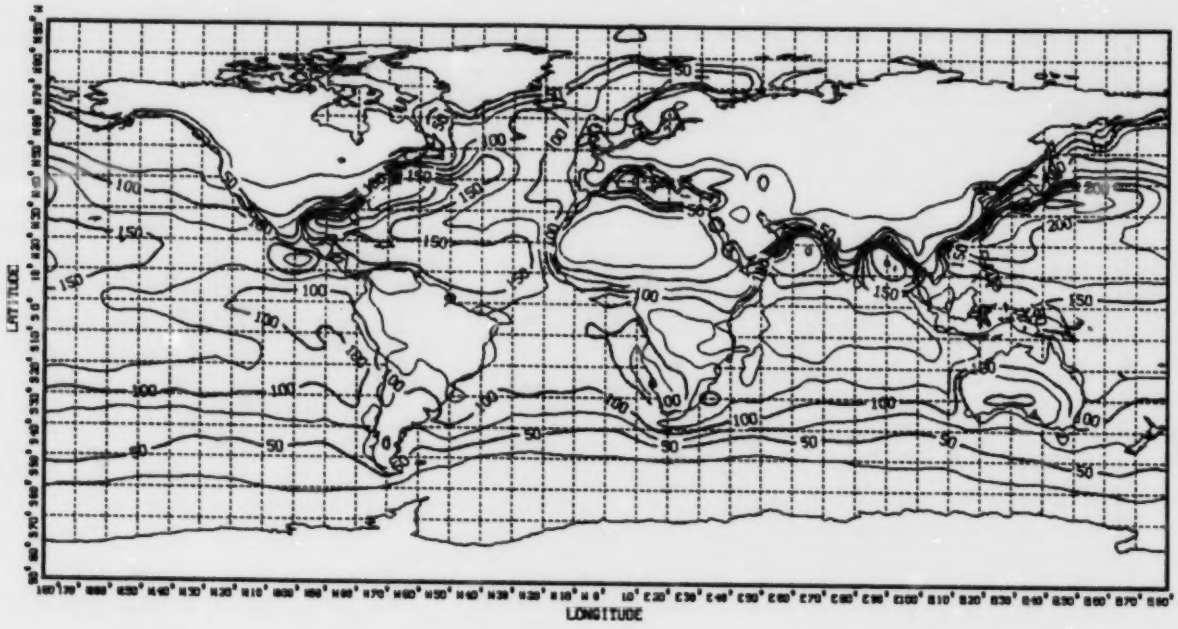

GRAND MEAN JULY LATENT HEAT (W/M**2)

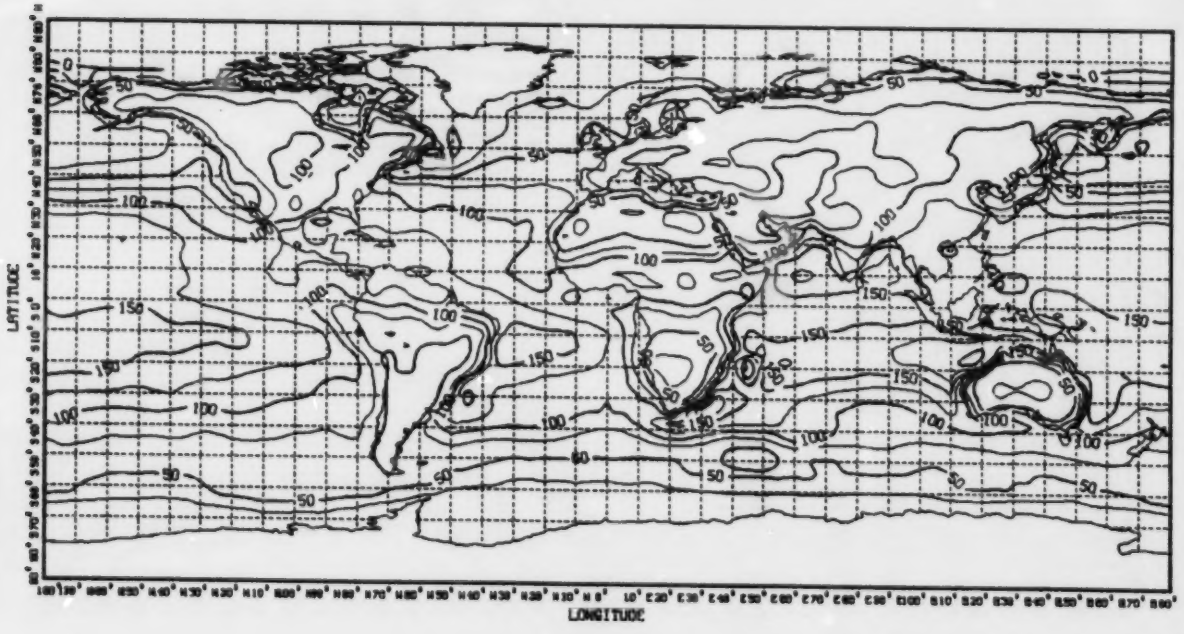

Figure 18

T-STATISTIC JANUARY LATENT HEAT

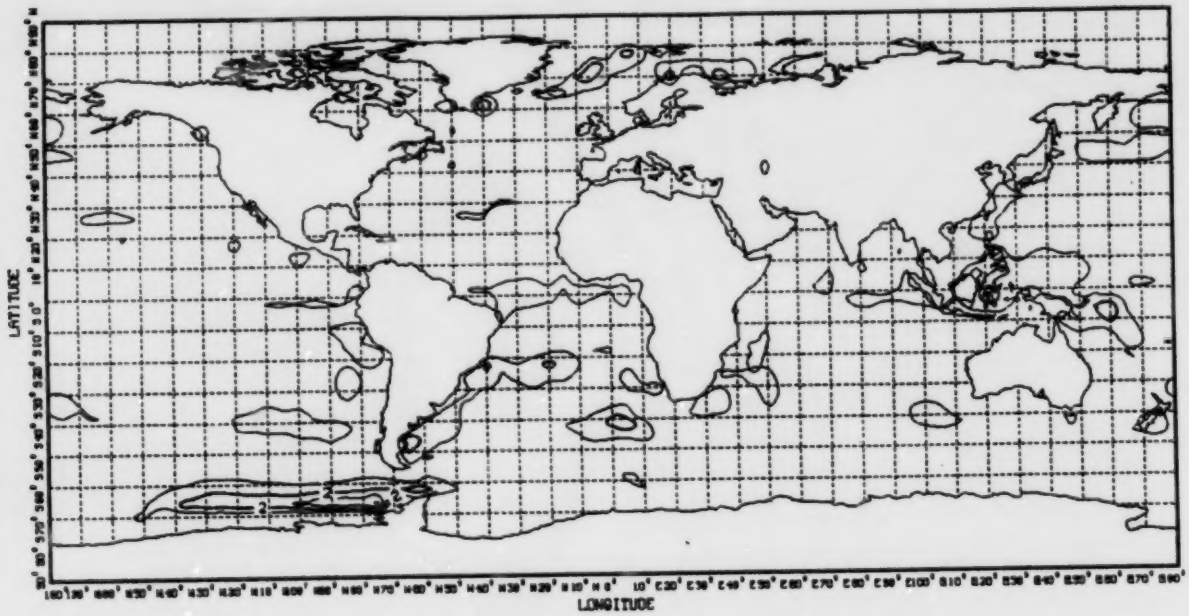

T-STATISTIC JULY LATENT HEAT

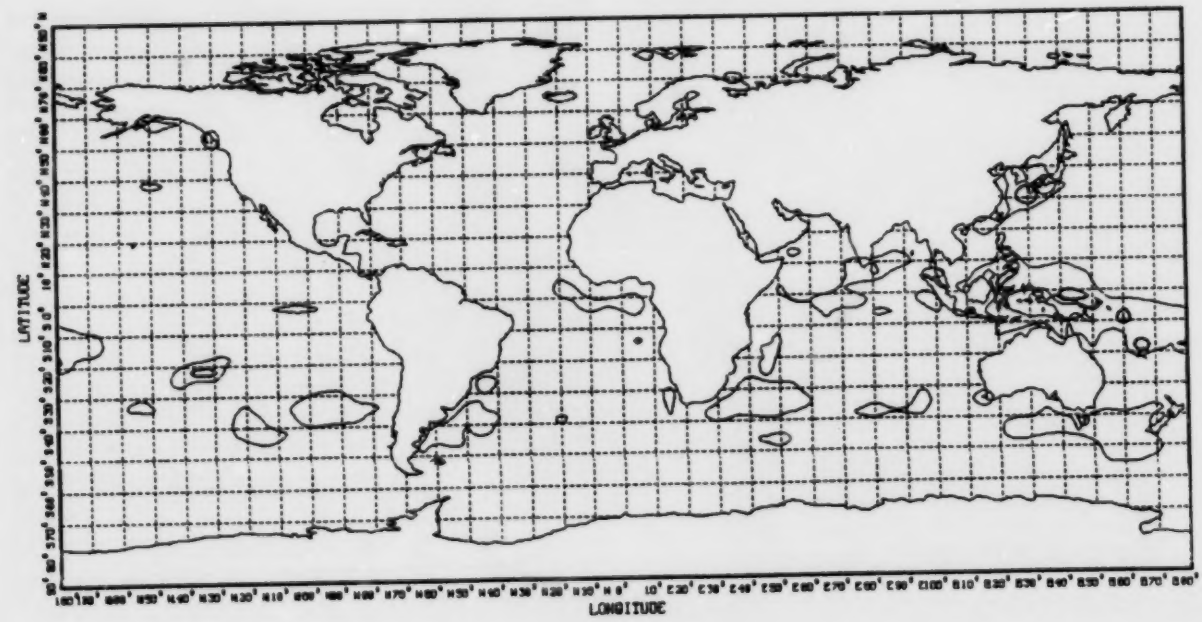

Figure 19

STANDARD DEVIATION JANUARY LATENT HEAT (W/M××2)

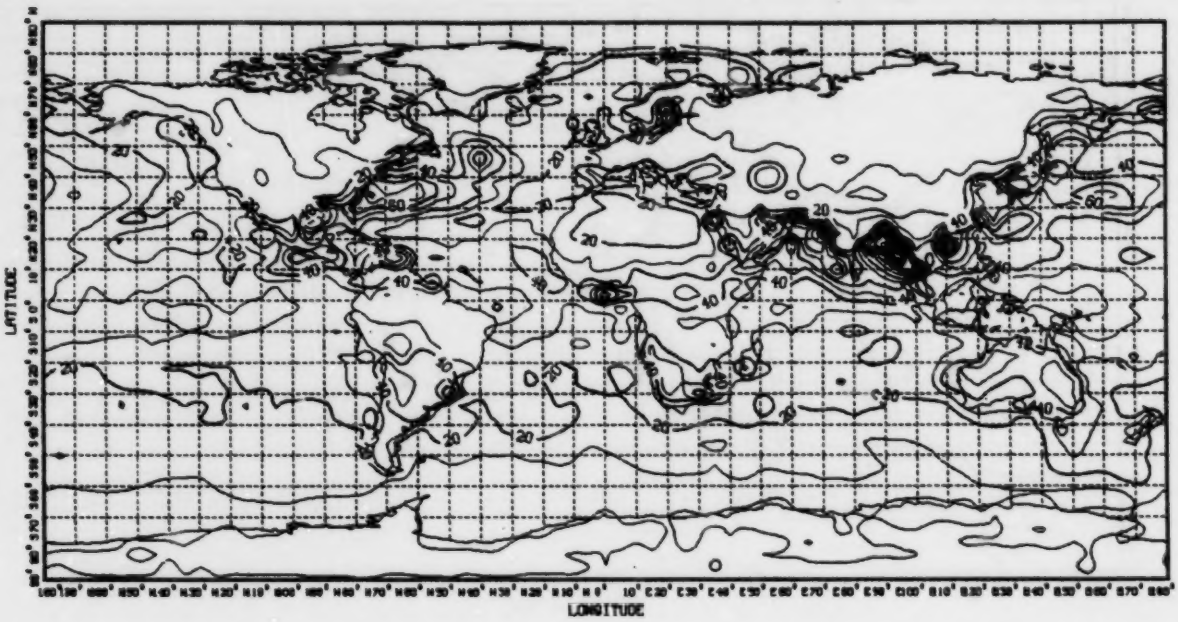

STANDARD DEVIATION JULY LATENT HEAT (W/M××2)

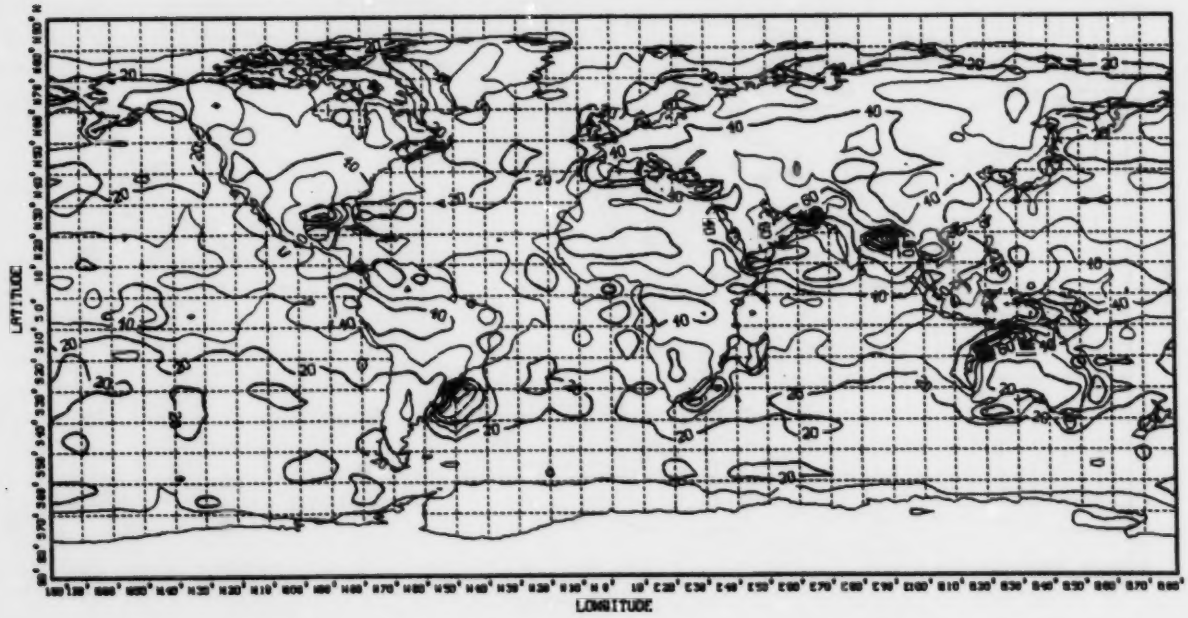

Figure 20

ESBENSEN AND KUSHNIR JANUARY SENSIBLE HEAT (W/M**2)

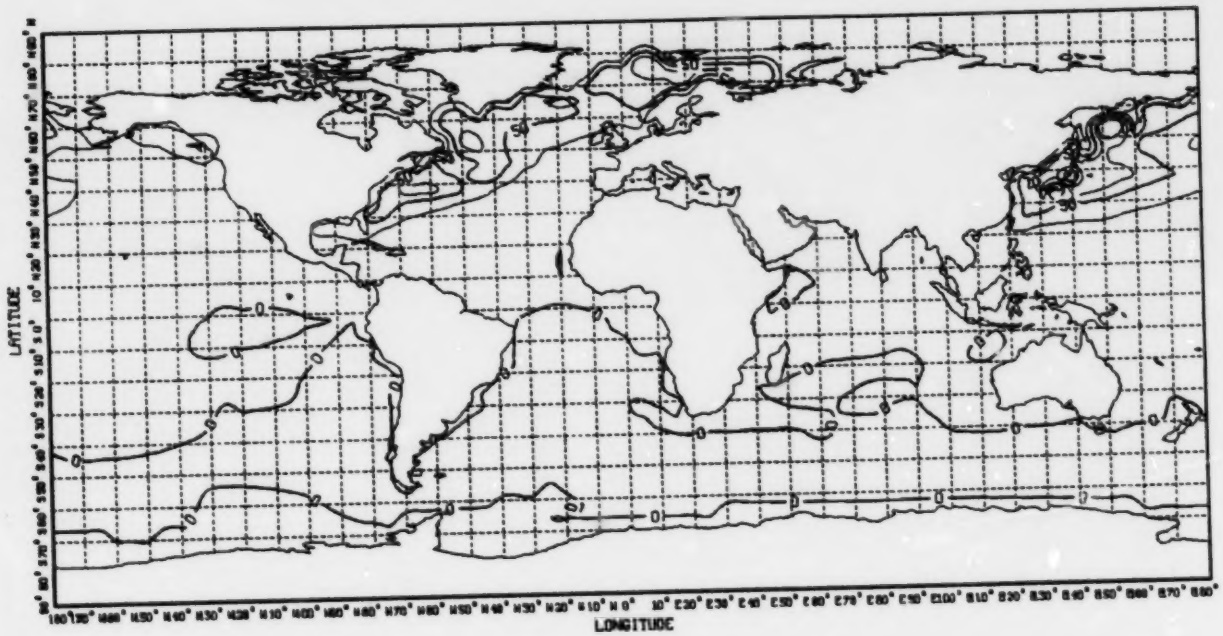

ESBENSEN AND KUSHNIR JULY SENSIBLE HEAT (W/M**2)

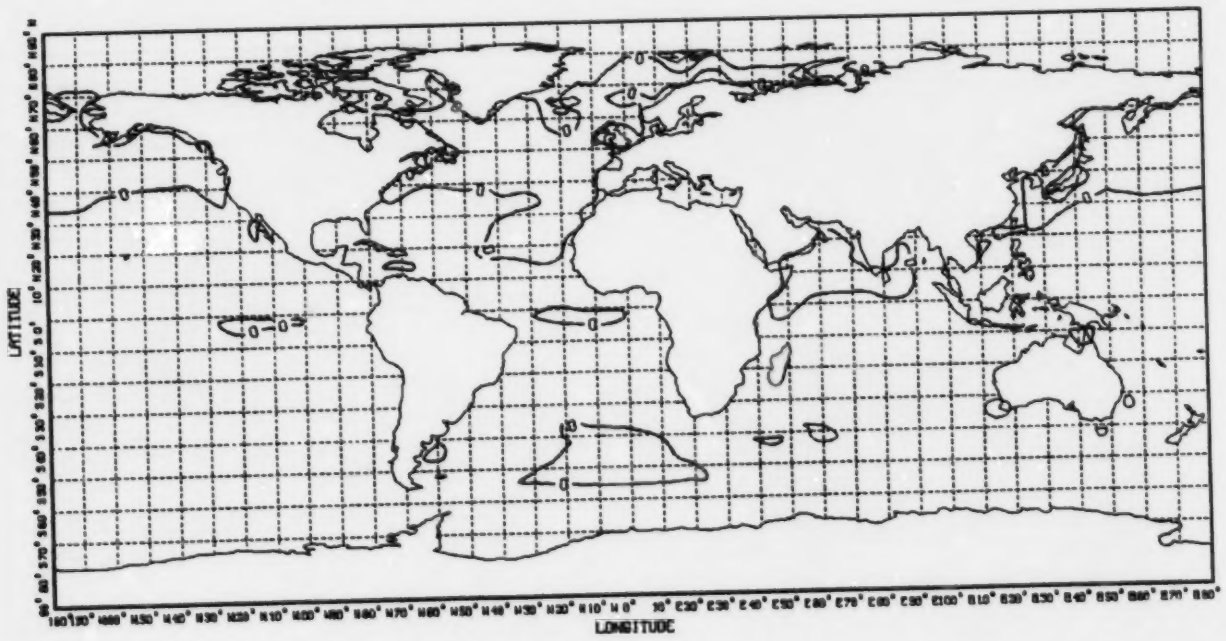

Figure 21

GRAND MEAN JANUARY SENSIBLE HEAT (W/M××2)

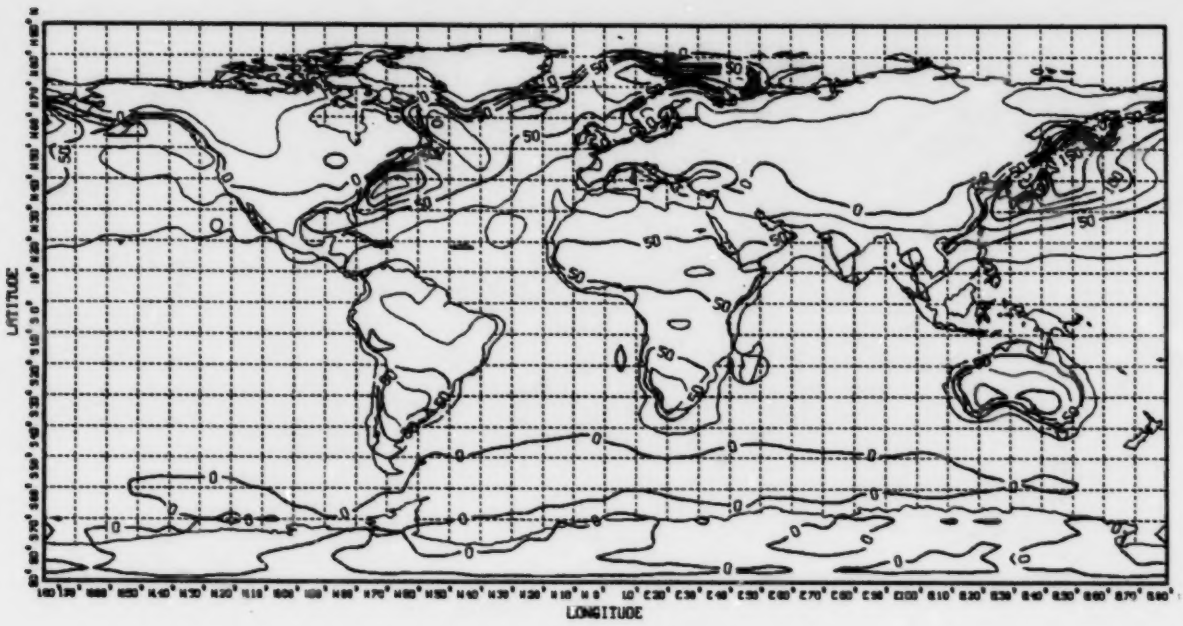

GRAND MEAN JULY SENSIBLE HEAT (W/M××2)

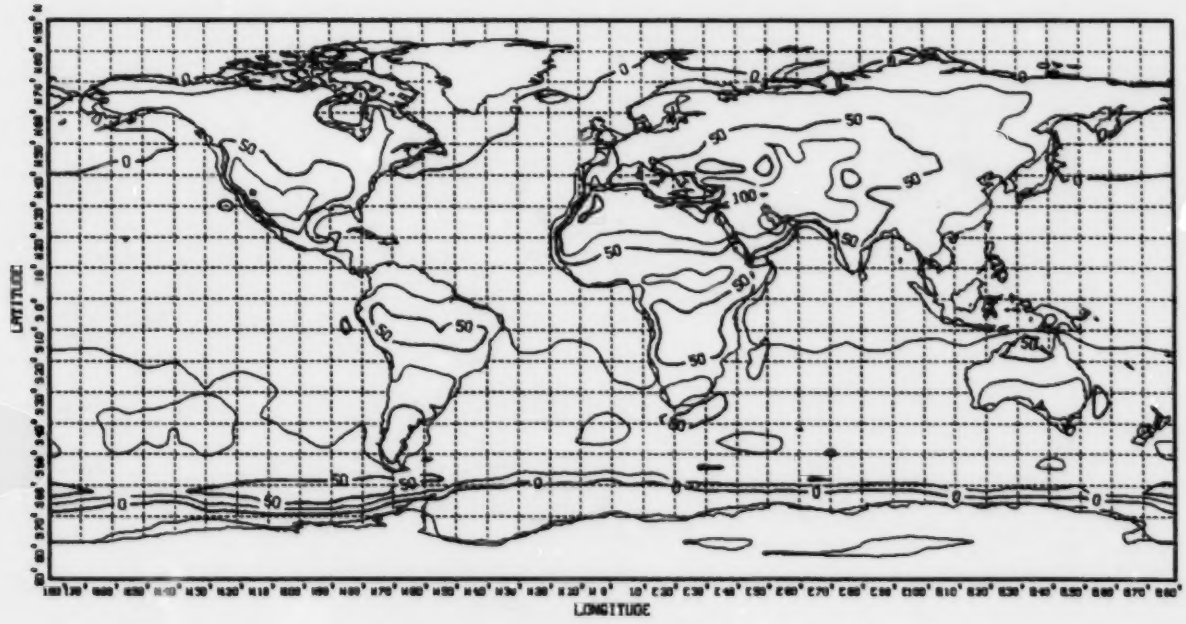

Figure 22

T-STATISTIC JANUARY SENSIBLE HEAT

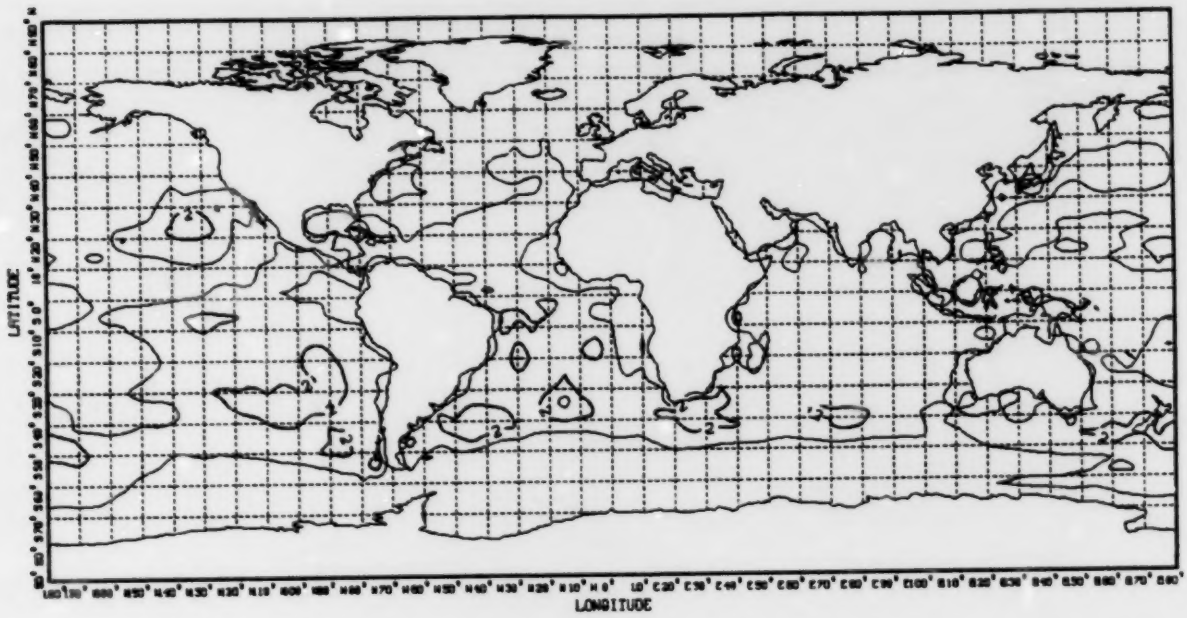

T-STATISTIC JULY SENSIBLE HEAT

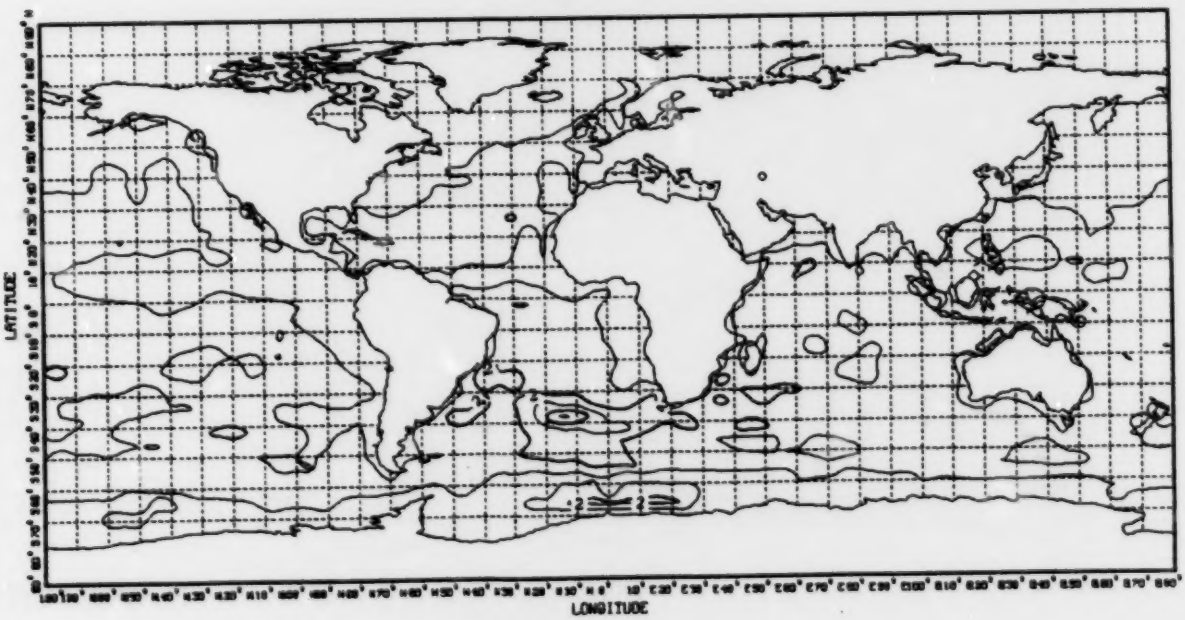

Figure 23

STANDARD DEVIATION JANUARY SENSIBLE HEAT (W/M**2)

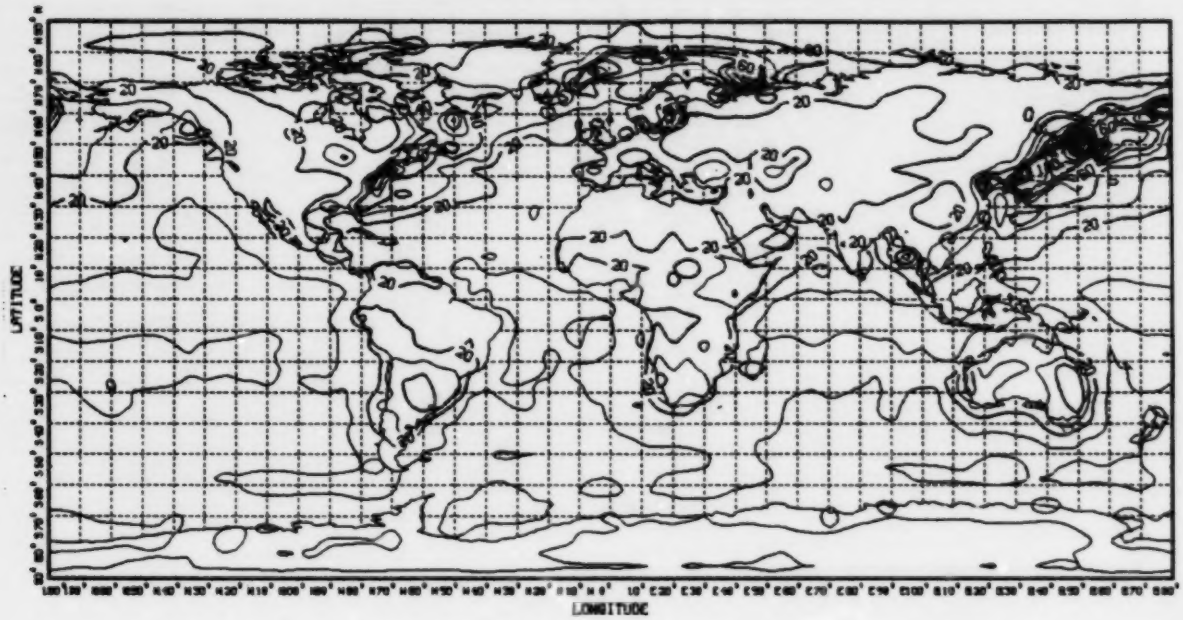

STANDARD DEVIATION JULY SENSIBLE HEAT (W/M**2)

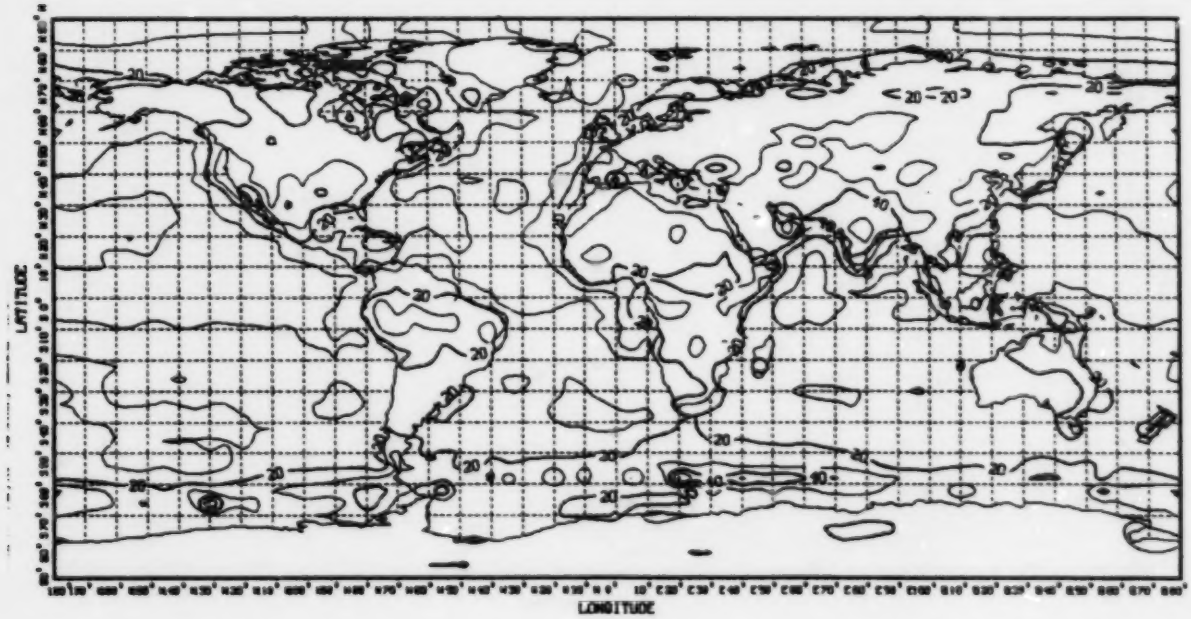

Figure 24

HAN AND LEE JANUARY U SURFACE STRESS .001*(N/M**2)

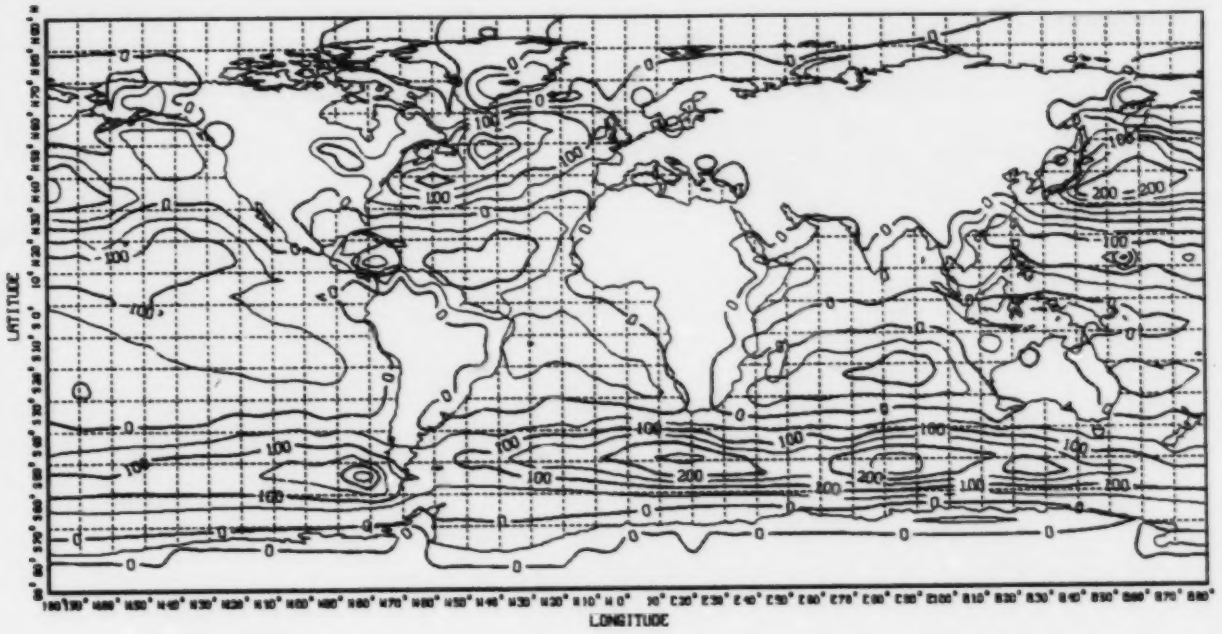

HAN AND LEE JULY U SURFACE STRESS .001*(N/M**2)

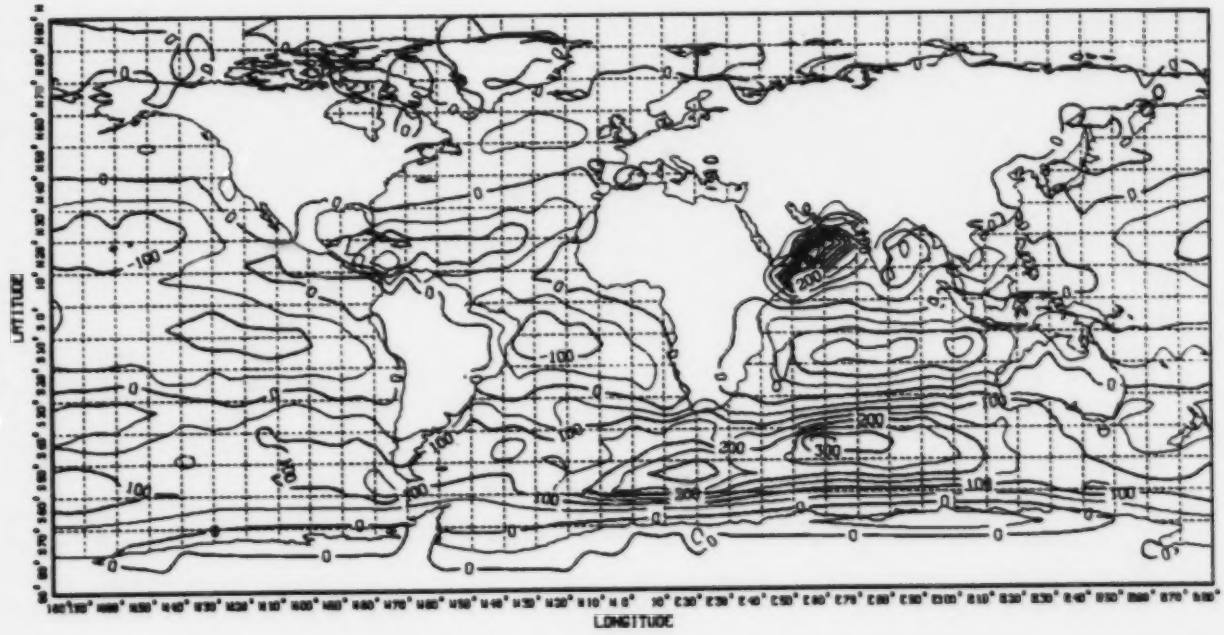

Figure 25

GRAND MEAN JANUARY U SURFACE STRESS .001×(N/M××2)

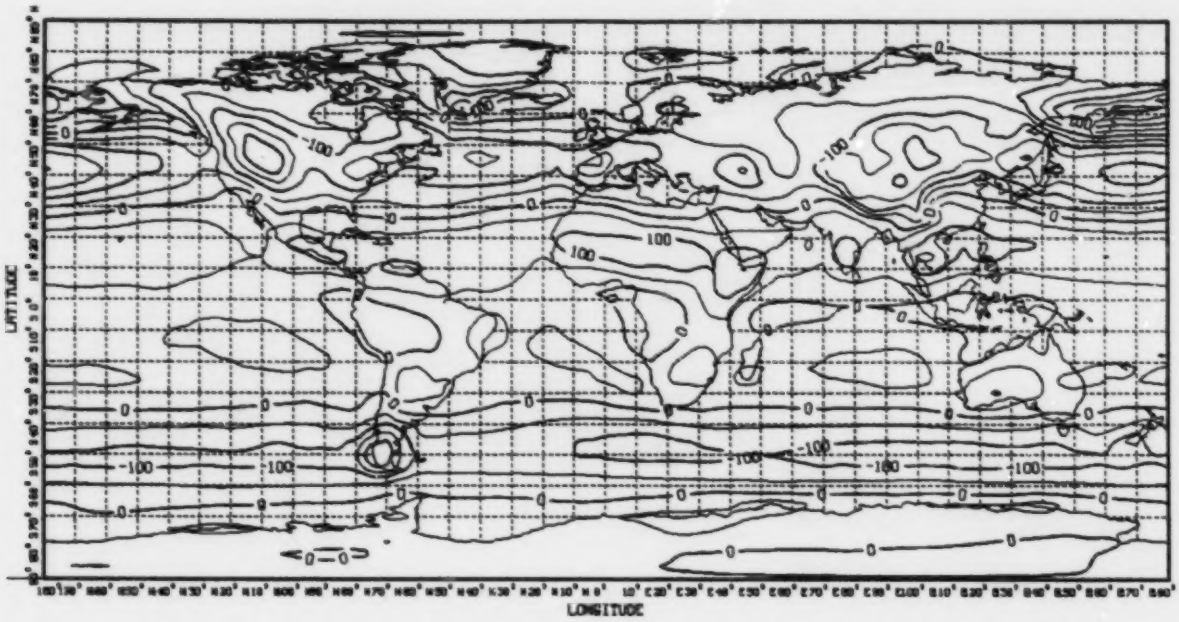

GRAND MEAN JULY U SURFACE STRESS .001×(N/M××2)

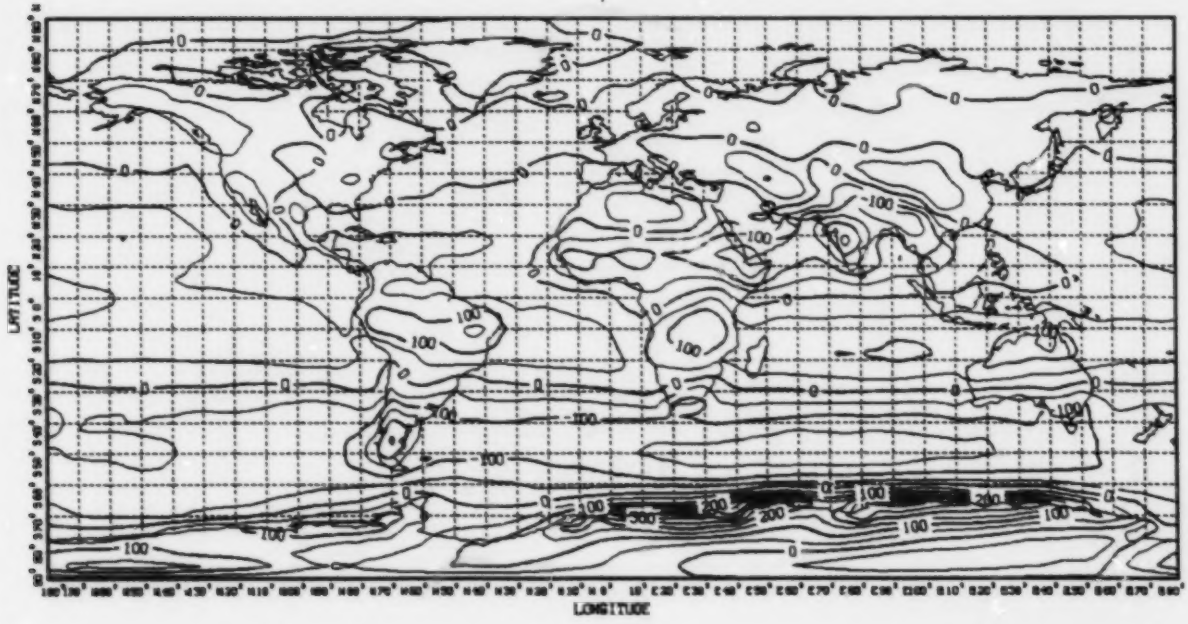

Figure 26

T-STATISTIC JANUARY U SURFACE STRESS

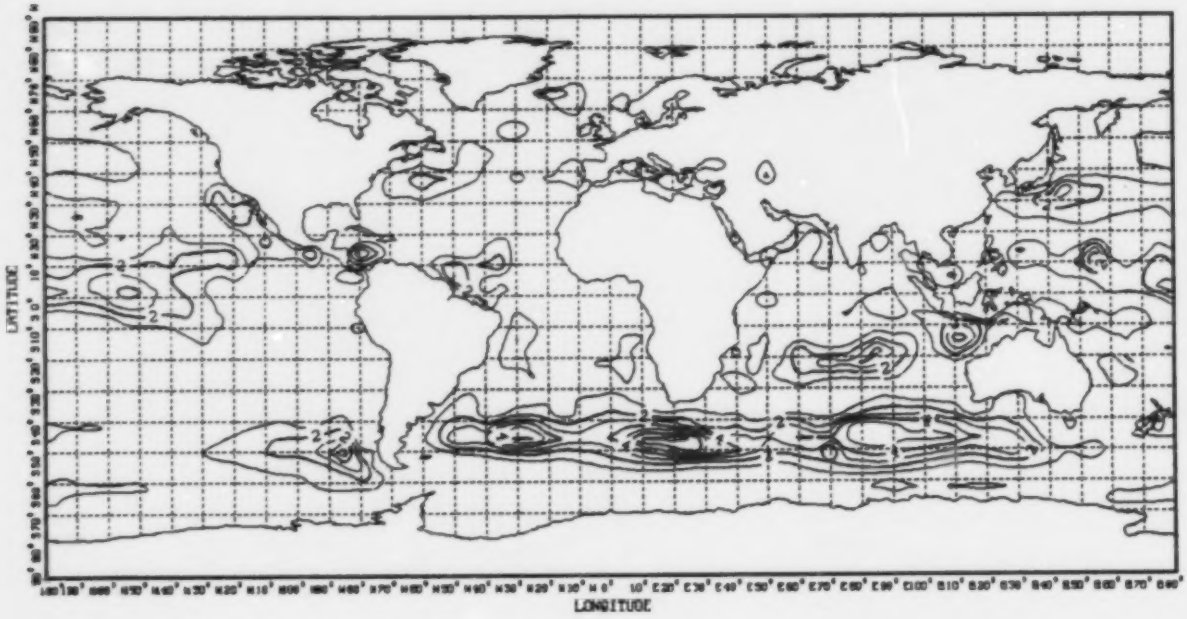

T-STATISTIC JULY U SURFACE STRESS

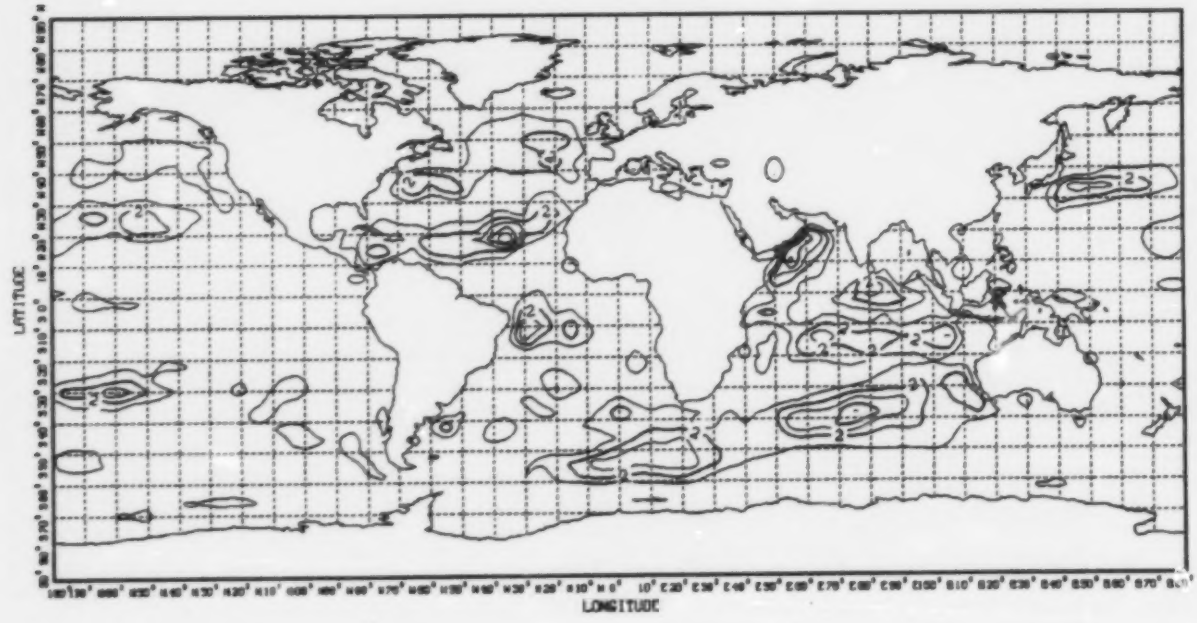

Figure 27

STANDARD DEVIATION JANUARY U SFC STRESS .001*(N/M**2)

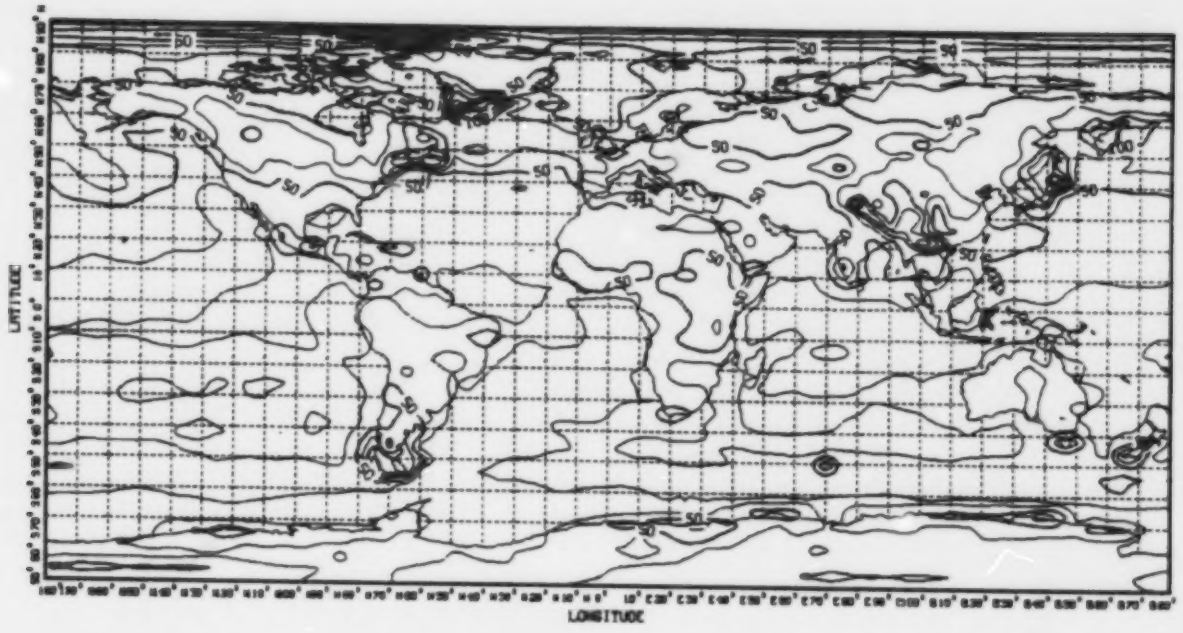

STANDARD DEVIATION JULY U SFC STRESS .001*(N/M**2)

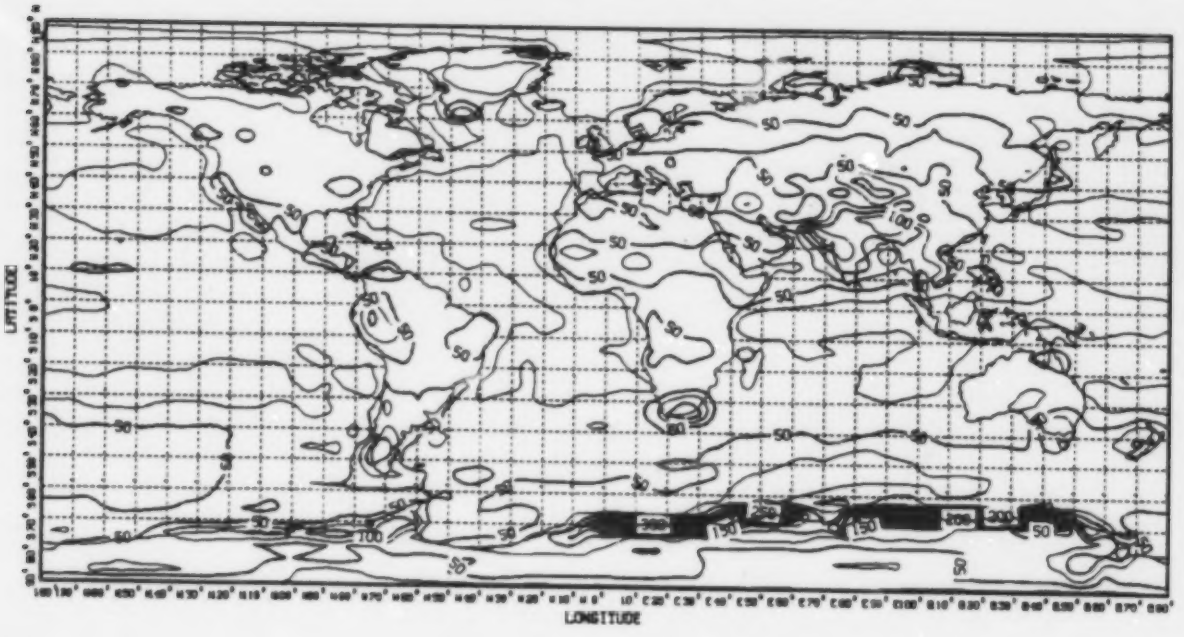

Figure 28

HAN AND LEE JANUARY V SURFACE STRESS .001*(N/M**2)

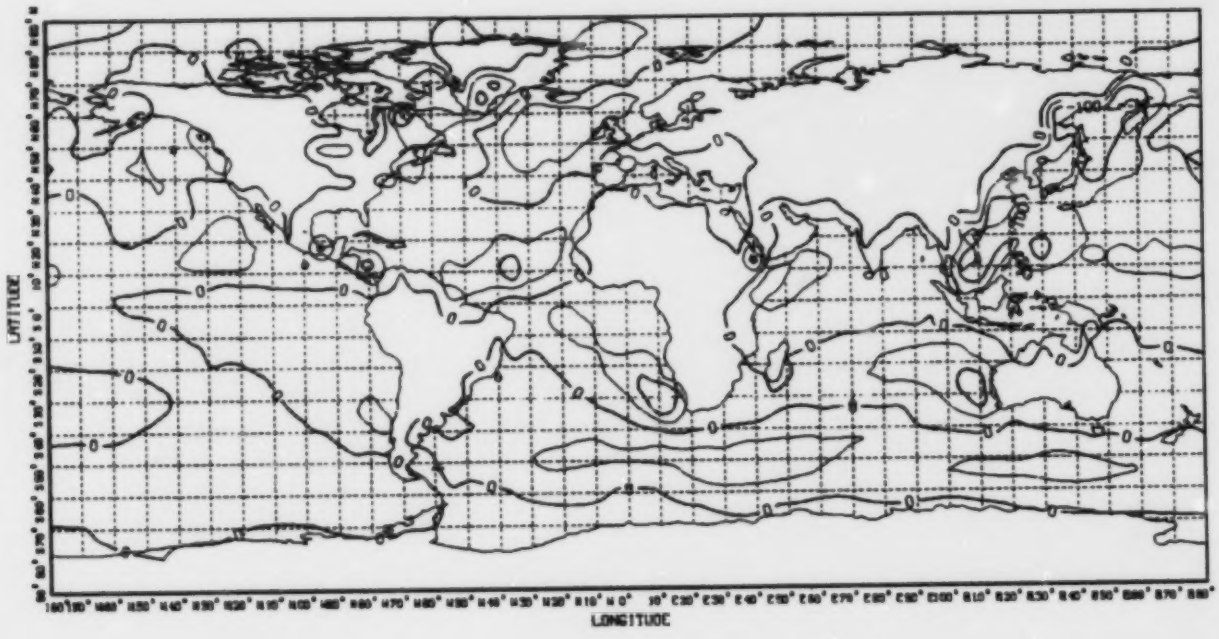

HAN AND LEE JULY V SURFACE STRESS .001*(N/M**2)

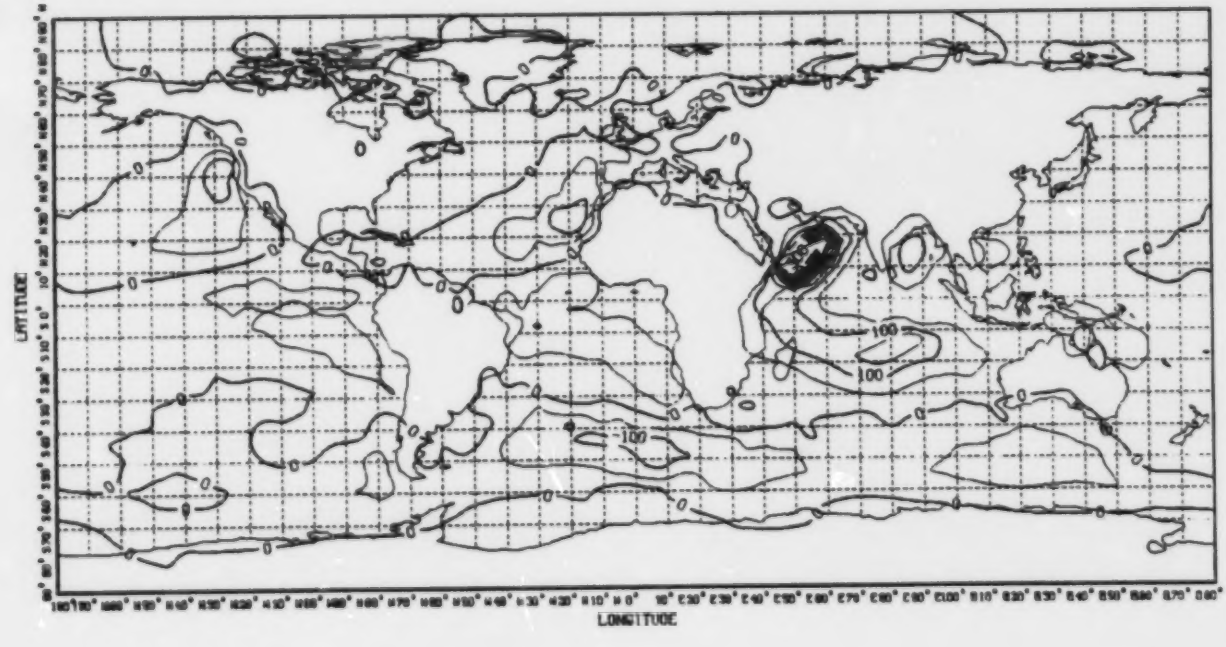

Figure 29

GRAND MEAN JANUARY V SURFACE STRESS .001*(N/M**2)

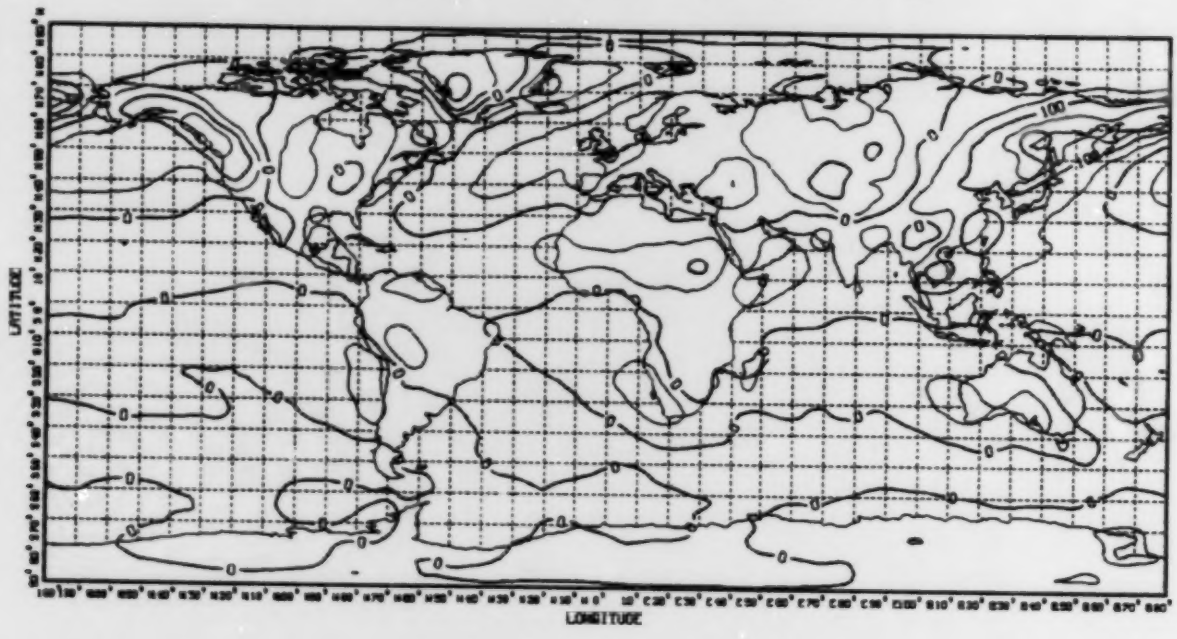

GRAND MEAN JULY V SURFACE STRESS .001*(N/M**2)

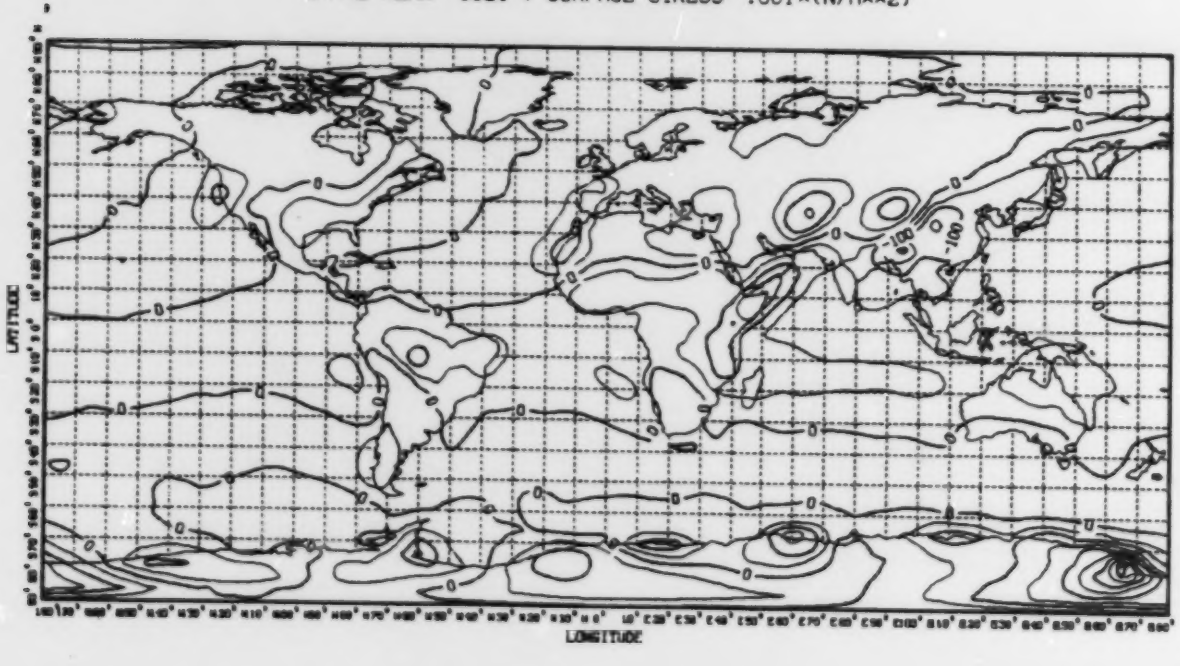

Figure 30

T-STATISTIC JANUARY V SURFACE STRESS

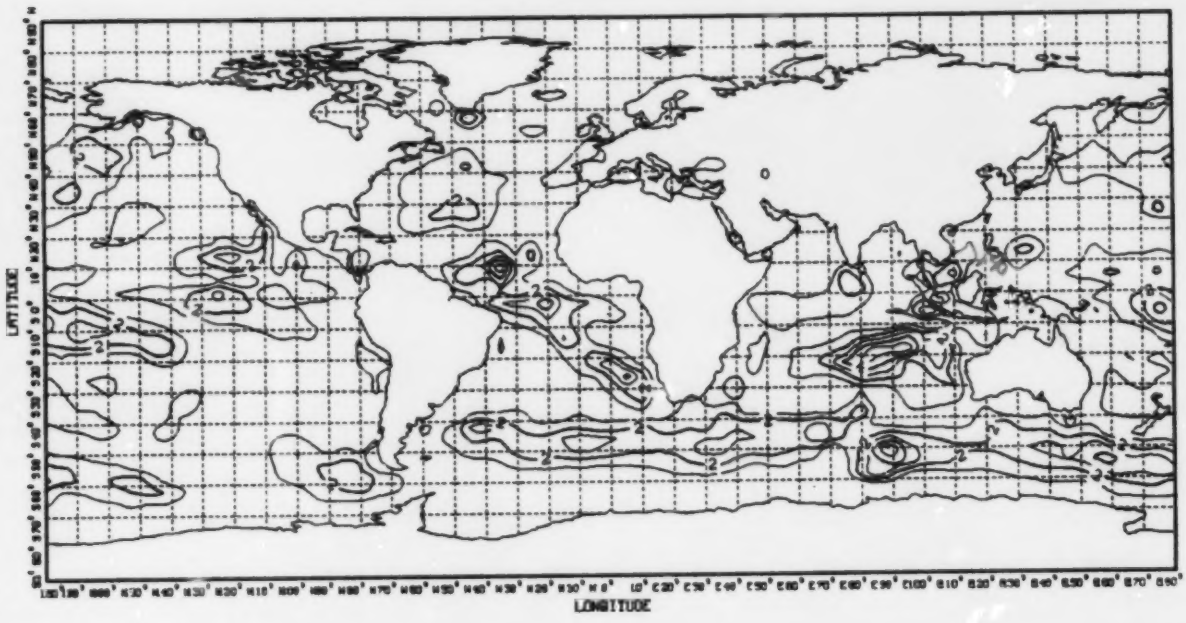

T-STATISTIC JULY V SURFACE STRESS

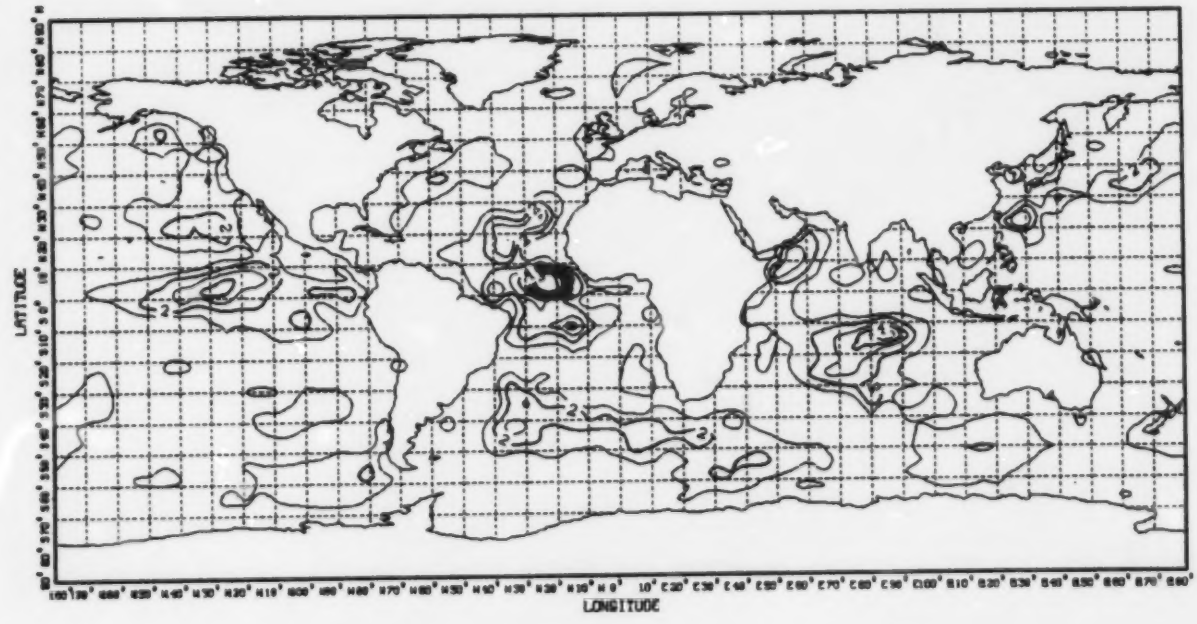

Figure 31

STANDARD DEVIATION JANUARY V SFC STRESS .001×(N/M××2)

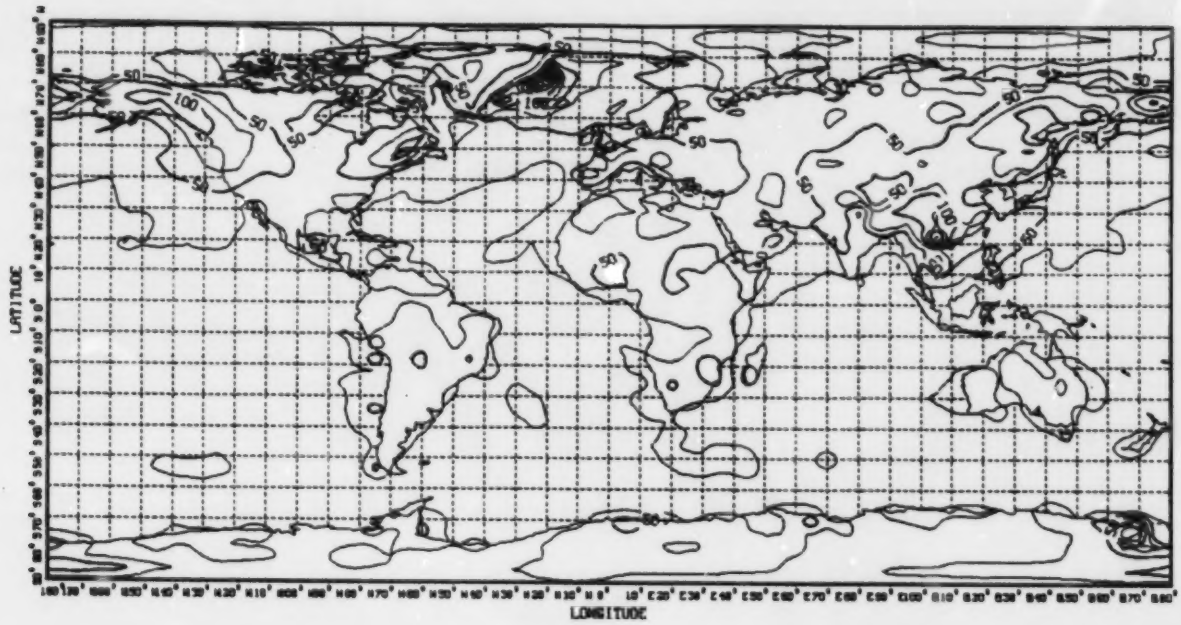

STANDARD DEVIATION JULY V SFC STRESS .001×(N/M××2)

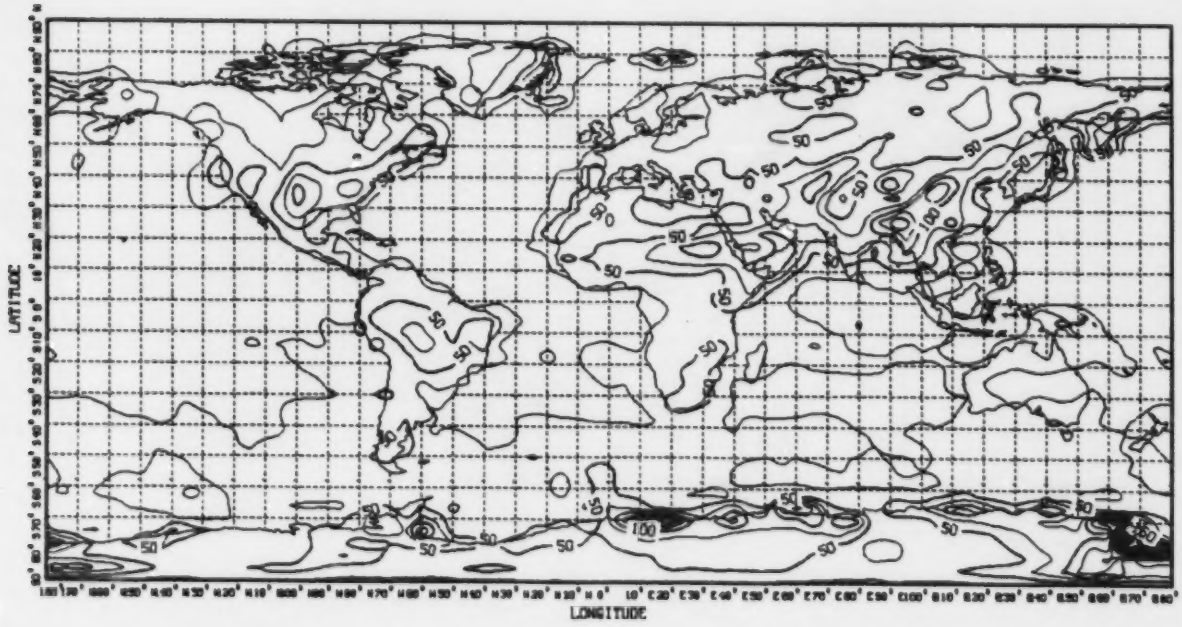

Figure 32

OBS JANUARY PRECIPITATION-EVAPORATION (MM/DAY)

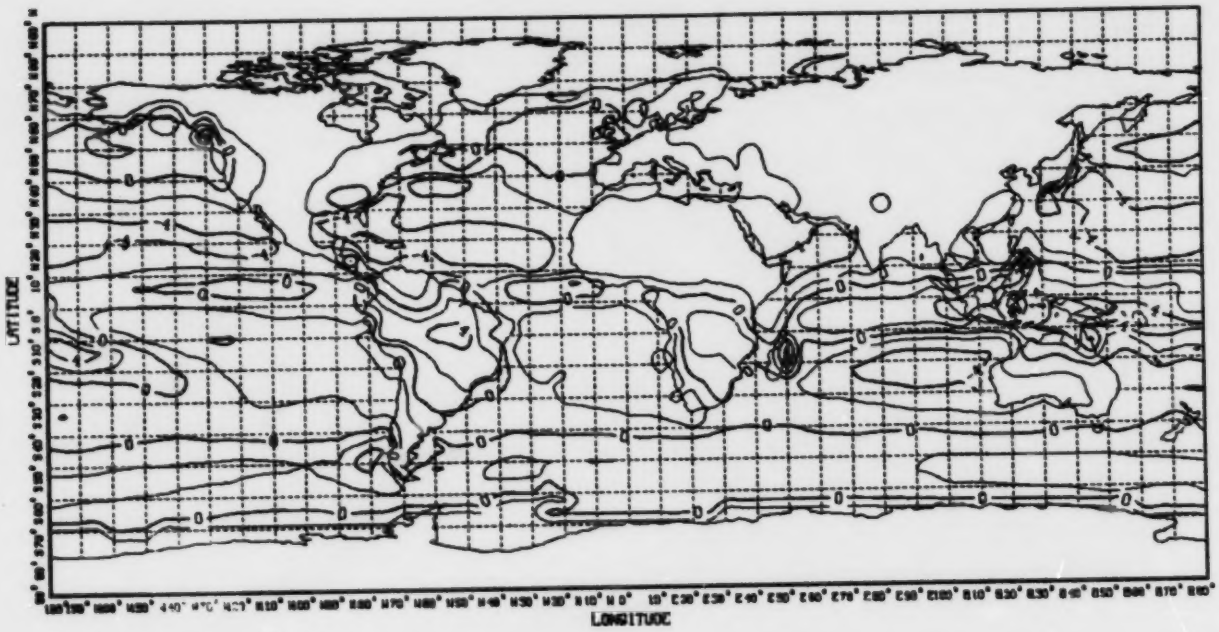

OBS JULY PRECIPITATION-EVAPORATION (MM/DAY)

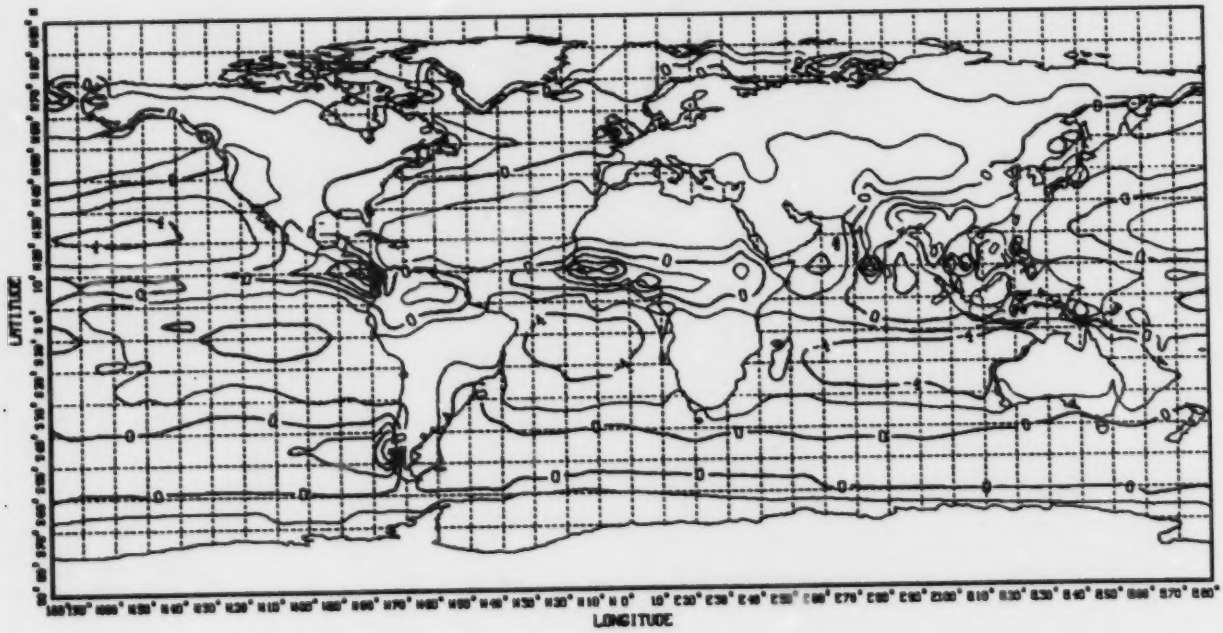

Figure 33

GRAND MEAN JANUARY PRECIPITATION-EVAPORATION (MM/DAY)

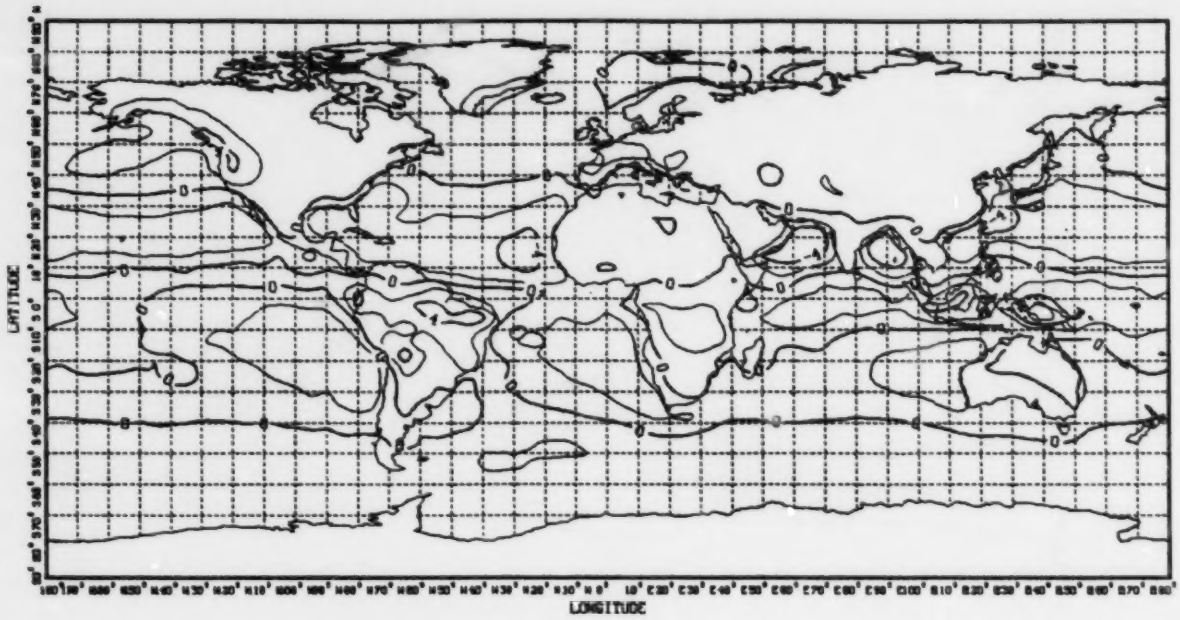

GRAND MEAN JULY PRECIPITATION-EVAPORATION (MM/DAY)

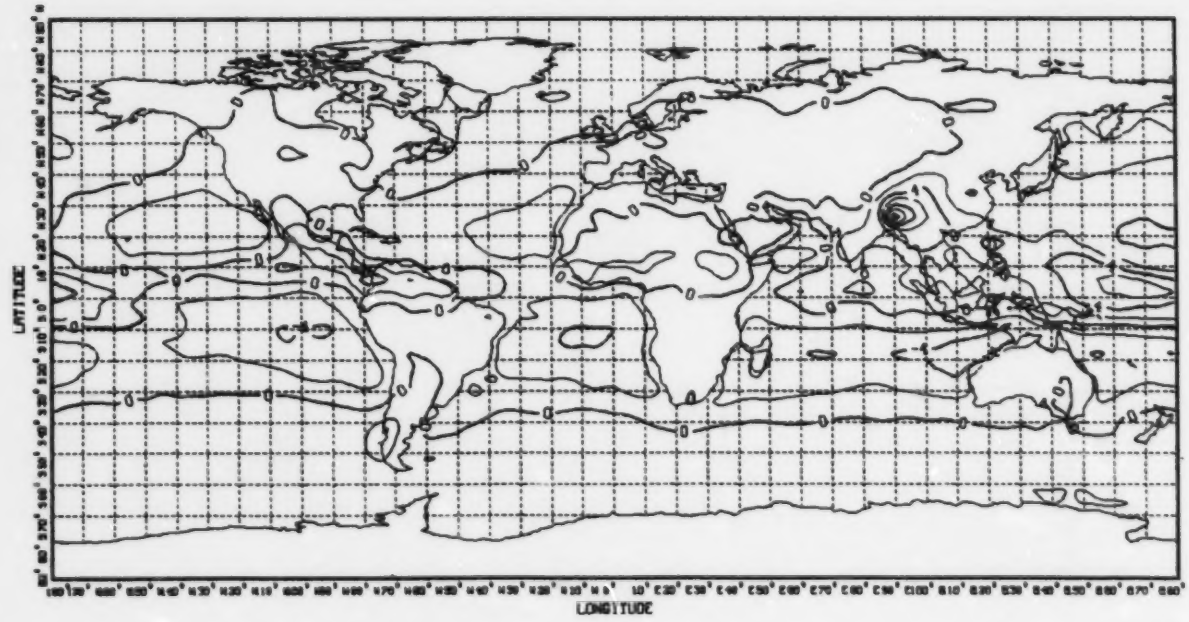

Figure 34

T-STATISTIC JANUARY PRECIPITATION-EVAPORATION

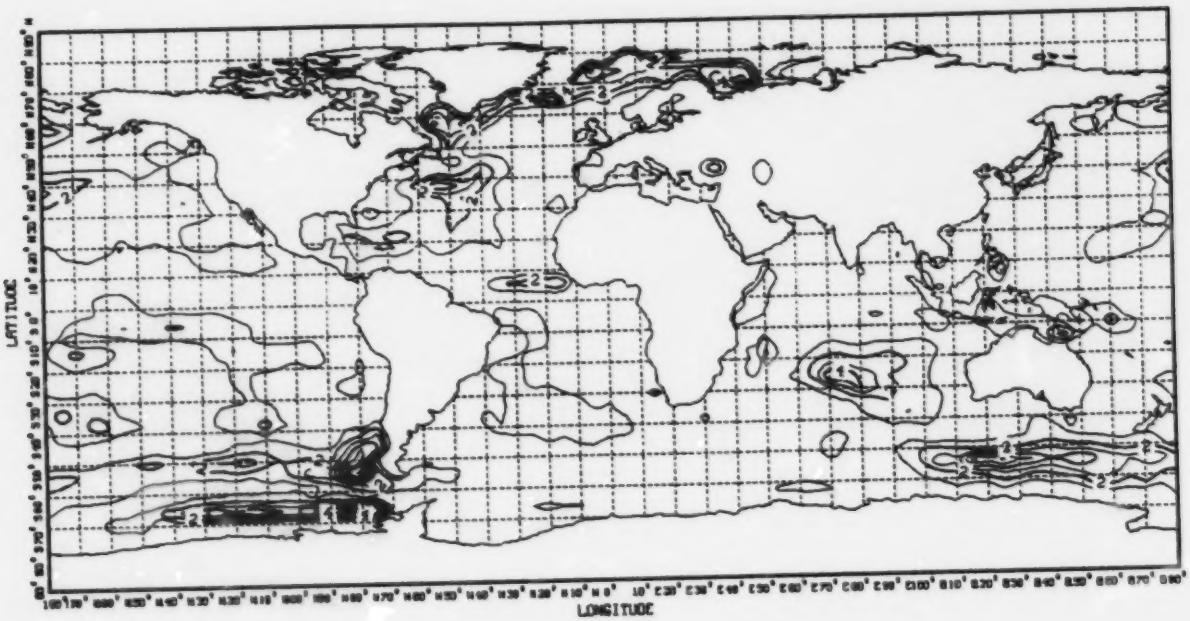

T-STATISTIC JULY PRECIPITATION-EVAPORATION

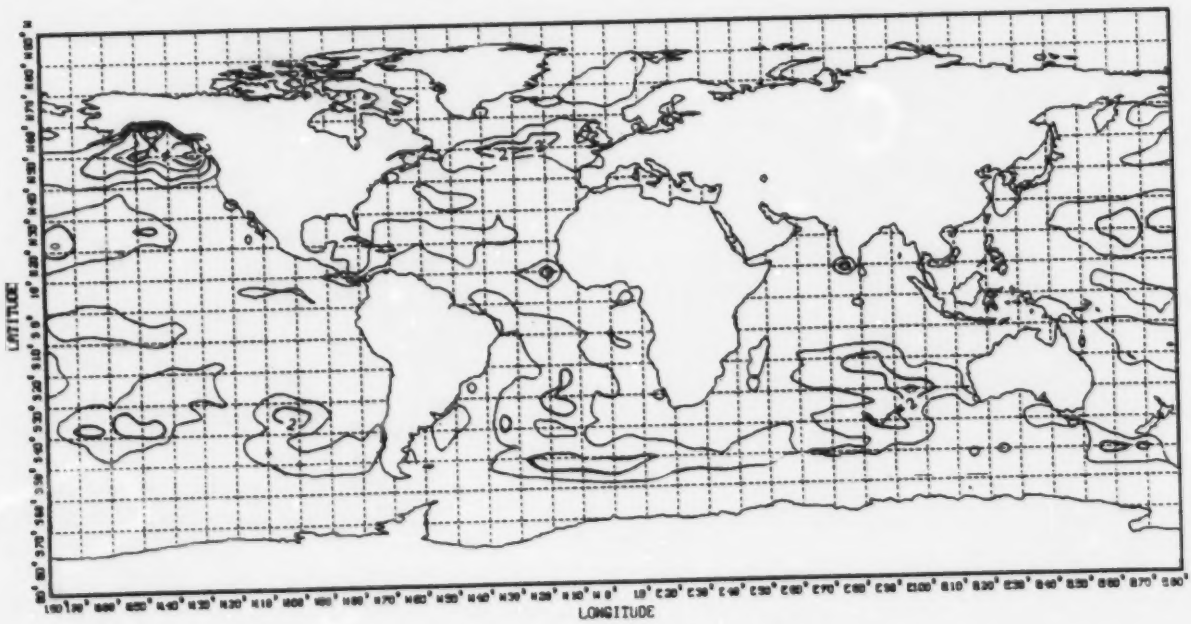

Figure 35

STANDARD DEVIATION JANUARY PRECIP-EVAP (MM/DAY)

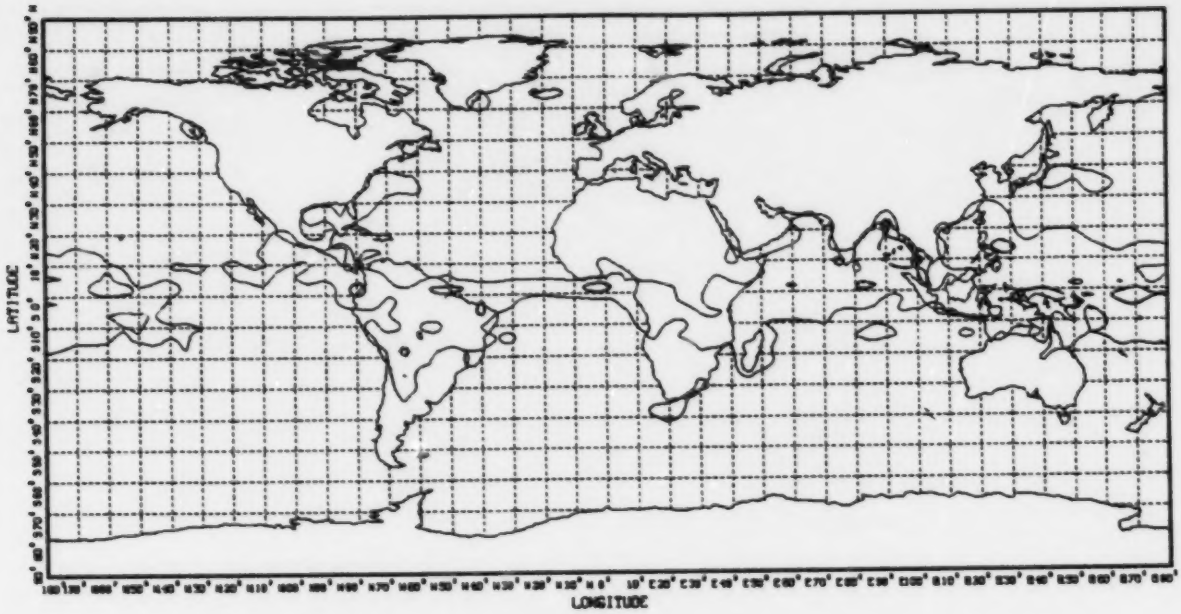

STANDARD DEVIATION JULY PRECIP-EVAP (MM/DAY)

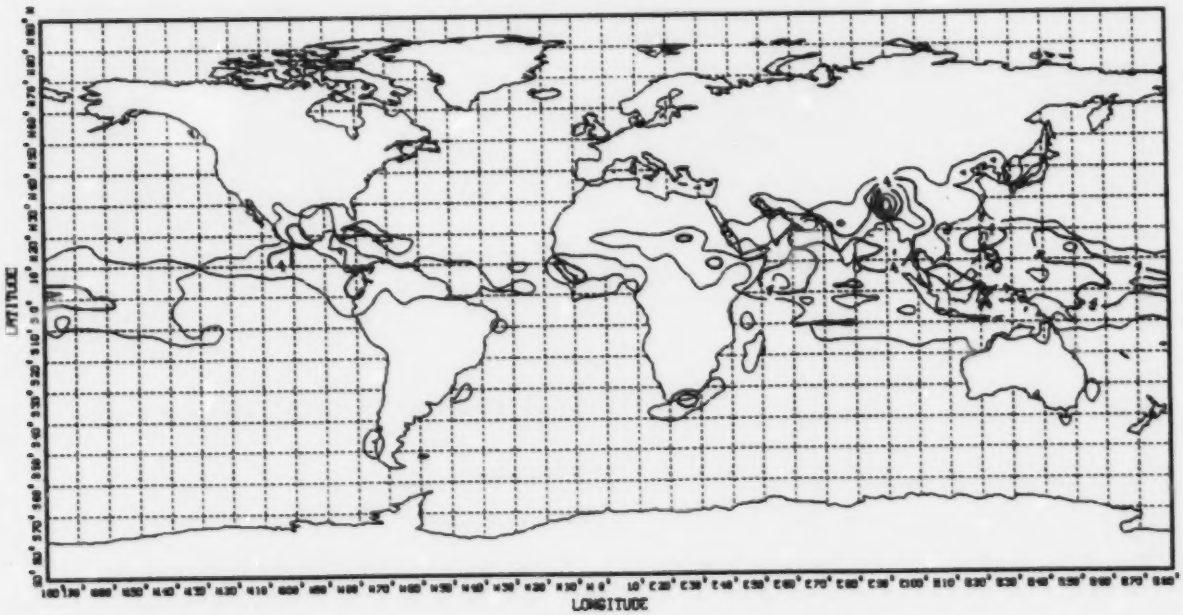

Figure 36

MOLLER WINTER PRECIPITATION (MM/DAY)

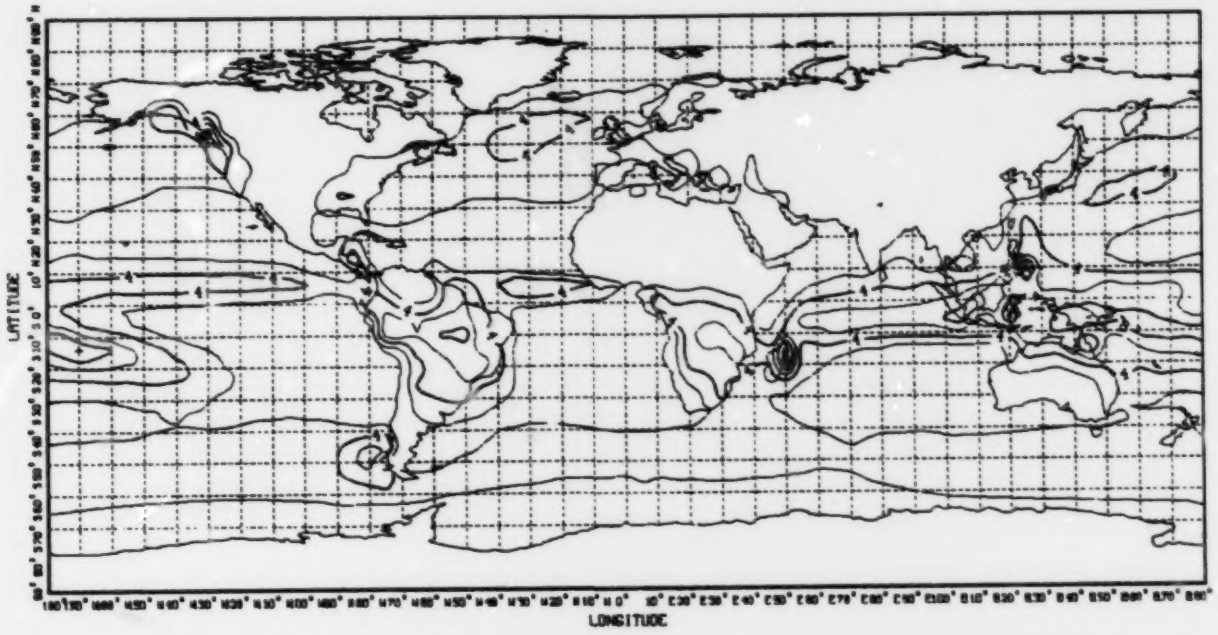

MÖLLER SUMMER PRECIPITATION (MM/DAY)

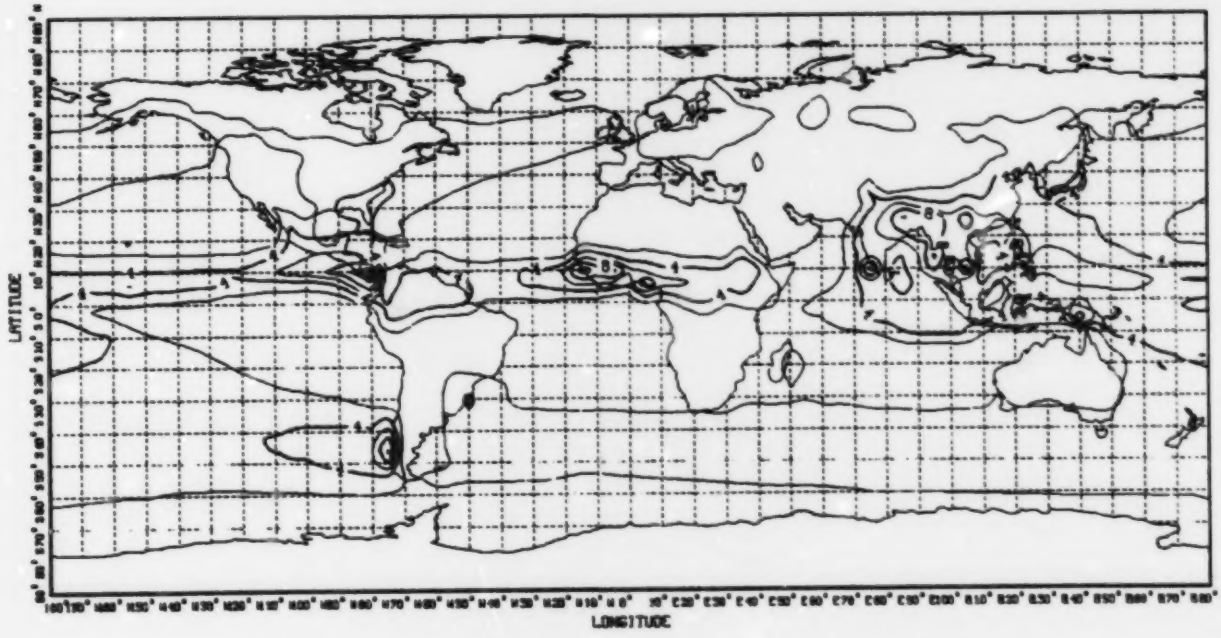

Figure 37

GRAND MEAN JANUARY PRECIPITATION (MM/DAY)

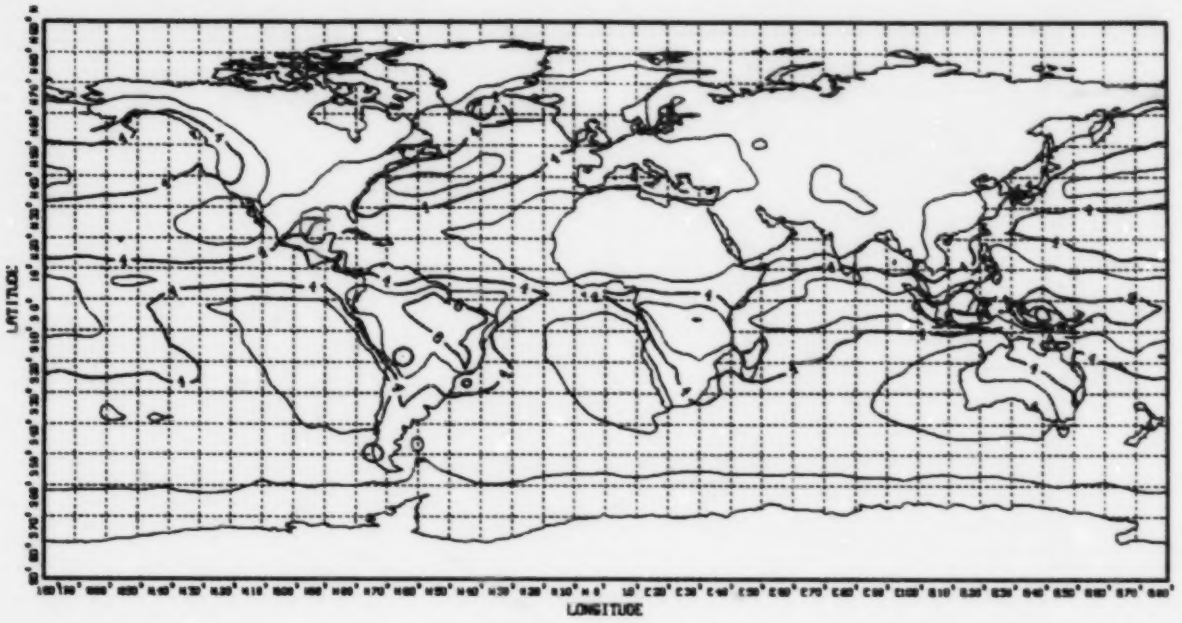

GRAND MEAN JULY PRECIPITATION (MM/DAY)

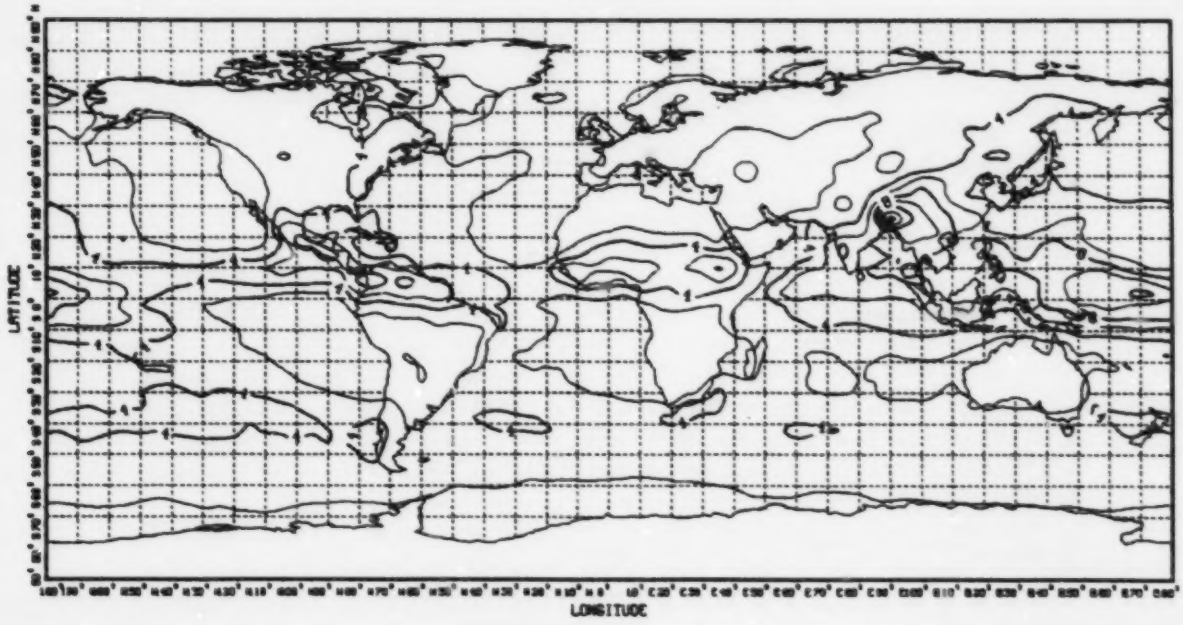

Figure 38

T-STATISTIC JANUARY PRECIPITATION

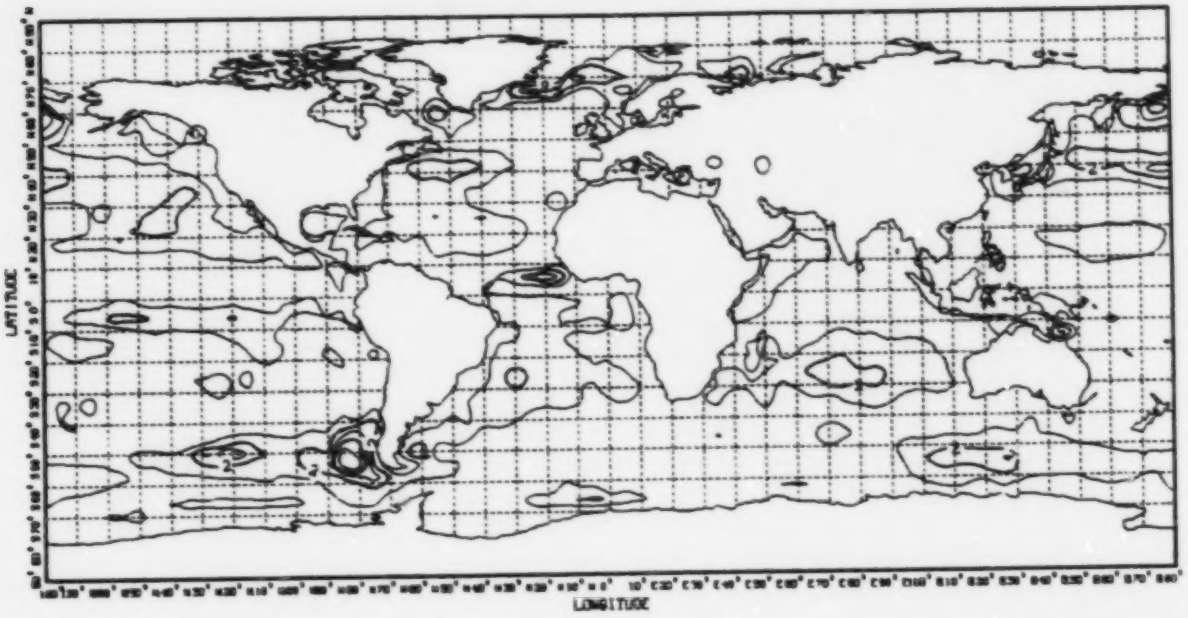

T-STATISTIC JULY PRECIPITATION

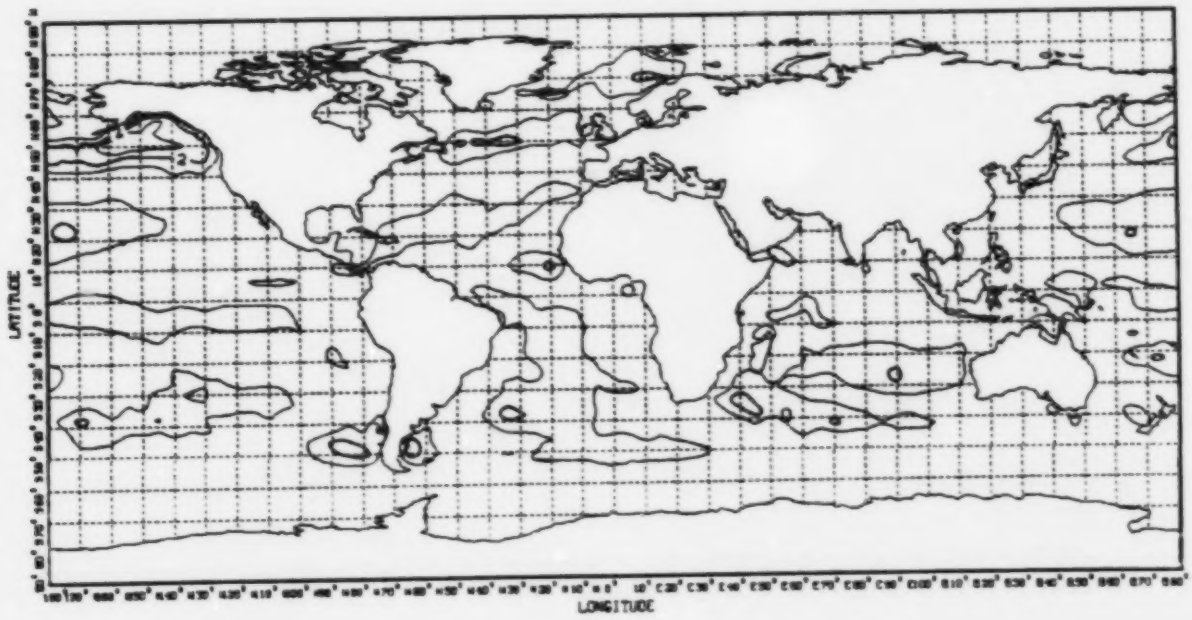

Figure 39

STANDARD DEVIATION JANUARY PRECIPITATION (MM/DAY)

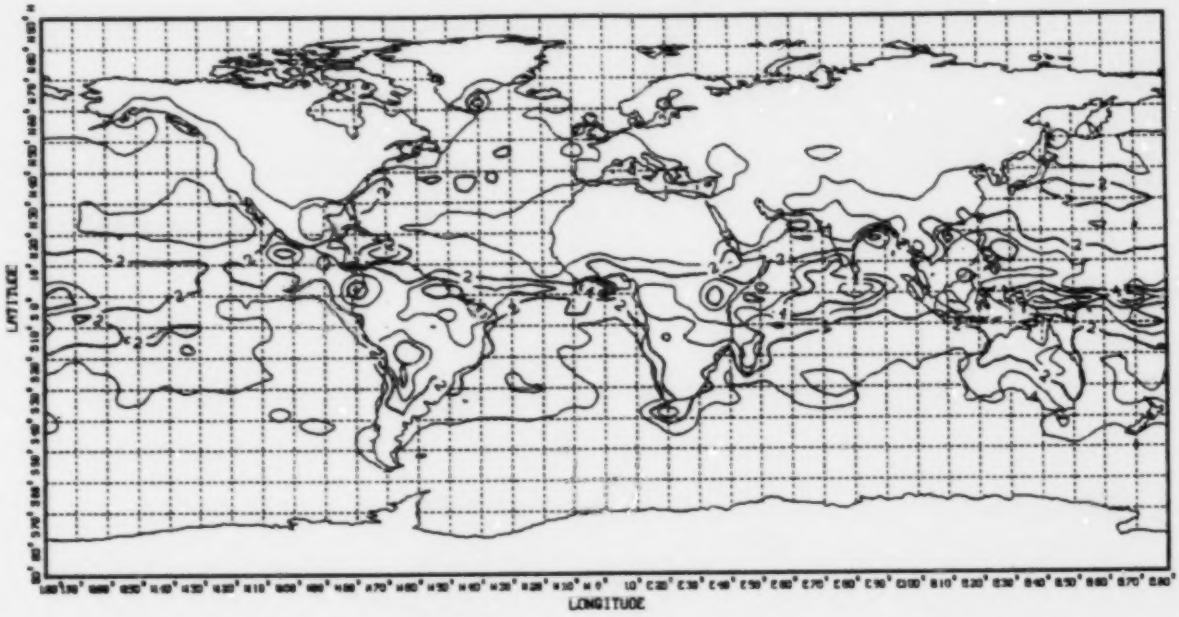

STANDARD DEVIATION JULY PRECIPITATION (MM/DAY)

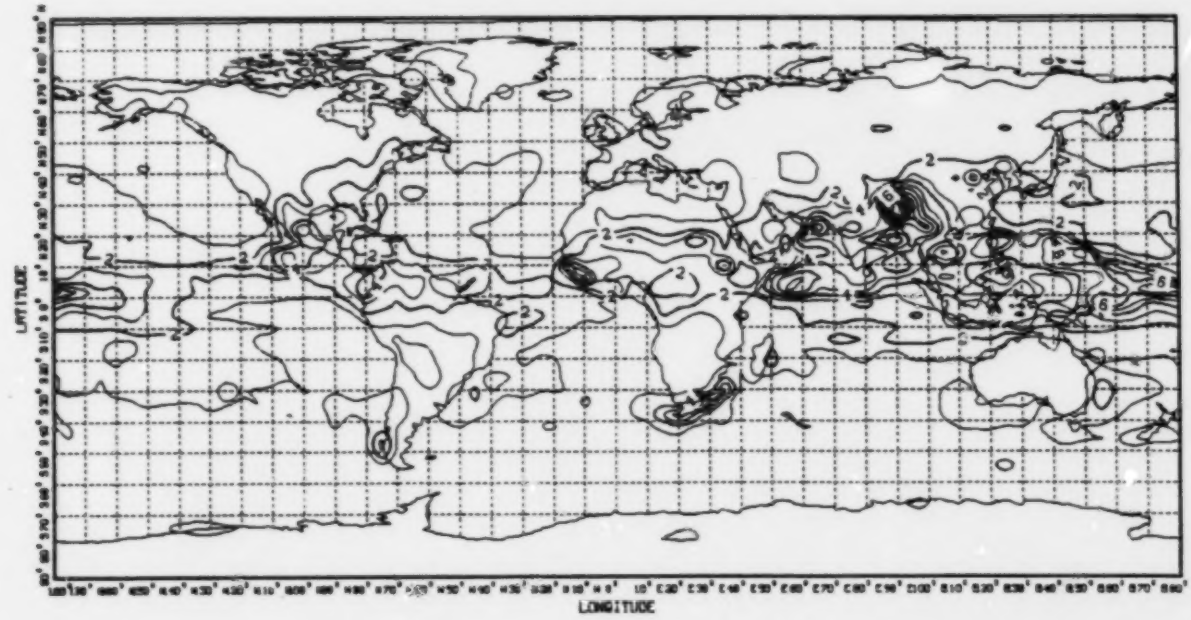

Figure 40

Appendix I. Zonally averaged values of atmosphere/ocean fluxes from individual models.

Each panel displays the January (or December-February) and July (or June-August) values of the climatological estimate, the dark solid line, and the values from up to three individual models.

The information is given as follows:

Net energy flux at the surface.	Figures (41-44)
East-west surface stress.	Figures (45-48)
North-south surface stress.	Figures (49-52)
Moisture flux, P - E, at the surface.	Figures (53-56)

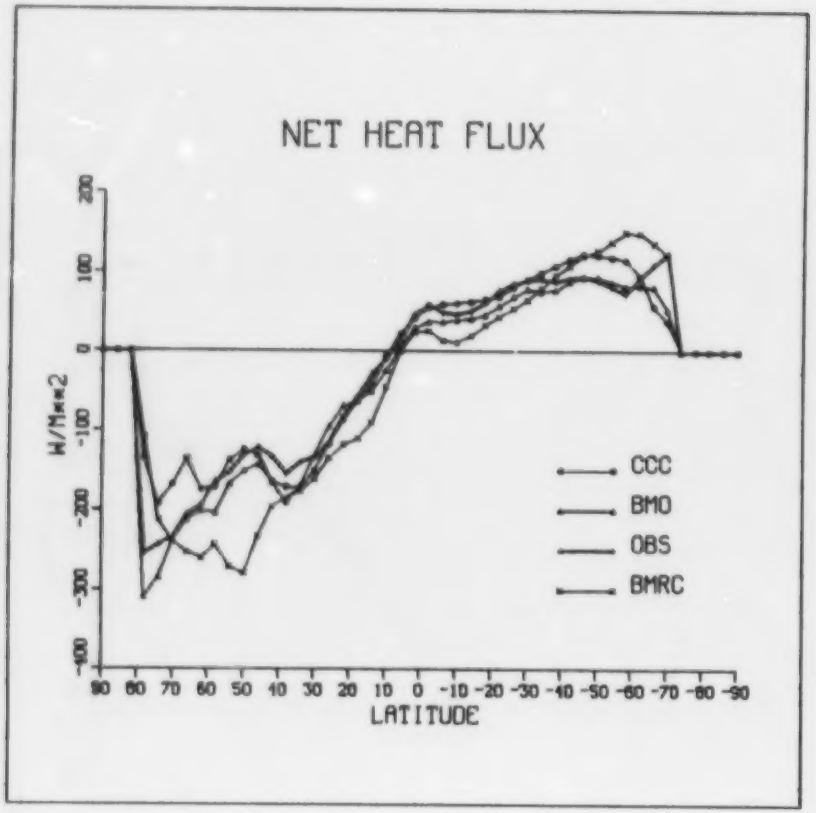
NET HEAT FLUX
W/M**2
200
100
0
-100
-200
-300
-400
90 80 70 60 50 40 30 20 10 0 -10 -20 -30 -40 -50 -60 -70 -80 -90
LATITUDE
CCC
BMO
OBS
BMRC

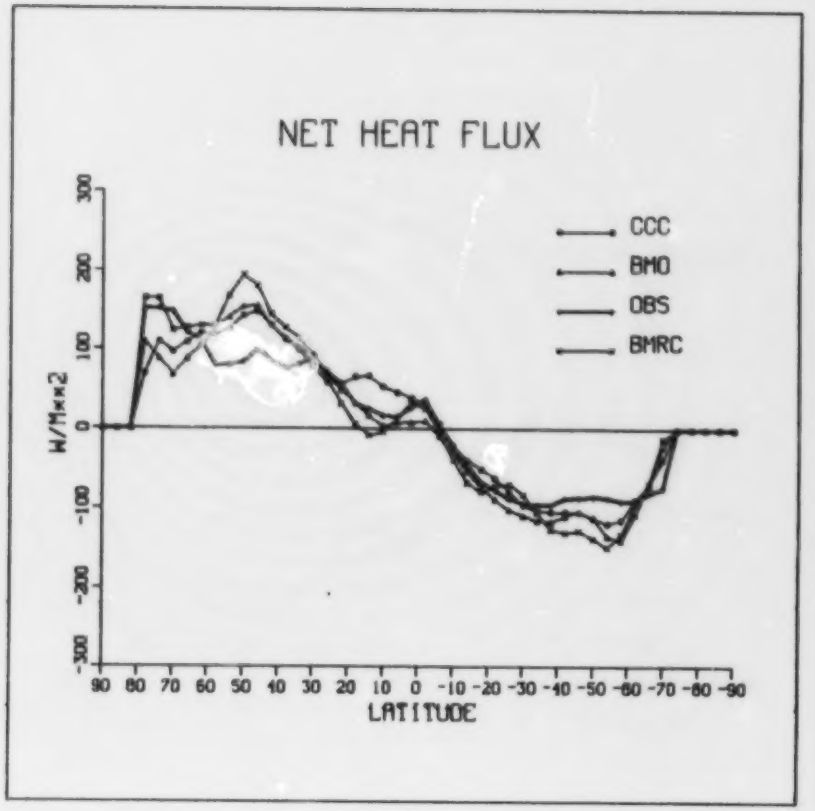
NET HEAT FLUX
W/M**2
300
200
100
0
-100
-200
-300
90 80 70 60 50 40 30 20 10 0 -10 -20 -30 -40 -50 -60 -70 -80 -90
LATITUDE
CCC
BMO
OBS
BMRC

Figure 41

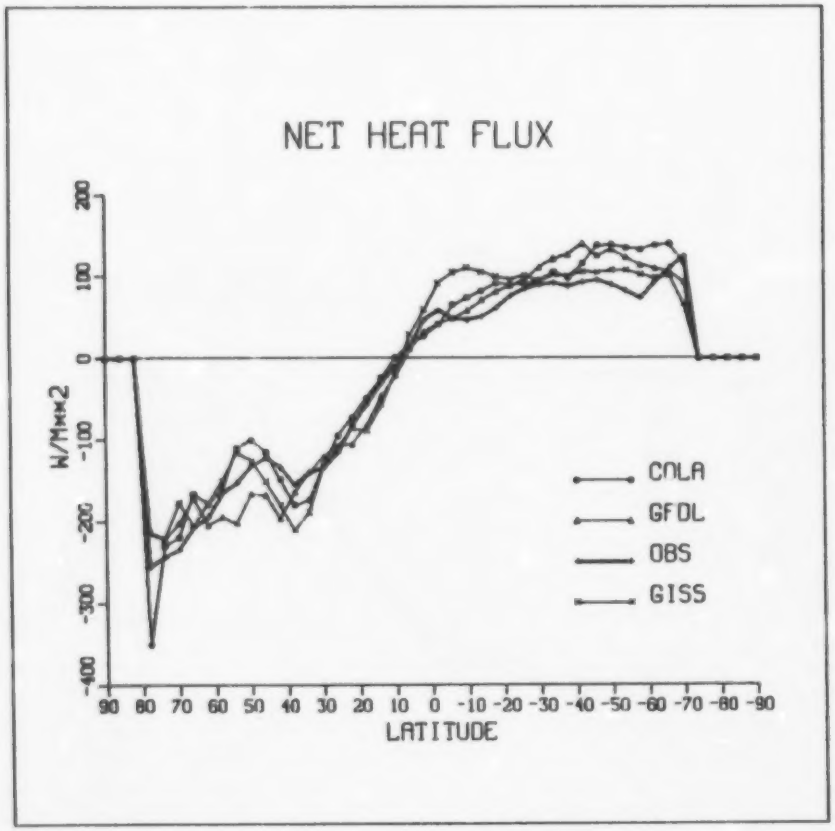
NET HEAT FLUX
W/M**2
200
100
0
-100
-200
-300
-400
90 80 70 60 50 40 30 20 10 0 -10 -20 -30 -40 -50 -60 -70 -80 -90
LATITUDE
COLA
GFDL
OBS
GISS

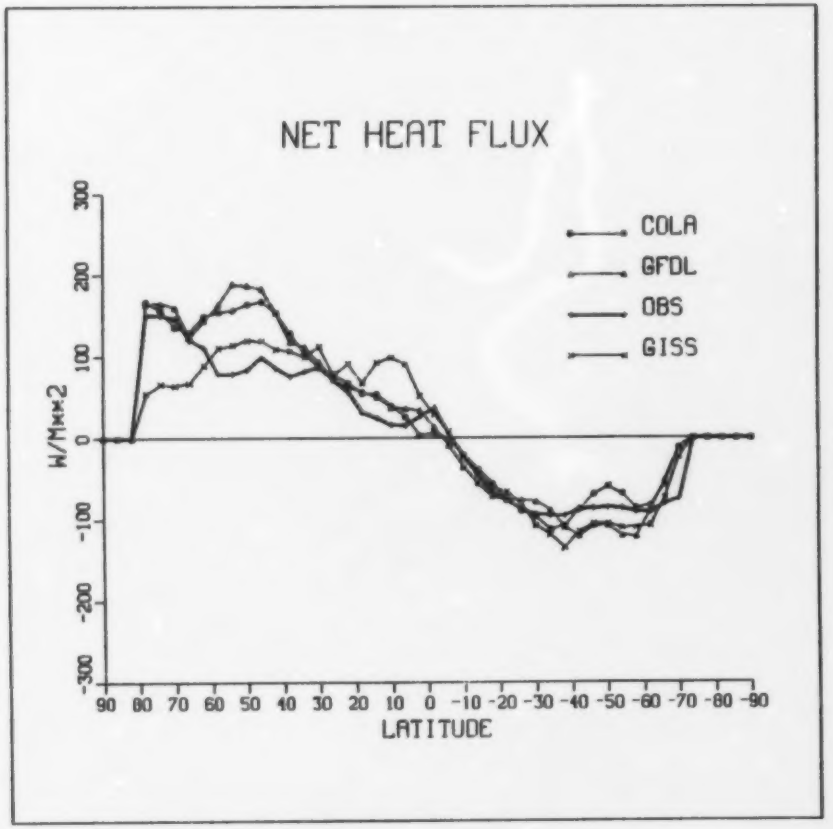
NET HEAT FLUX
W/M**2
300
200
100
0
-100
-200
-300
90 80 70 60 50 40 30 20 10 0 -10 -20 -30 -40 -50 -60 -70 -80 -90
LATITUDE
COLA
GFDL
OBS
GISS

Figure 42

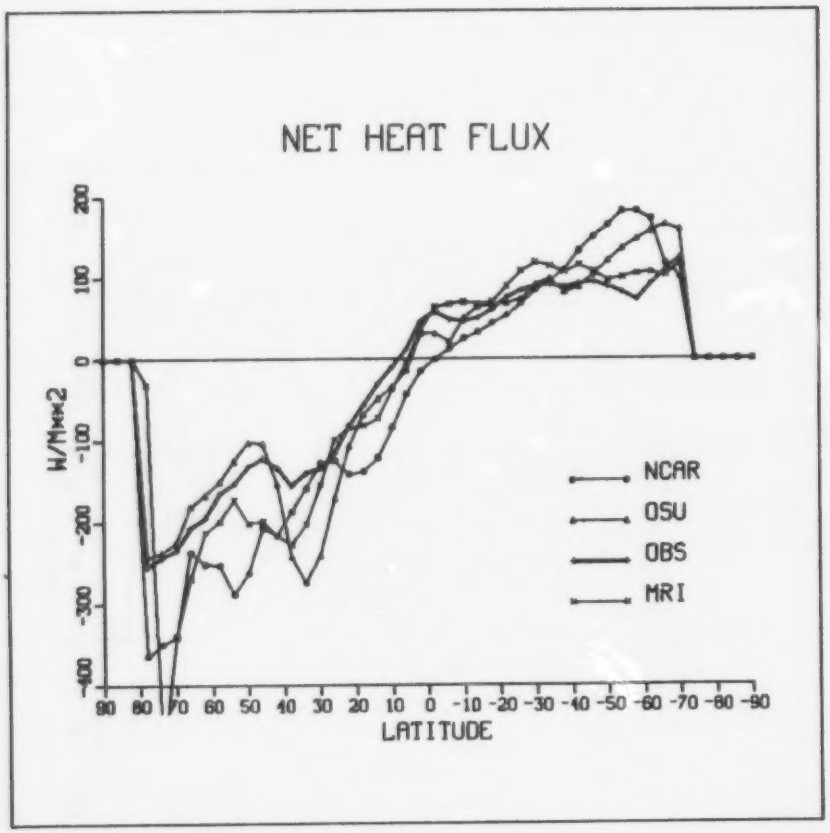
NET HEAT FLUX
W/M**2
200
100
0
-100
-200
-300
-400
90 80 70 60 50 40 30 20 10 0 -10 -20 -30 -40 -50 -60 -70 -80 -90
LATITUDE
NCAR
OSU
OBS
MRI

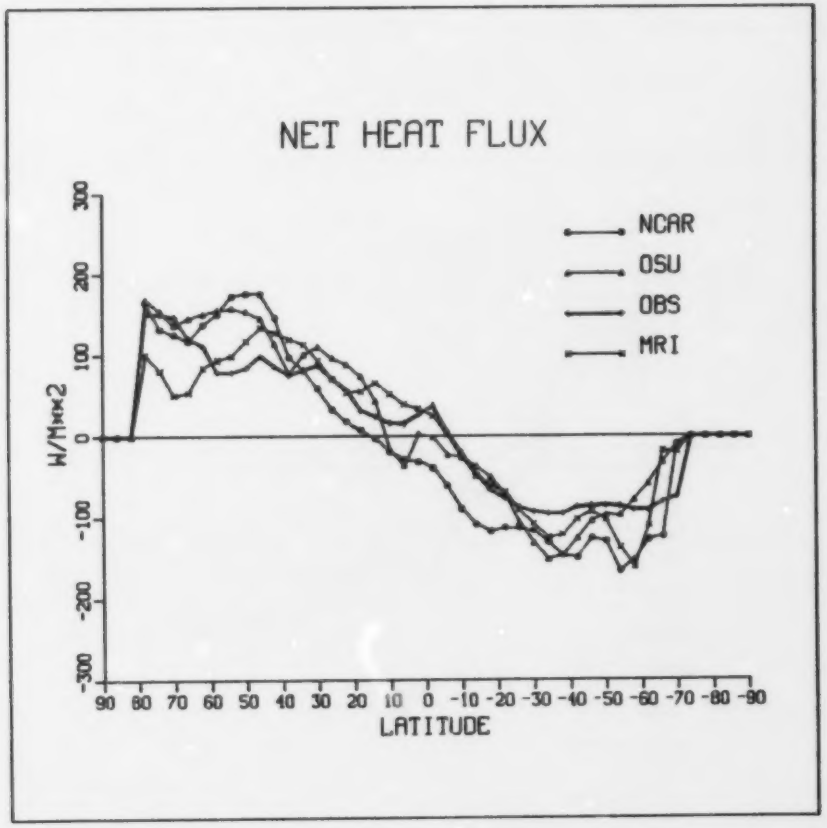
NET HEAT FLUX
W/M**2
300
200
100
0
-100
-200
-300
90 80 70 60 50 40 30 20 10 0 -10 -20 -30 -40 -50 -60 -70 -80 -90
LATITUDE
NCAR
OSU
OBS
MRI

Figure 43

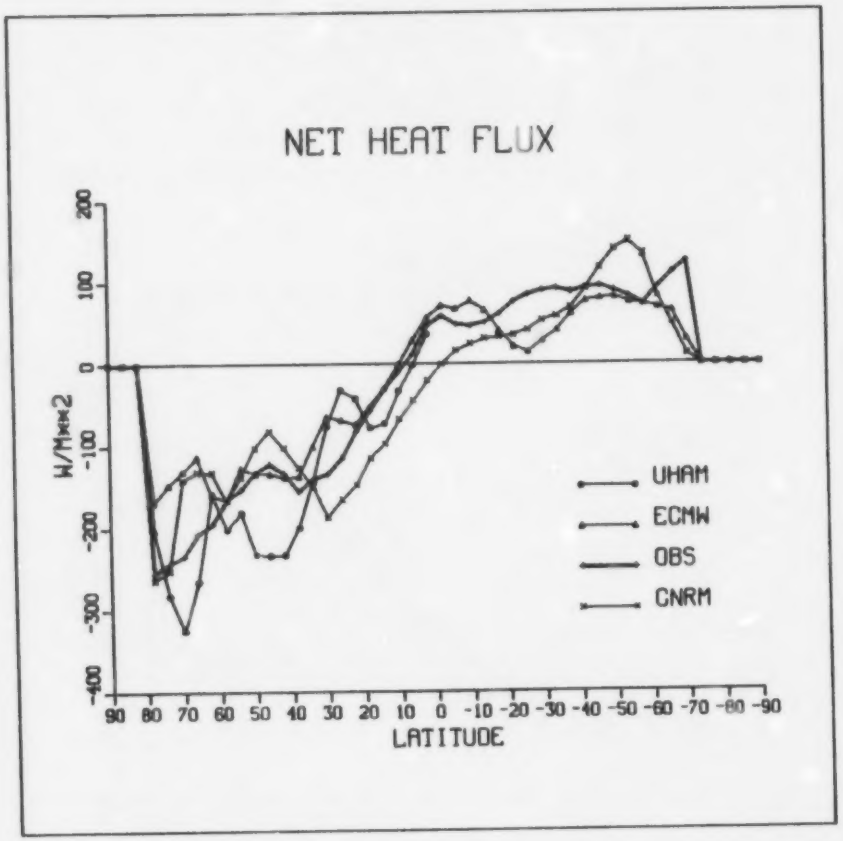
NET HEAT FLUX
W/M**2
200
100
0
-100
-200
-300
-400
90 80 70 60 50 40 30 20 10 0 -10 -20 -30 -40 -50 -60 -70 -80 -90
LATITUDE
UHAM
ECMW
OBS
CNRM

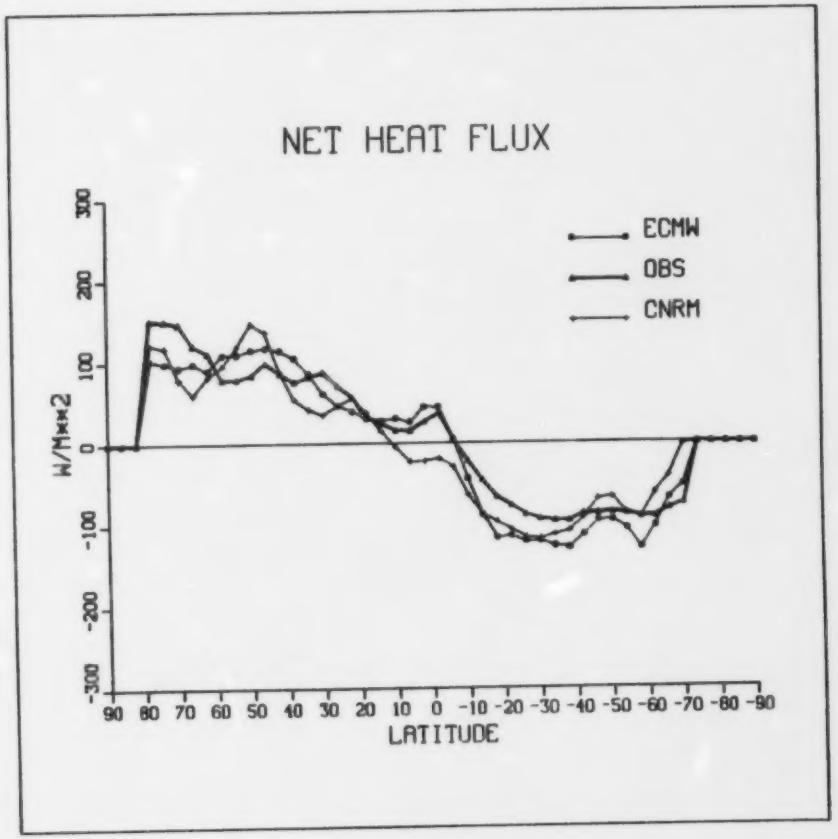
NET HEAT FLUX
W/M**2
300
200
100
0
-100
-200
-300
90 80 70 60 50 40 30 20 10 0 -10 -20 -30 -40 -50 -60 -70 -80 -90
LATITUDE
ECMW
OBS
CNRM

Figure 44

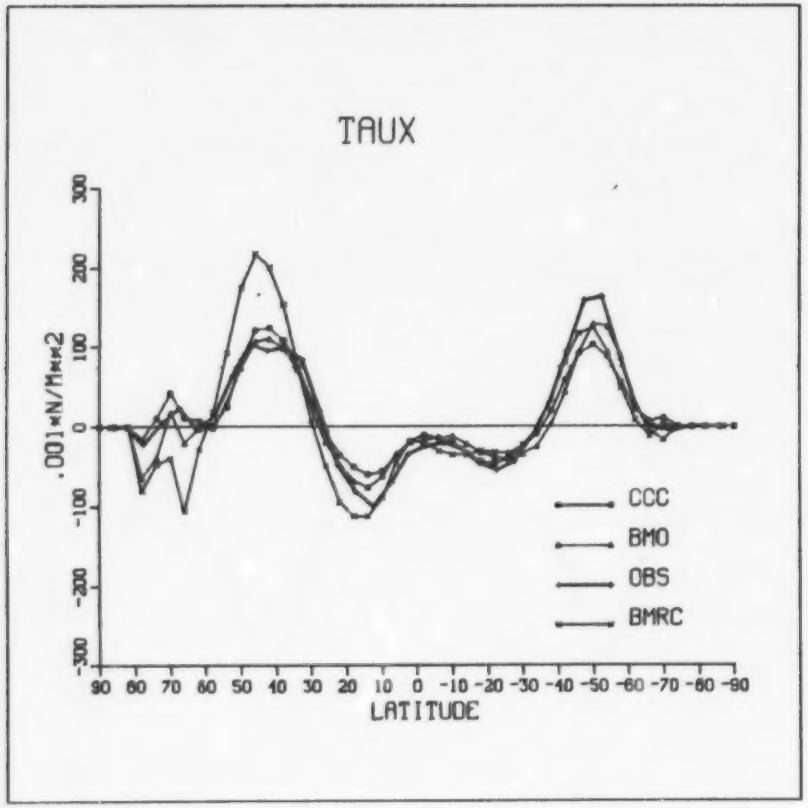
TAUX
.001*N/M**2
300
200
100
0
-100
-200
-300
90 80 70 60 50 40 30 20 10 0 -10 -20 -30 -40 -50 -60 -70 -80 -90
LATITUDE
CCC
BMO
OBS
BMRC

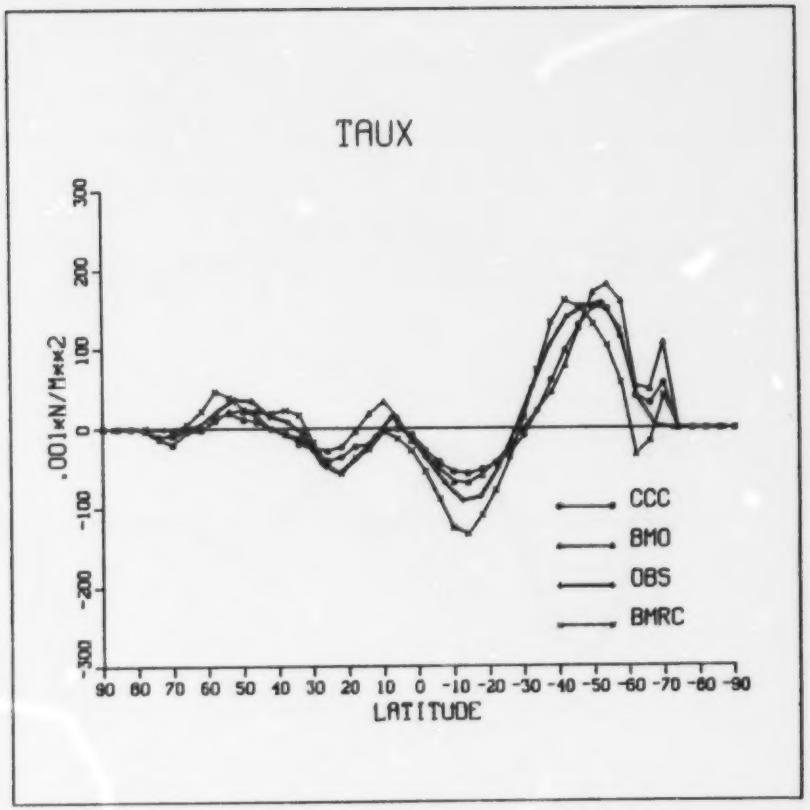
TAUX
.001*N/M**2
300
200
100
0
-100
-200
-300
90 80 70 60 50 40 30 20 10 0 -10 -20 -30 -40 -50 -60 -70 -80 -90
LATITUDE
CCC
BMO
OBS
BMRC

Figure 45

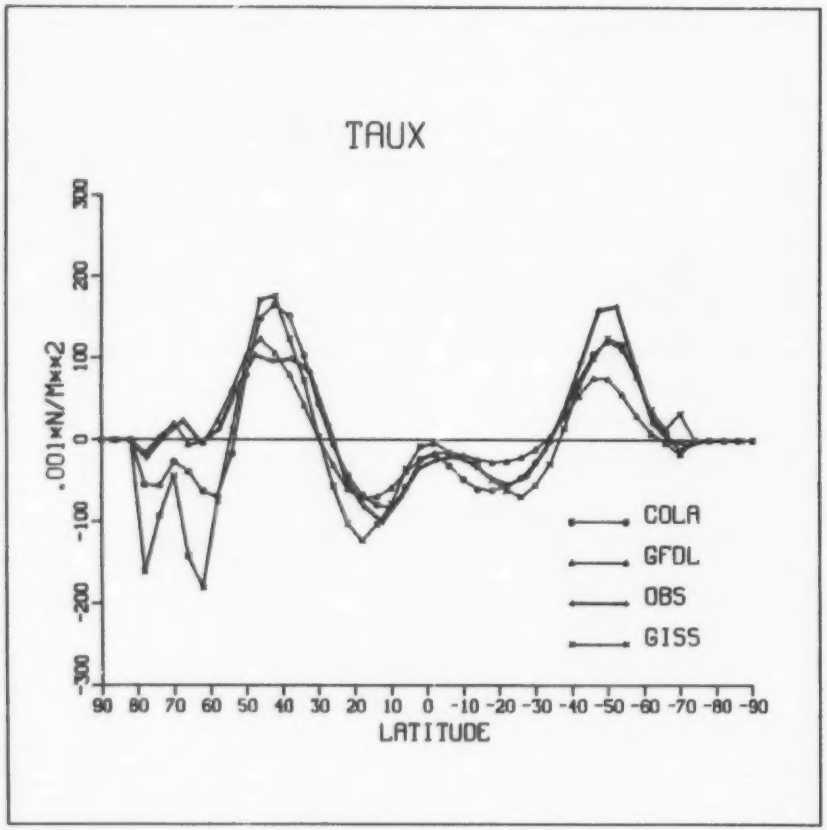
TAUX
.001*N/M**2
300
200
100
0
-100
-200
-300
90 80 70 60 50 40 30 20 10 0 -10 -20 -30 -40 -50 -60 -70 -80 -90
LATITUDE
COLA
GFDL
OBS
GISS

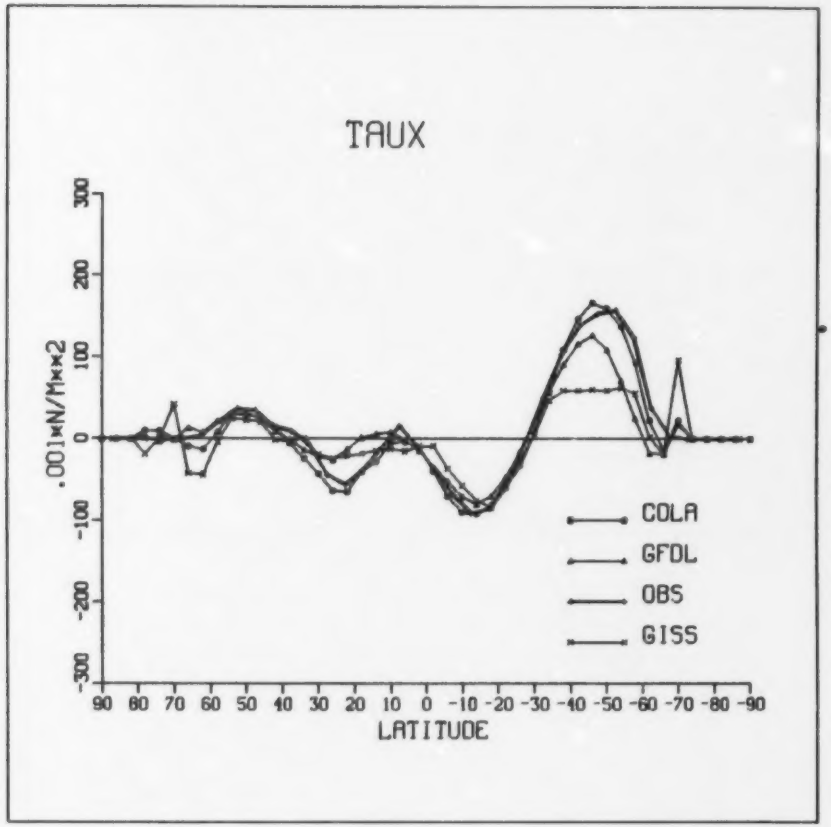
TAUX
.001*N/M**2
300
200
100
0
-100
-200
-300
90 80 70 60 50 40 30 20 10 0 -10 -20 -30 -40 -50 -60 -70 -80 -90
LATITUDE
COLA
GFDL
OBS
GISS

Figure 46

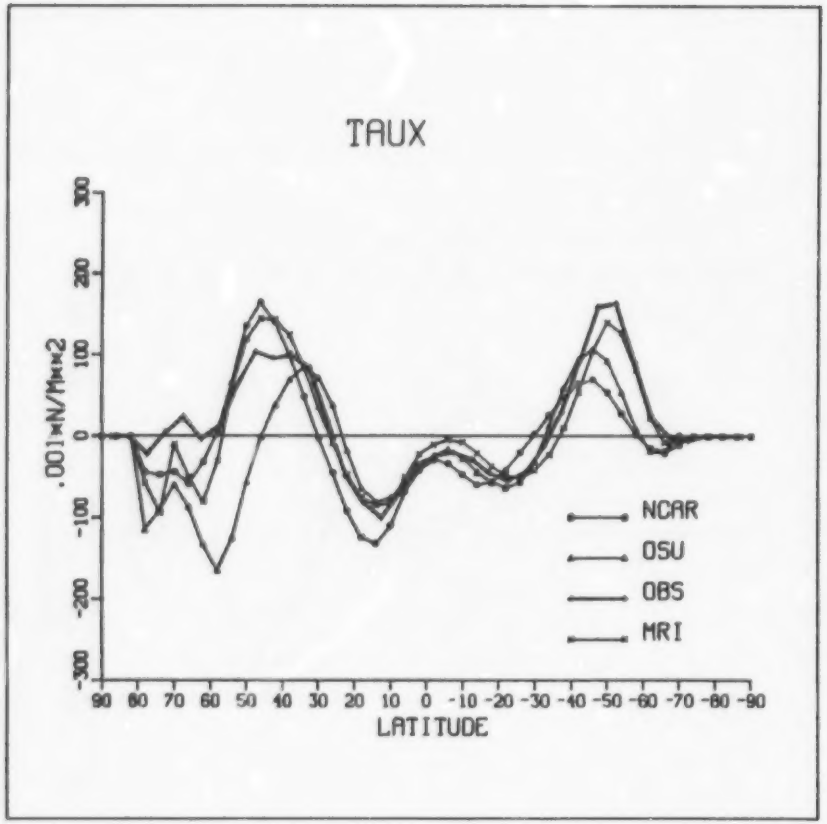
TAUX
.001*N/M**2
300
200
100
0
-100
-200
-300
90 80 70 60 50 40 30 20 10 0 -10 -20 -30 -40 -50 -60 -70 -80 -90
LATITUDE
NCAR
OSU
OBS
MRI

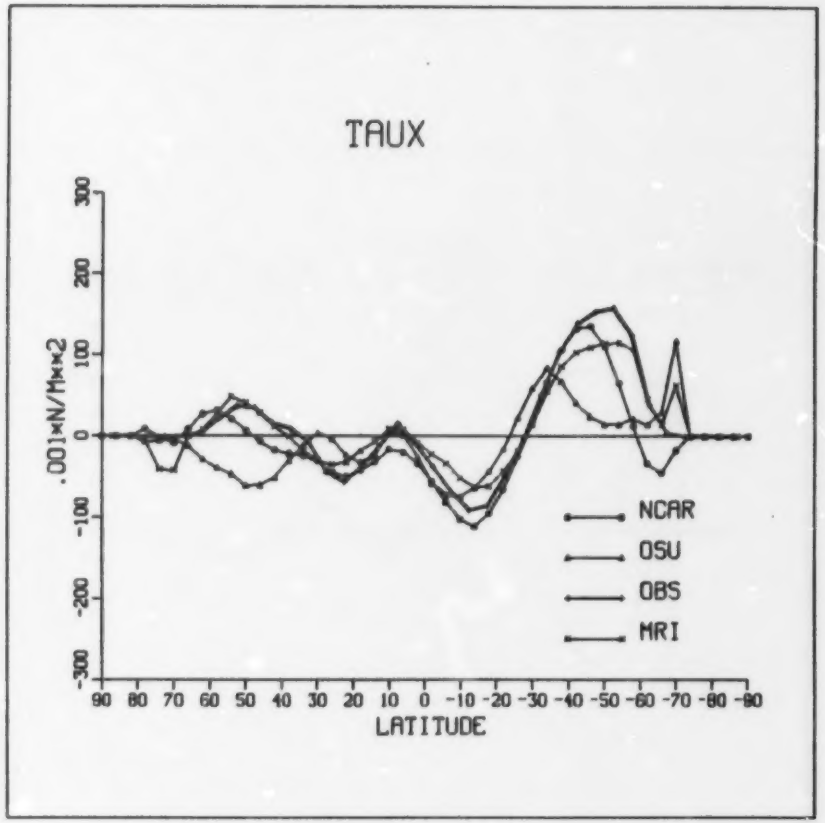
TAUX
.001*N/M**2
300
200
100
0
-100
-200
-300
90 80 70 60 50 40 30 20 10 0 -10 -20 -30 -40 -50 -60 -70 -80 -90
LATITUDE
NCAR
OSU
OBS
MRI

Figure 47

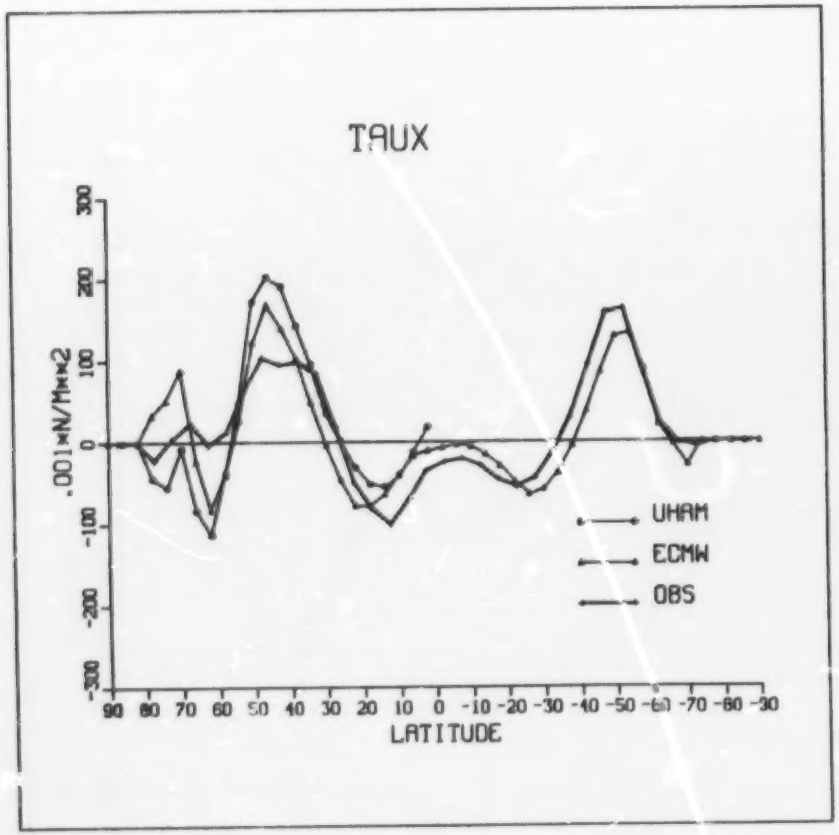
TAUX
.001*N/M**2*100.
300
200
100
0
-100
-200
-300
90 80 70 60 50 40 30 20 10 0 -10 -20 -30 -40 -50 -60 -70 -80 -90
LATITUDE
UHAM
ECMW
OBS

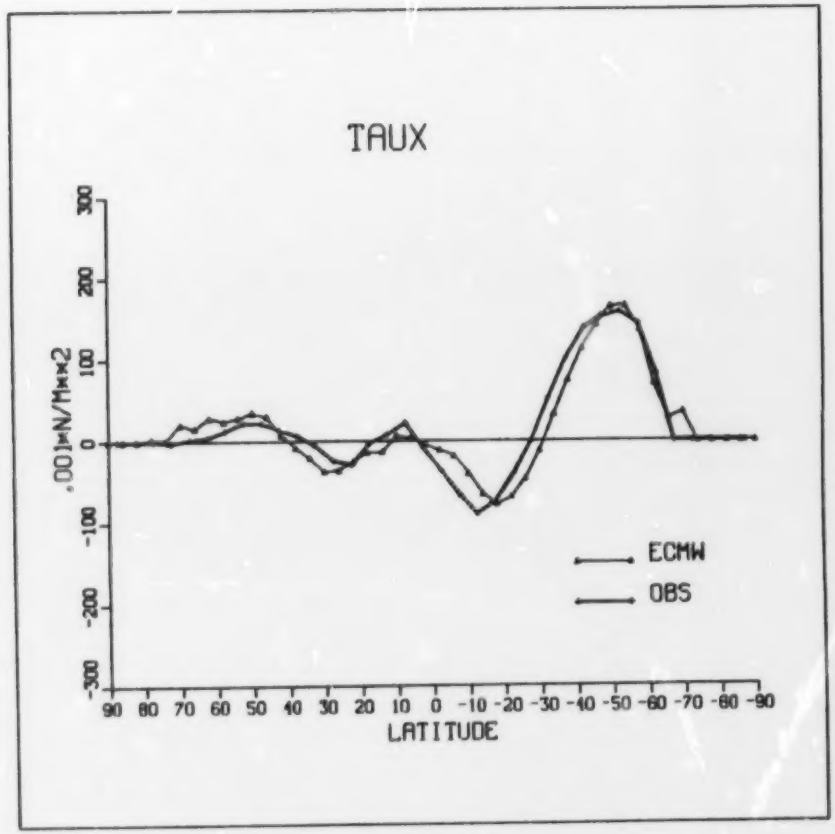
TAUX
.001*N/M**2
300
200
100
0
-100
-200
-300
90 80 70 60 50 40 30 20 10 0 -10 -20 -30 -40 -50 -60 -70 -80 -90
LATITUDE
ECMW
OBS

Figure 48

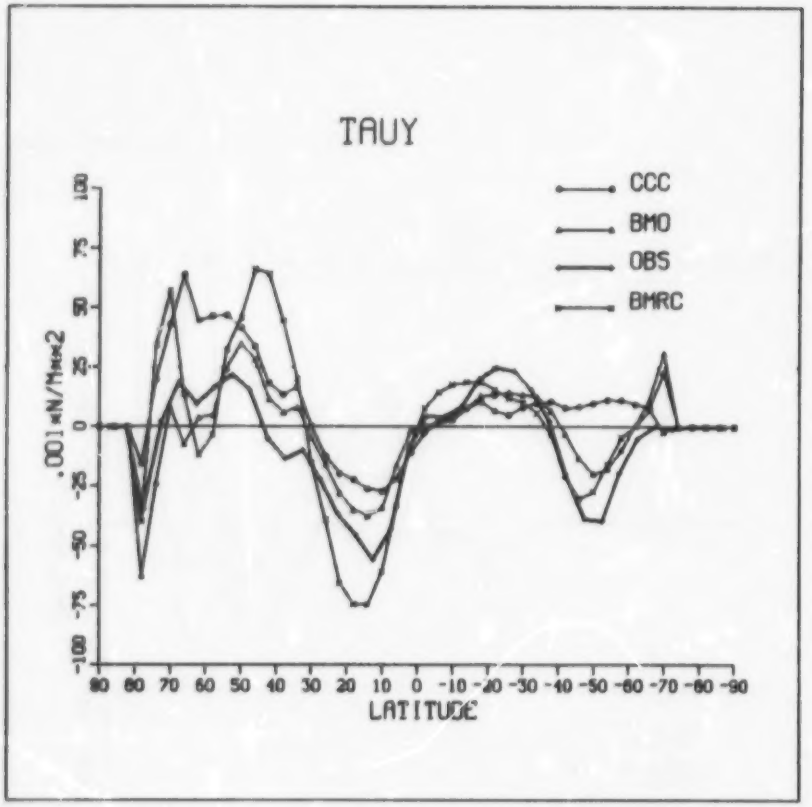
TAUY
CCC
BMO
OBS
BMRC
.001*N/M**2
100
75
50
25
0
-25
-50
-75
-100
90 80 70 60 50 40 30 20 10 0 -10 -20 -30 -40 -50 -60 -70 -80 -90
LATITUDE

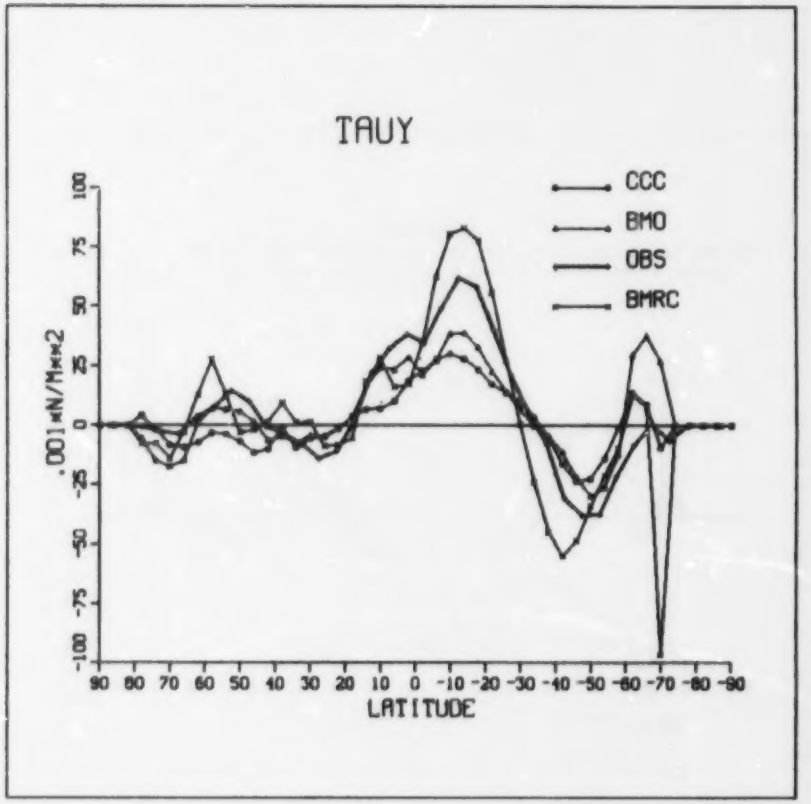
TAUY
CCC
BMO
OBS
BMRC
.001*N/M**2
100
75
50
25
0
-25
-50
-75
-100
90 80 70 60 50 40 30 20 10 0 -10 -20 -30 -40 -50 -60 -70 -80 -90
LATITUDE

Figure 49

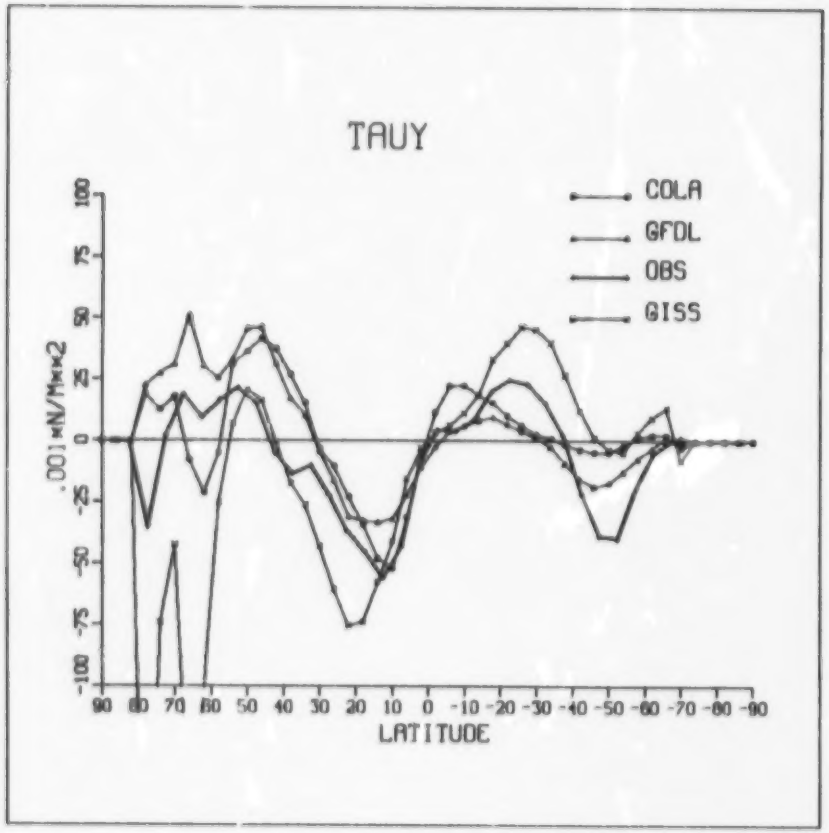
TAUY
COLA
GFDL
OBS
GISS
.001*N/M**2
100
75
50
25
0
-25
-50
-75
-100
90 80 70 60 50 40 30 20 10 0 -10 -20 -30 -40 -50 -60 -70 -80 -90
LATITUDE

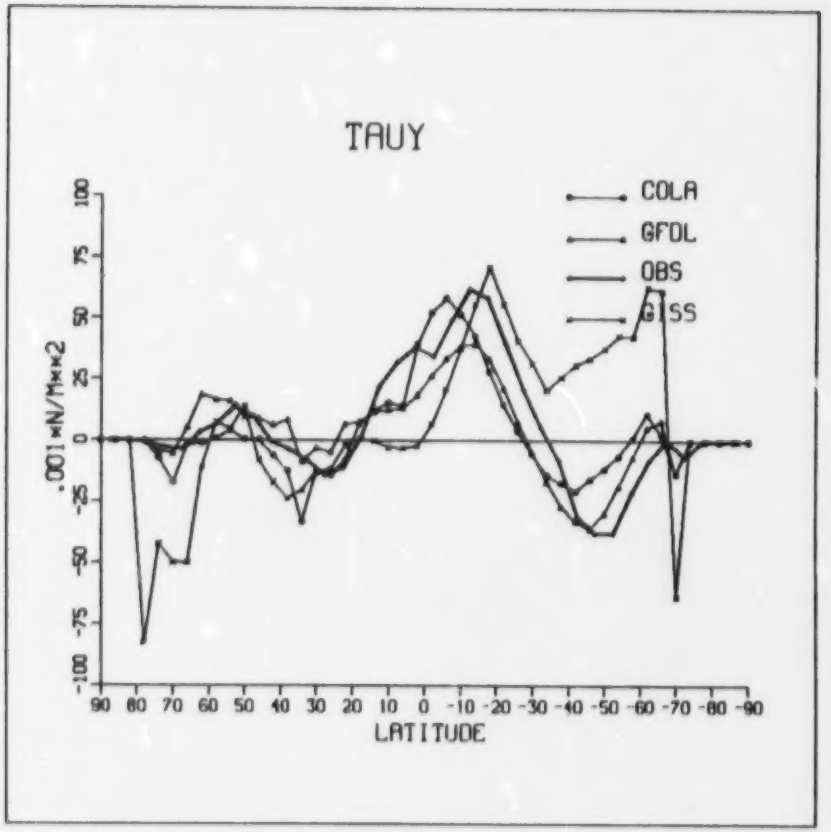
TAUY
COLA
GFDL
OBS
GISS
.001*N/M**2
100
75
50
25
0
-25
-50
-75
-100
90 80 70 60 50 40 30 20 10 0 -10 -20 -30 -40 -50 -60 -70 -80 -90
LATITUDE

Figure 50

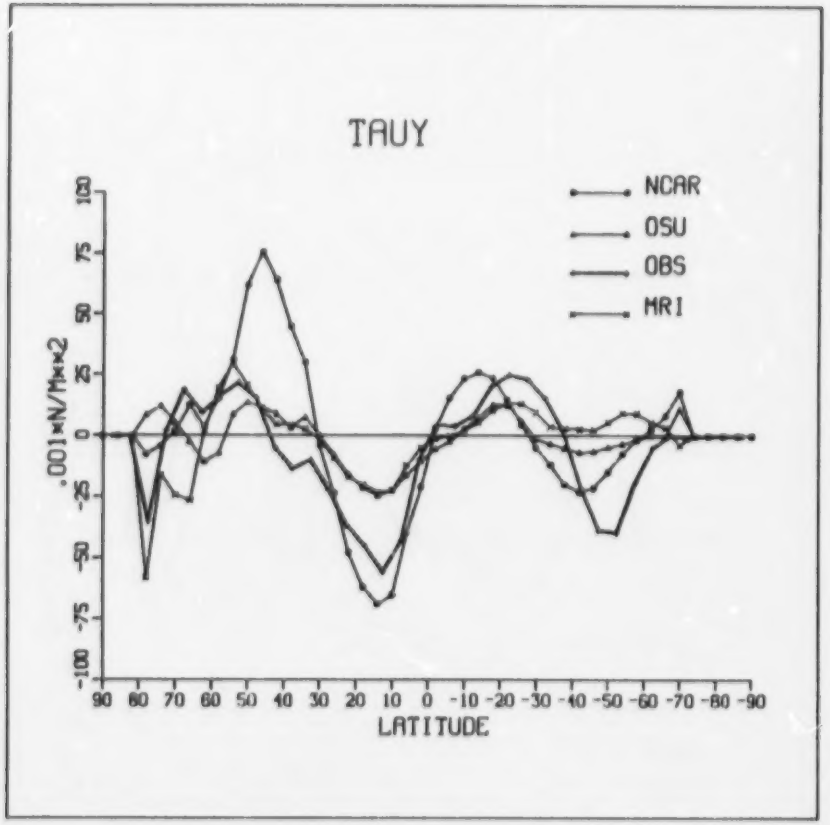
TAUY
NCAR
OSU
OBS
MRI
.001*N/M**2
100
75
50
25
0
-25
-50
-75
-100
90 80 70 60 50 40 30 20 10 0 -10 -20 -30 -40 -50 -60 -70 -80 -90
LATITUDE

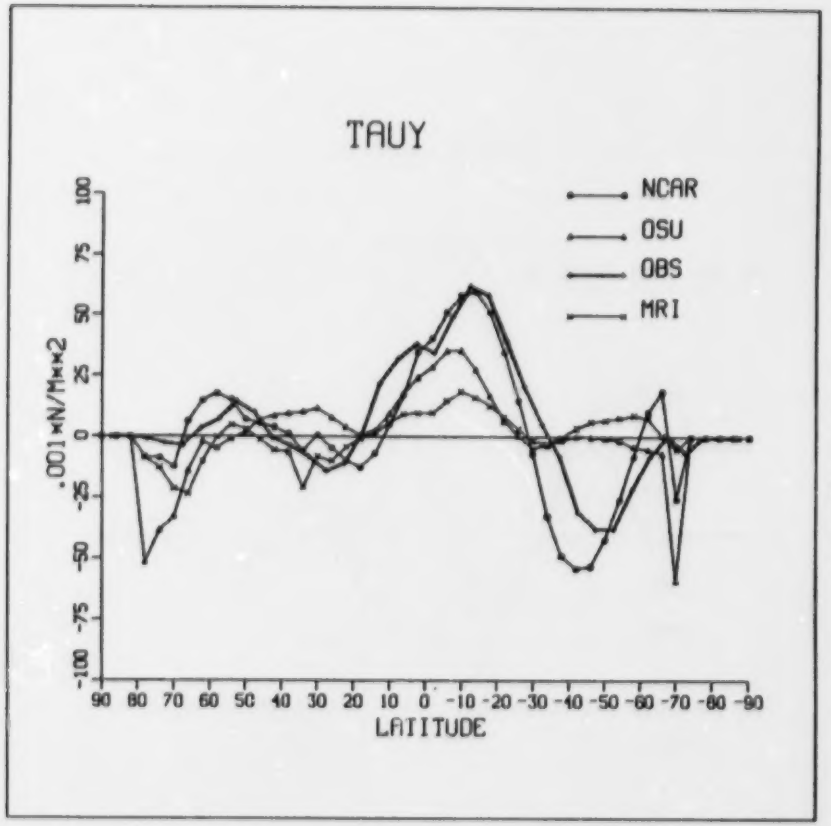
TAUY
NCAR
OSU
OBS
MRI
.001*N/M**2
100
75
50
25
0
-25
-50
-75
-100
90 80 70 60 50 40 30 20 10 0 -10 -20 -30 -40 -50 -60 -70 -80 -90
LATITUDE

Figure 51

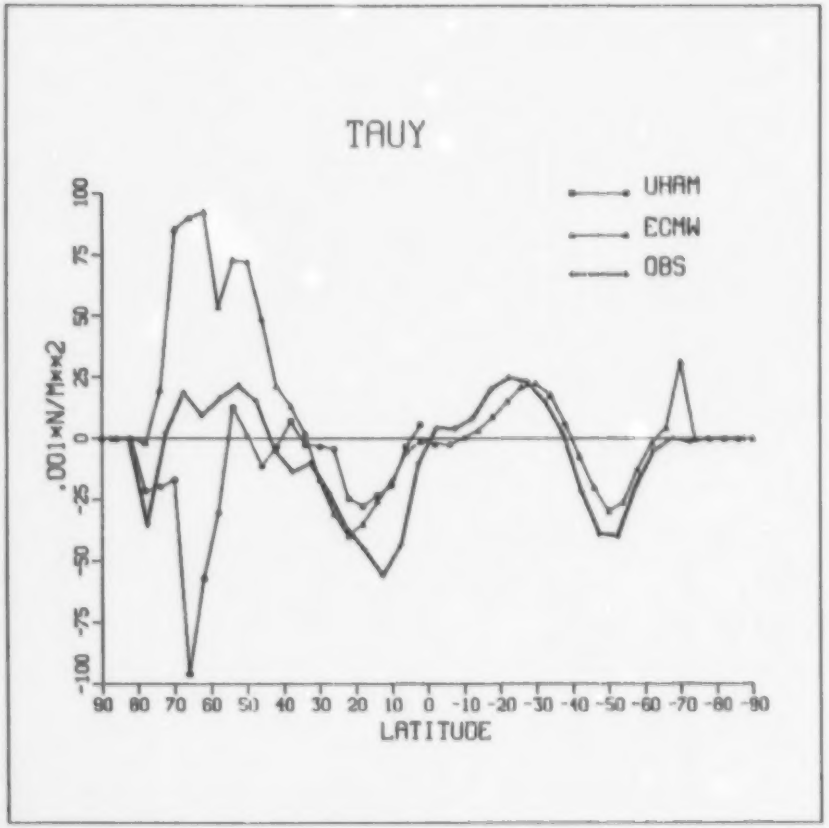
TAUY
UHAM
ECMW
OBS
.001*N/M**2
100
75
50
25
0
-25
-50
-75
-100
90 80 70 60 50 40 30 20 10 0 -10 -20 -30 -40 -50 -60 -70 -80 -90
LATITUDE

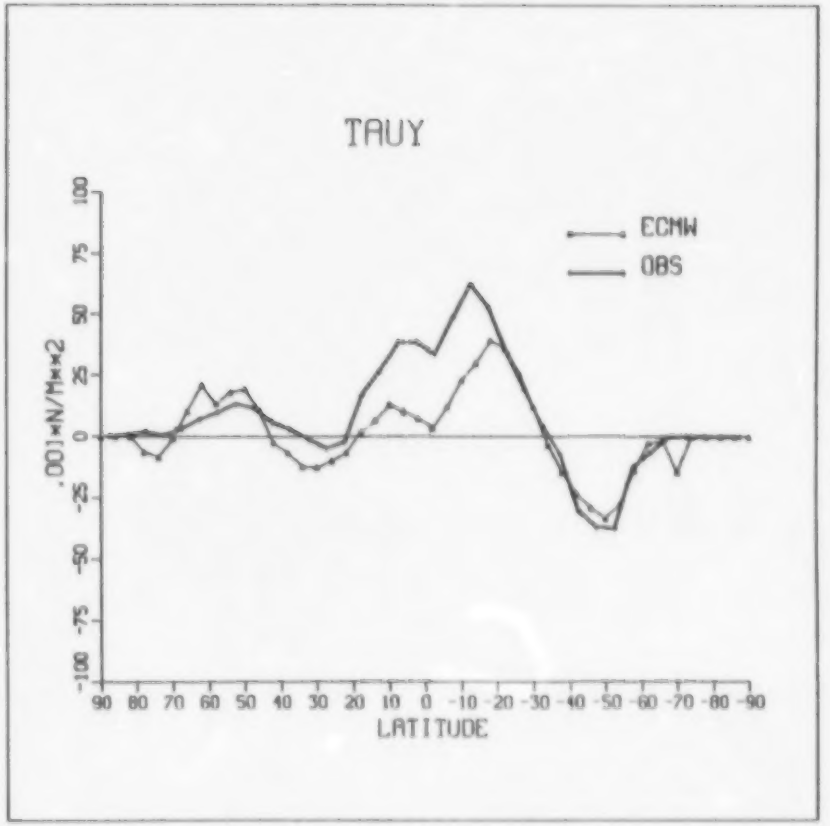
TAUY
ECMW
OBS
.001*N/M**2
100
75
50
25
0
-25
-50
-75
-100
90 80 70 60 50 40 30 20 10 0 -10 -20 -30 -40 -50 -60 -70 -80 -90
LATITUDE

Figure 52

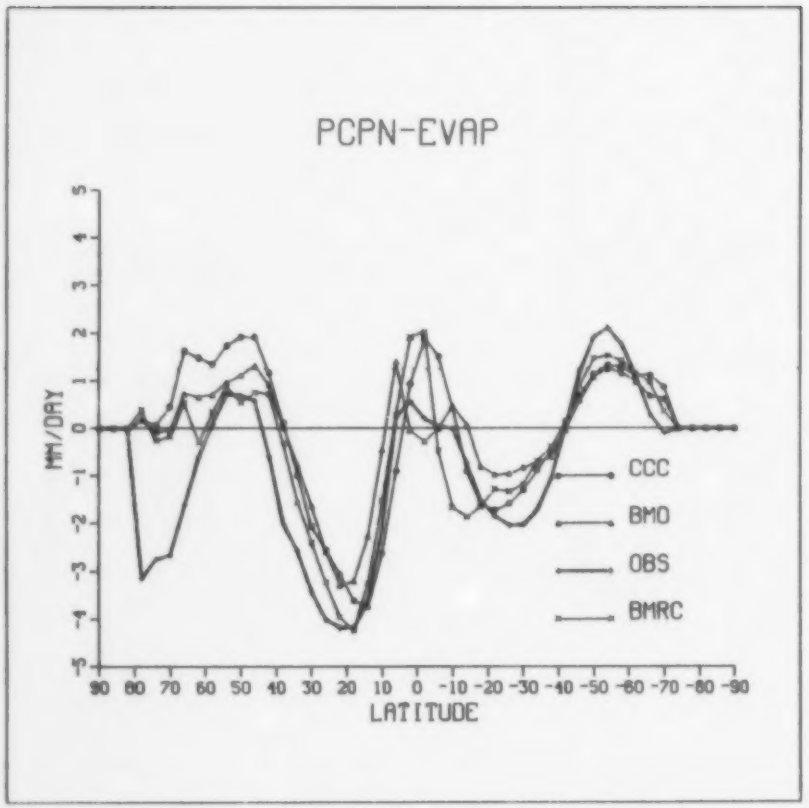
PCPN-EVAP
MM/DAY
5 4 3 2 1 0 -1 -2 -3 -4 -5
90 80 70 60 50 40 30 20 10 0 -10 -20 -30 -40 -50 -60 -70 -80 -90
LATITUDE
CCC
BMO
OBS
BMRC

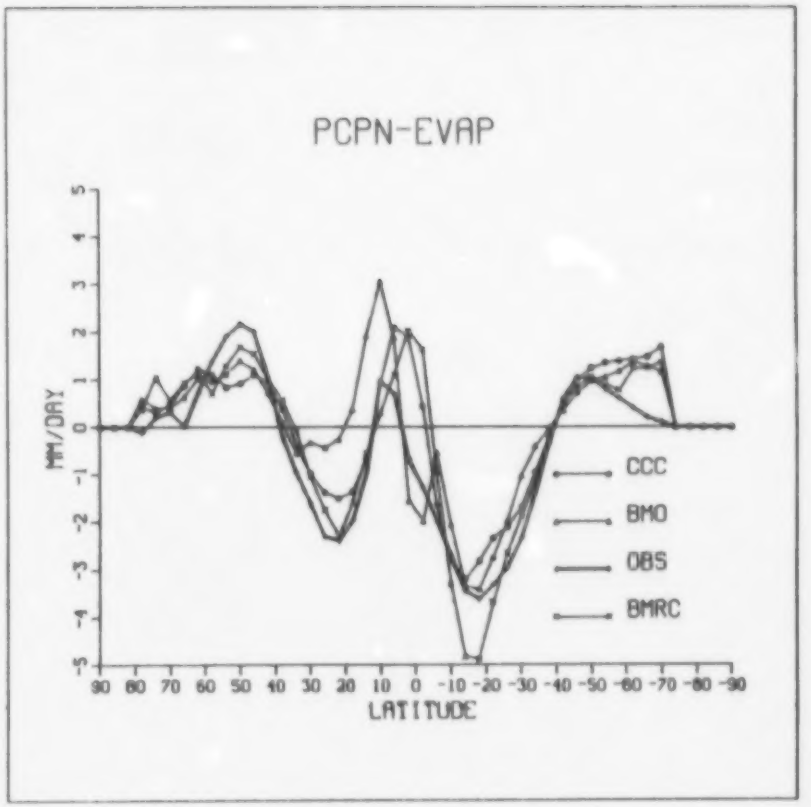
PCPN-EVAP
MM/DAY
5 4 3 2 1 0 -1 -2 -3 -4 -5
90 80 70 60 50 40 30 20 10 0 -10 -20 -30 -40 -50 -60 -70 -80 -90
LATITUDE
CCC
BMO
OBS
BMRC

Figure 53

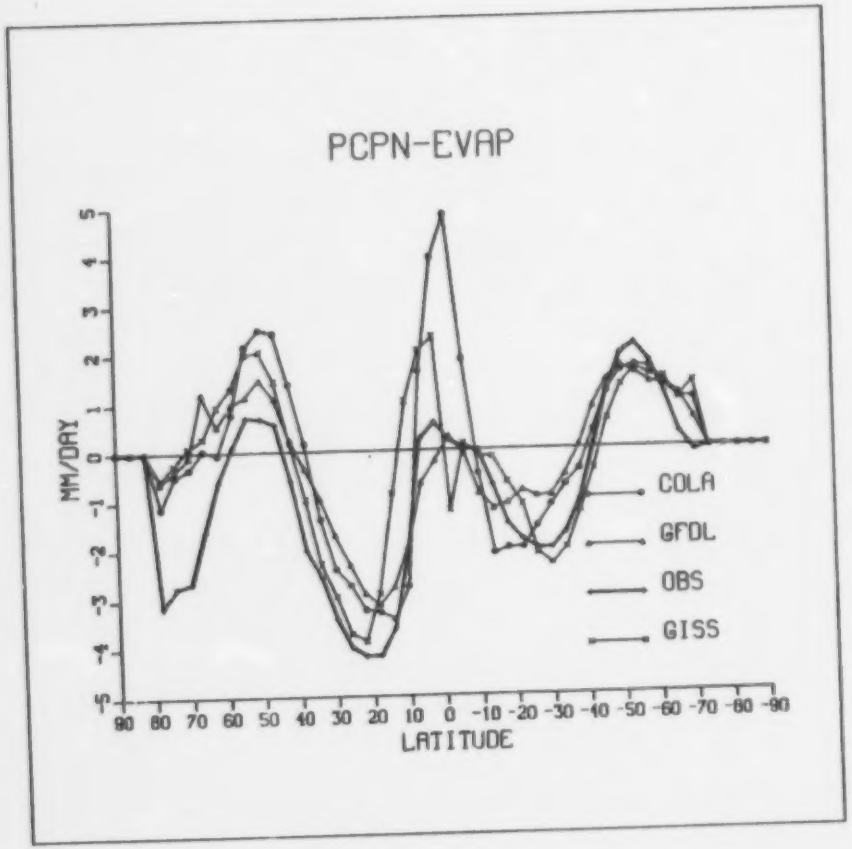
PCPN-EVAP
MM/DAY
5 4 3 2 1 0 -1 -2 -3 -4 -5
90 80 70 60 50 40 30 20 10 0 -10 -20 -30 -40 -50 -60 -70 -80 -90
LATITUDE
COLA
GFDL
OBS
GISS

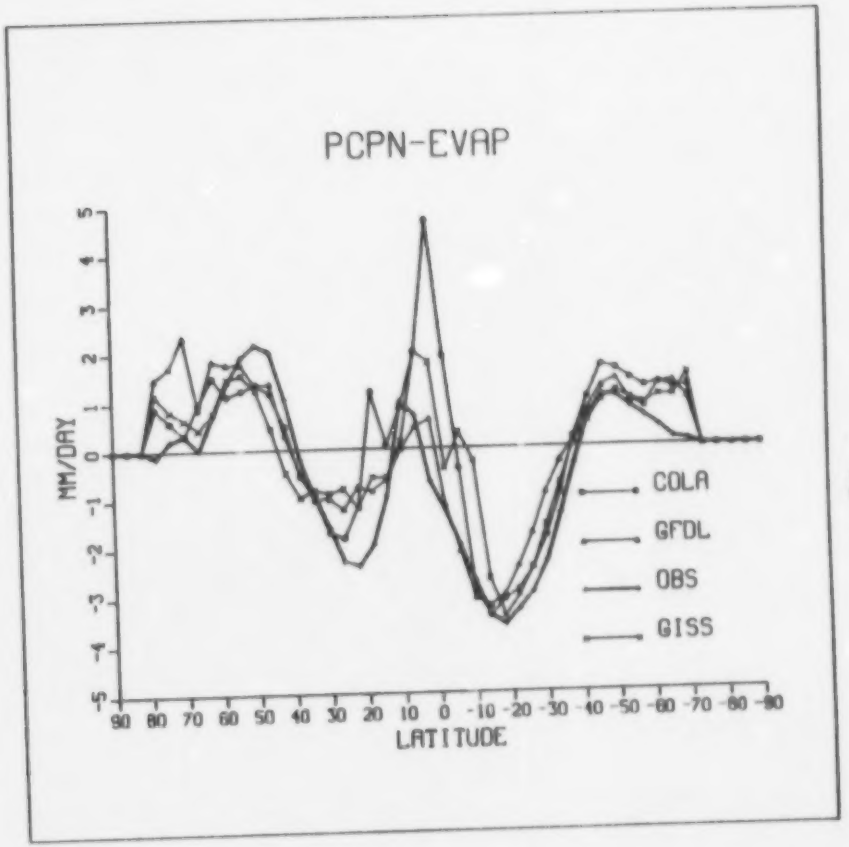
PCPN-EVAP
MM/DAY
5 4 3 2 1 0 -1 -2 -3 -4 -5
90 80 70 60 50 40 30 20 10 0 -10 -20 -30 -40 -50 -60 -70 -80 -90
LATITUDE
COLA
GFDL
OBS
GISS

Figure 54

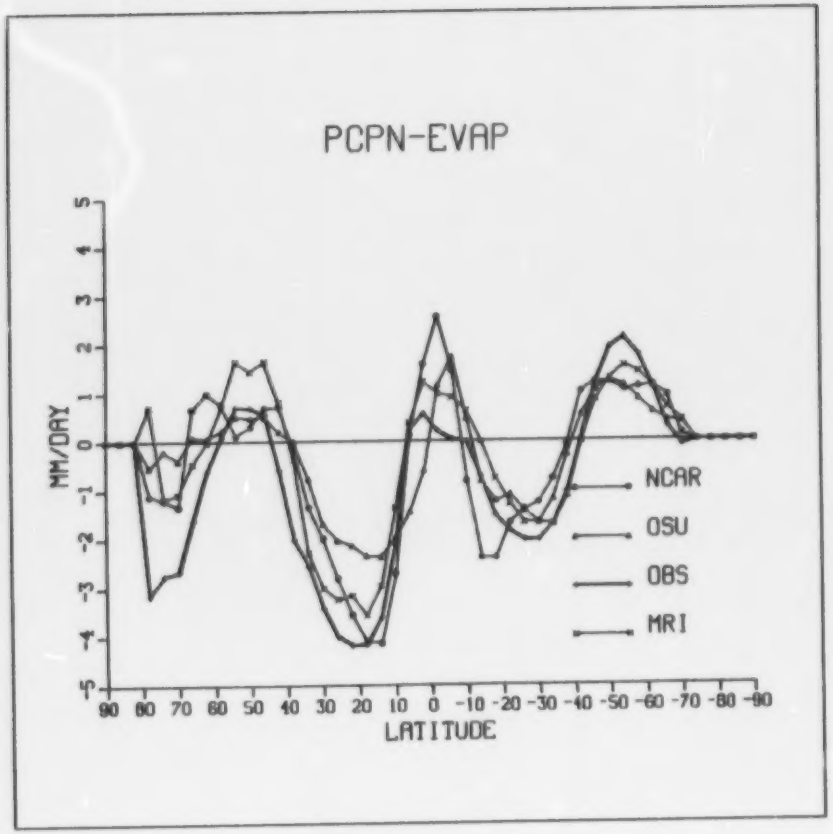
PCPN-EVAP
MM/DAY
5 4 3 2 1 0 -1 -2 -3 -4 -5
90 80 70 60 50 40 30 20 10 0 -10 -20 -30 -40 -50 -60 -70 -80 -90
LATITUDE
NCAR
OSU
OBS
MRI

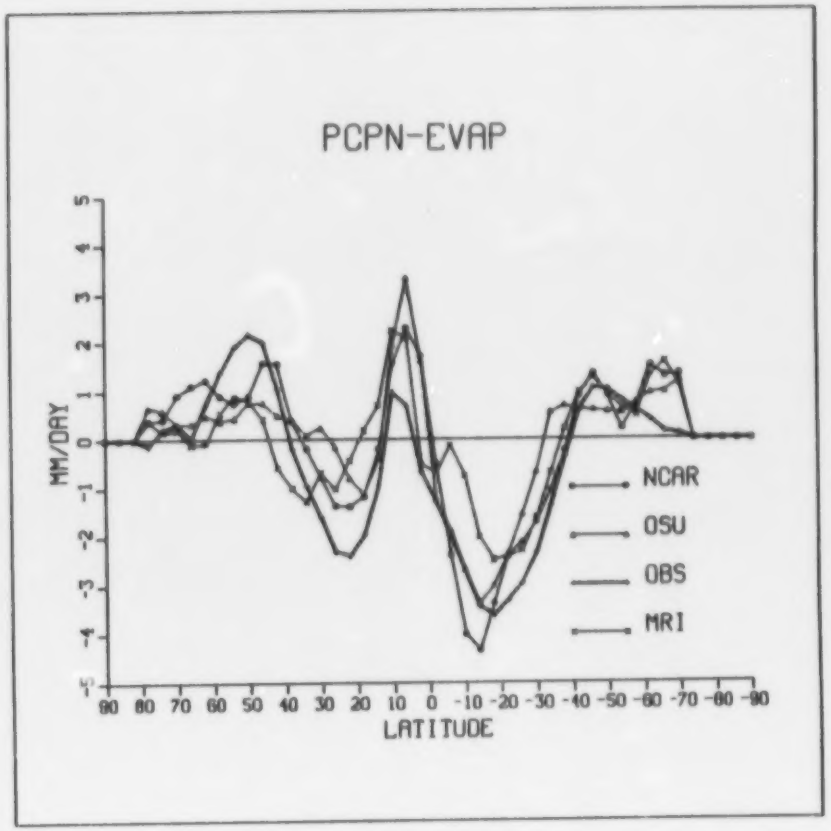
PCPN-EVAP
MM/DAY
5 4 3 2 1 0 -1 -2 -3 -4 -5
90 80 70 60 50 40 30 20 10 0 -10 -20 -30 -40 -50 -60 -70 -80 -90
LATITUDE
NCAR
OSU
OBS
MRI

Figure 55

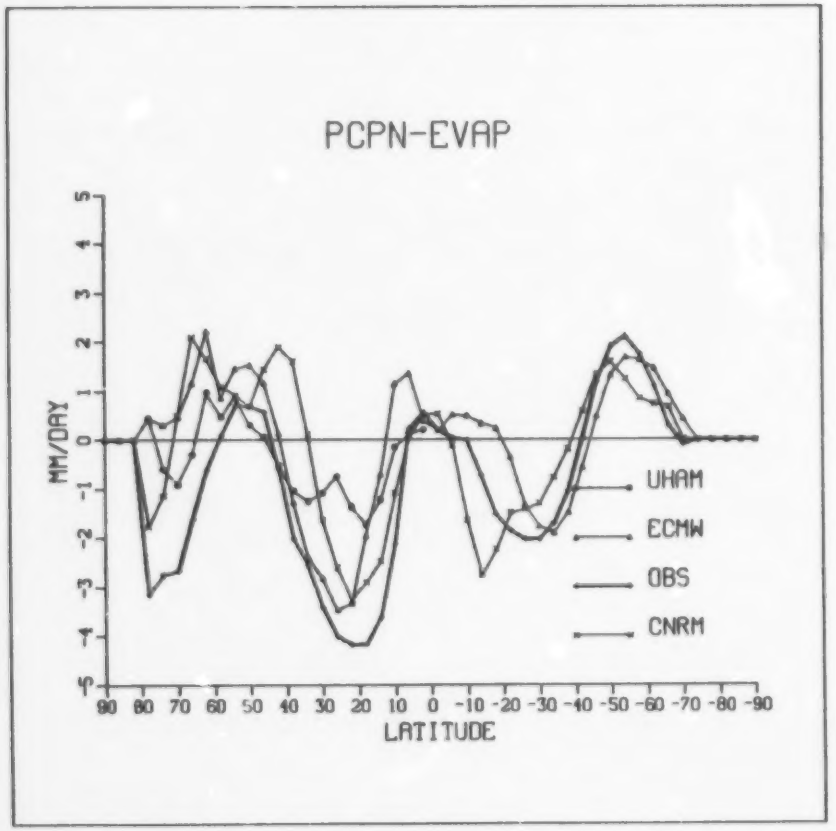
PCPN-EVAP
MM/DAY
5 4 3 2 1 0 -1 -2 -3 -4 -5
90 80 70 60 50 40 30 20 10 0 -10 -20 -30 -40 -50 -60 -70 -80 -90
LATITUDE
UHAM
ECMW
OBS
CNRM

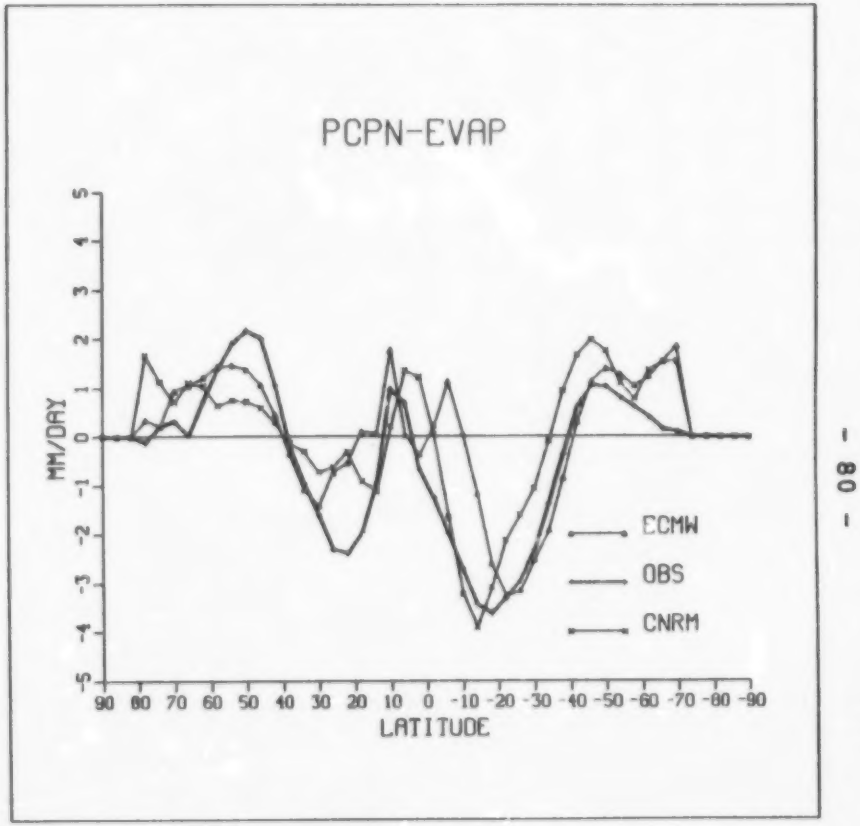
PCPN-EVAP
MM/DAY
5 4 3 2 1 0 -1 -2 -3 -4 -5
90 80 70 60 50 40 30 20 10 0 -10 -20 -30 -40 -50 -60 -70 -80 -90
LATITUDE
ECMW
OBS
CNRM

Figure 56

Appendix II. Geographically distributed values of atmosphere/ocean fluxes from individual models.

Each panel displays the geographical distribution of the flux for a particular model for January (or December-February) and July (or June-August). To put the values in context, the climatological estimate of the term is repeated as the first figure in each section.

The information is given as follows:

Net energy flux at the surface.	Figures (57-69)
Radiative energy flux at the surface.	Figures (70-82)
Latent heat flux at the surface.	Figures (83-95)
Sensible heat flux at the surface.	Figures (96-108)
East-west surface stress.	Figures (109-120)
North-south surface stress.	Figures (121-132)
Moisture flux, P - E, at the surface.	Figures (133-145)
Precipitation rate.	Figures (146-158)

ESBENSEN AND KUSHNIR JANUARY NET HEAT (W/M**2)

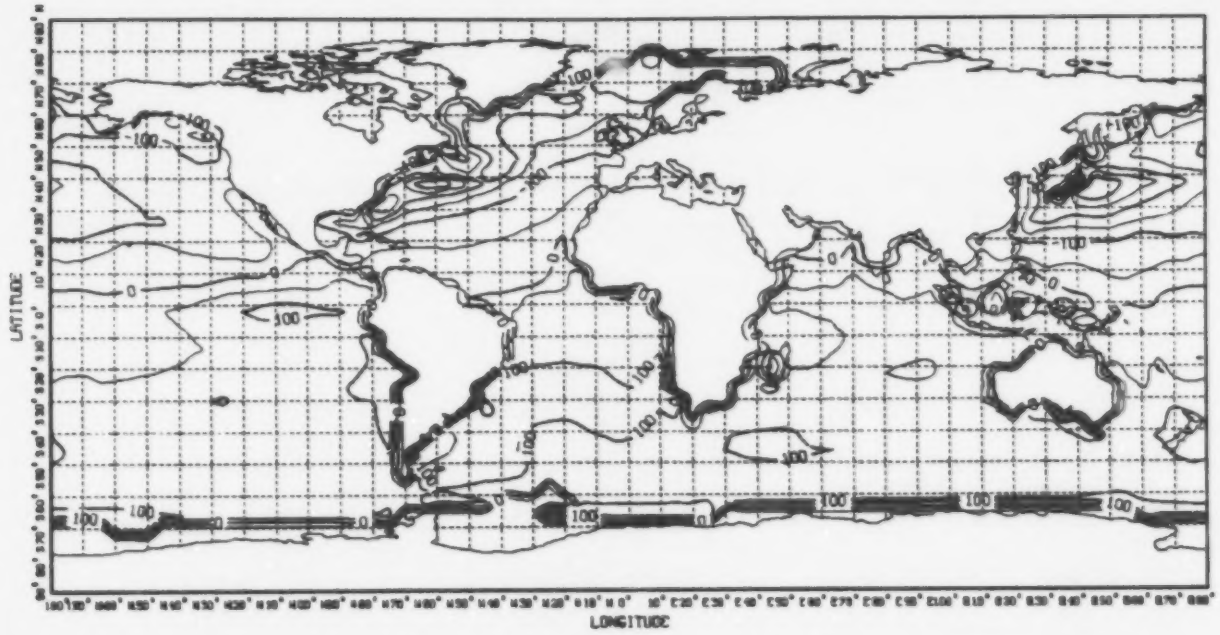

ESBENSEN AND KUSHNIR JULY NET HEAT (W/M**2)

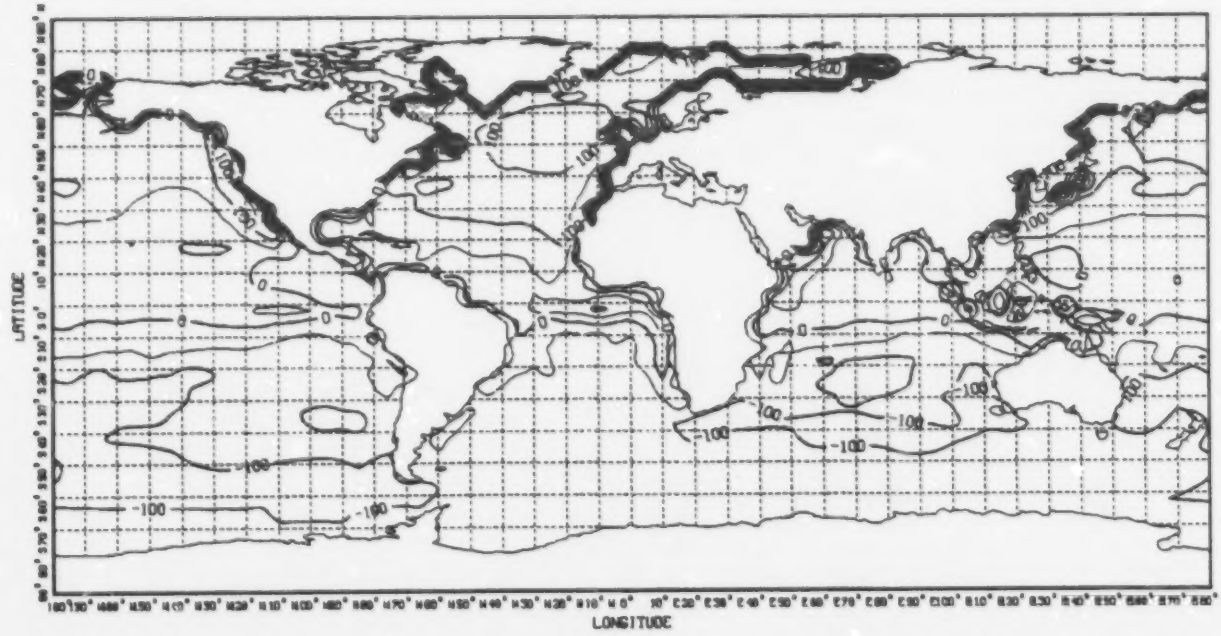

Figure 57

CANADA (CCC) WINTER NET HEAT (W/M**2)

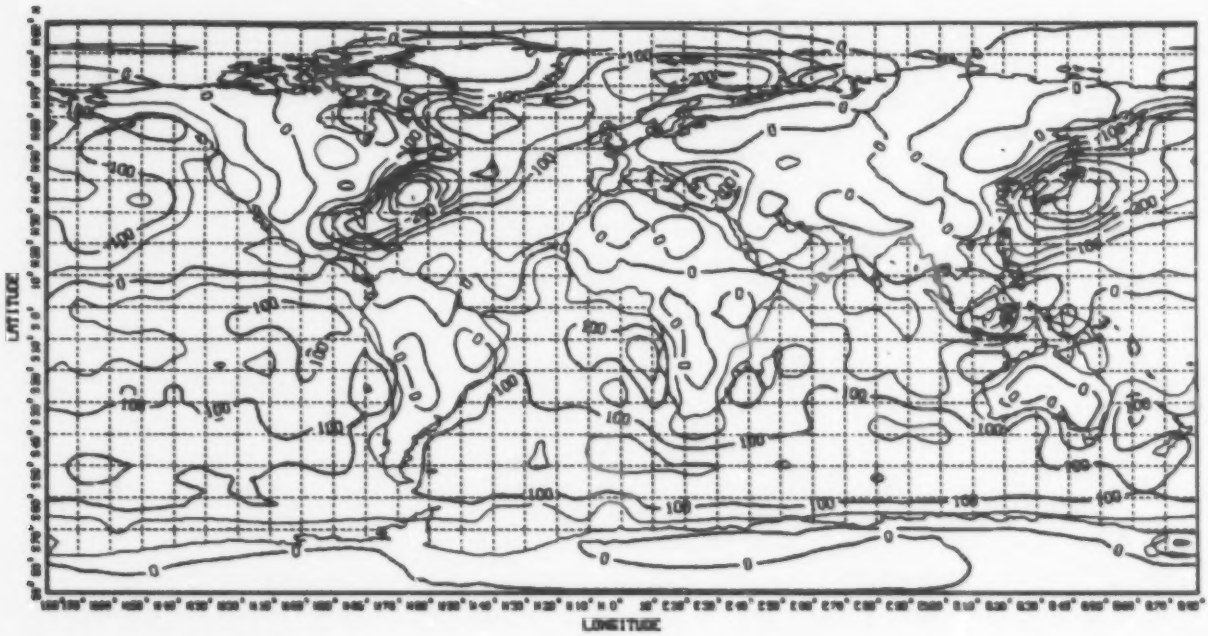

CANADA (CCC) SUMMER NET HEAT (W/M**2)

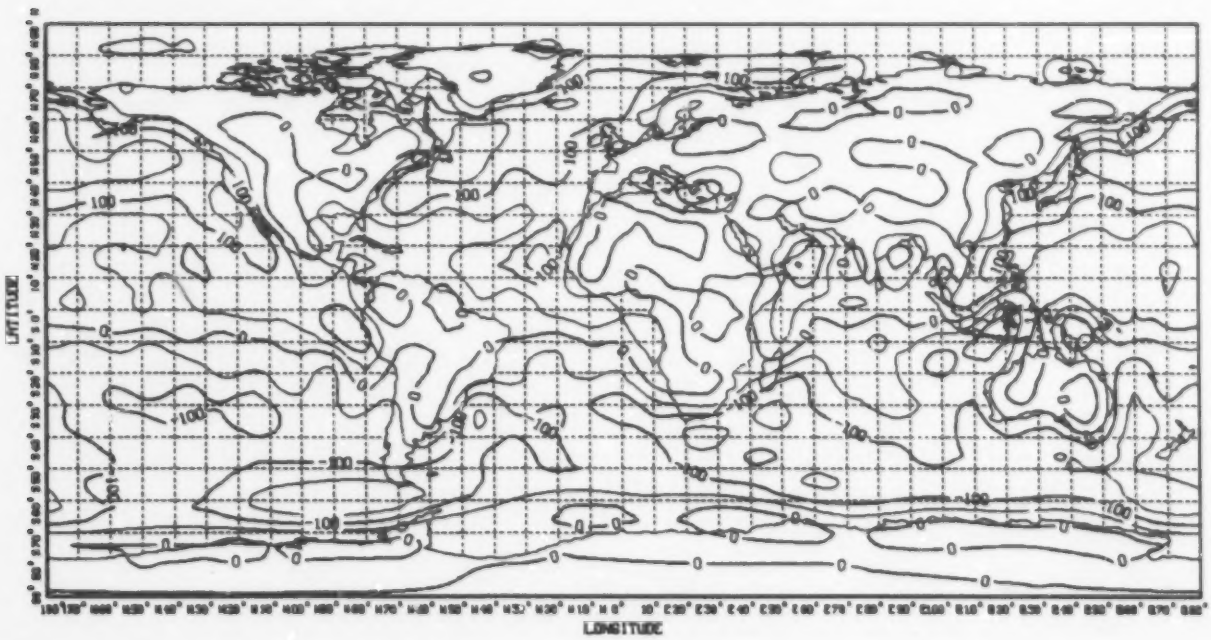

Figure 58

ENGLAND (BMO) WINTER NET HEAT (W/M**2)

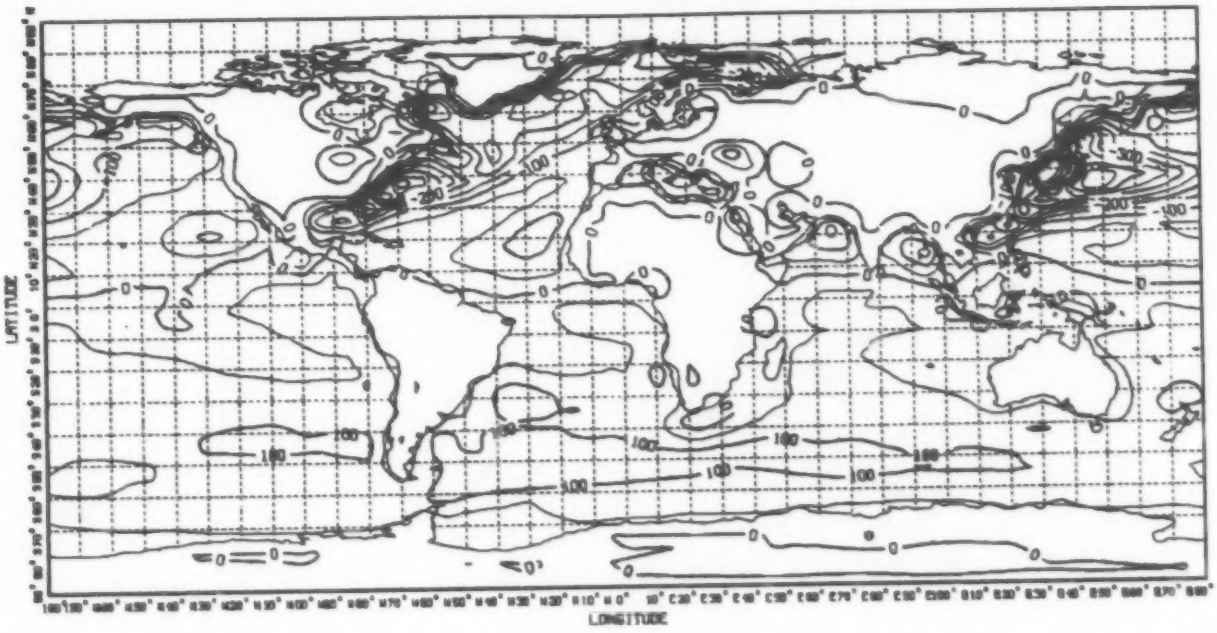

ENGLAND (BMO) SUMMER NET HEAT (W/M**2)

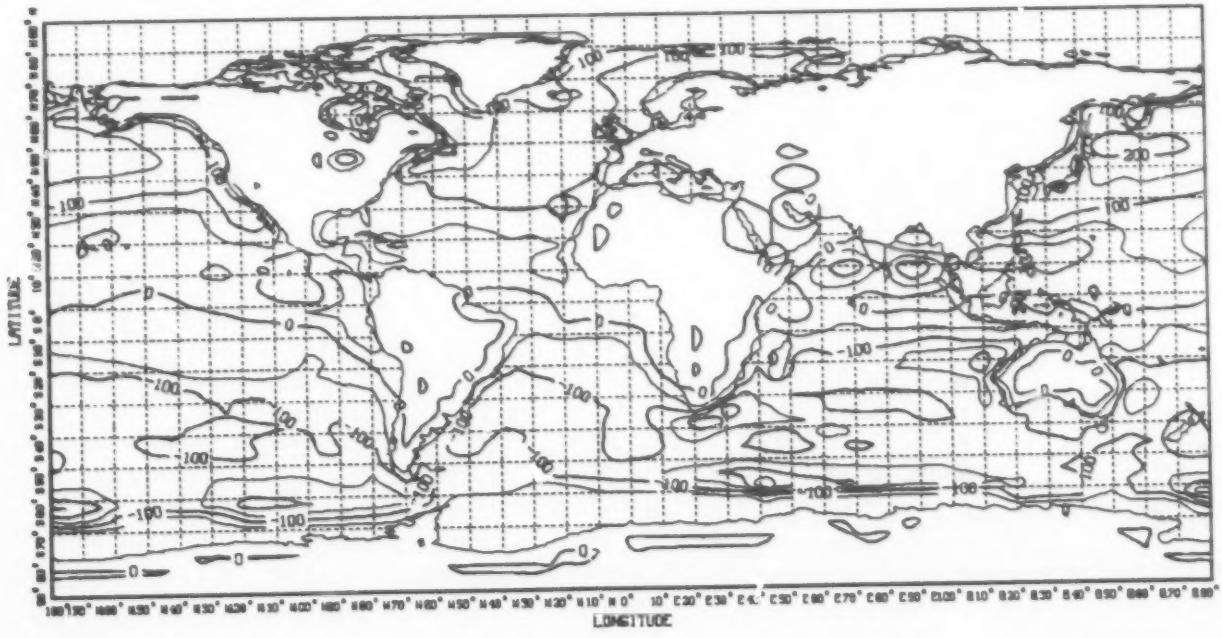

Figure 59

AUSTRALIA (BMRC) JANUARY NET HEAT (W/M**2)

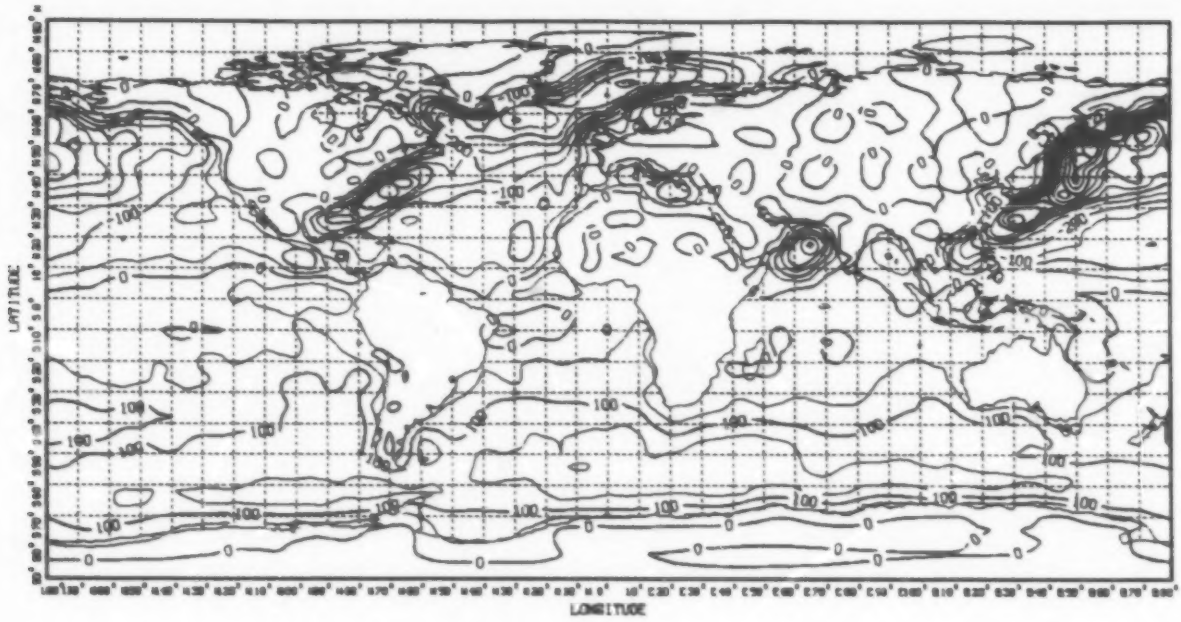

AUSTRALIA (BMRC) JULY NET HEAT (W/M**2)

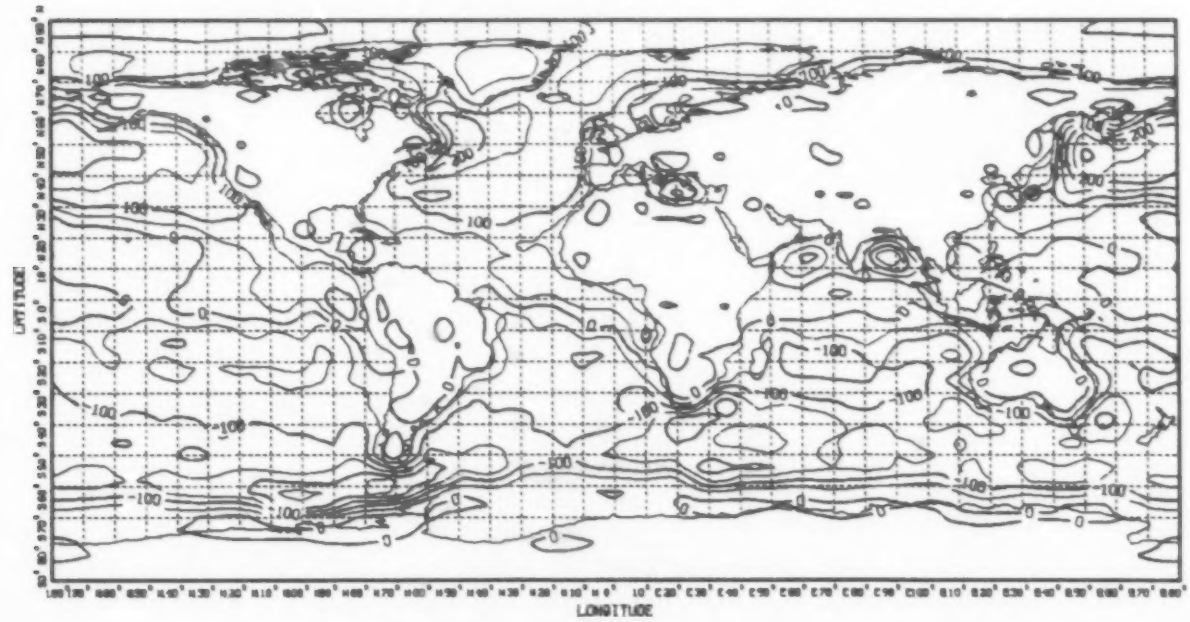

Figure 60

U S A (COLAI) JANUARY NET HEAT (W/M**2)

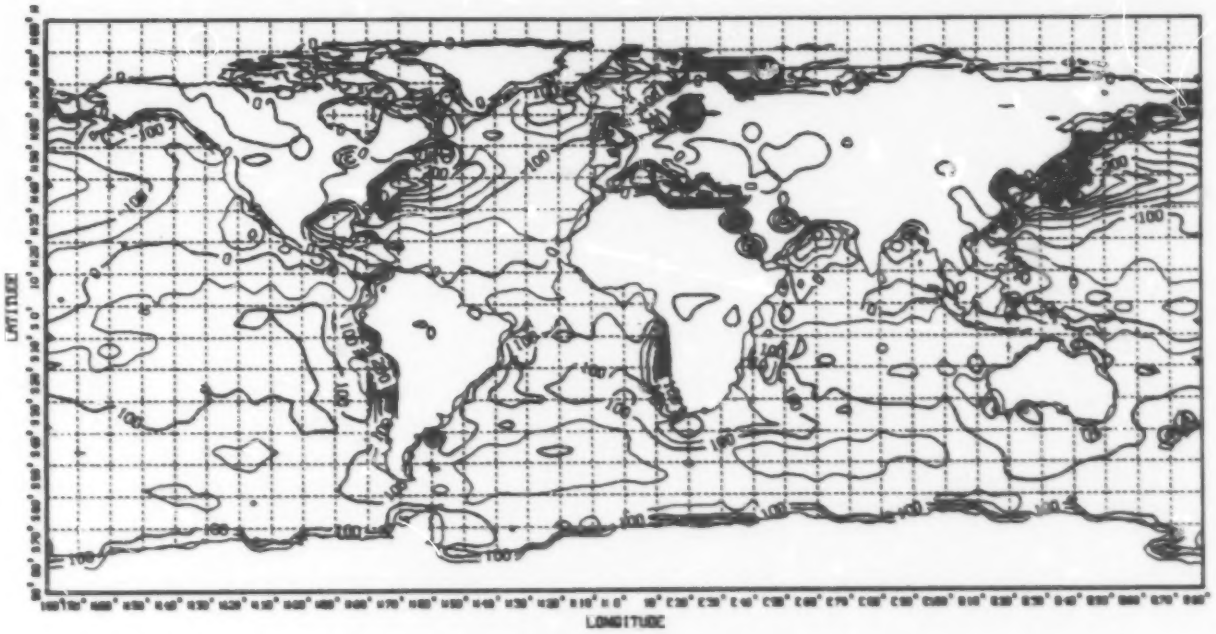

U S A (COLAI) JULY NET HEAT (W/M**2)

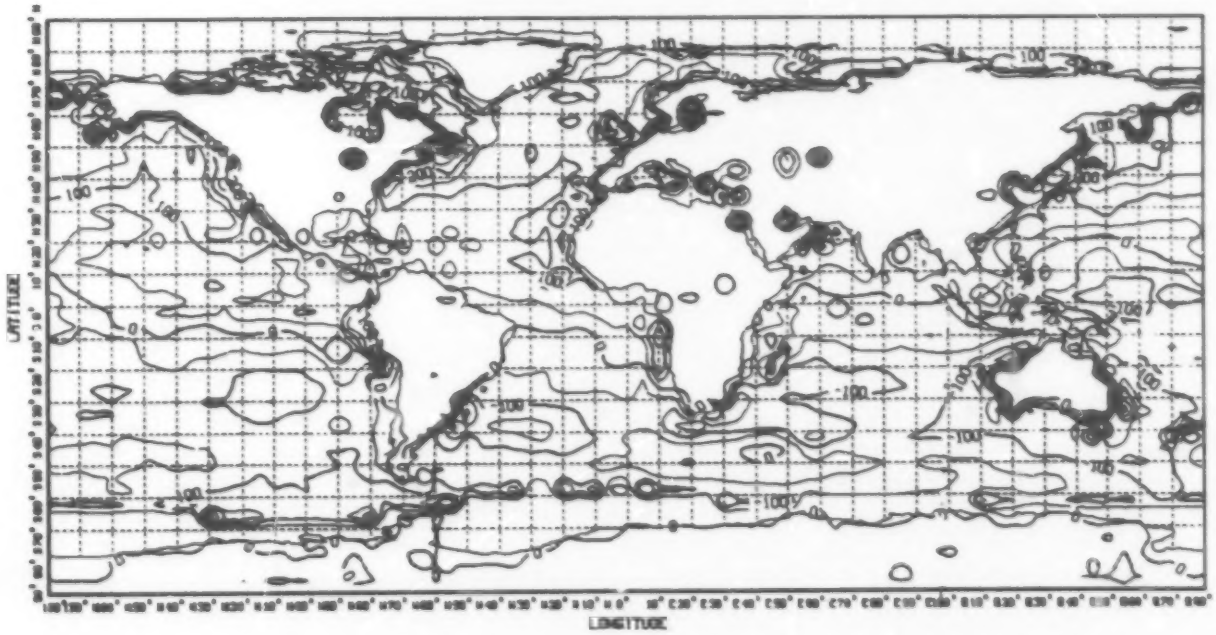

Figure 61

U S A (GFDL) JANUARY NET HEAT (W/M**2)

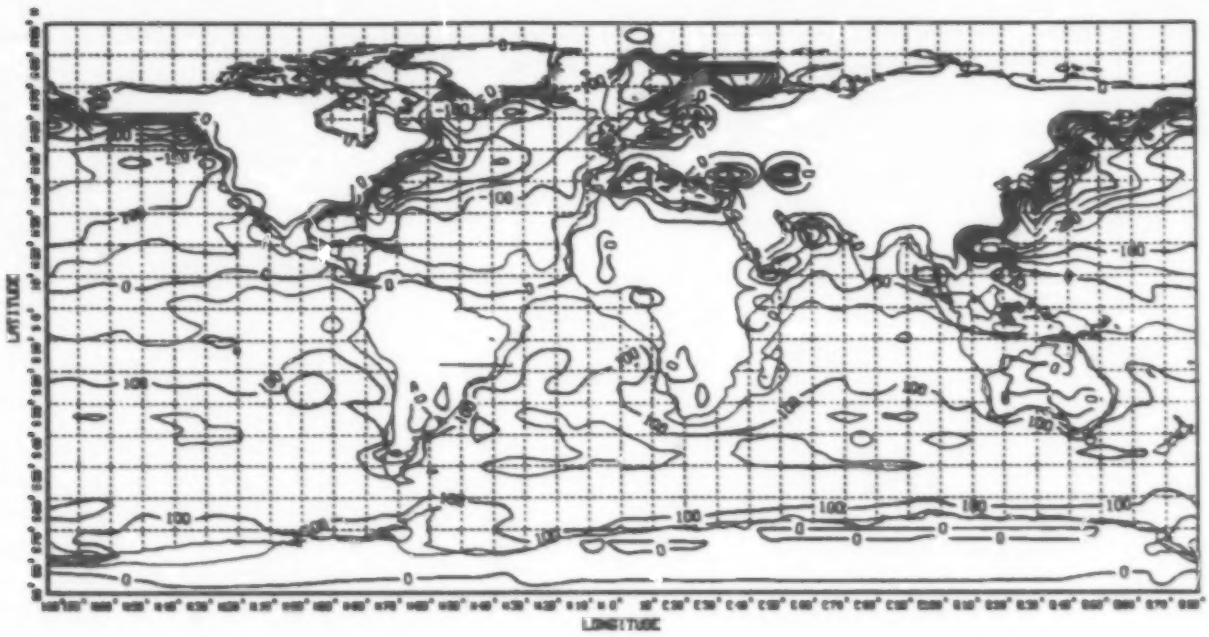

U S A (GFDL) JULY NET HEAT (W/M**2)

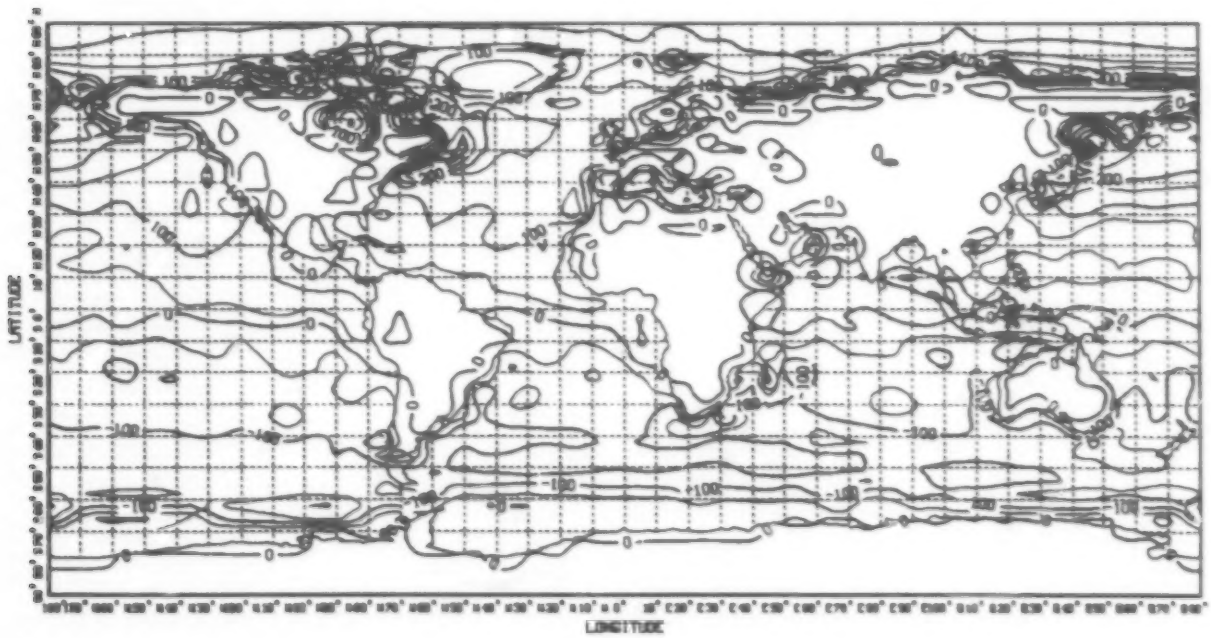

Figure 62

U S A (GISS) WINTER NET HEAT (W/M**2)

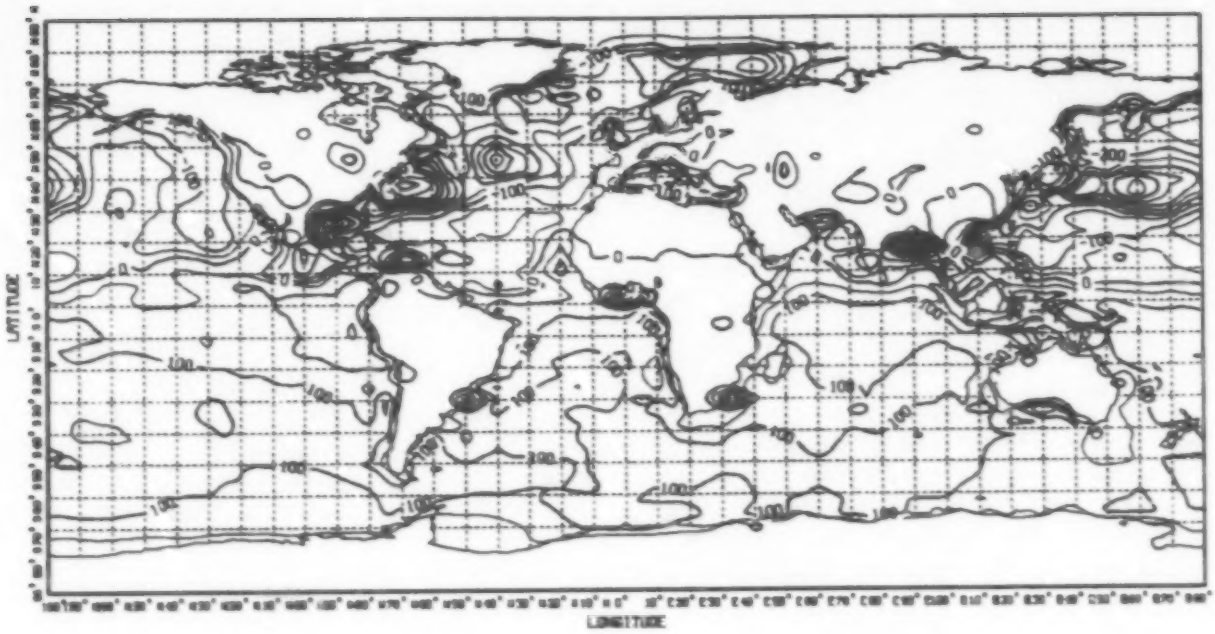

U S A (GISS) SUMMER NET HEAT (W/M**2)

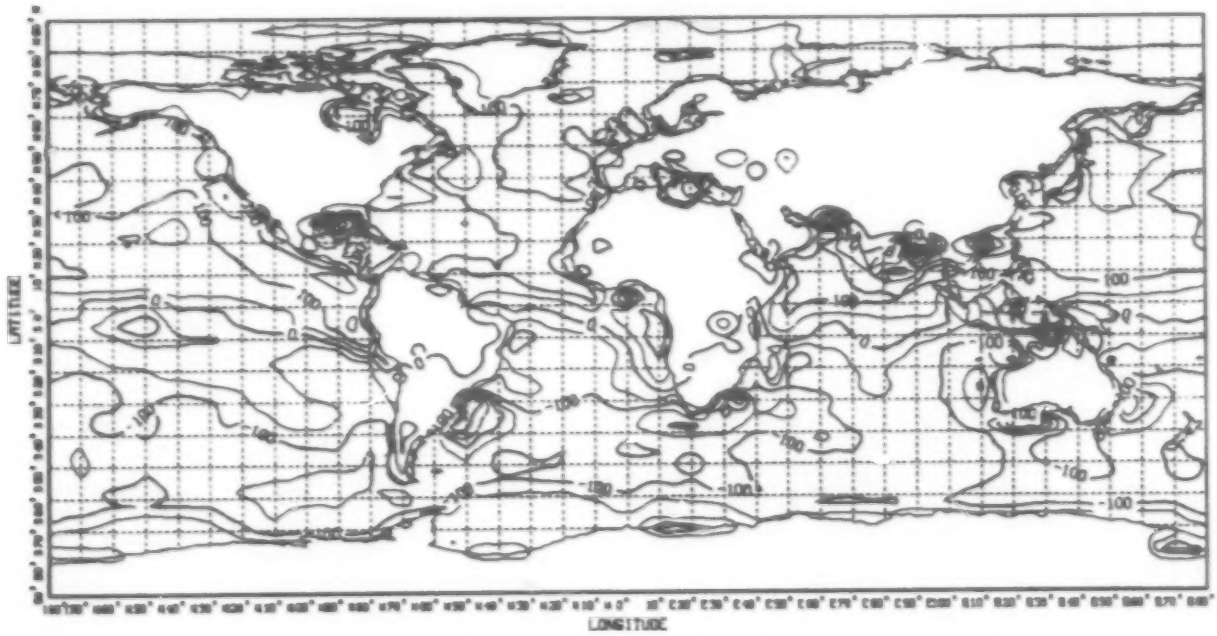

Figure 63

JAPAN (MRI) JANUARY NET HEAT (W/M**2)

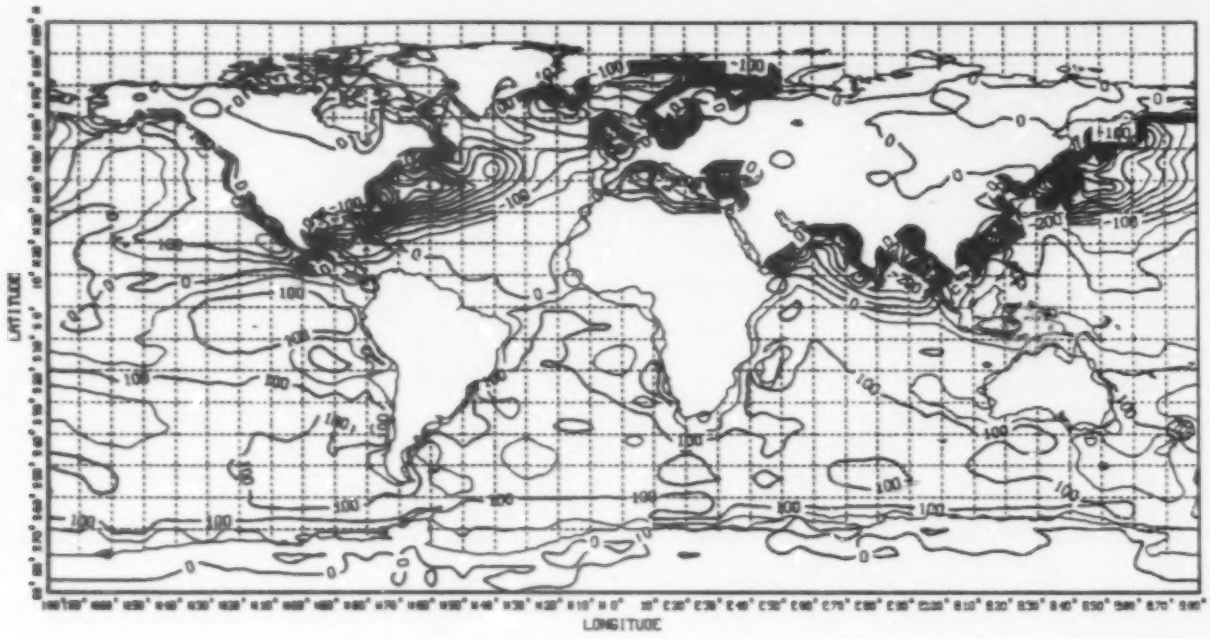

JAPAN (MRI) JULY NET HEAT (W/M**2)

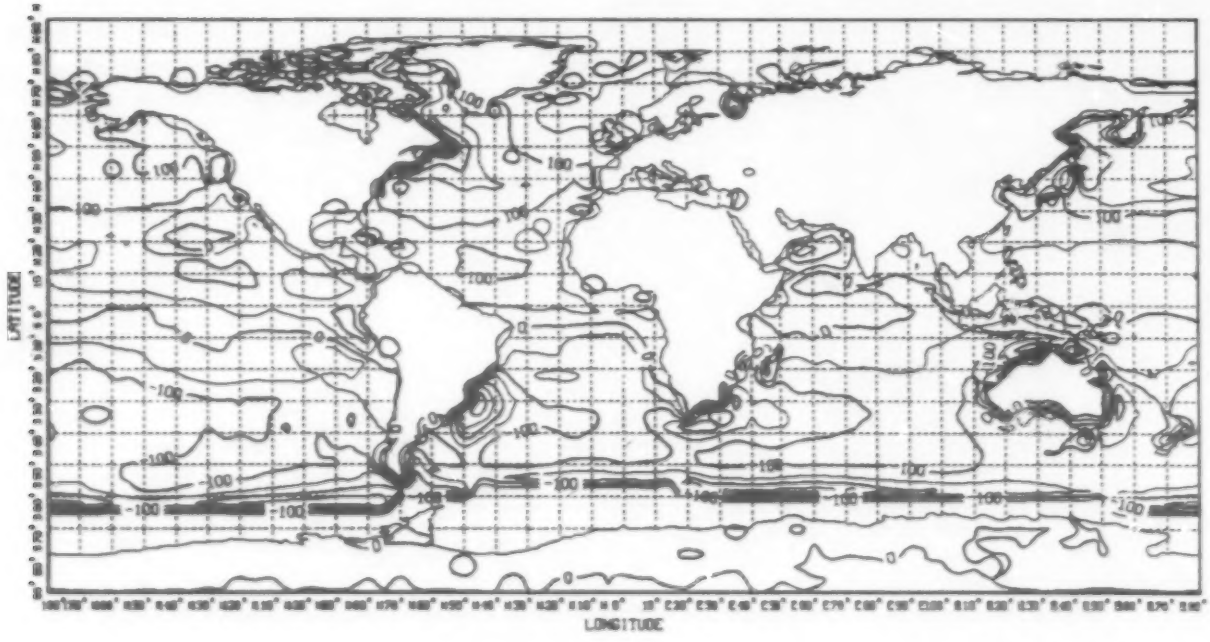

Figure 66

U S A (NCAR) JANUARY NET HEAT (W/M**2)

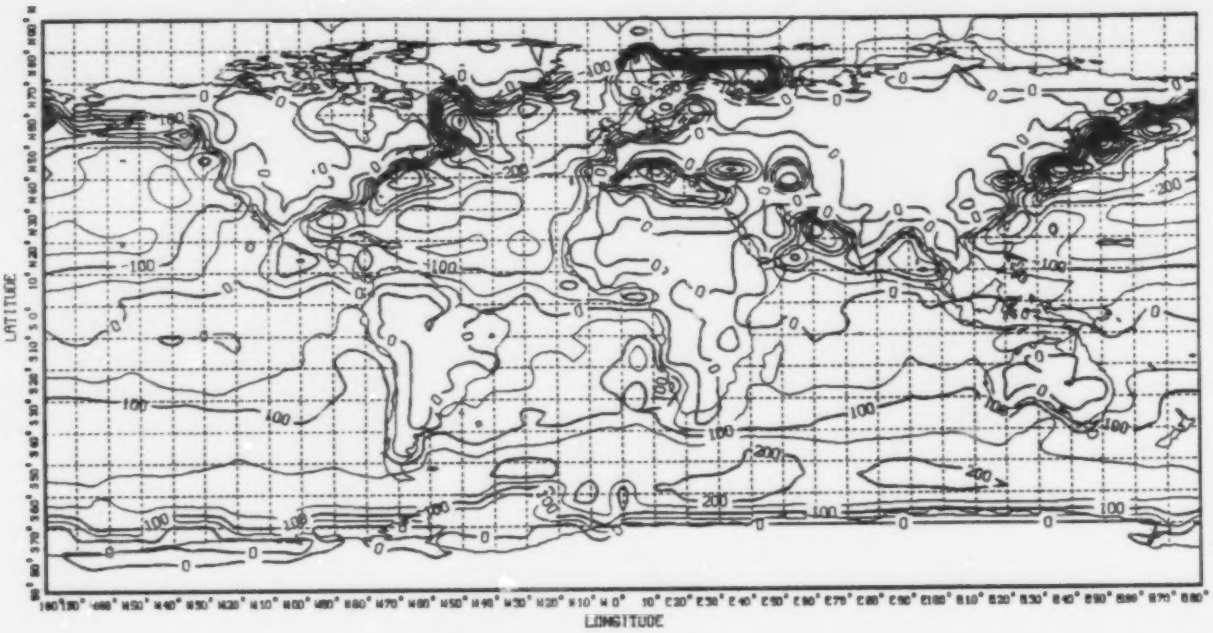

U S A (NCAR) JULY NET HEAT (W/M**2)

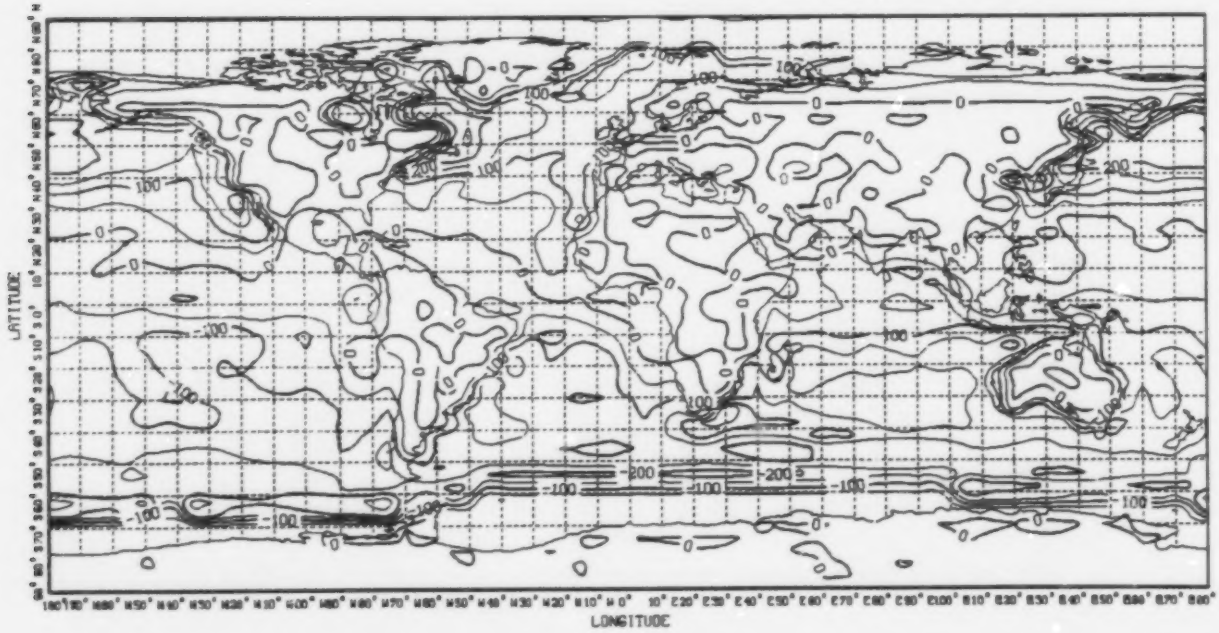

Figure 64

U S A (OSU) JANUARY NET HEAT (W/M**2)

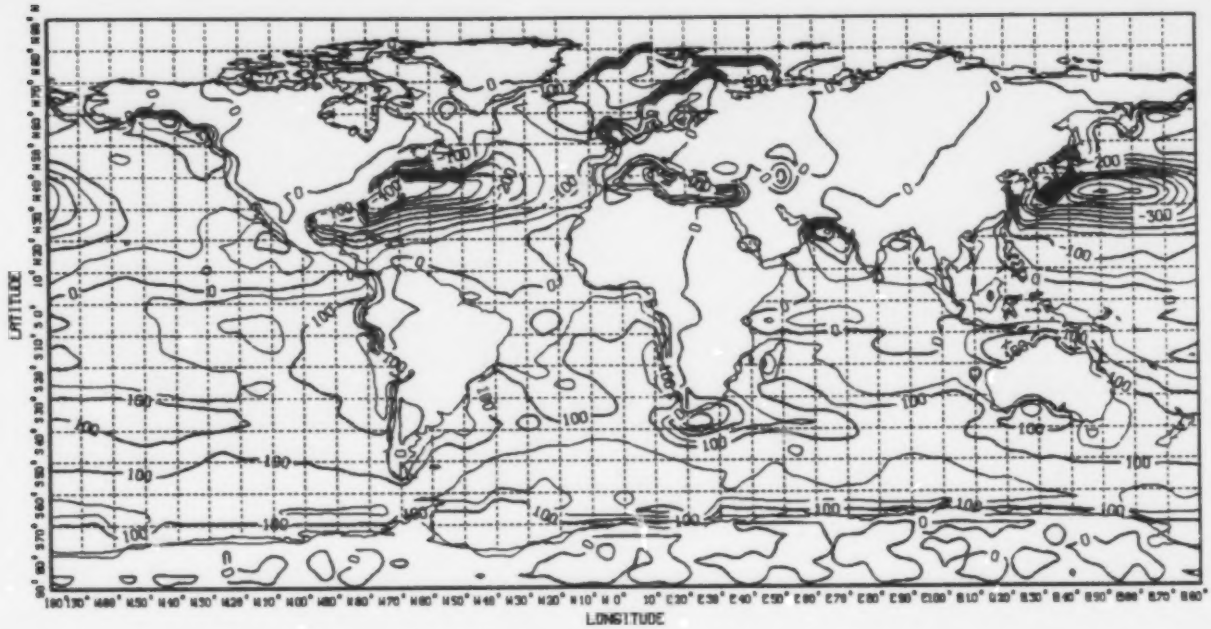

U S A (OSU) JULY NET HEAT (W/M**2)

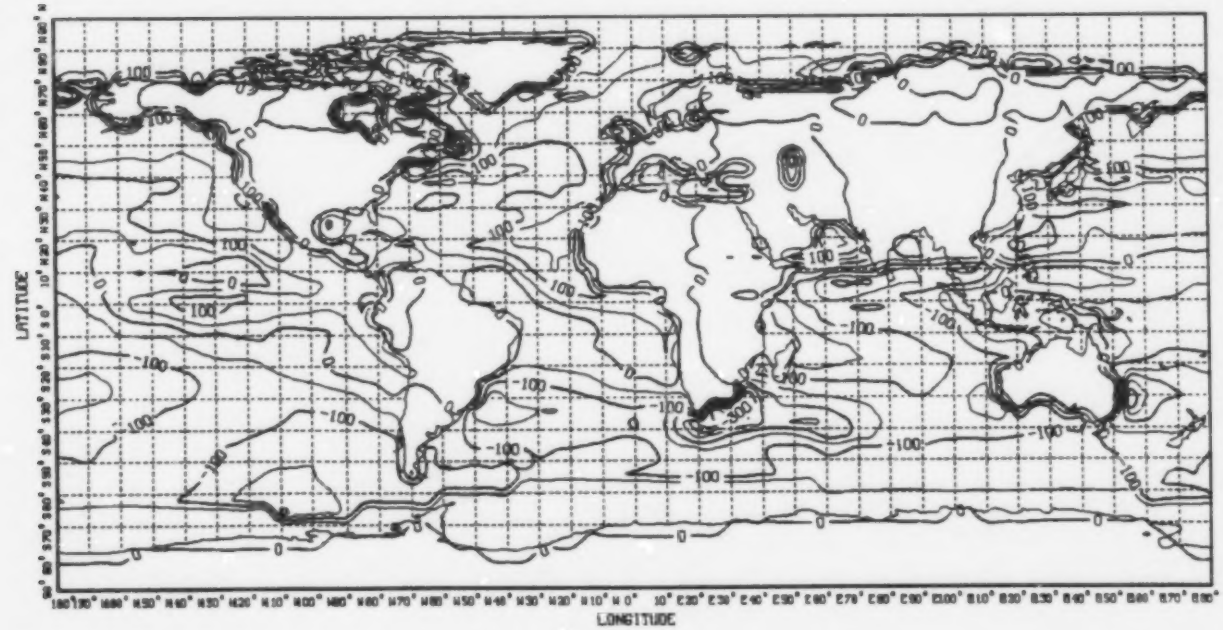

Figure 65

ECMWF JANUARY NET HEAT (W/M**2)

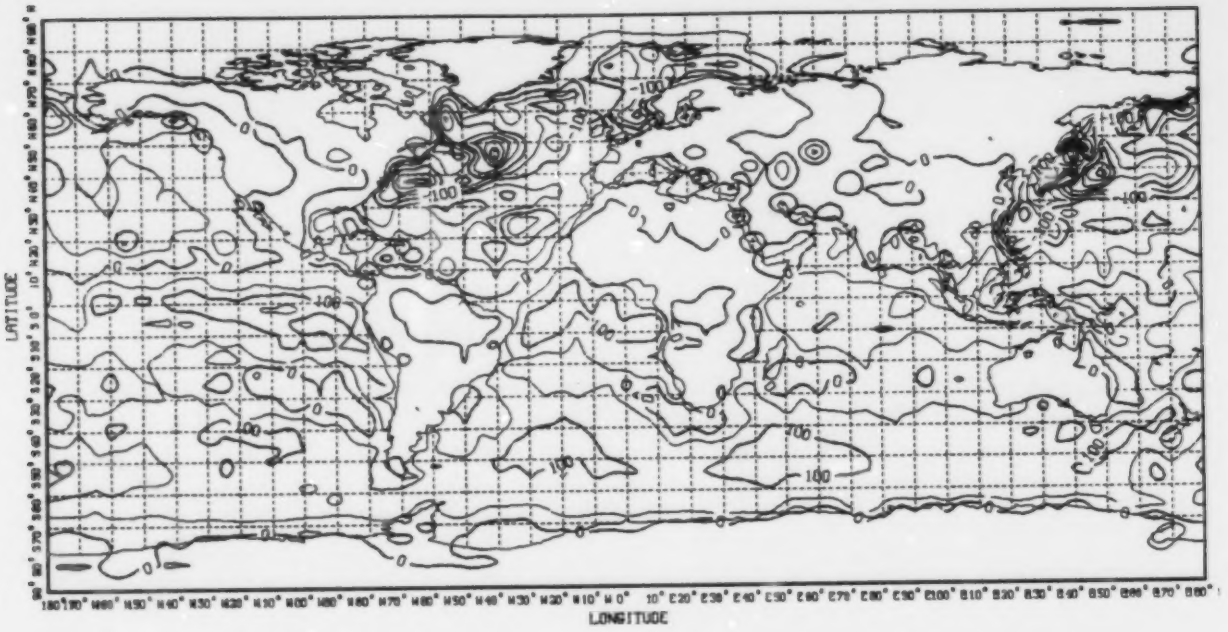

ECMWF JUNE NET HEAT (W/M**2)

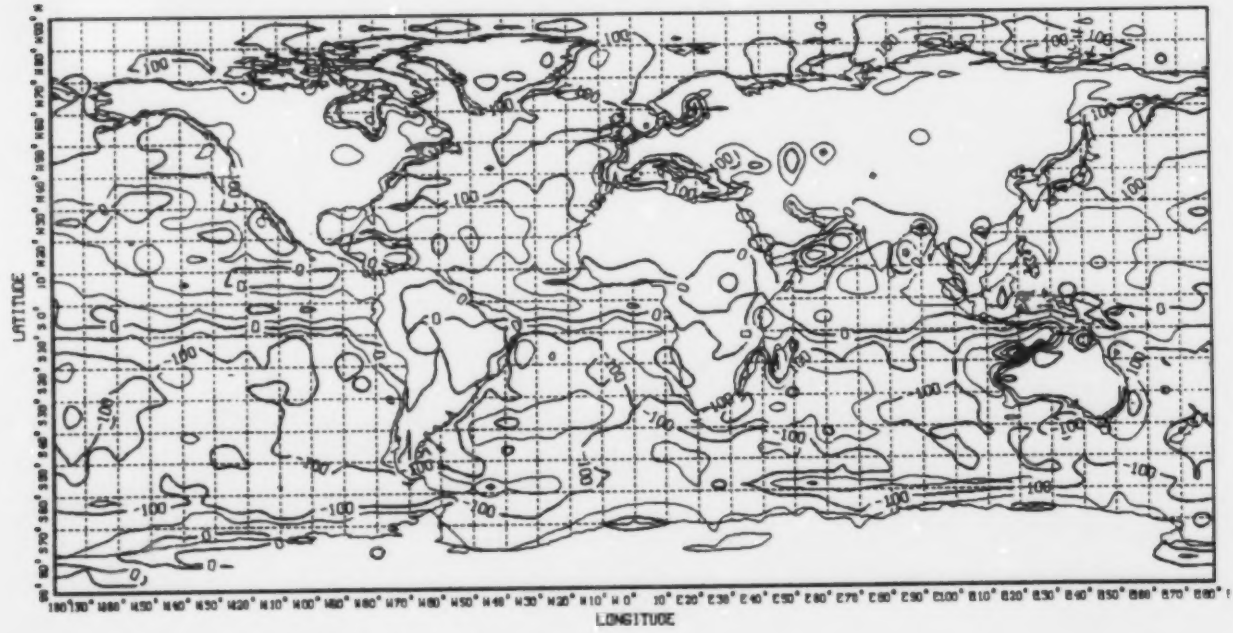

Figure 67

FRANCE (CNRM) WINTER NET HEAT (W/M**2)

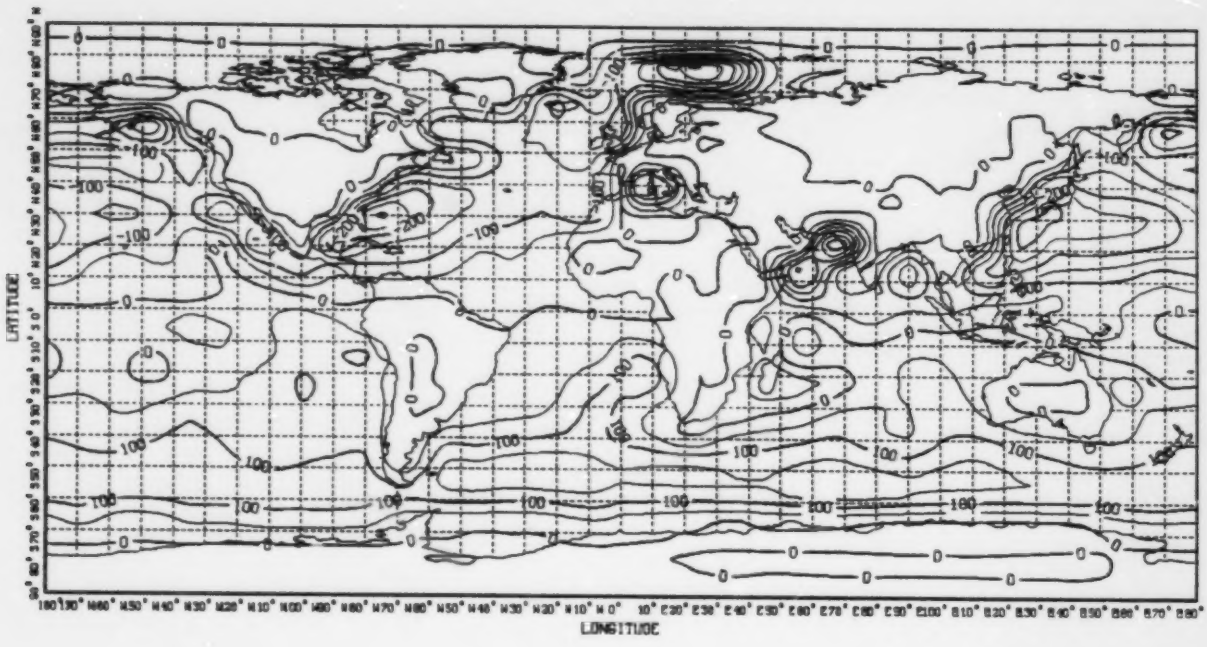

FRANCE (CNRM) SUMMER NET HEAT (W/M**2)

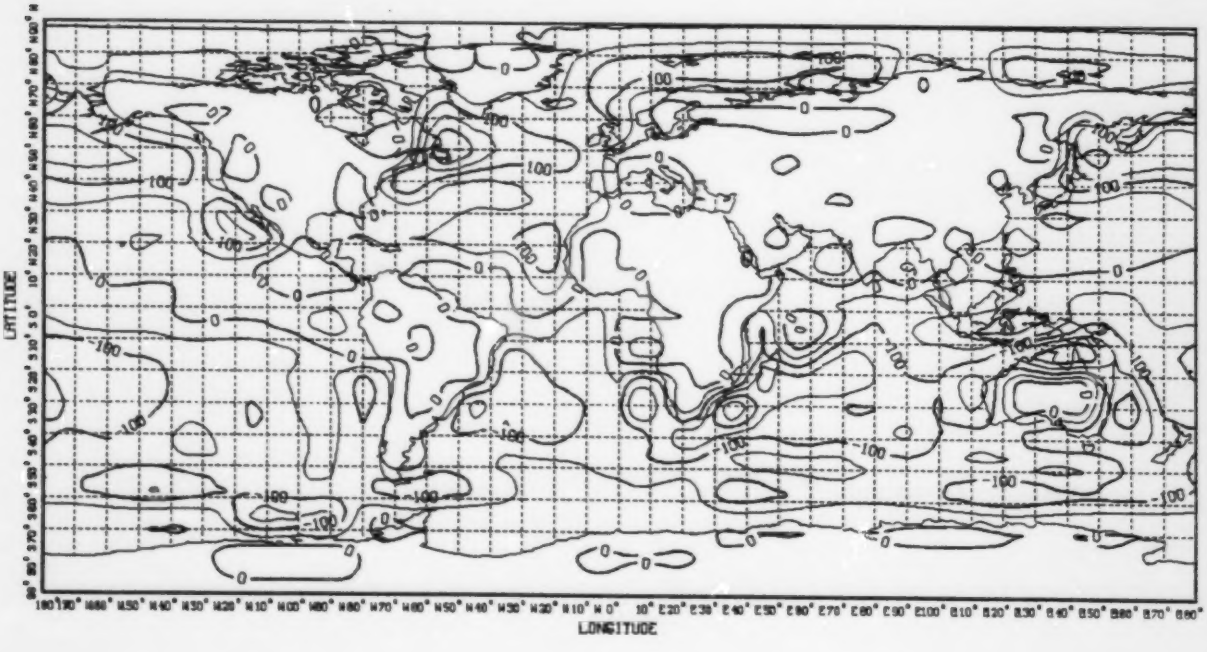

Figure 68

F R G (HAMBURG U) JANUARY NET HEAT (W/M**2)

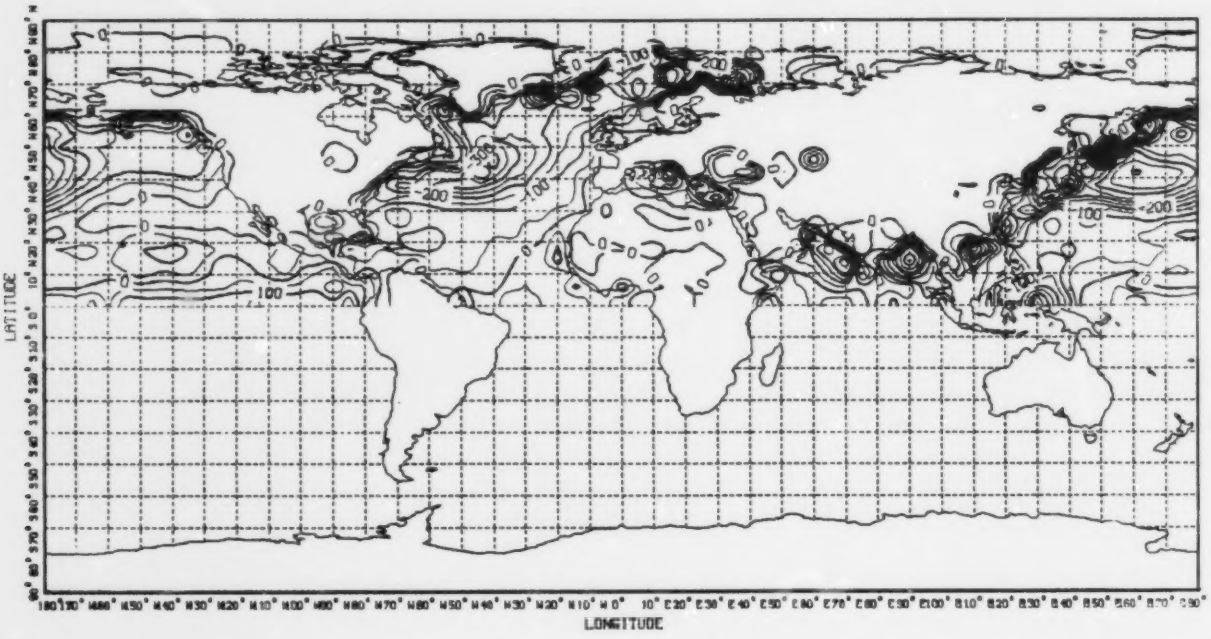

Figure 69

ESBENSEN AND KUSHNIR JANUARY NET RADIATION (W/M**2)

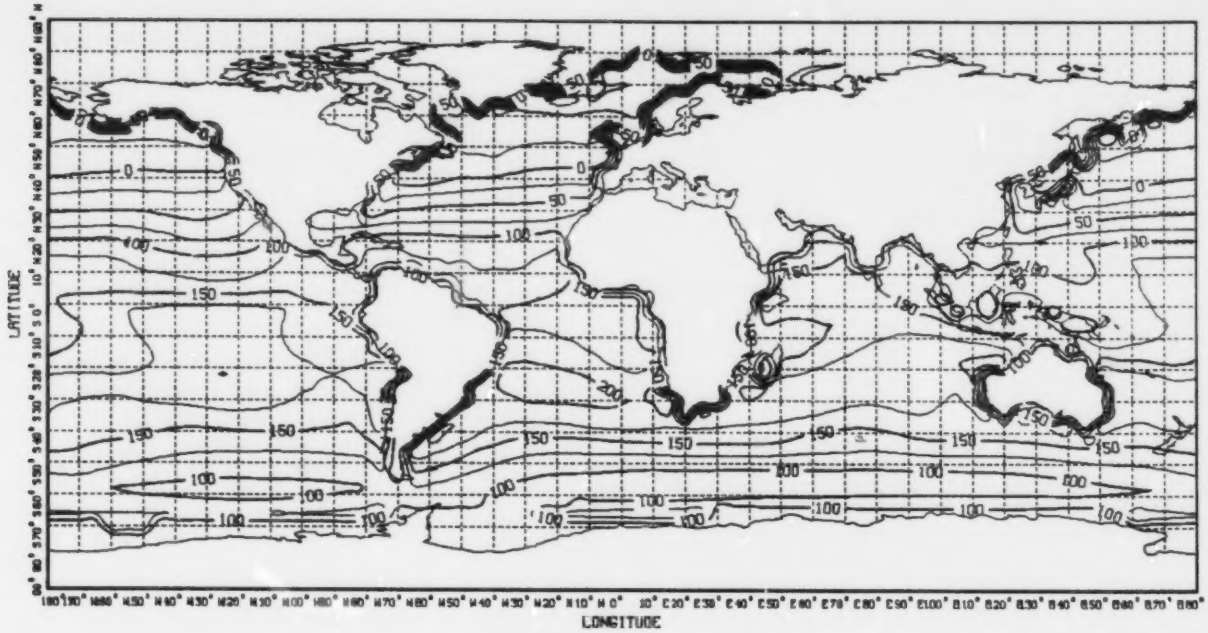

ESBENSEN AND KUSHNIR JULY NET RADIATION (W/M**2)

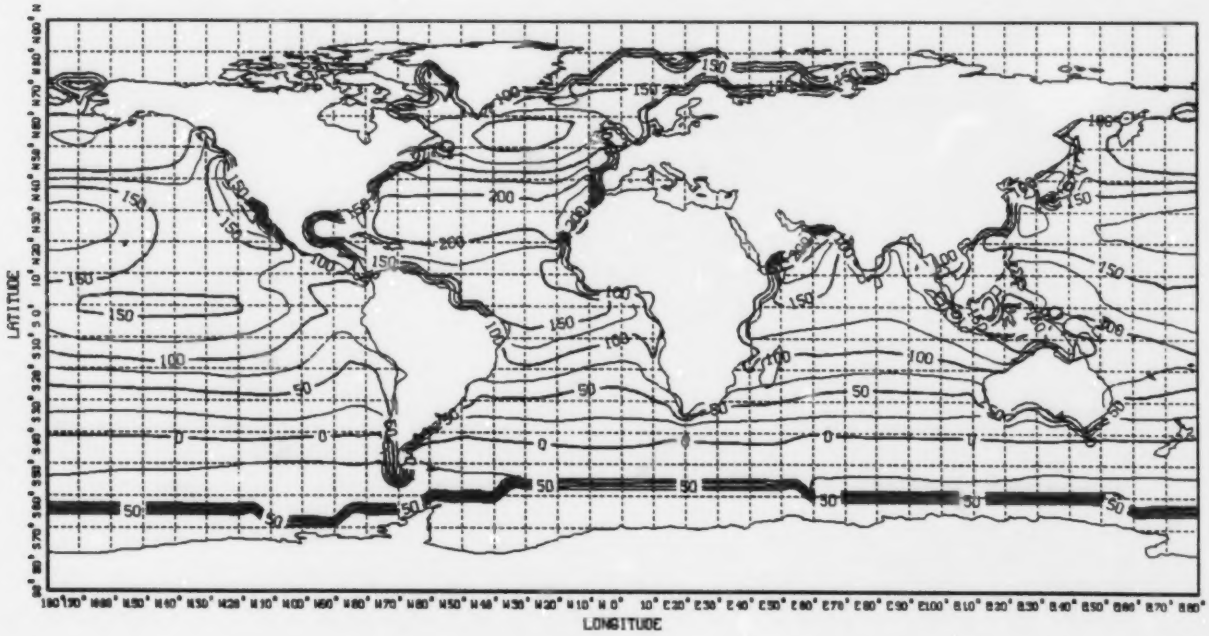

Figure 70

CANADA (CCC) WINTER NET RADIATION (W/M**2)

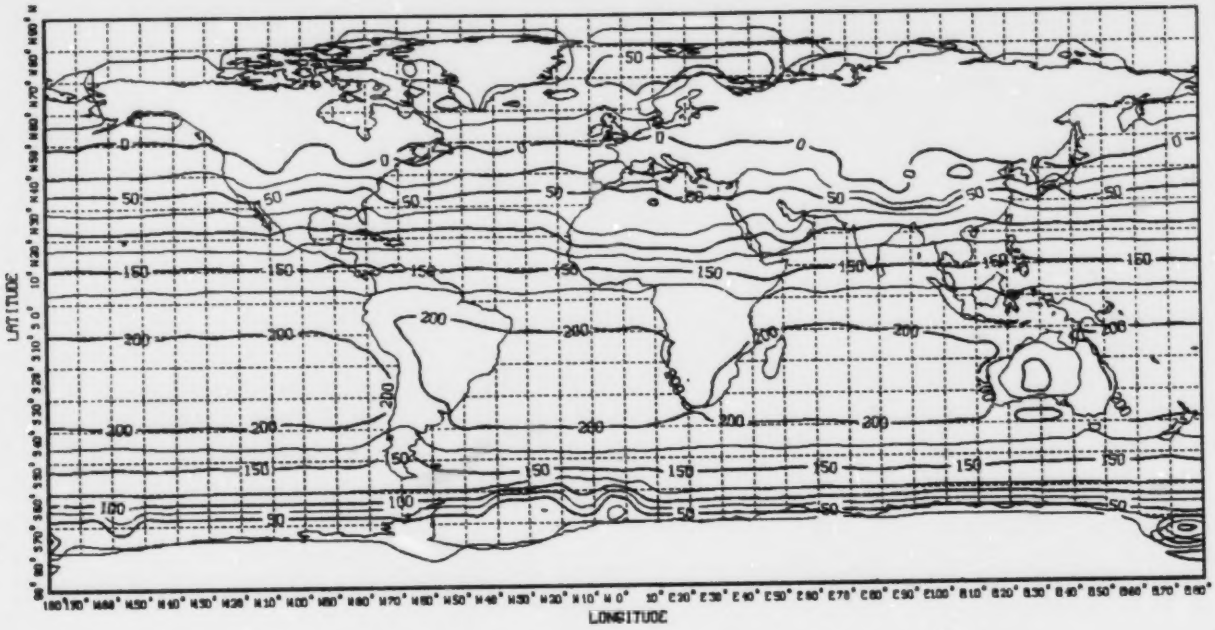

CANADA (CCC) SUMMER NET RADIATION (W/M**2)

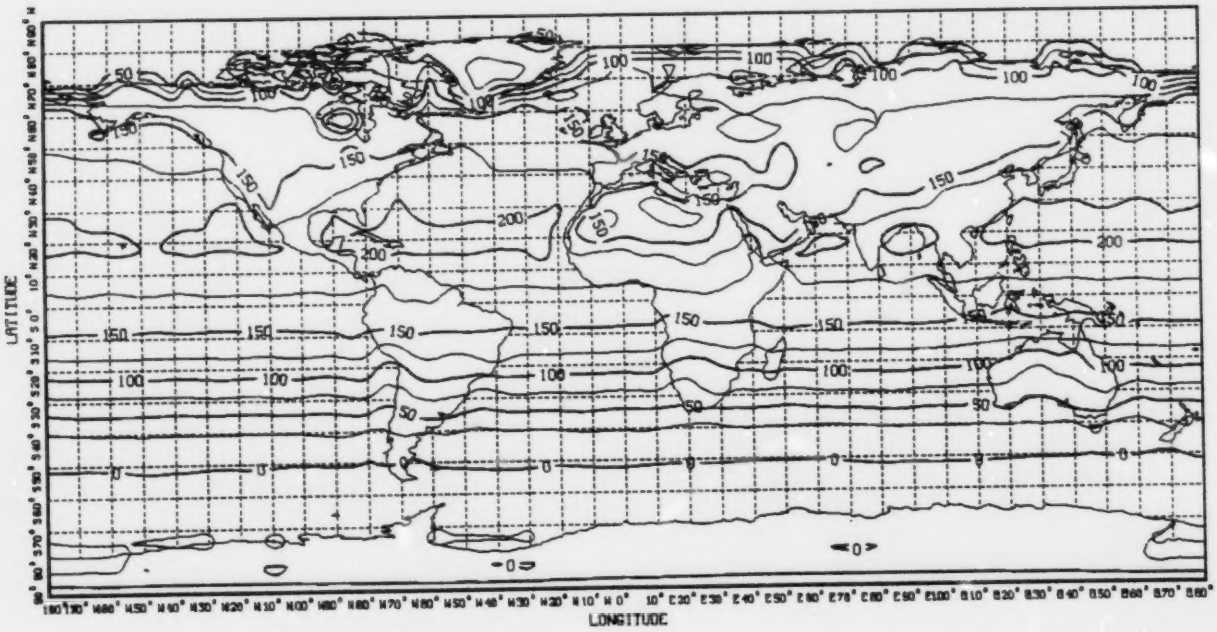

Figure 71

ENGLAND (BMO) WINTER NET RADIATION (W/M××2)

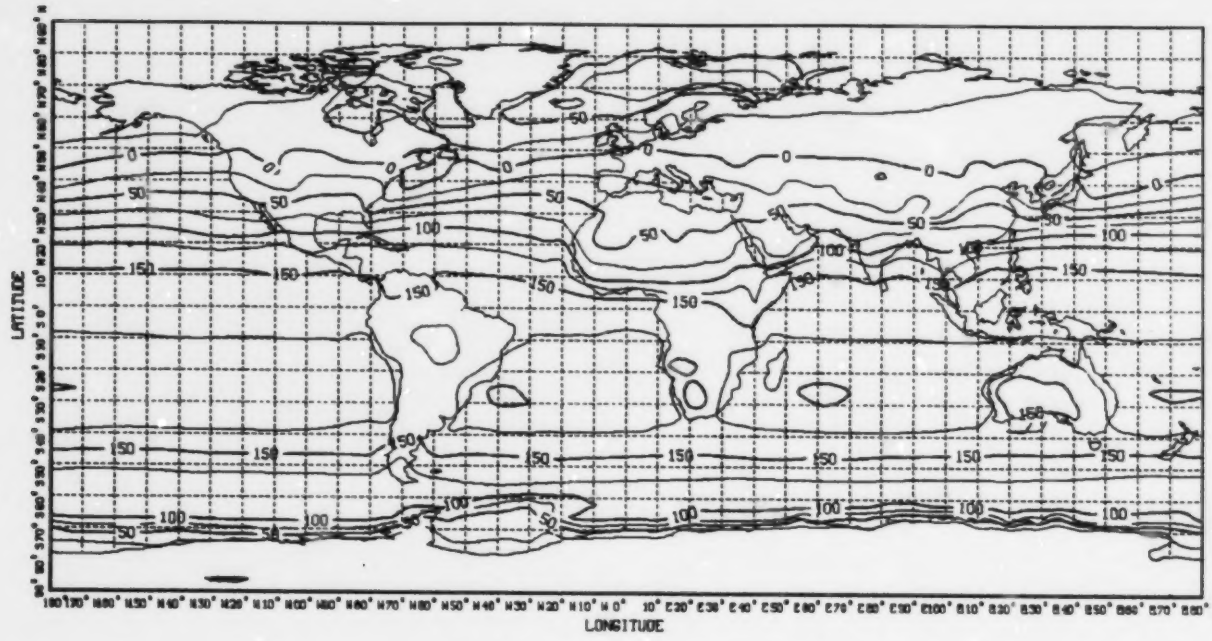

ENGLAND (BMO) SUMMER NET RADIATION (W/M××2)

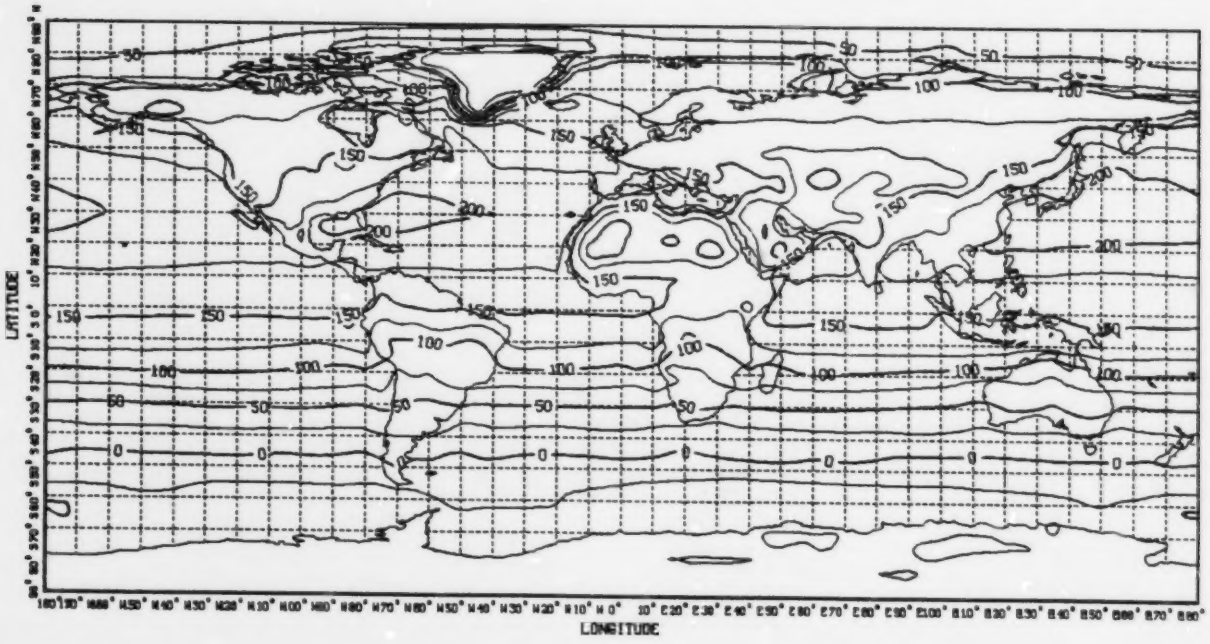

Figure 72

AUSTRALIA (BMRC) JANUARY NET RADIATION (W/M**2)

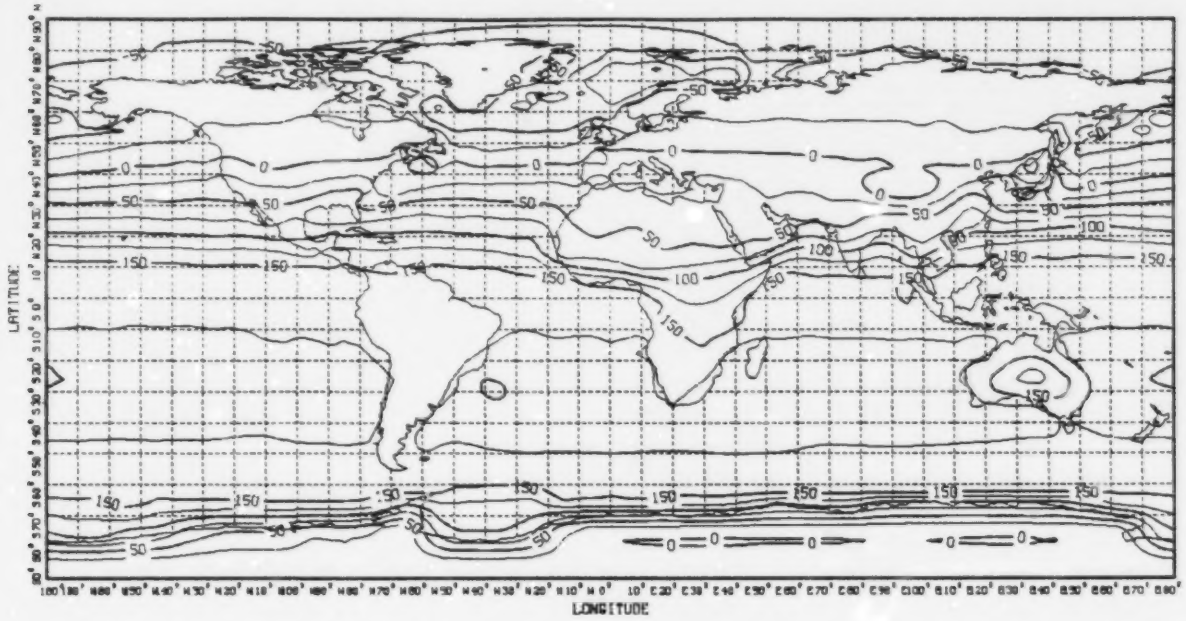

AUSTRALIA (BMRC) JULY NET RADIATION (W/M**2)

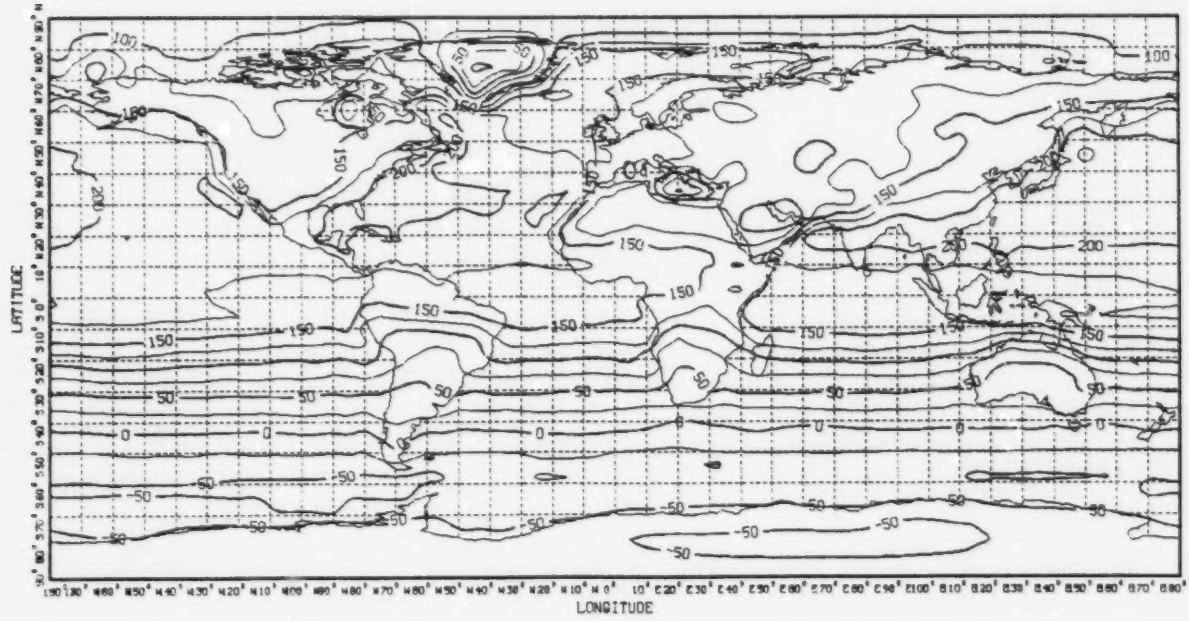

Figure 73

U S A (COLAI) JANUARY NET RADIATION (W/M××2)

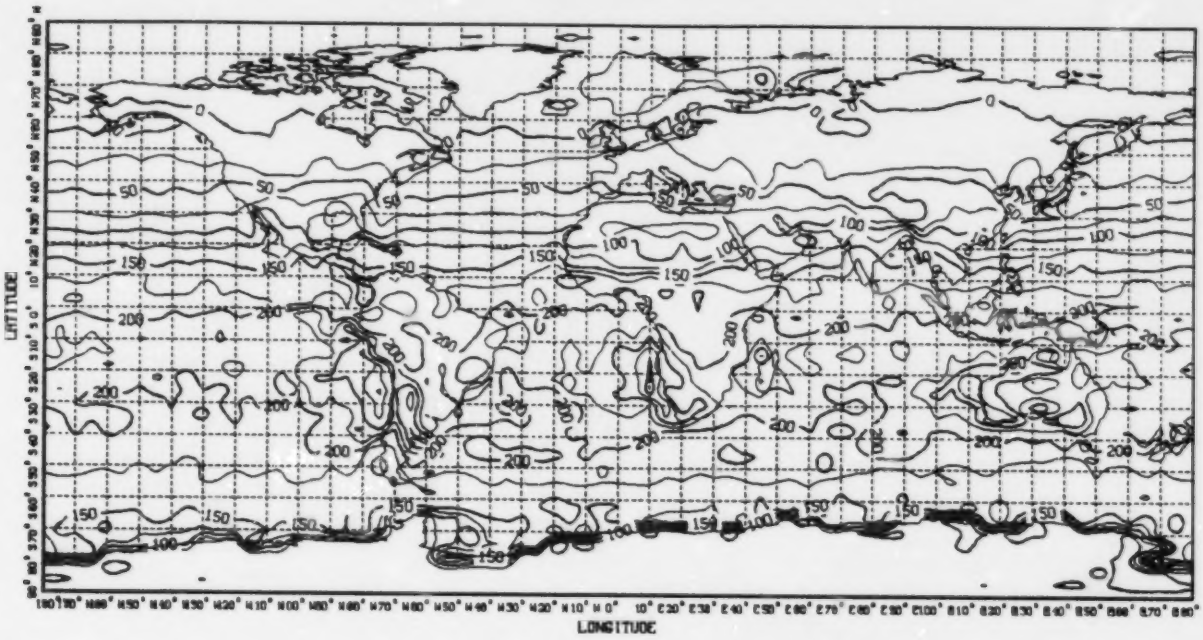

U S A (COLAI) JULY NET RADIATION (W/M××2)

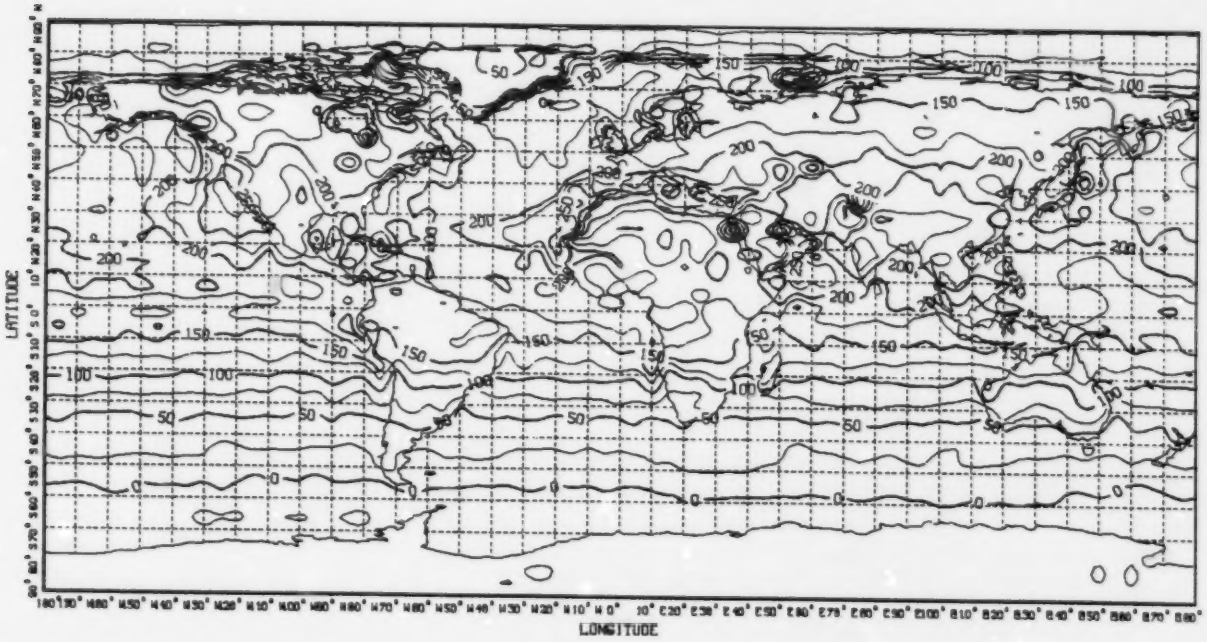

Figure 74

U S A (GFDL) JANUARY NET RADIATION (W/M**2)

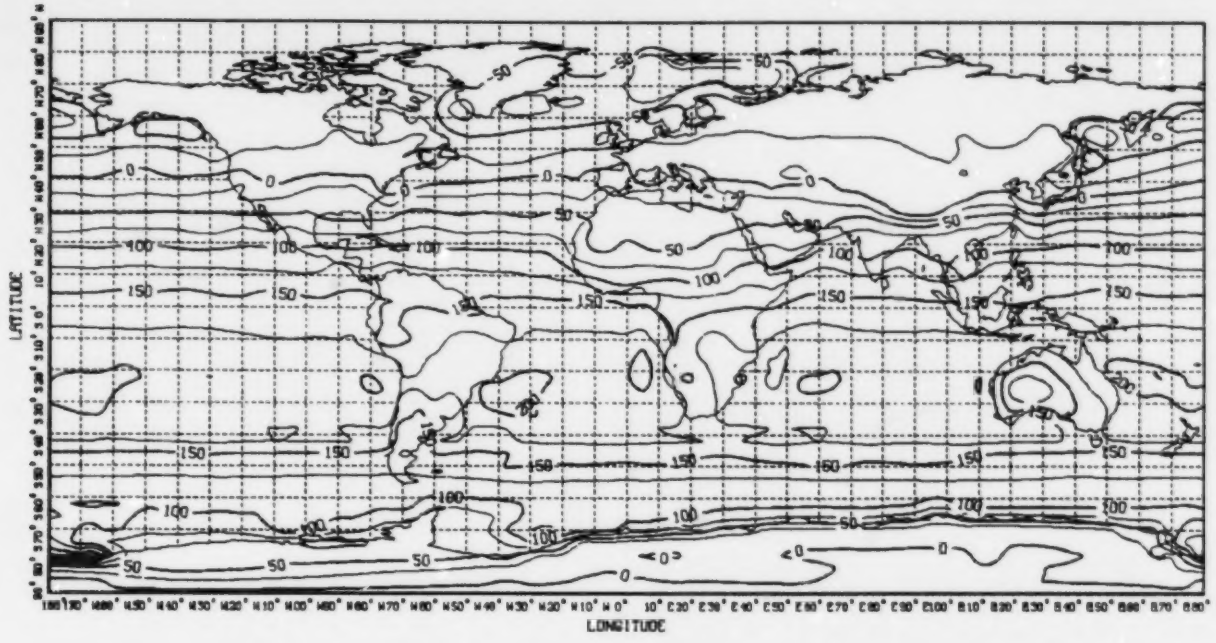

U S A (GFDL) JULY NET RADIATION (W/M**2)

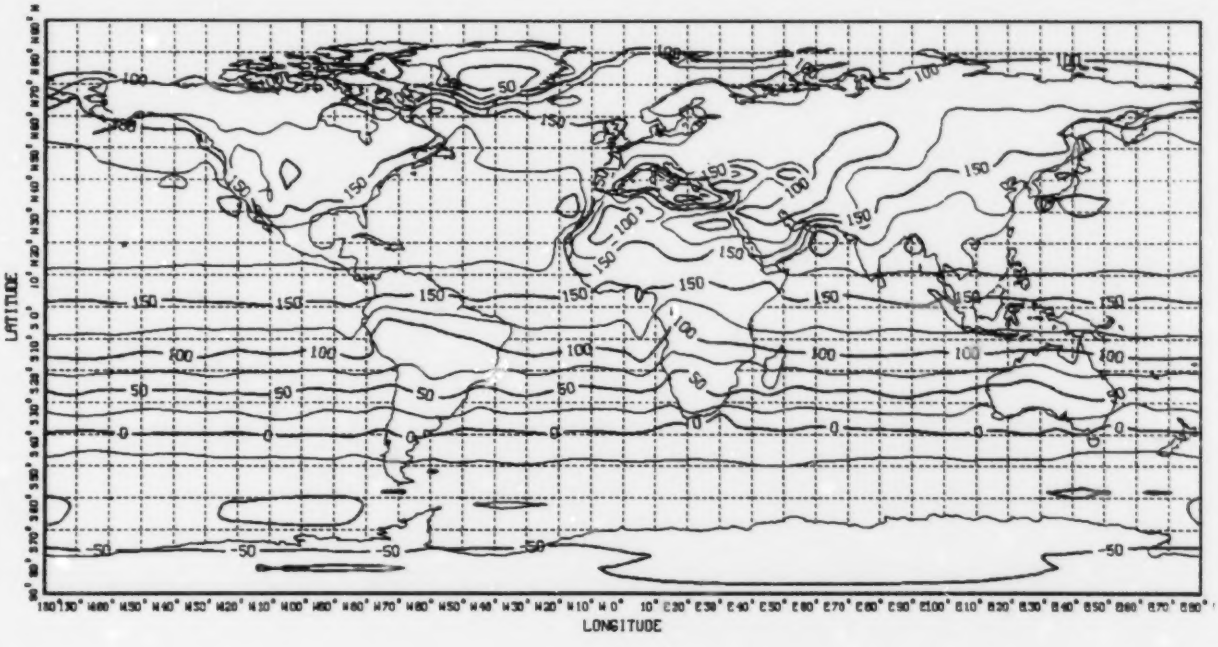

Figure 75

U S A (GISS) WINTER NET RADIATION (W/M**2)

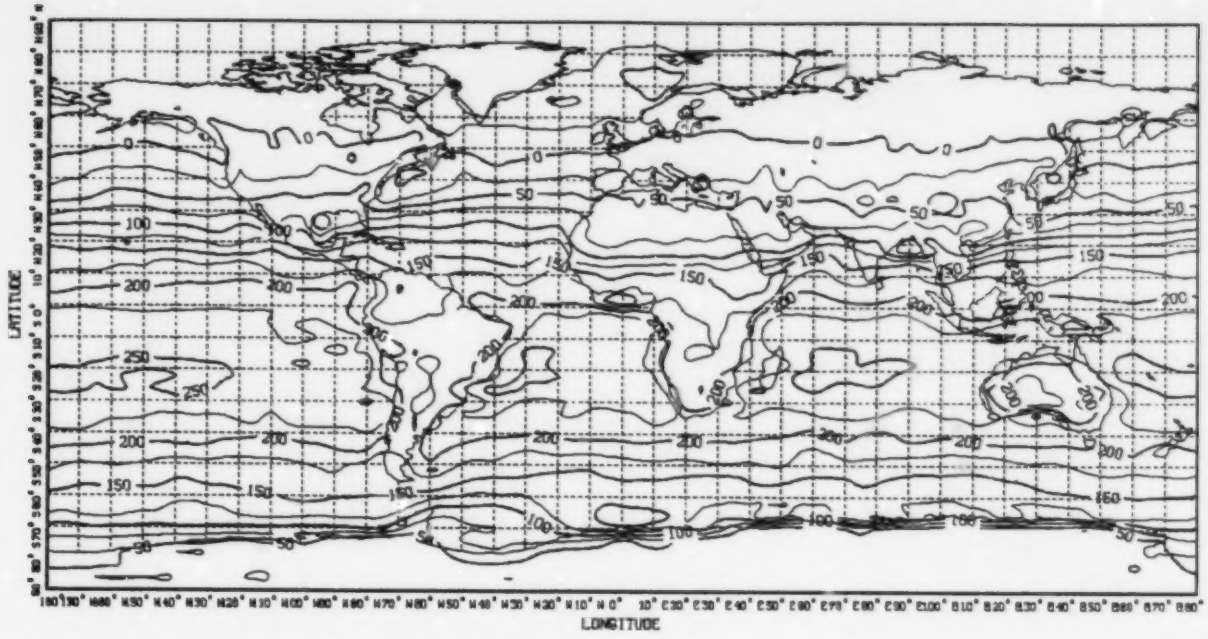

U S A (GISS) SUMMER NET RADIATION (W/M**2)

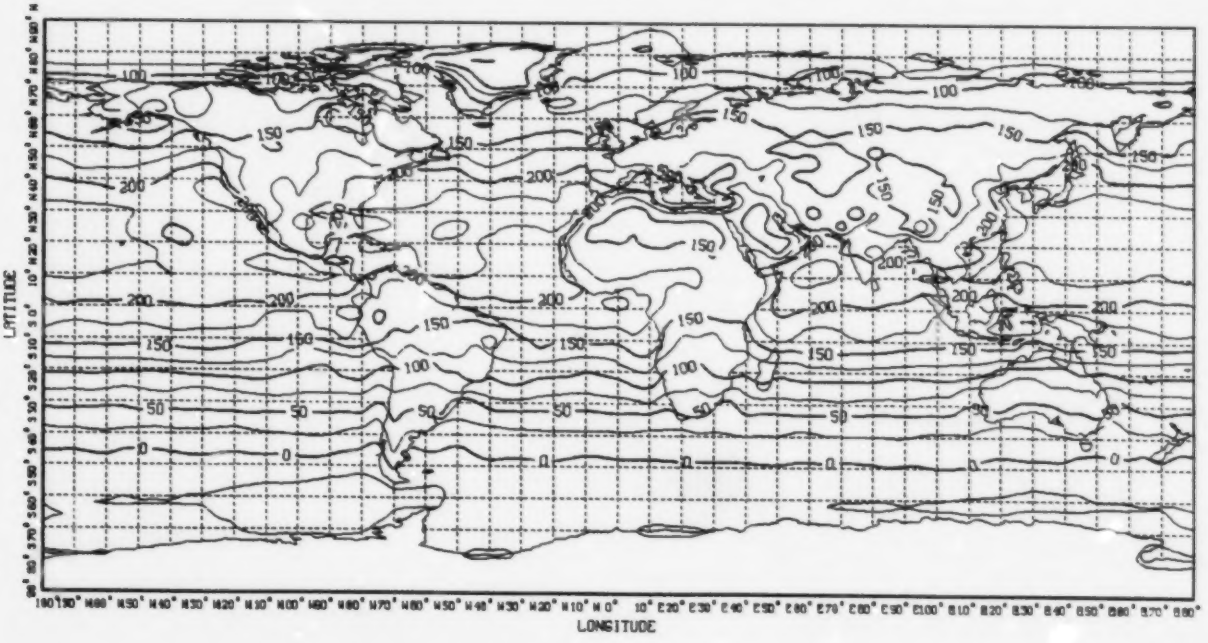

Figure 76

U S A (NCAR) JANUARY NET RADIATION (W/M**2)

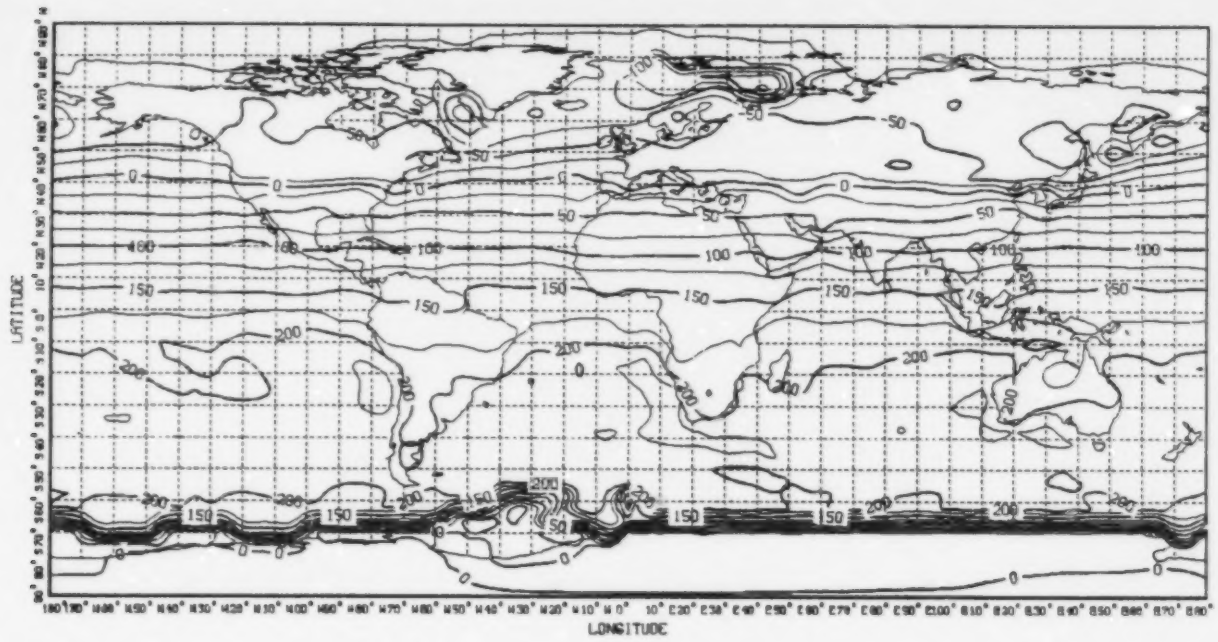

U S A (NCAR) JULY NET RADIATION (W/M**2)

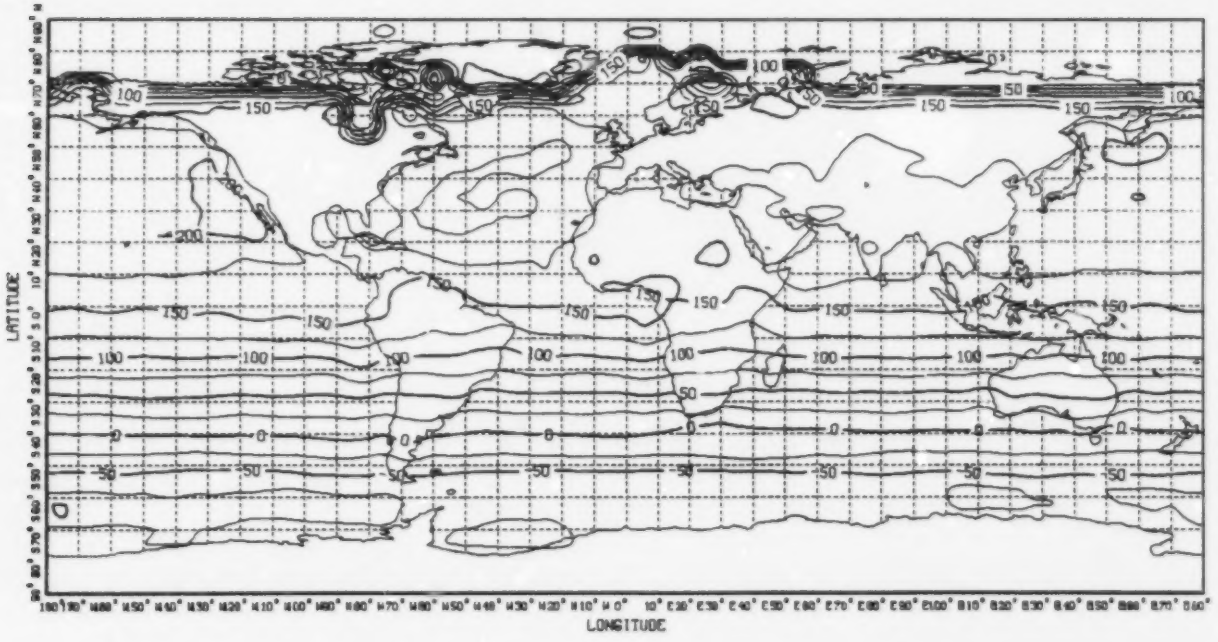

Figure 77

U S A (OSU) JANUARY NET RADIATION (W/M**2)

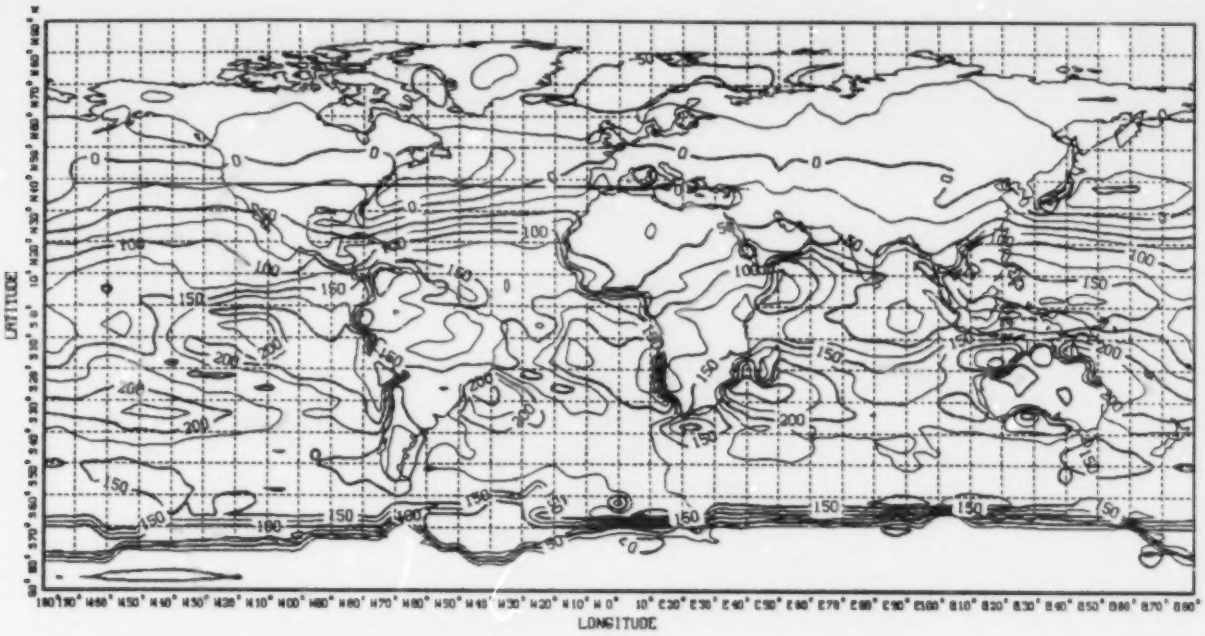

U S A (OSU) JULY NET RADIATION (W/M**2)

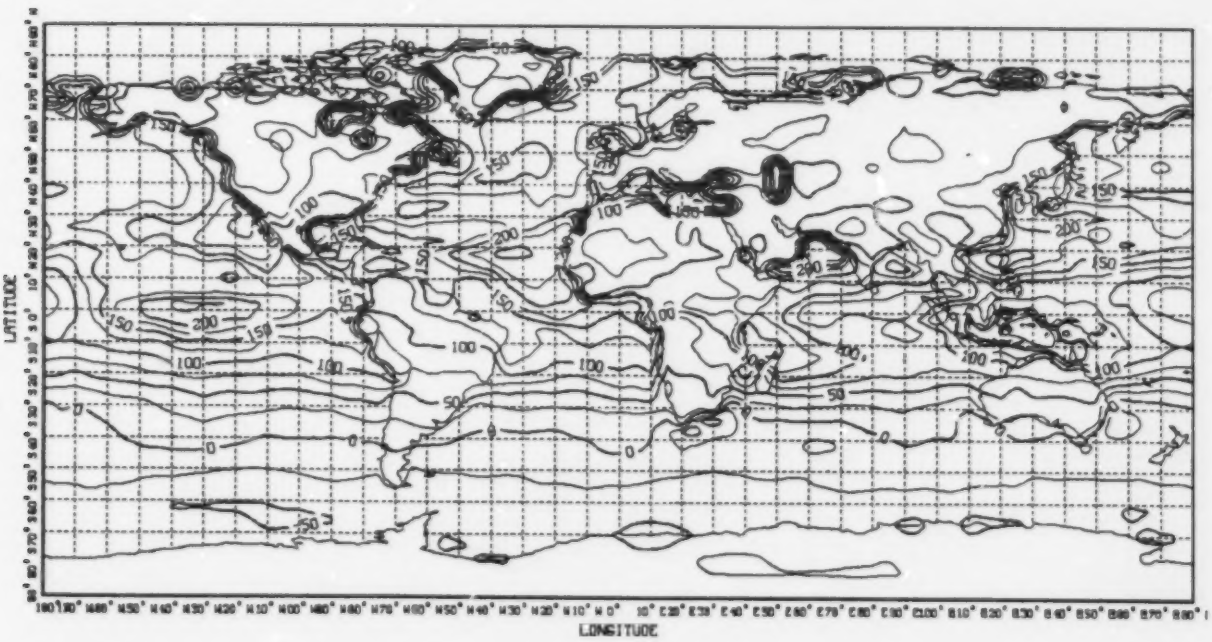

Figure 78

JAPAN (MRI) JANUARY NET RADIATION (W/M××2)

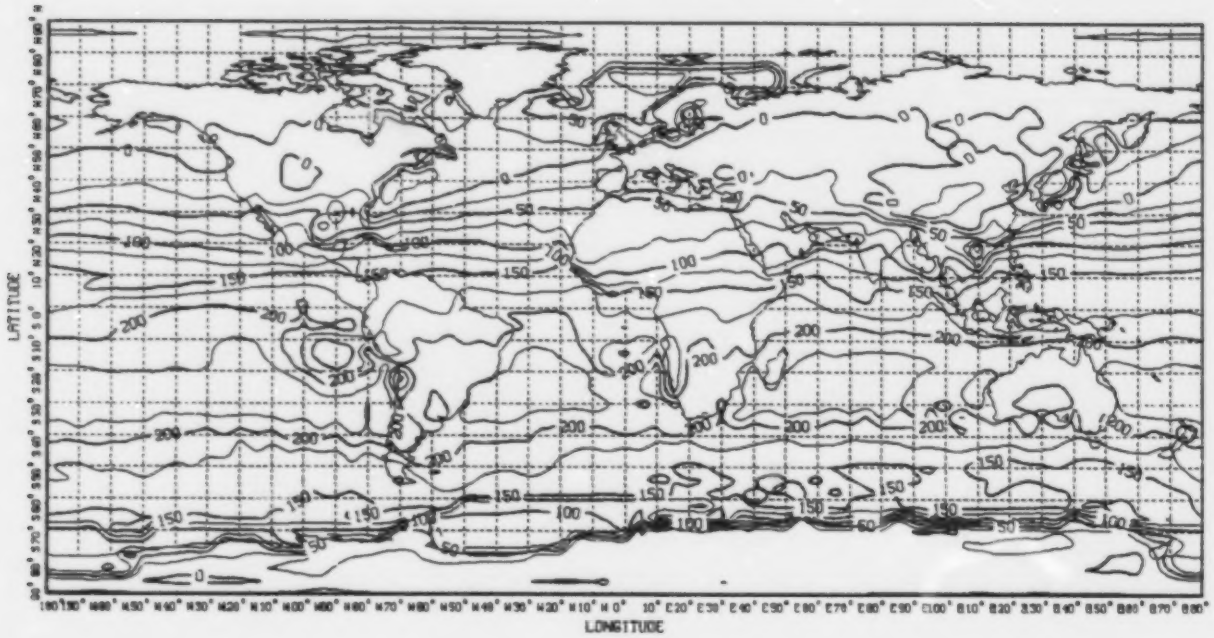

JAPAN (MRI) JULY NET RADIATION (W/M××2)

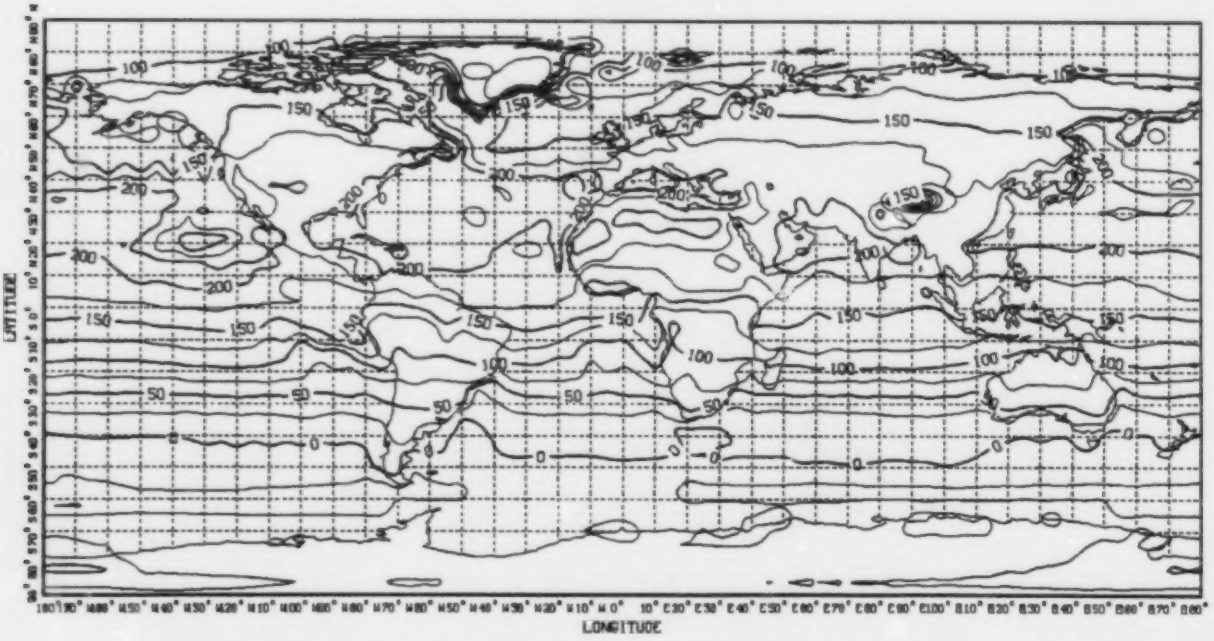

Figure 79

ECMWF JANUARY NET RADIATION (W/M××2)

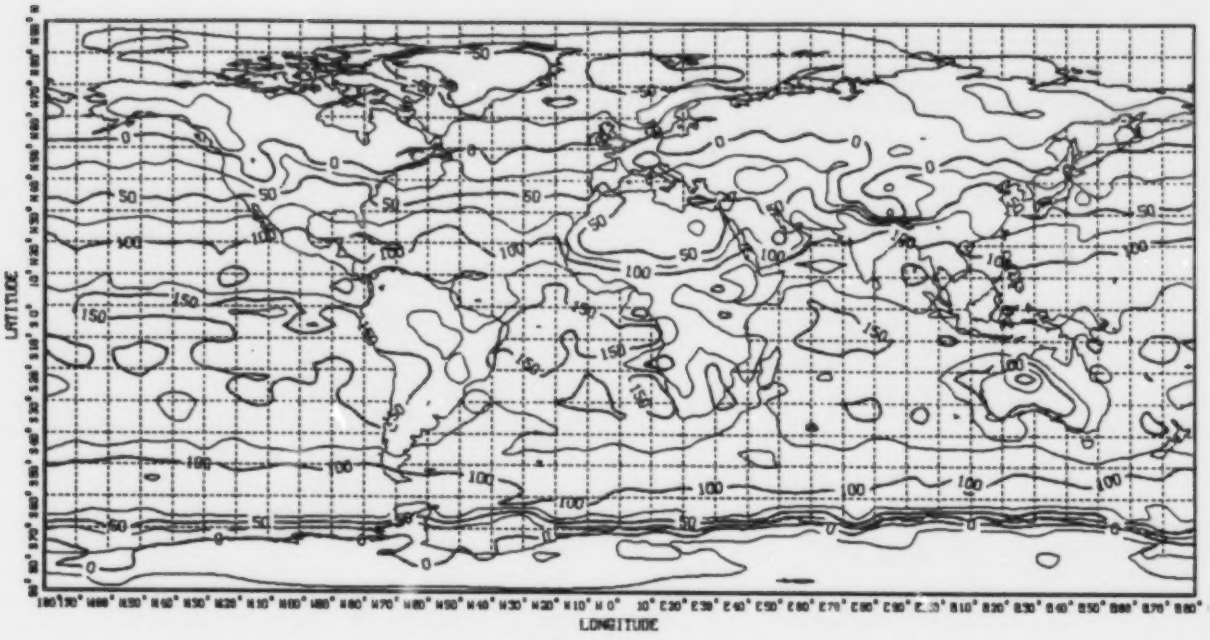

ECMWF JUNE NET RADIATION (W/M××2)

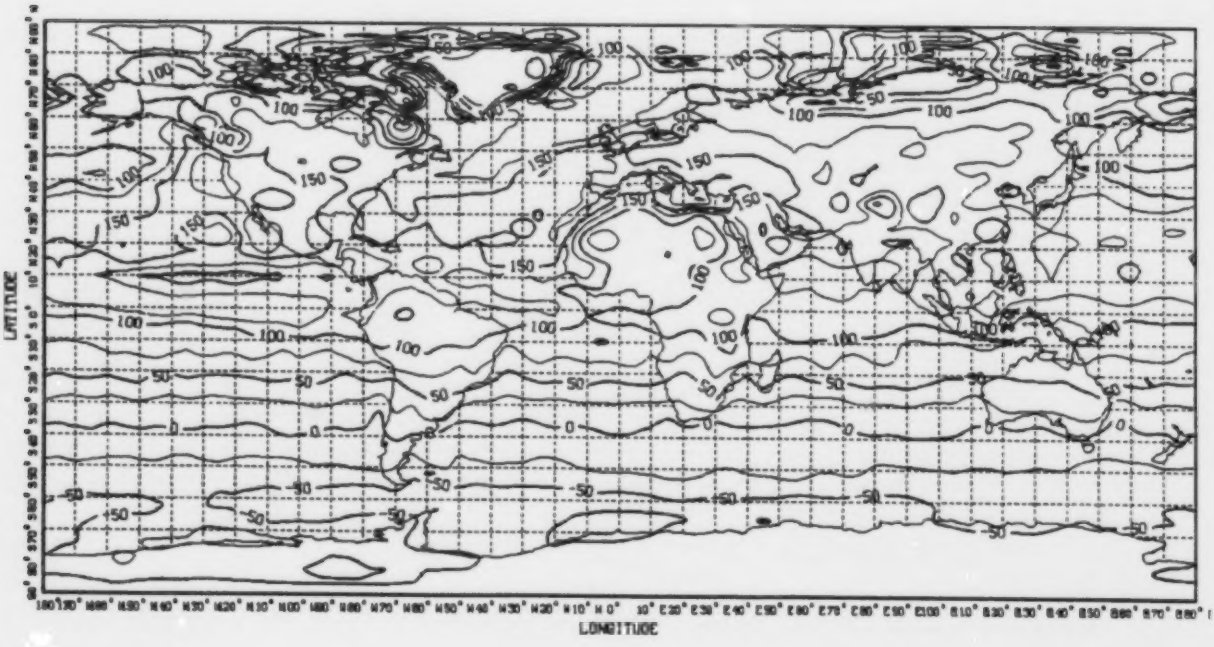

Figure 80

FRANCE (CNRM) WINTER NET RADIATION (W/M**2)

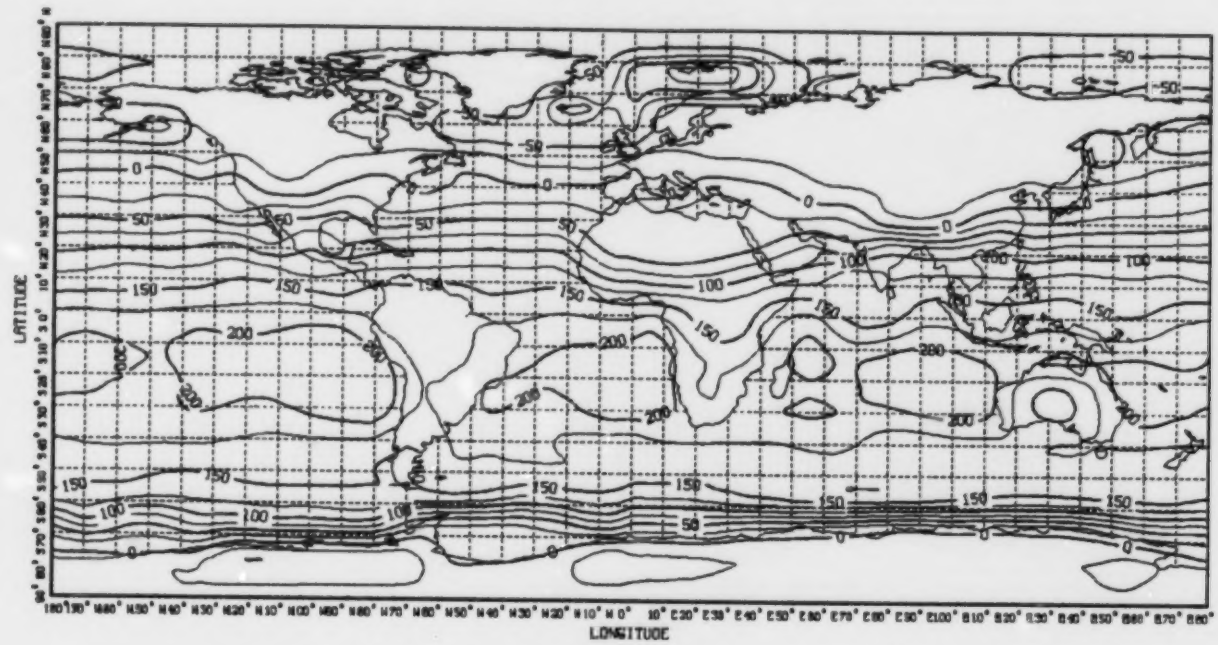

FRANCE (CNRM) SUMMER NET RADIATION (W/M**2)

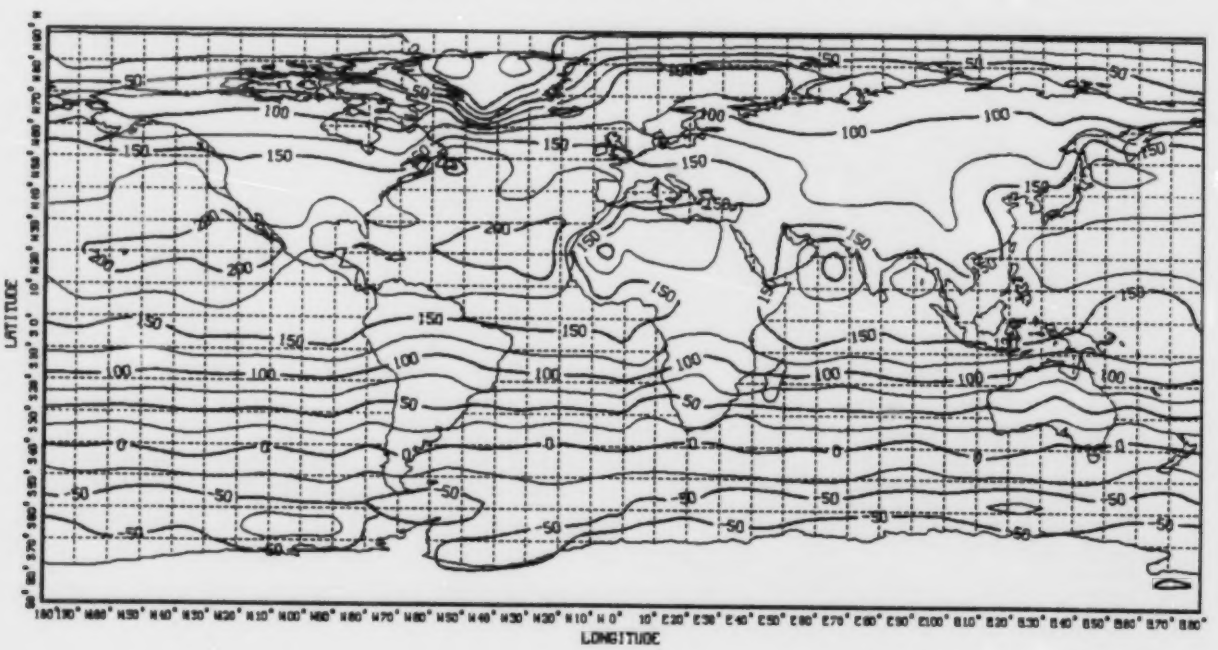

Figure 81

F R G (HAMBURG U) JANUARY NET RADIATION (W/M**2)

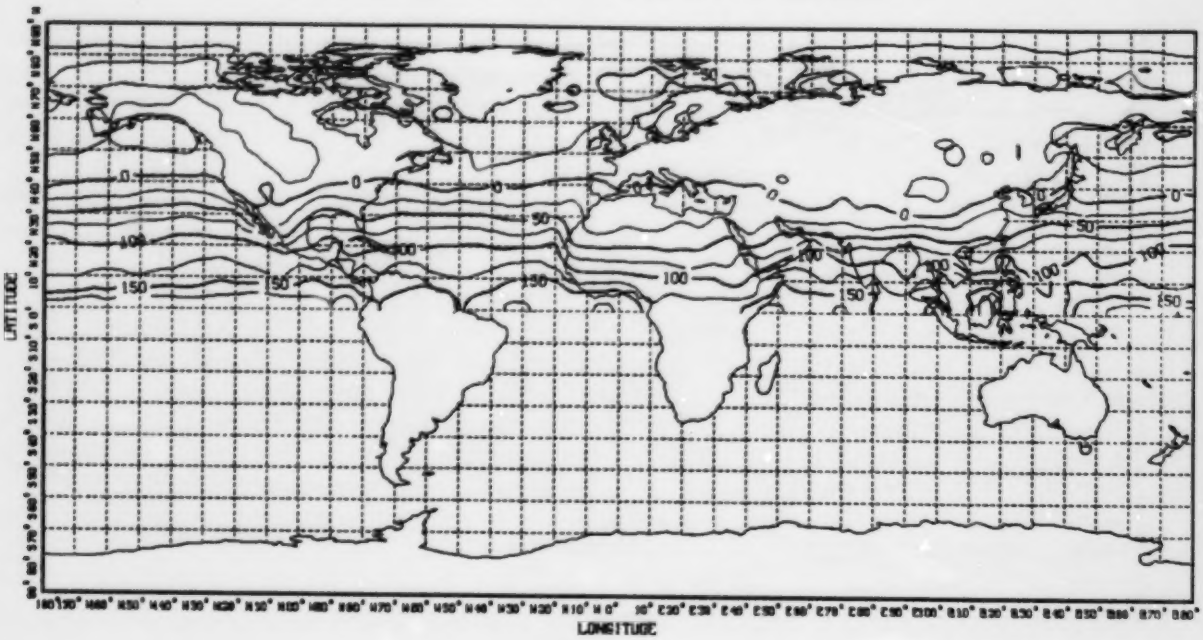

Figure 82

ESBENSEN AND KUSHNIR JANUARY LATENT HEAT (W/M**2)

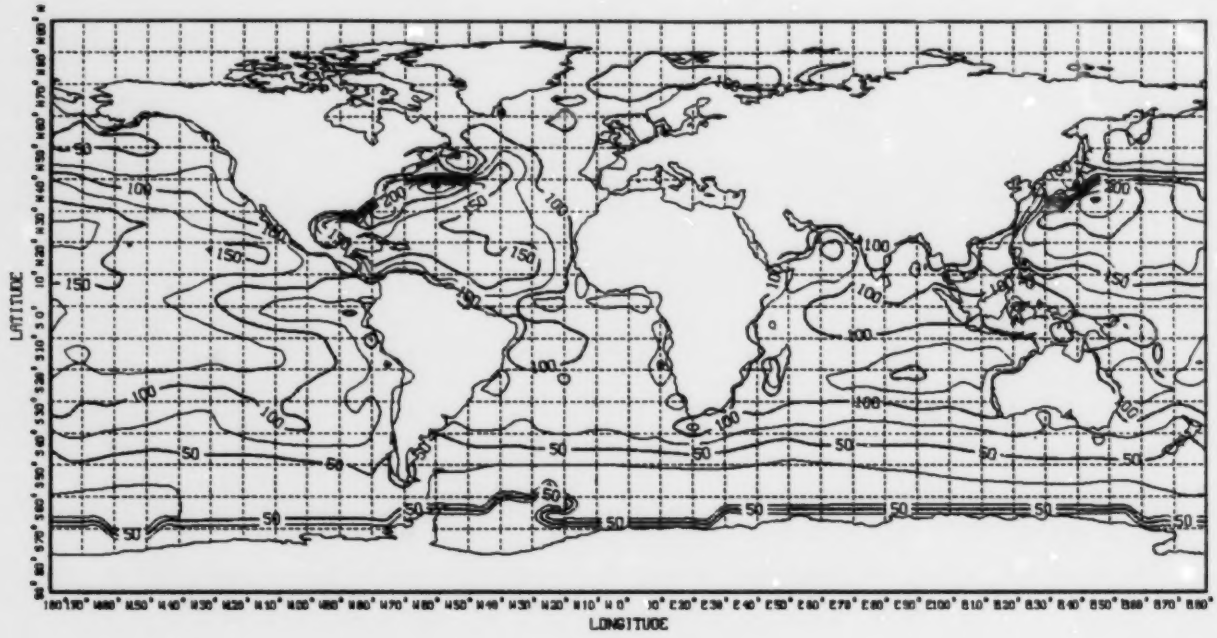

ESBENSEN AND KUSHNIR JULY LATENT HEAT (W/M**2)

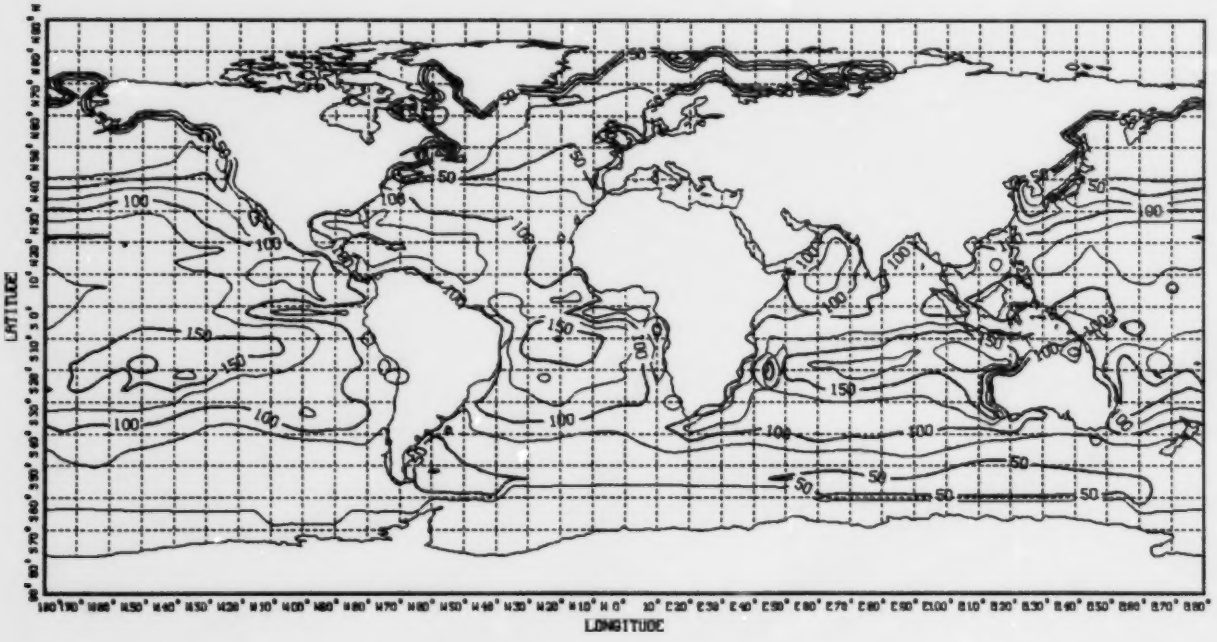

Figure 83

CANADA (CCC) WINTER LATENT HEAT (W/M**2)

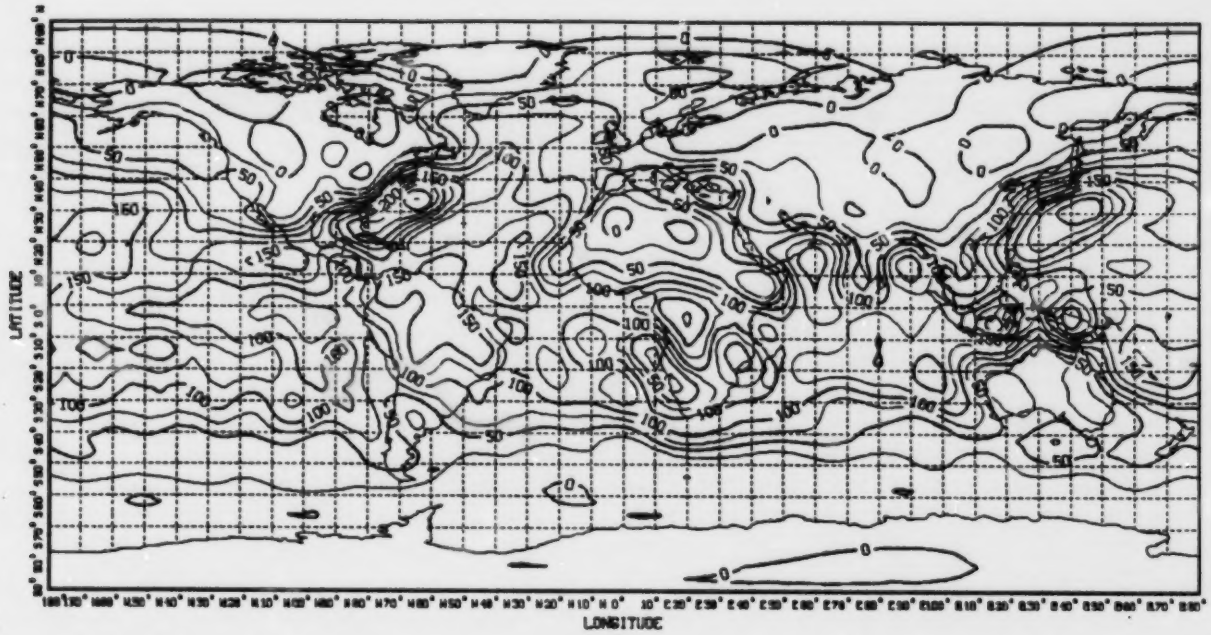

CANADA (CCC) SUMMER LATENT HEAT (W/M**2)

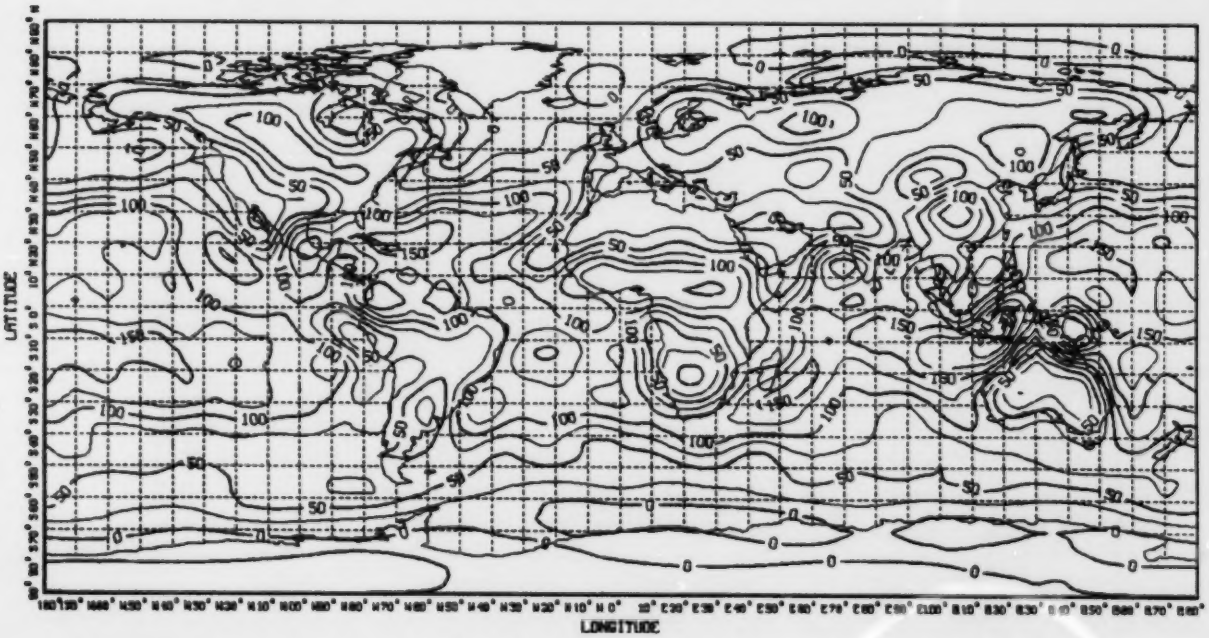

Figure 84

ENGLAND (BMO) WINTER LATENT HEAT (W/M××2)

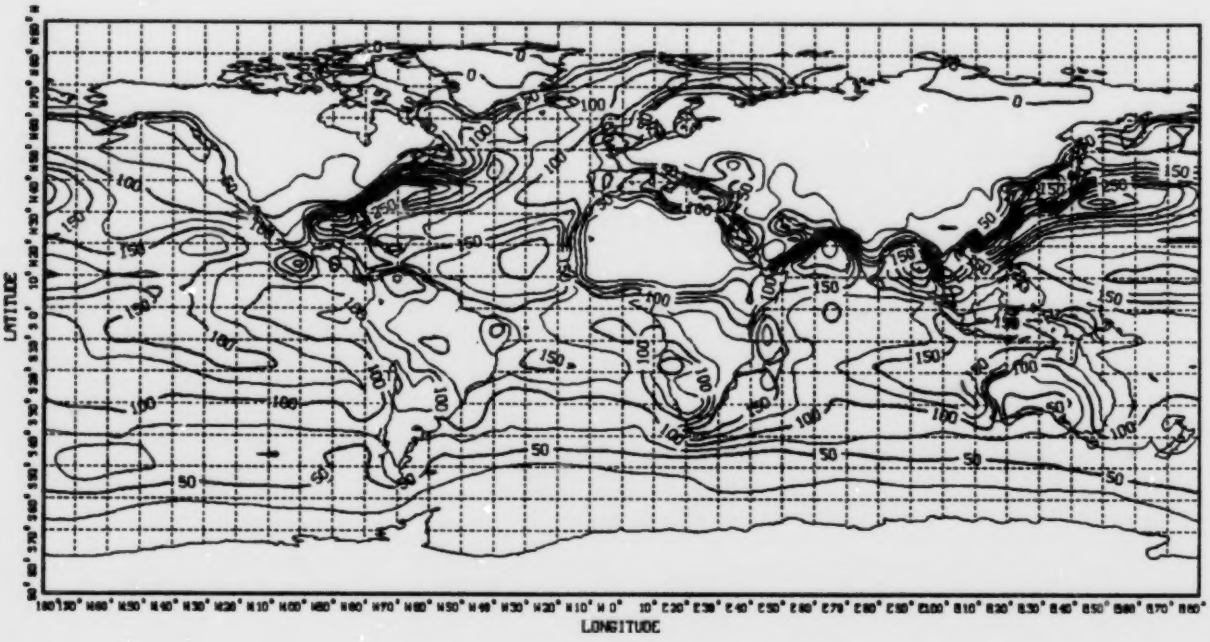

ENGLAND (BMO) SUMMER LATENT HEAT (W/M××2)

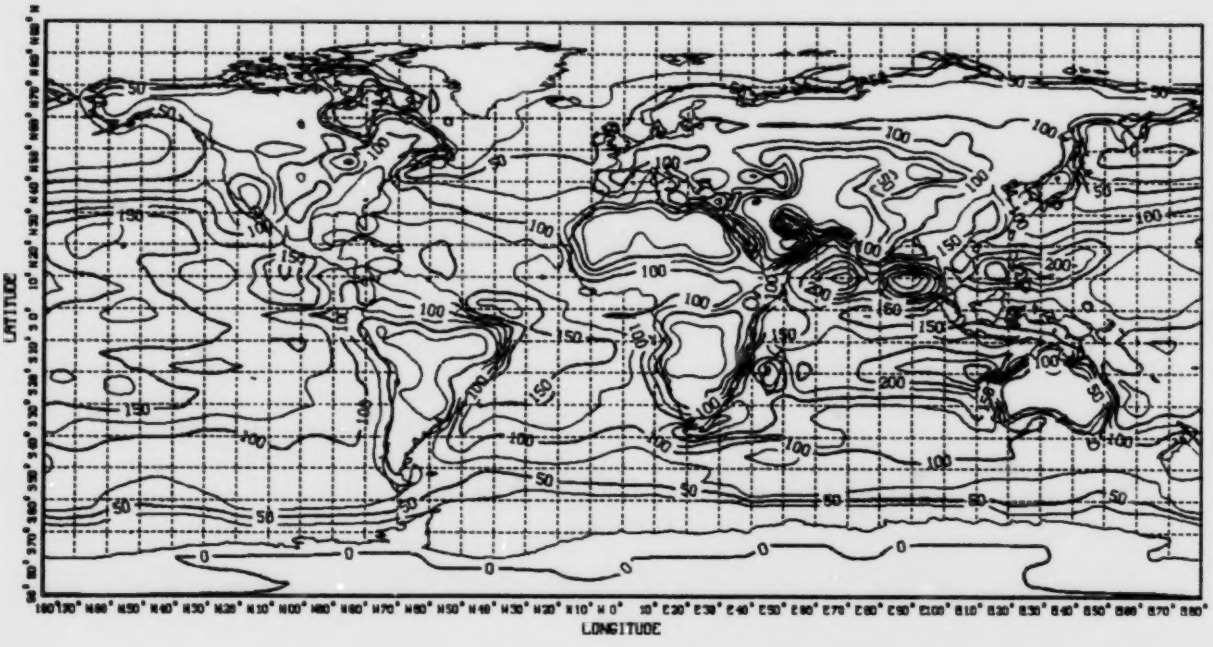

Figure 85

AUSTRALIA (BMRC) JANUARY LATENT HEAT (W/M**2)

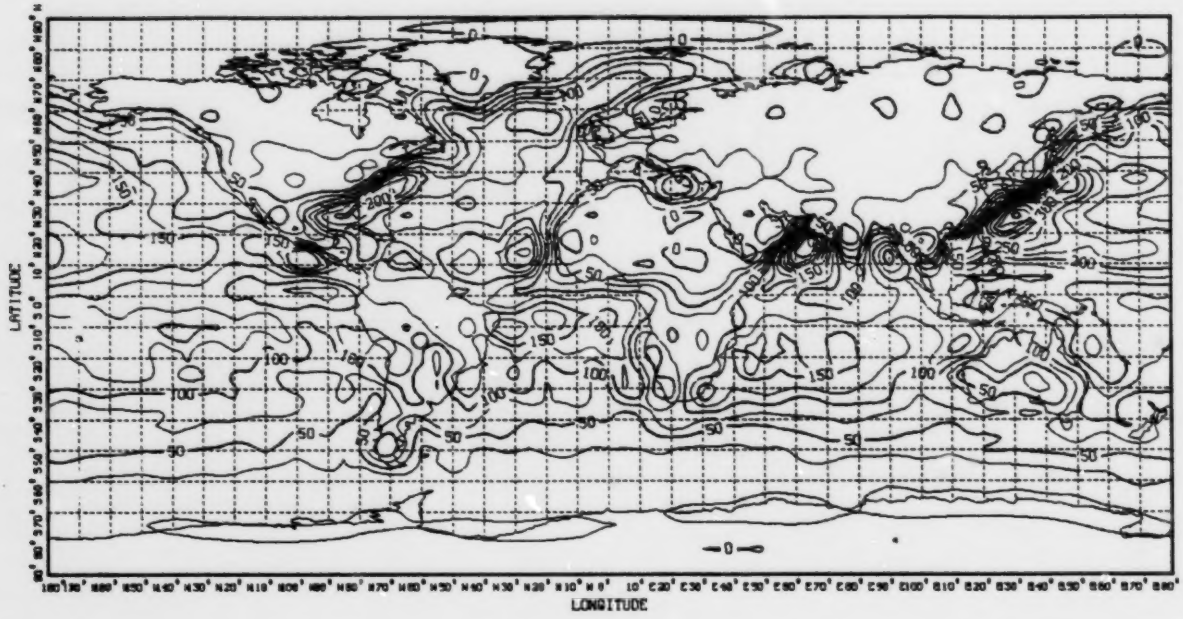

AUSTRALIA (BMRC) JULY LATENT HEAT (W/M**2)

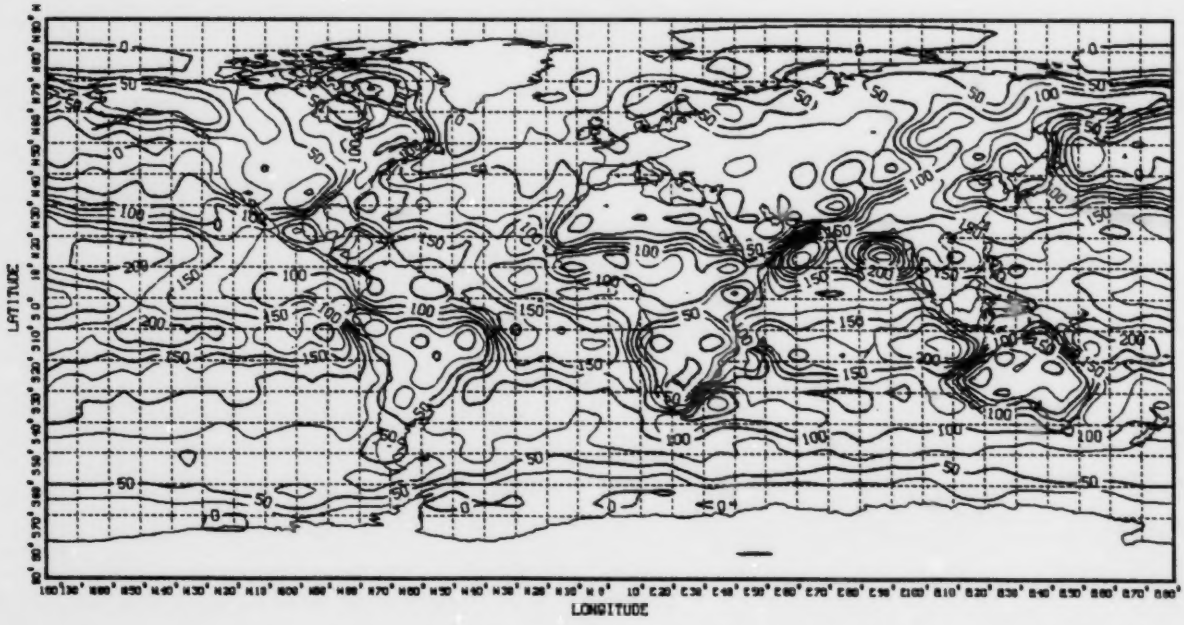

Figure 86

U S A (COLAI) JANUARY LATENT HEAT (W/M**2)

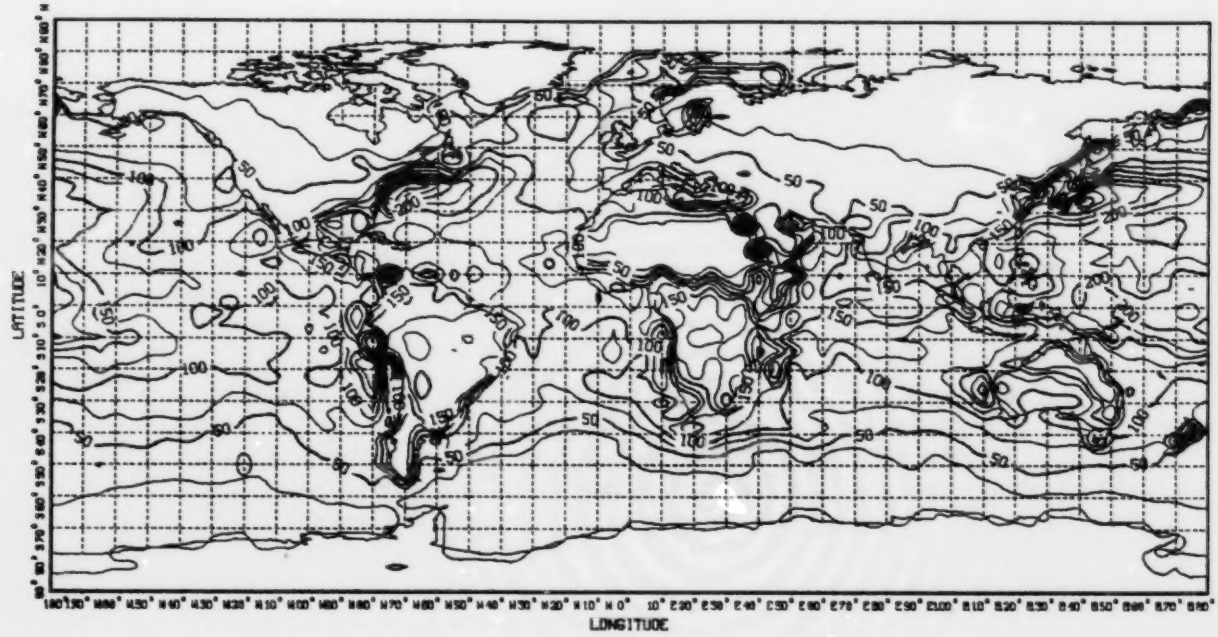

U S A (COLAI) JULY LATENT HEAT (W/M**2)

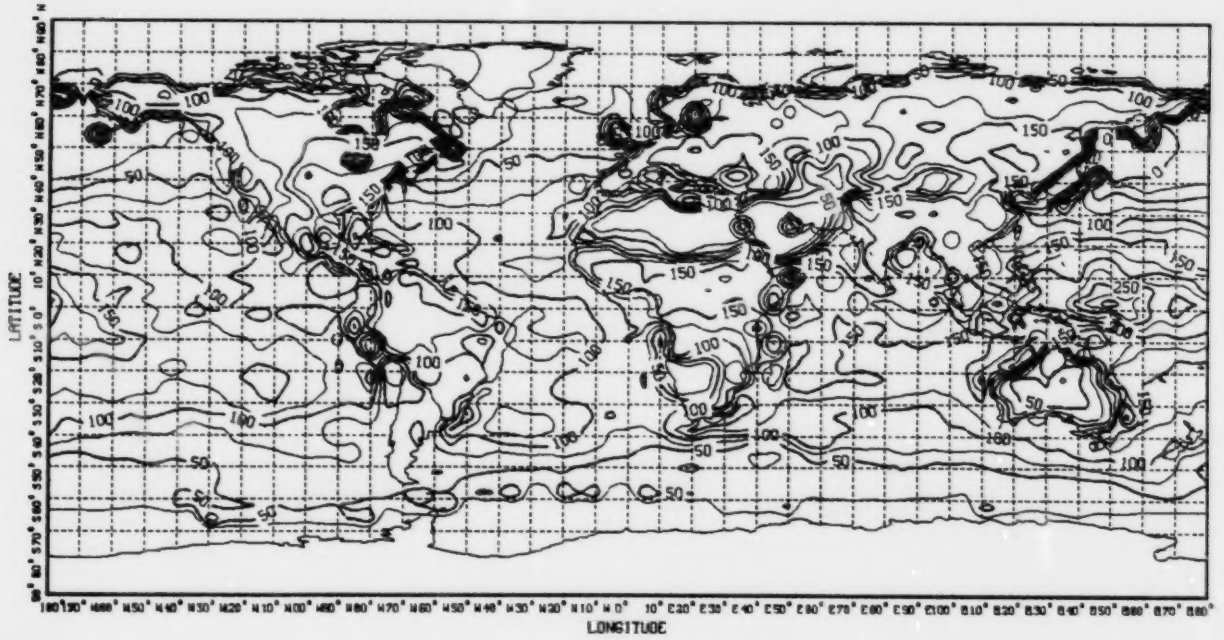

Figure 87

U S A (GFDL) JANUARY LATENT HEAT (W/M**2)

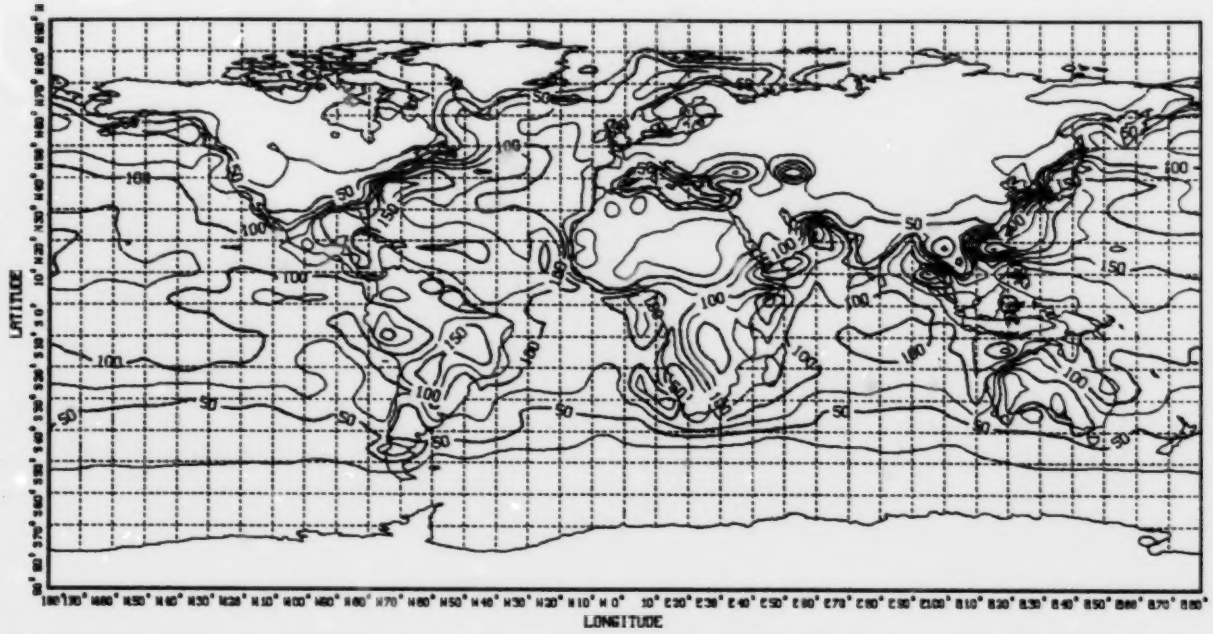

U S A (GFDL) JULY LATENT HEAT (W/M**2)

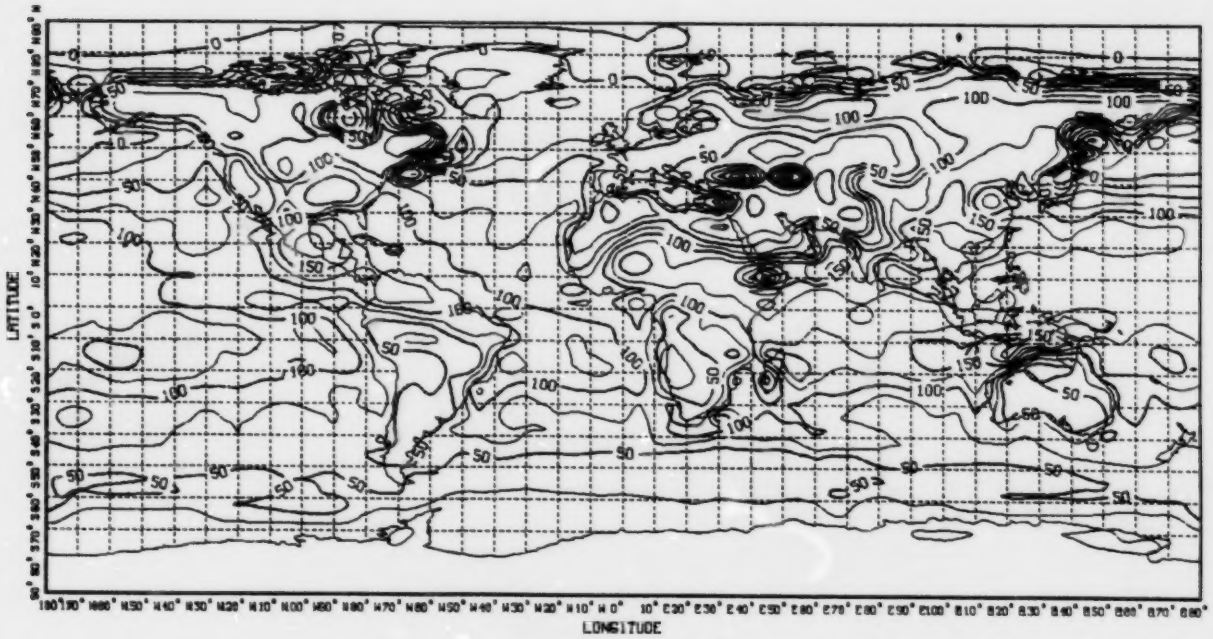

Figure 88

U S A (GISS) WINTER LATENT HEAT (W/M**2)

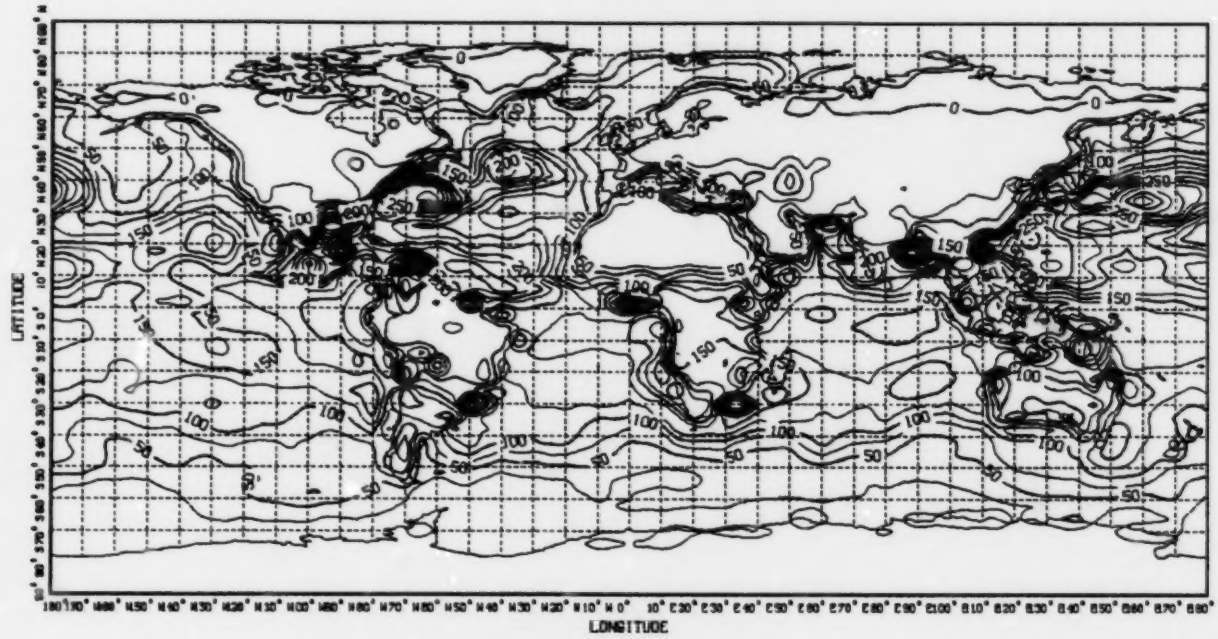

U S A (GISS) SUMMER LATENT HEAT (W/M**2)

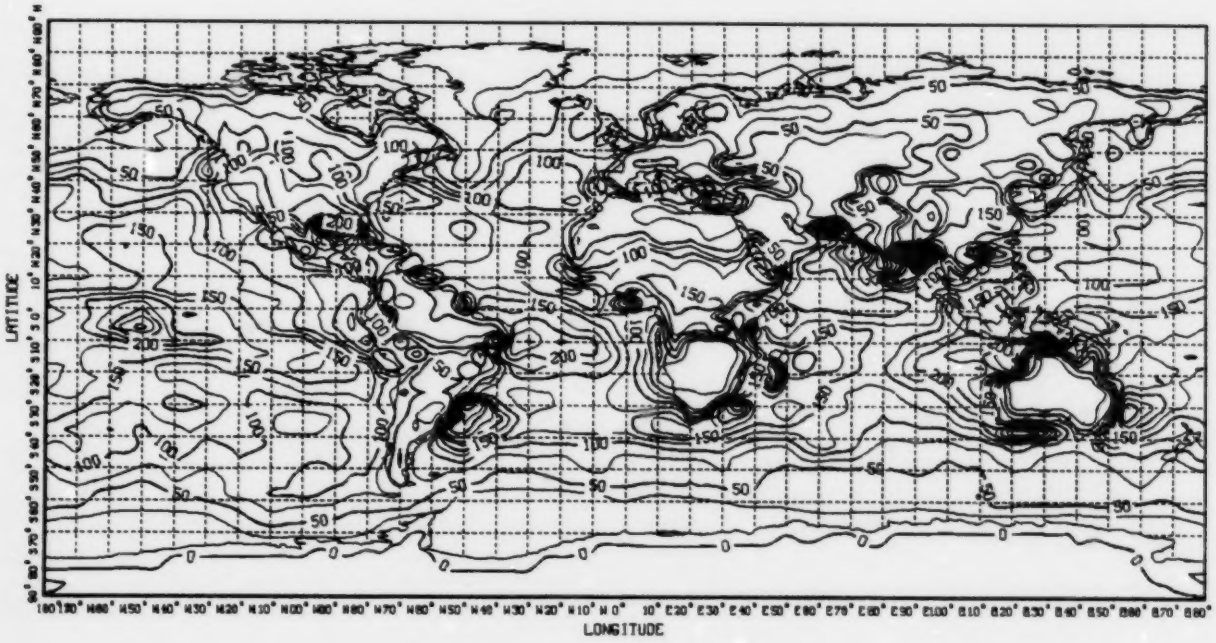

Figure 89

U S A (NCAR) JANUARY LATENT HEAT (W/M**2)

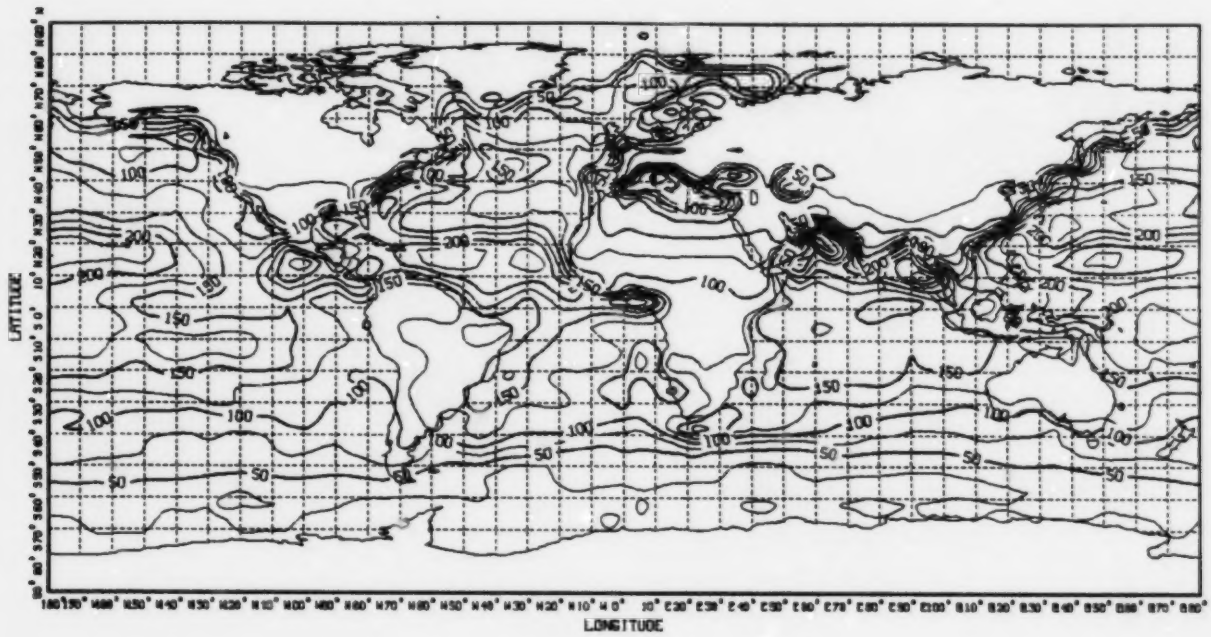

U S A (NCAR) JULY LATENT HEAT (W/M**2)

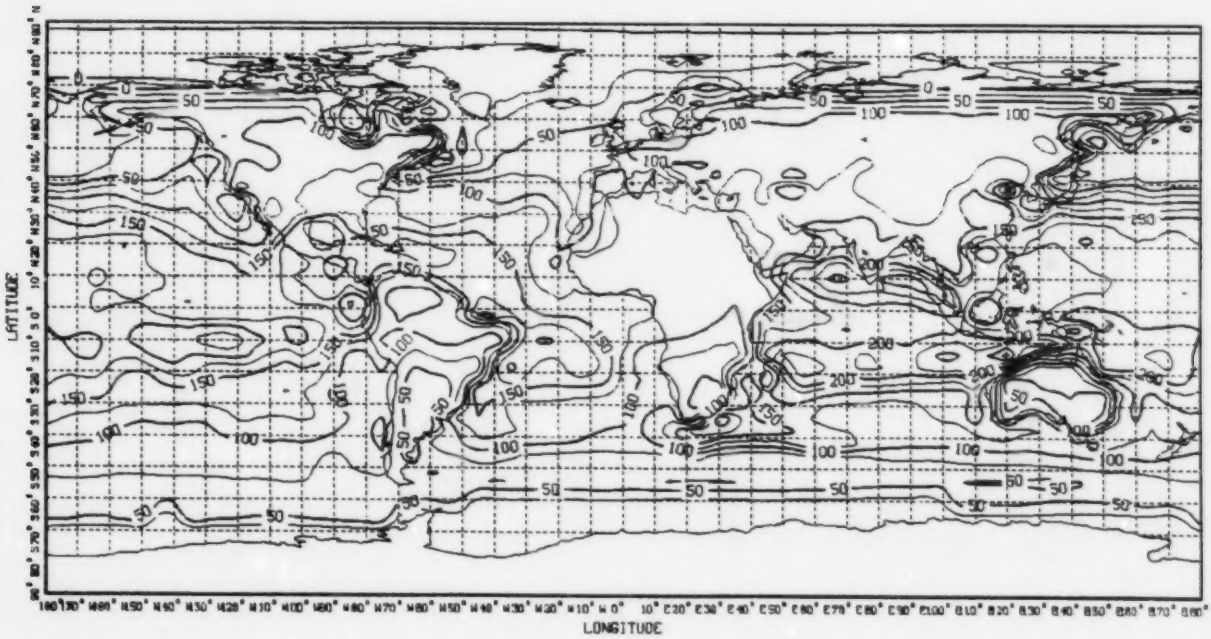

Figure 90

U S A (OSU) JANUARY LATENT HEAT (W/M**2)

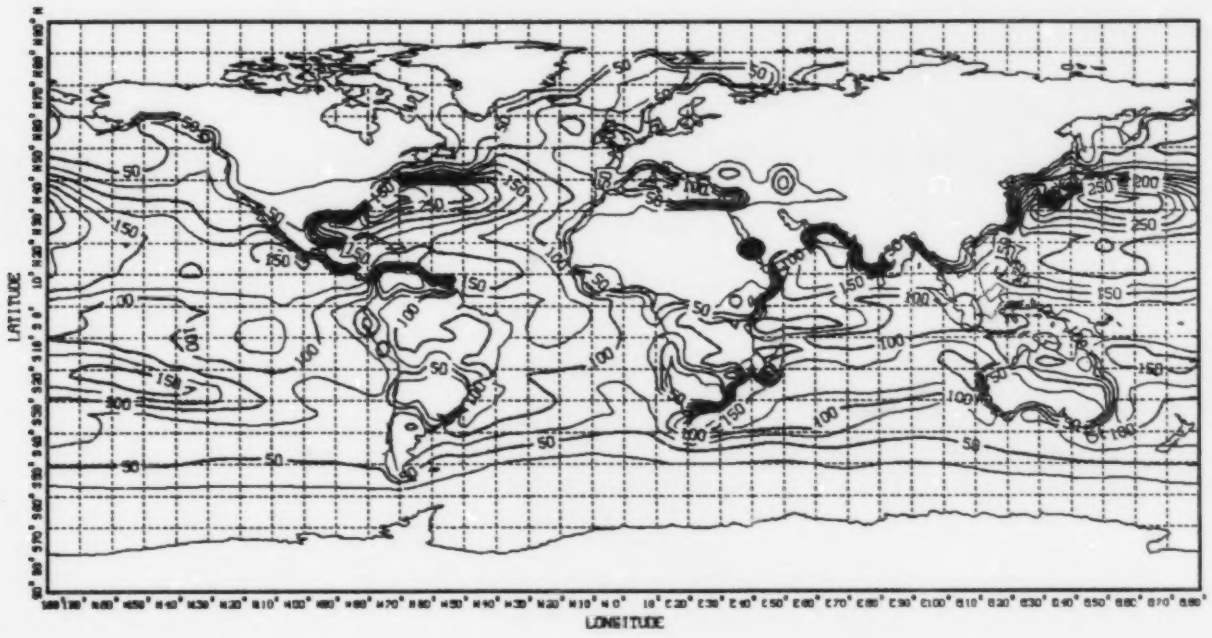

U S A (OSU) JULY LATENT HEAT (W/M**2)

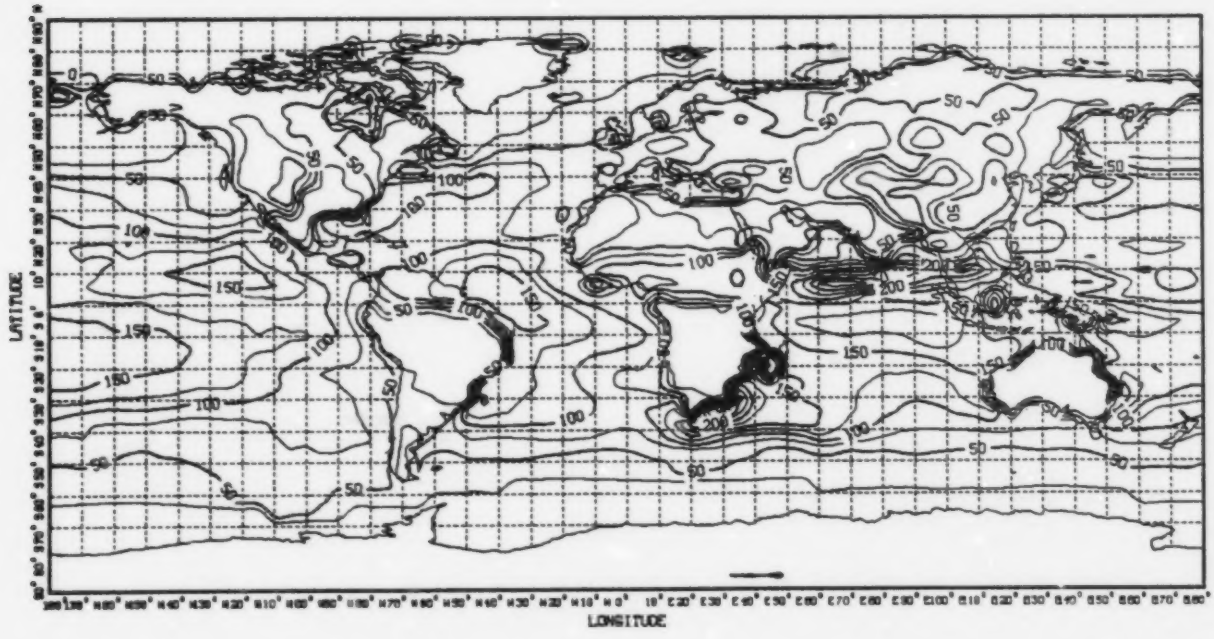

Figure 91

JAPAN (MRI) JANUARY LATENT HEAT (W/M**2)

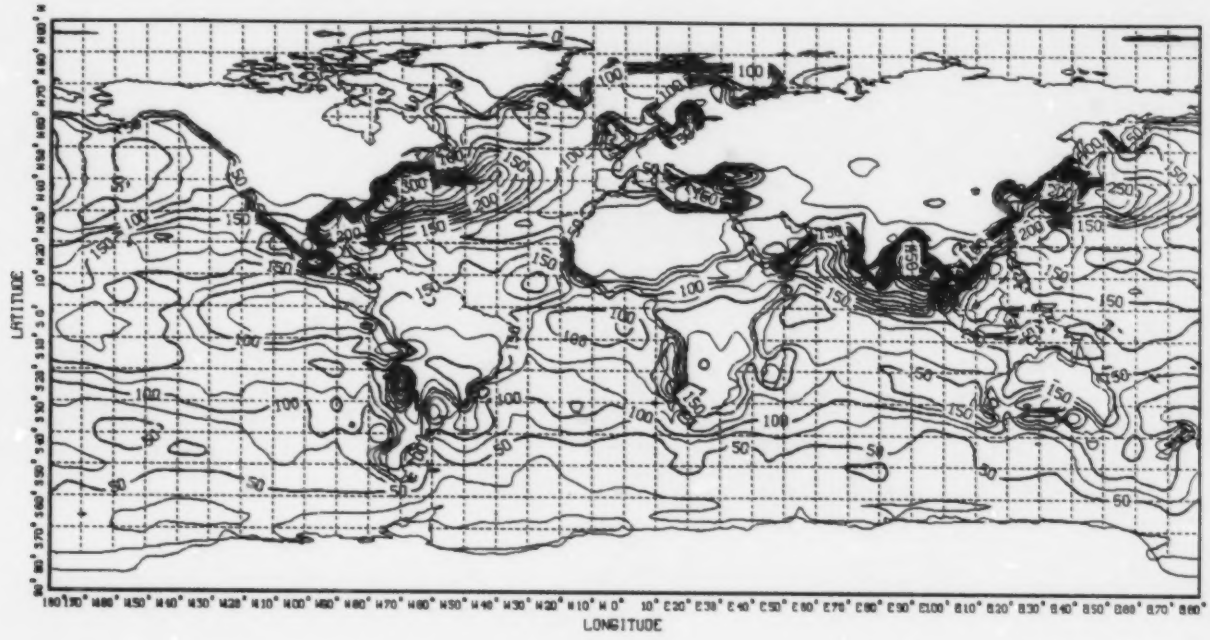

JAPAN (MRI) JULY LATENT HEAT (W/M**2)

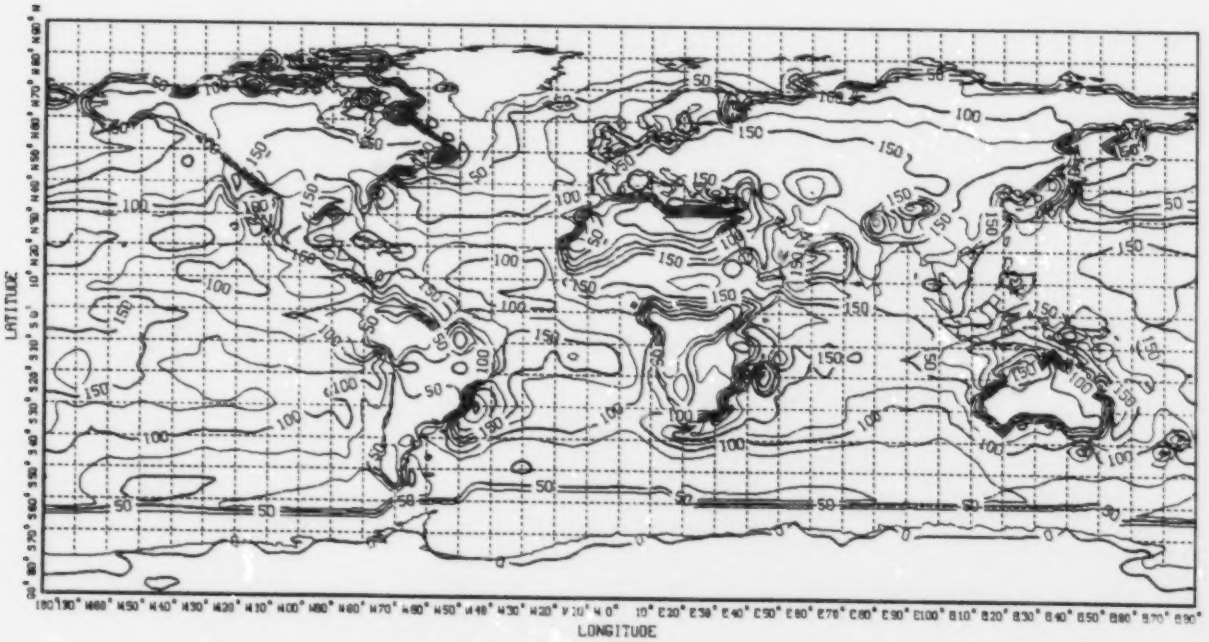

Figure 92

ECMWF JANUARY LATENT HEAT (W/M**2)

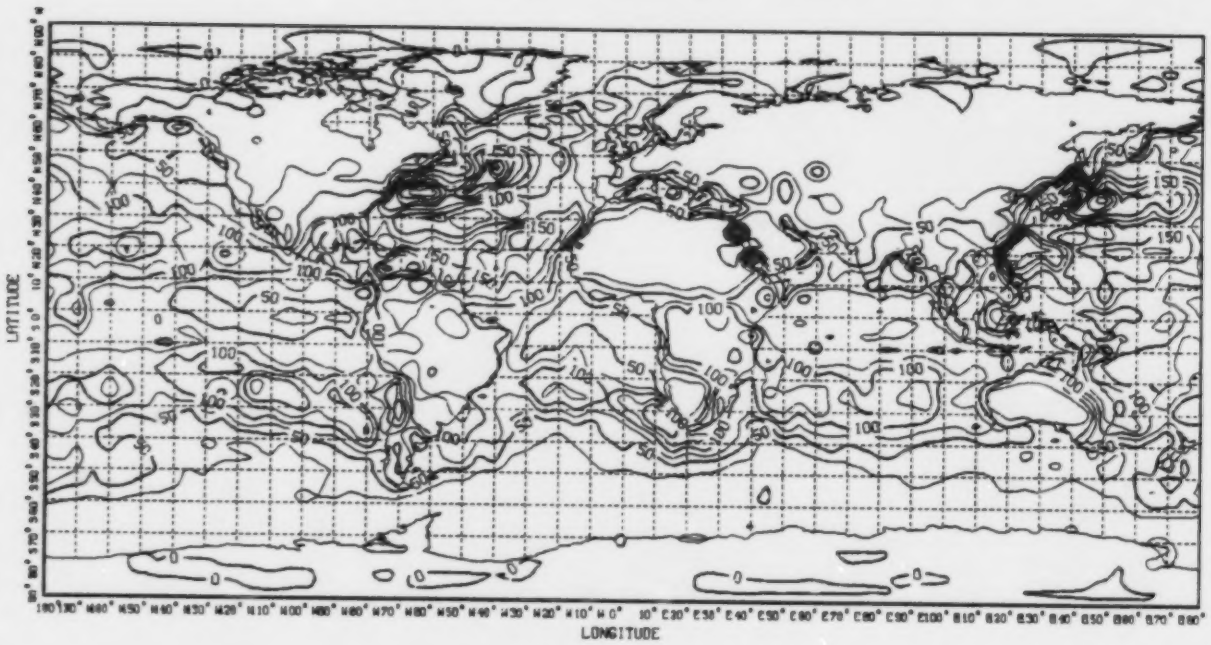

ECMWF JUNE LATENT HEAT (W/M**2)

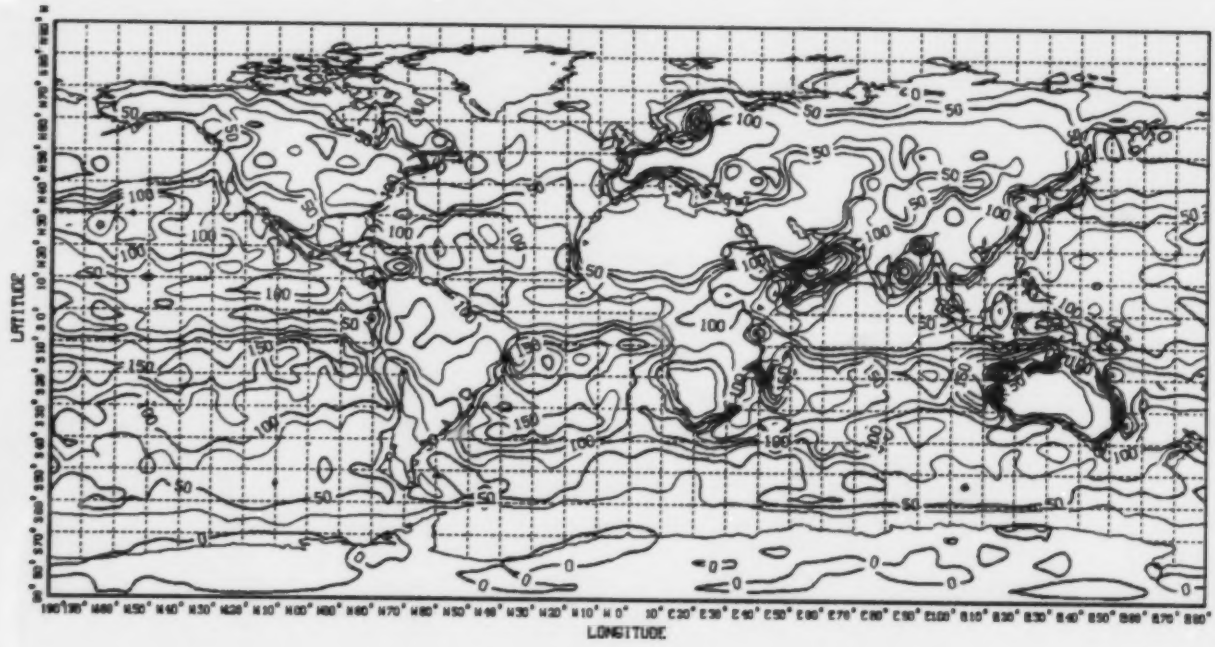

Figure 93

FRANCE (CNRM) JANUARY LATENT HEAT (W/M**2)

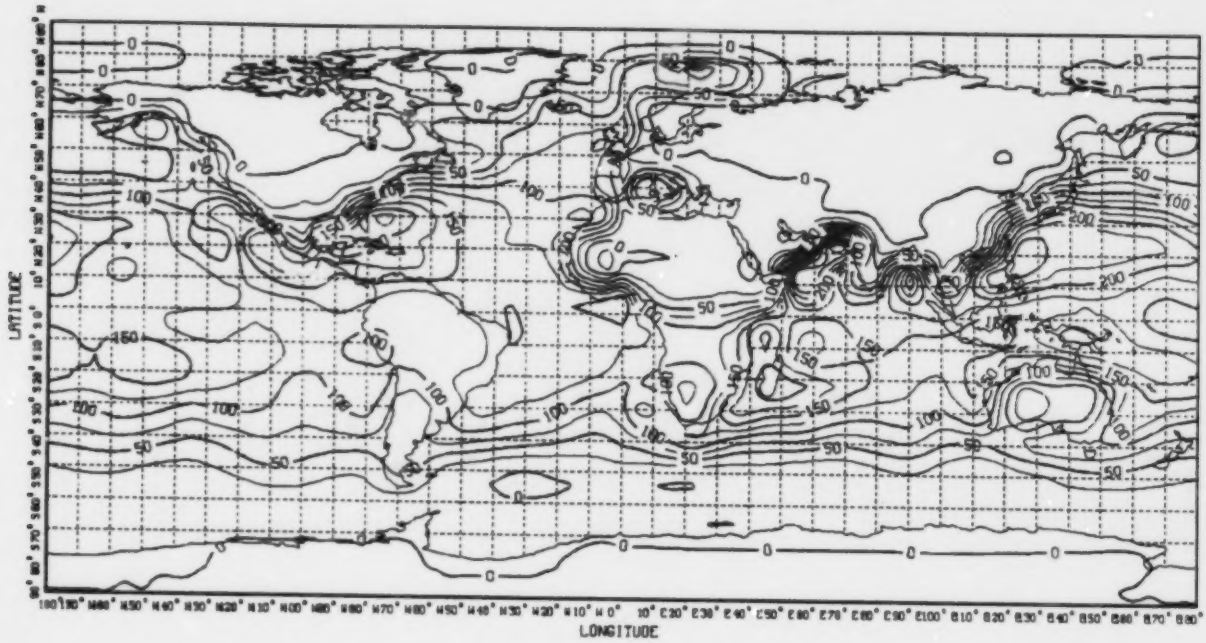

FRANCE (CNRM) SUMMER LATENT HEAT (W/M**2)

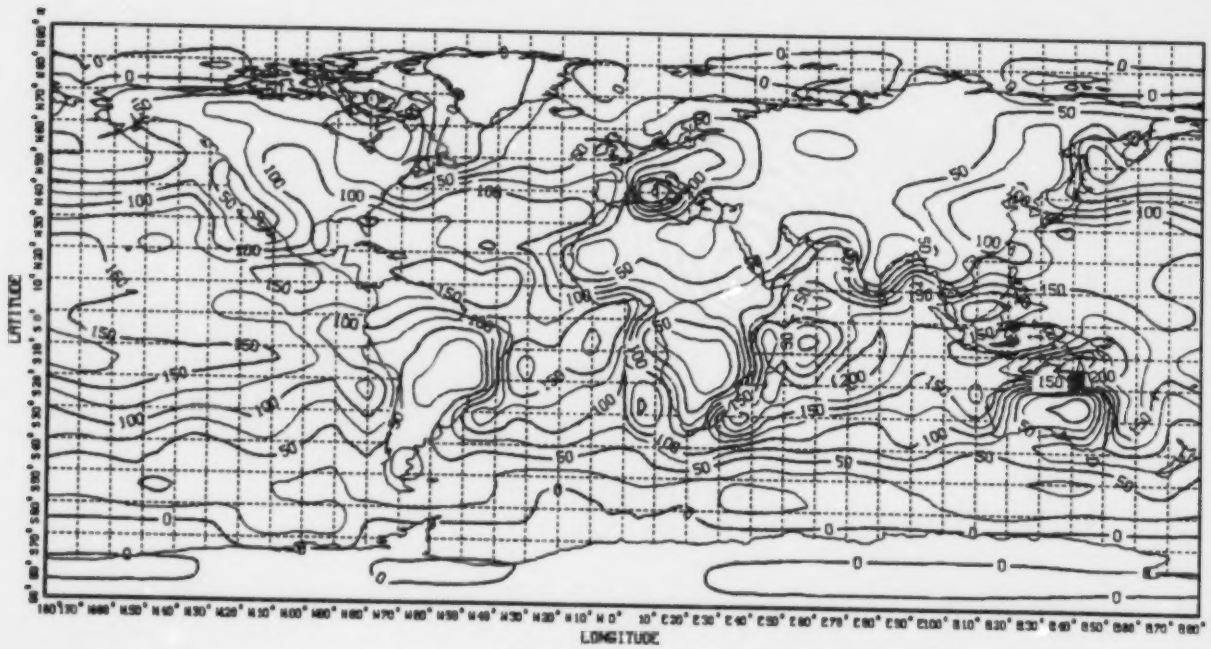

Figure 94

F R G (HAMBURG U) JANUARY LATENT HEAT (W/M**2)

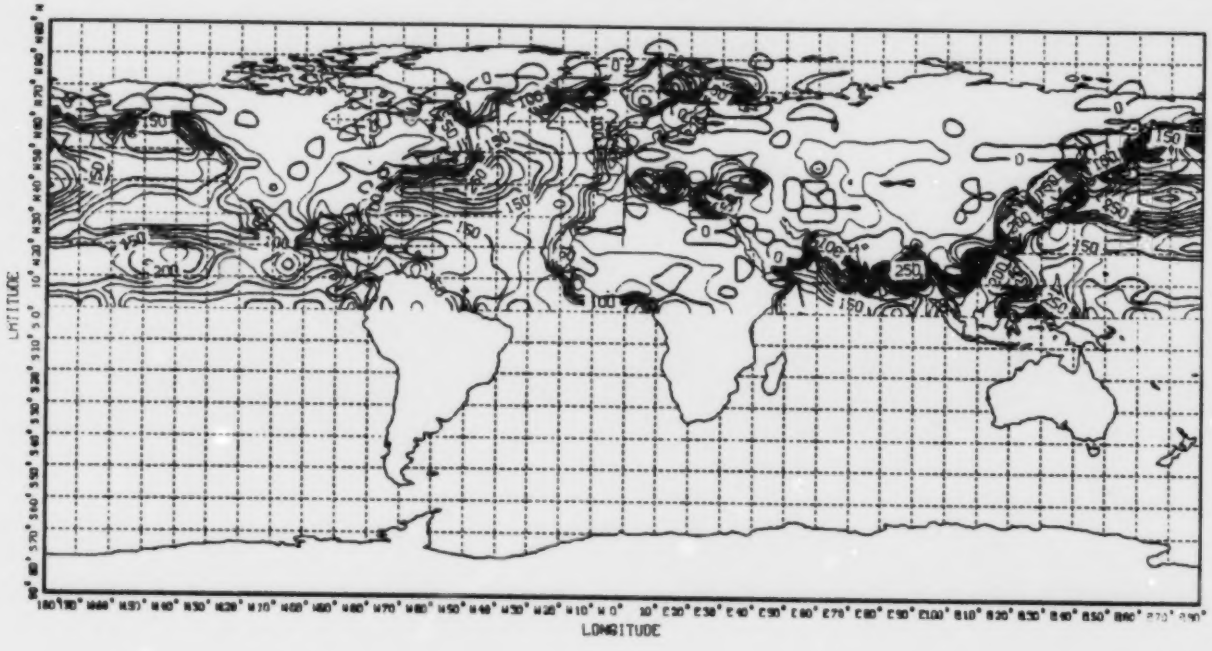

Figure 95

ESBENSEN AND KUSHNIR JANUARY SENSIBLE HEAT (W/M**2)

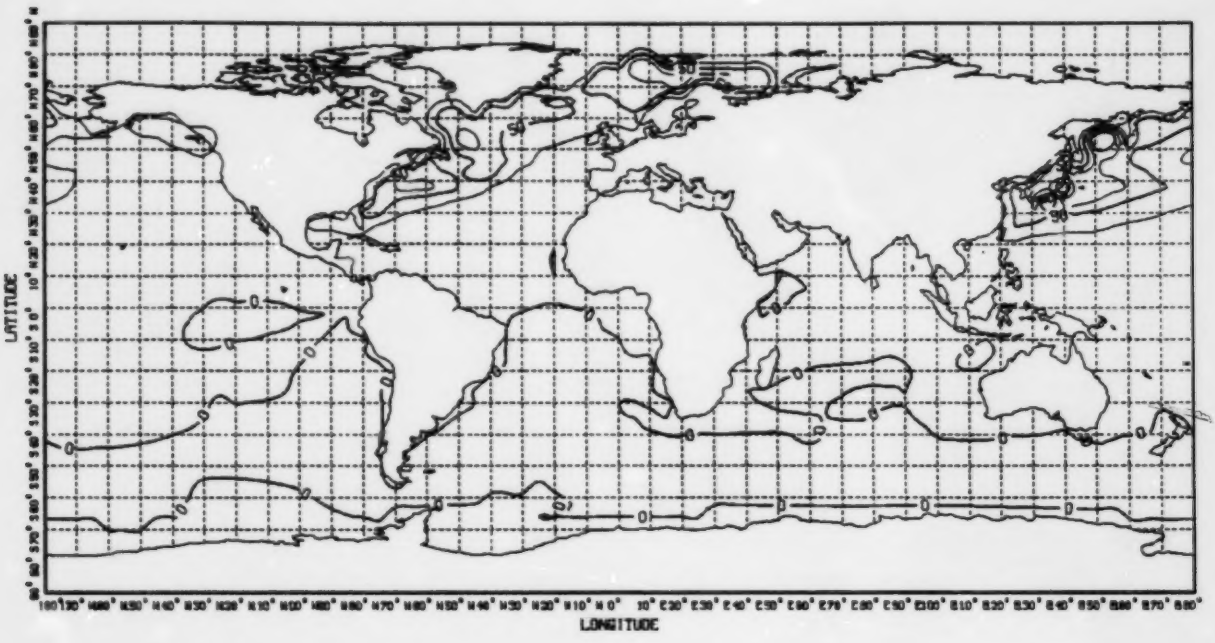

ESBENSEN AND KUSHNIR JULY SENSIBLE HEAT (W/M**2)

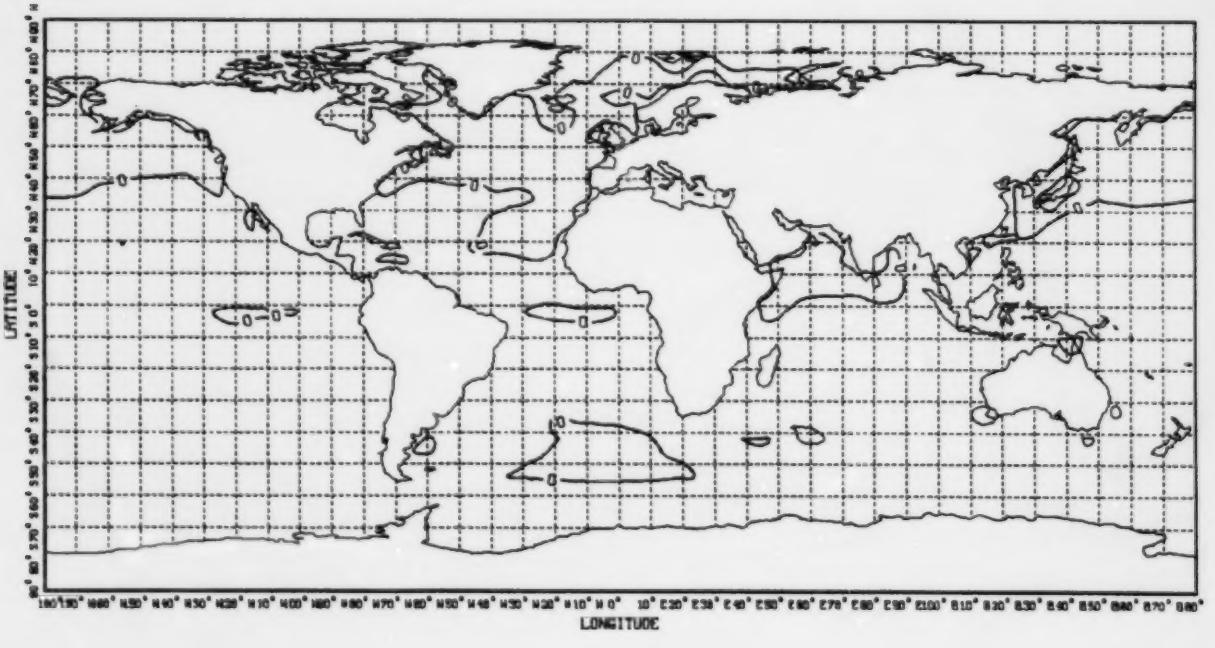

Figure 96

CANADA (CCC) WINTER SENSIBLE HEAT (W/M**2)

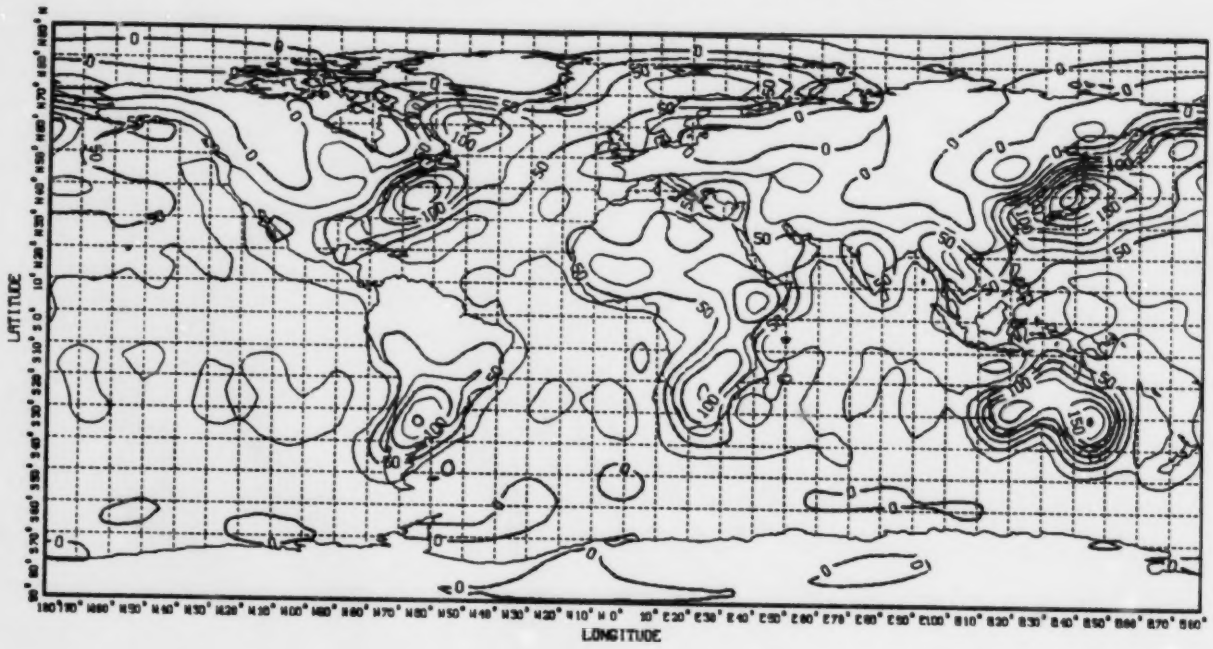

CANADA (CCC) SUMMER SENSIBLE HEAT (W/M**2)

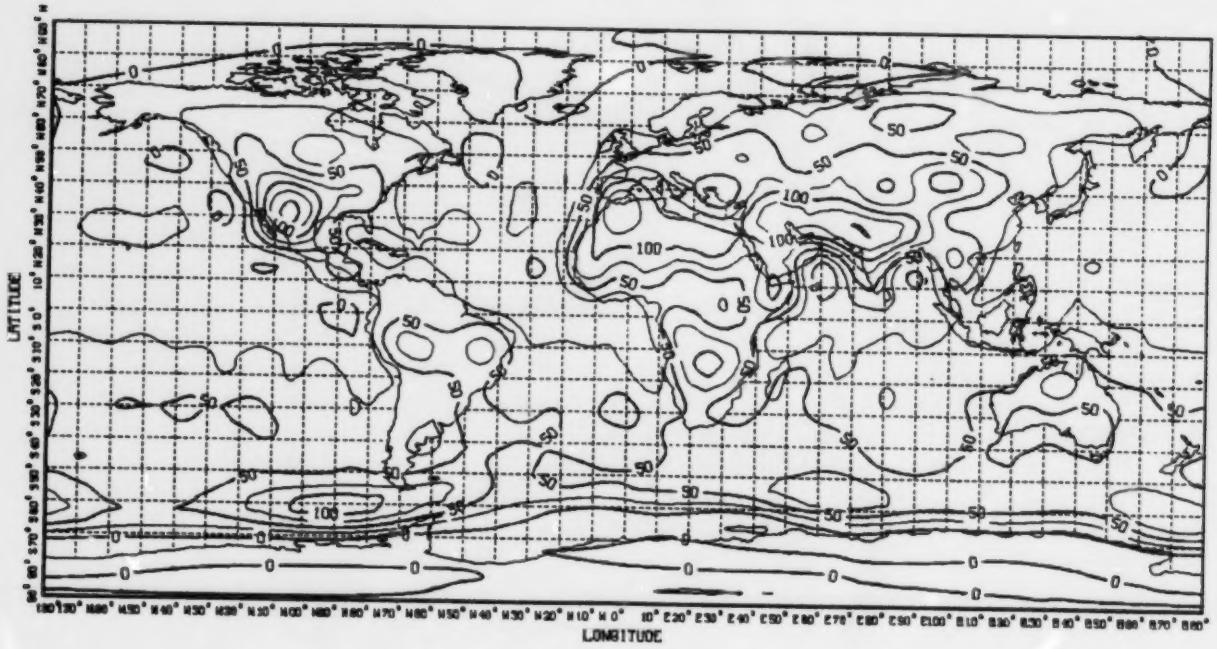

Figure 97

ENGLAND (BMO) WINTER SENSIBLE HEAT (W/M**2)

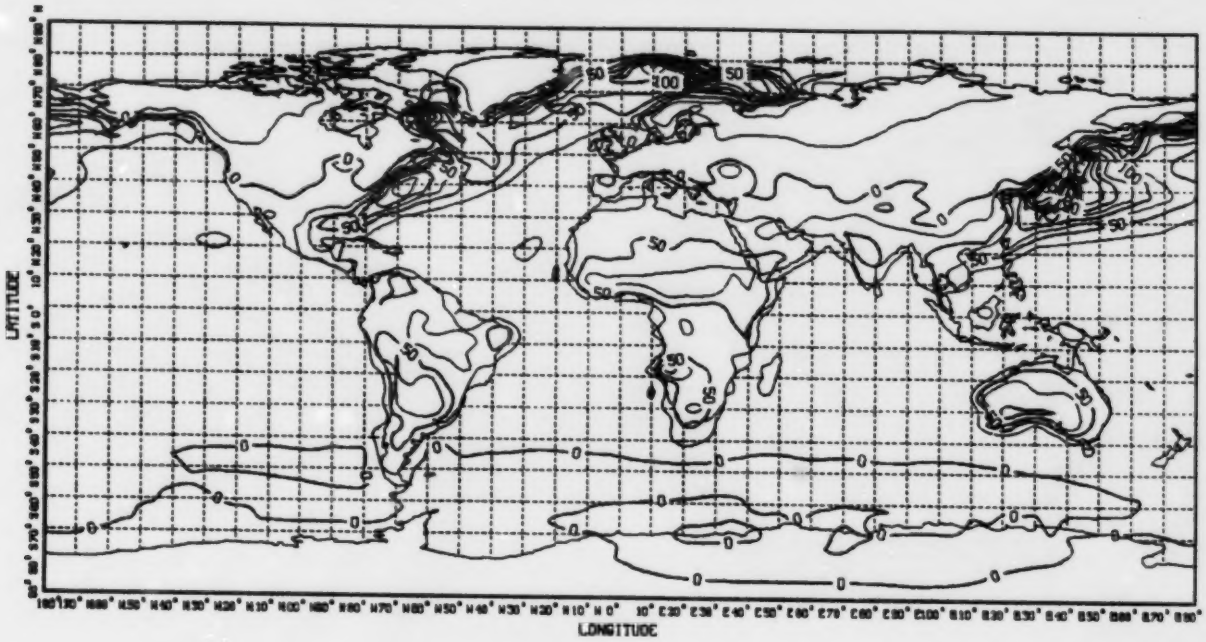

ENGLAND (BMO) SUMMER SENSIBLE HEAT (W/M**2)

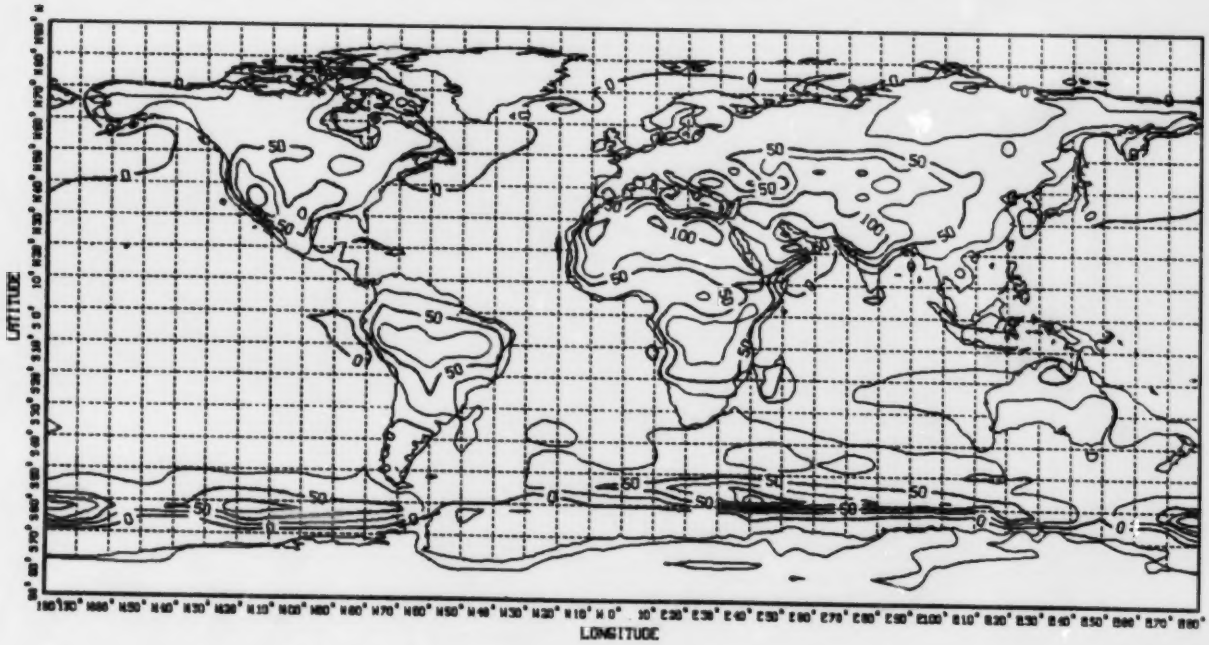

Figure 98

AUSTRALIA (BMRC) JANUARY SENSIBLE HEAT (W/M**2)

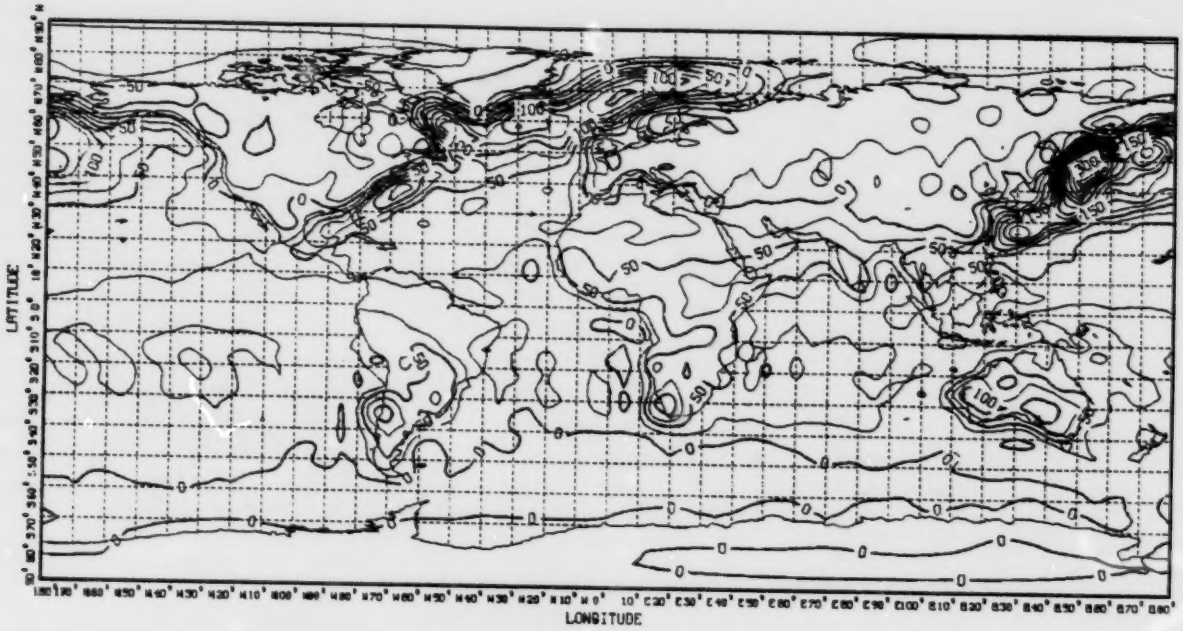

AUSTRALIA (BMRC) JULY SENSIBLE HEAT (W/M**2)

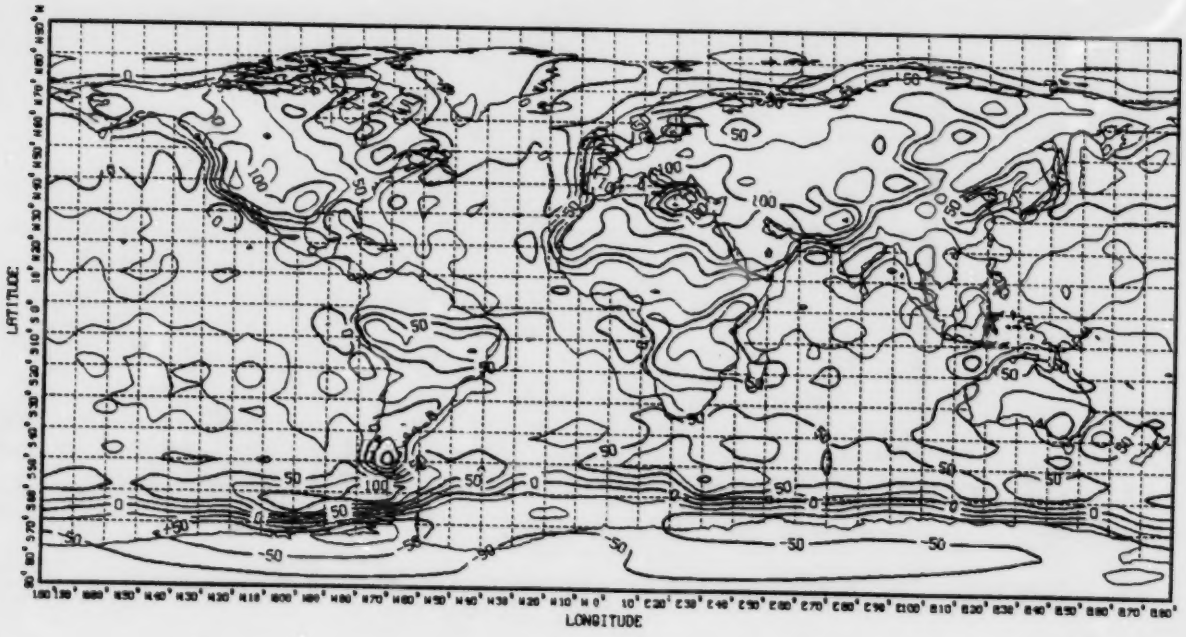

Figure 99

U S A (COLAI) JANUARY SENSIBLE HEAT (W/M**2)

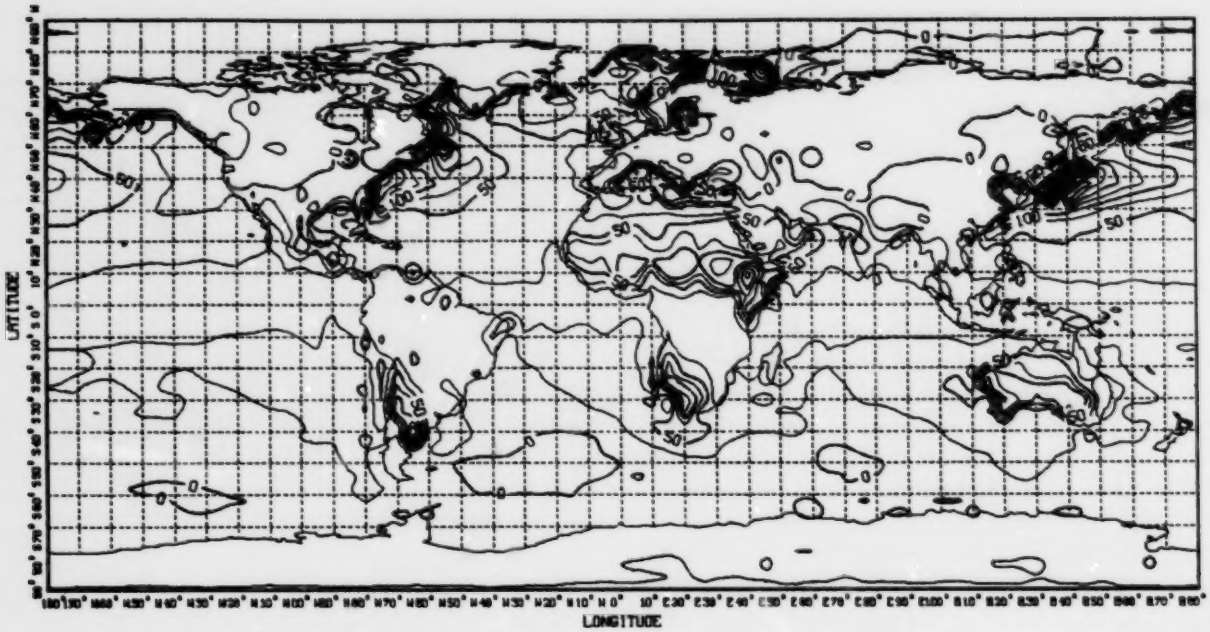

U S A (COLAI) JULY SENSIBLE HEAT (W/M**2)

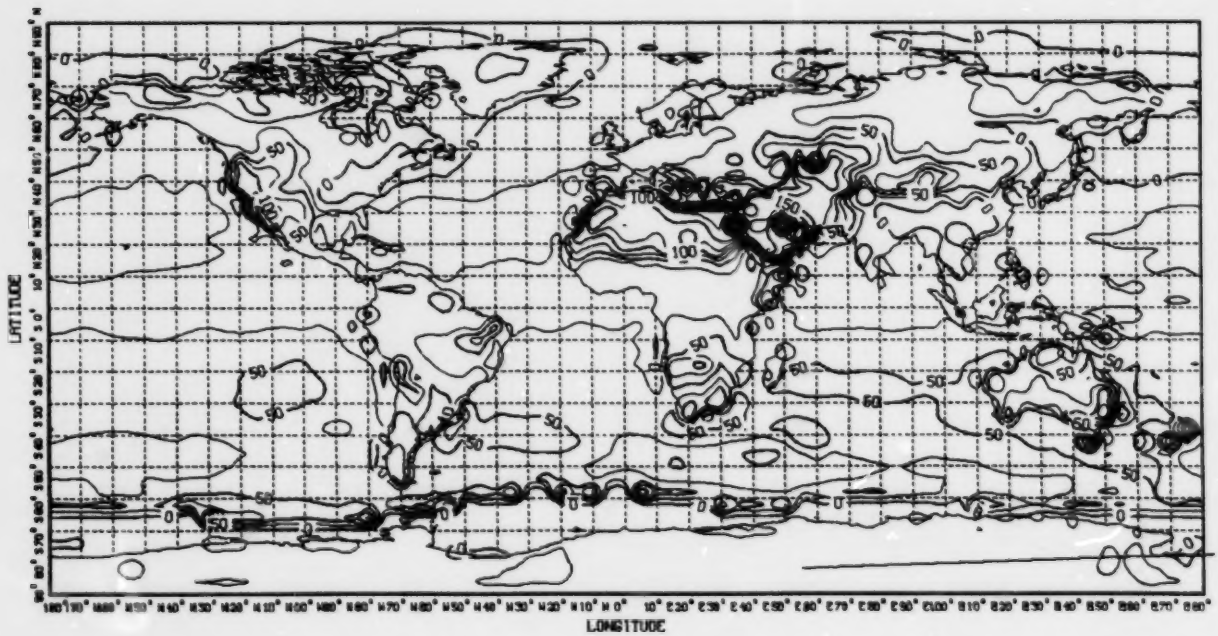

Figure 100

U S A (GFDL) JANUARY SENSIBLE HEAT (W/M**2)

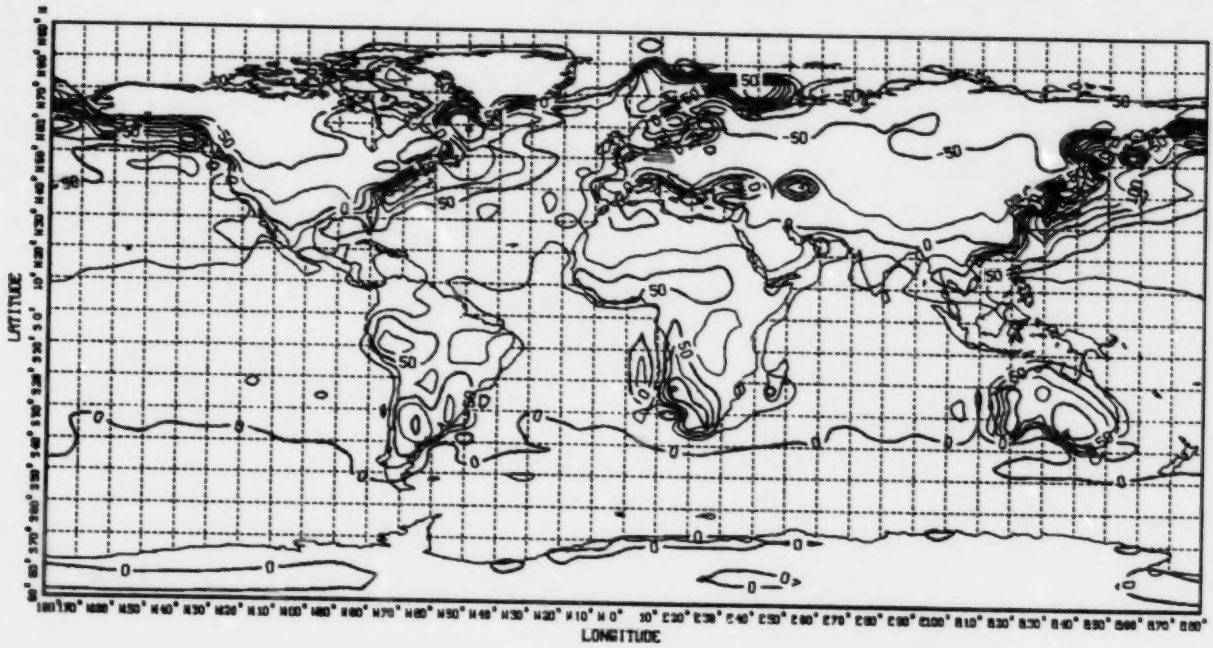

U S A (GFDL) JULY SENSIBLE HEAT (W/M**2)

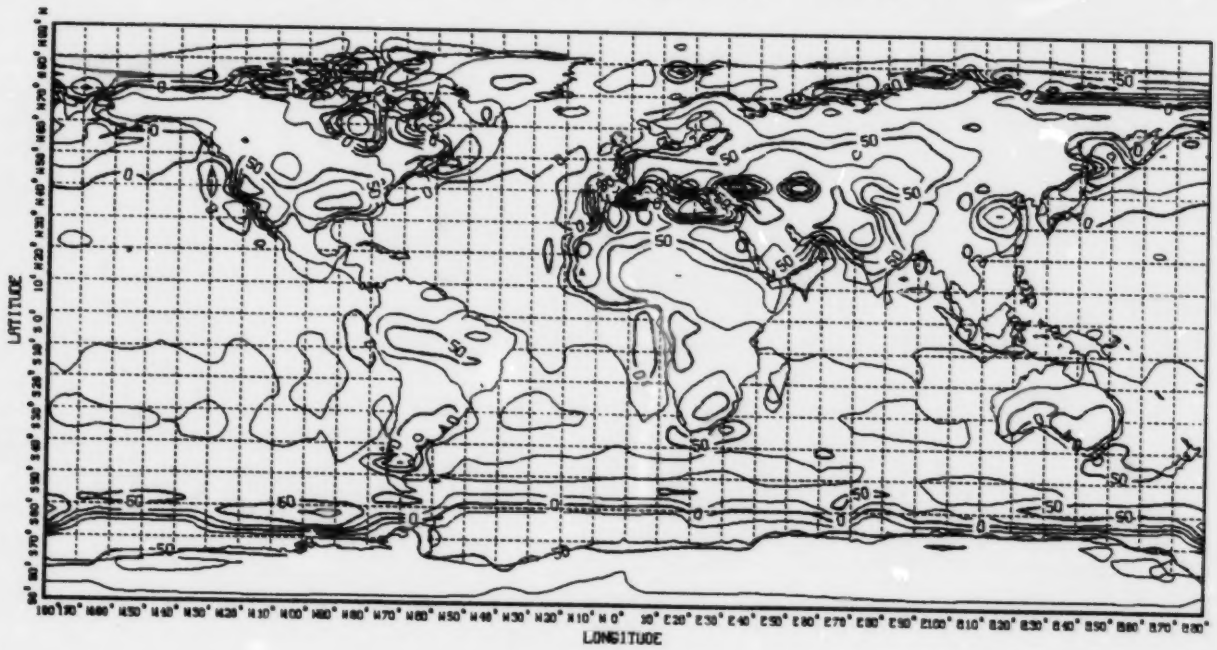

Figure 101

U S A (GISS) WINTER SENSIBLE HEAT (W/M××2)

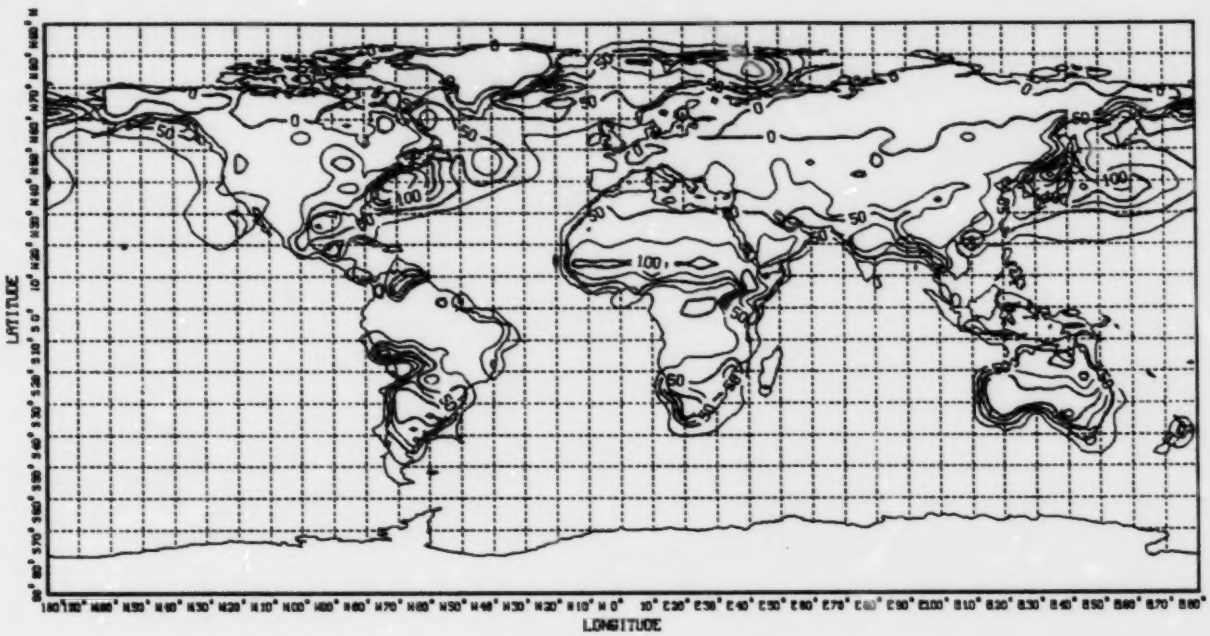

U S A (GISS) SUMMER SENSIBLE HEAT (W/M××2)

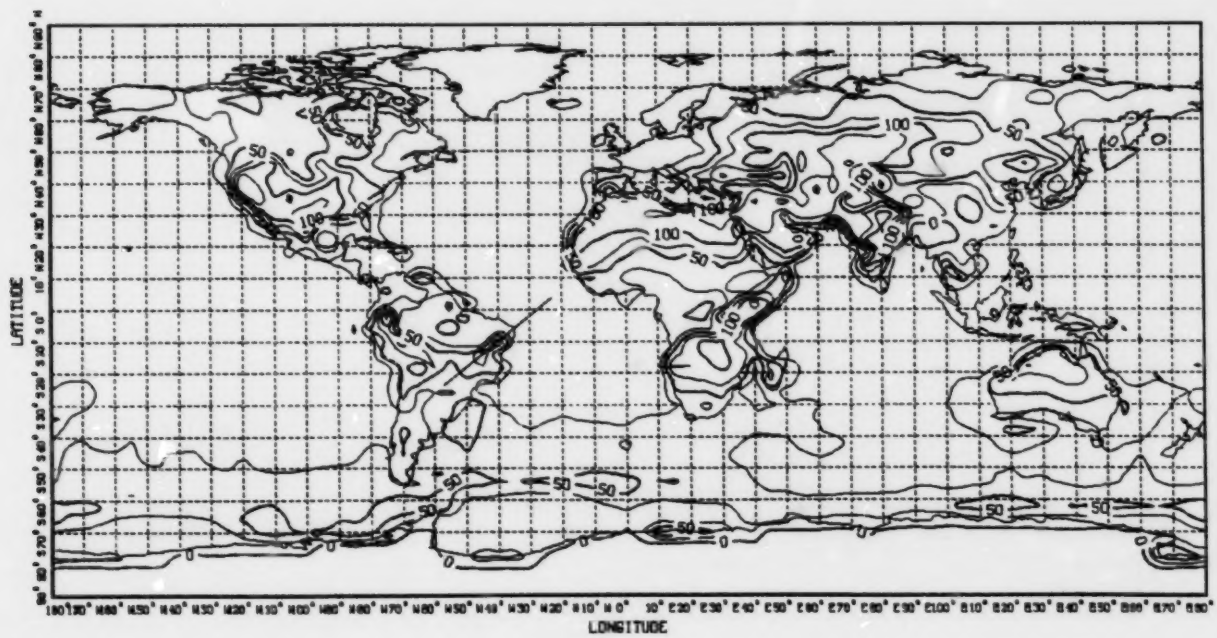

Figure 102

U S A (NCAR) JANUARY SENSIBLE HEAT (W/M**2)

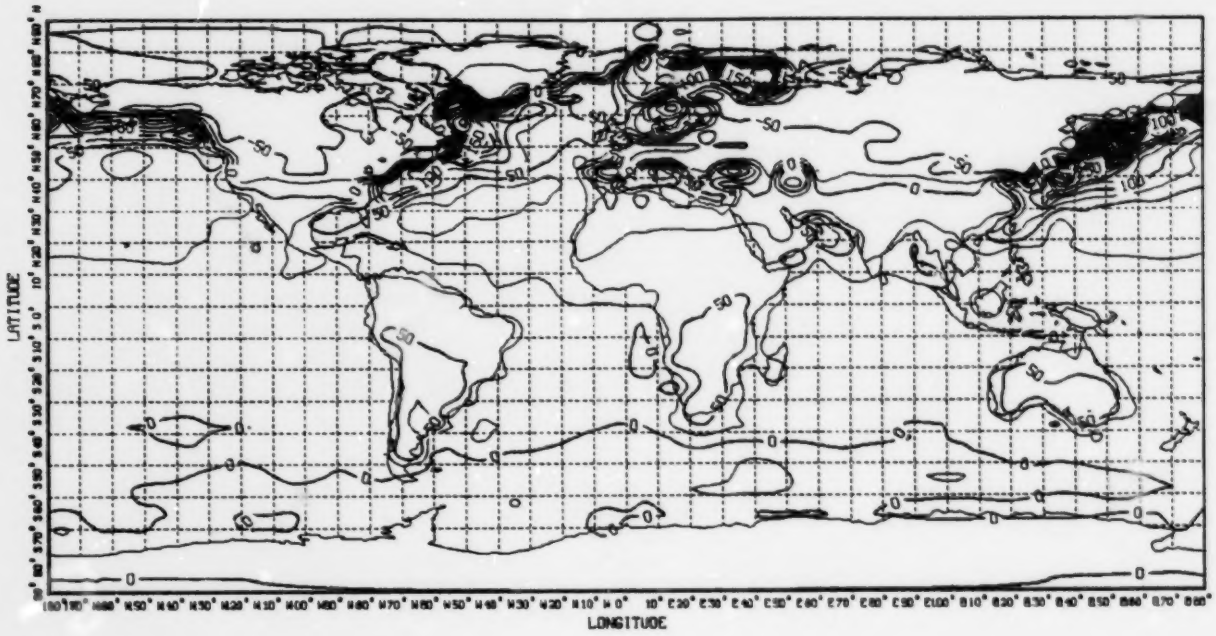

U S A (NCAR) JULY SENSIBLE HEAT (W/M**2)

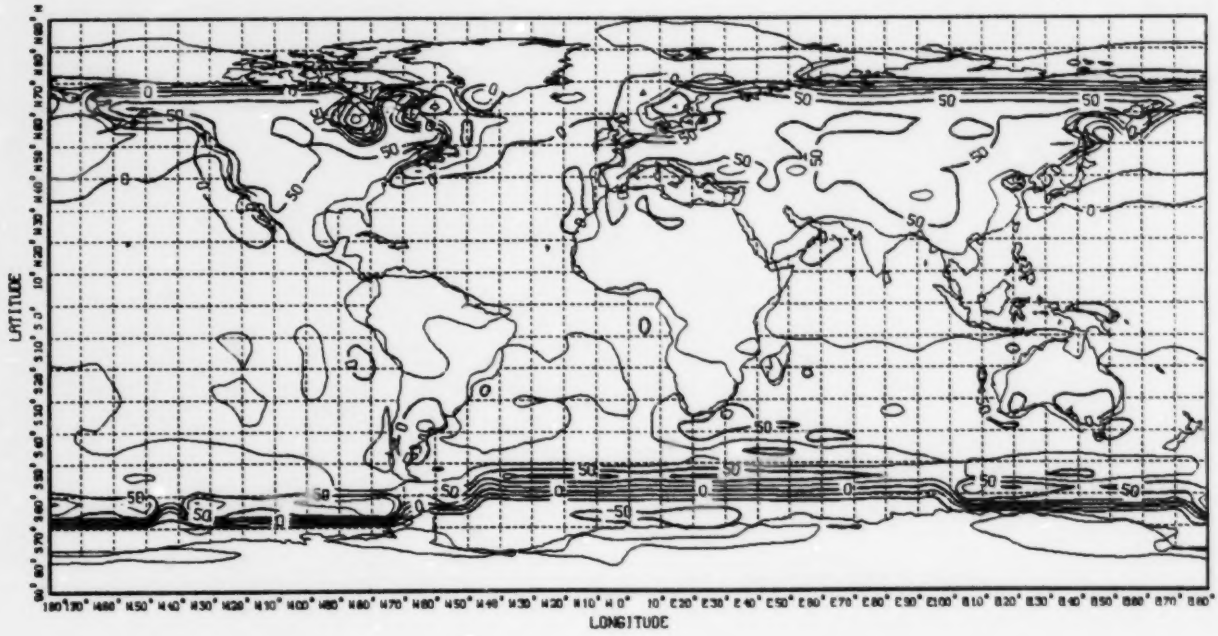

Figure 103

U S A (OSU) JANUARY SENSIBLE HEAT (W/M**2)

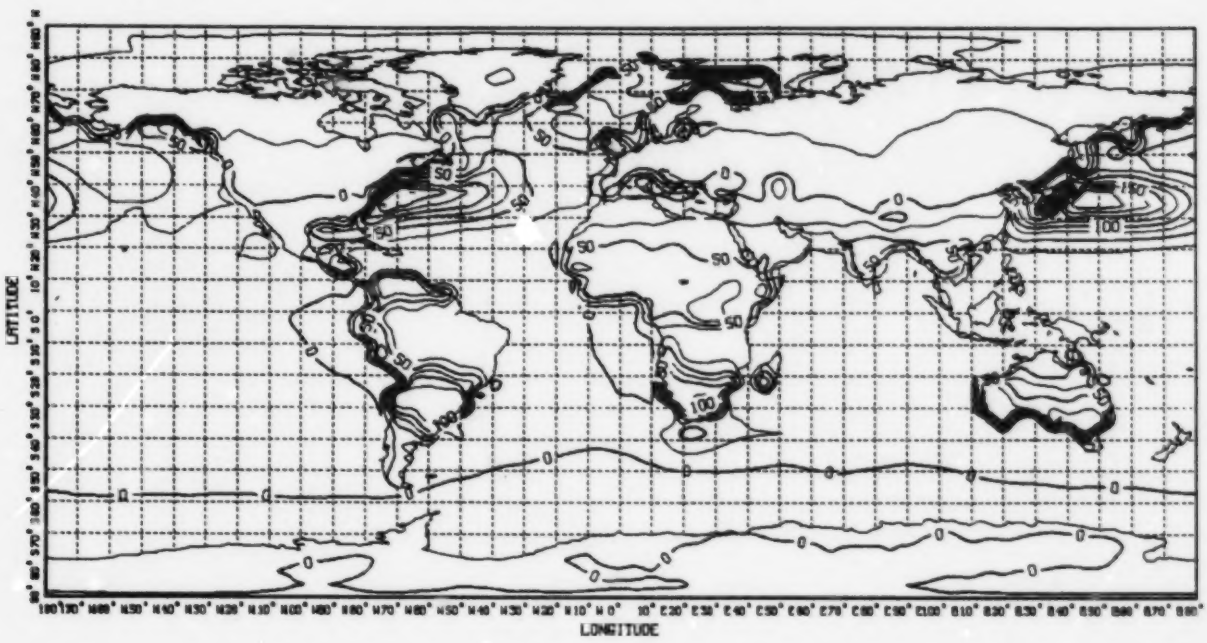

U S A (OSU) JULY SENSIBLE HEAT (W/M**2)

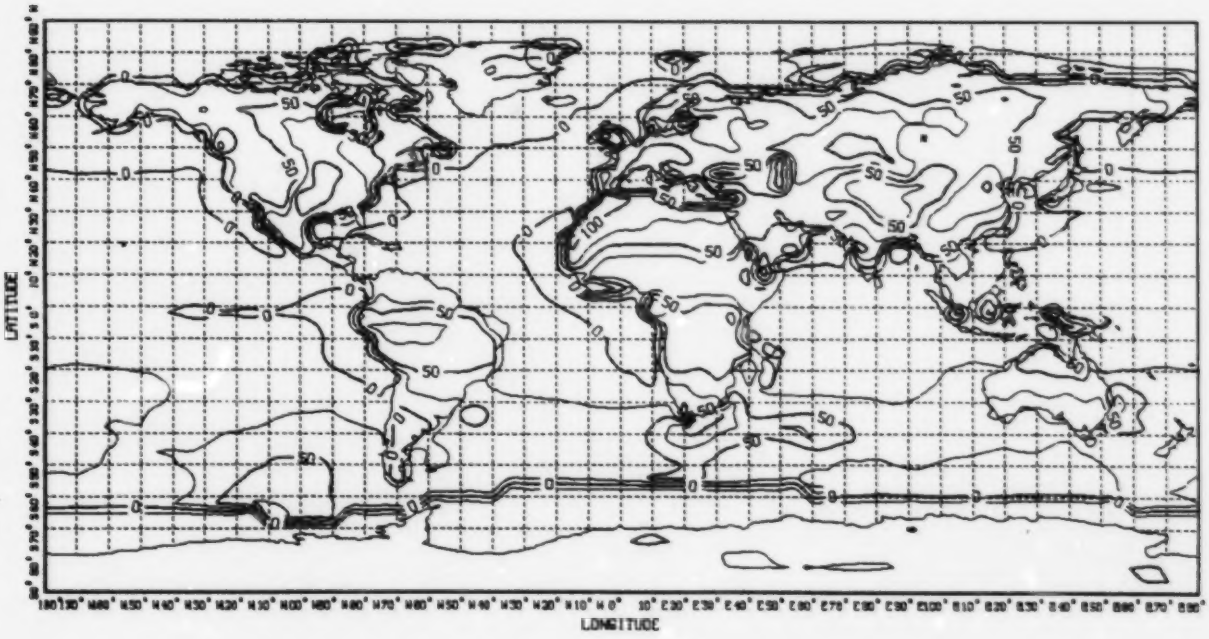

Figure 104

JAPAN (MRI) JANUARY SENSIBLE HEAT (W/M**2)

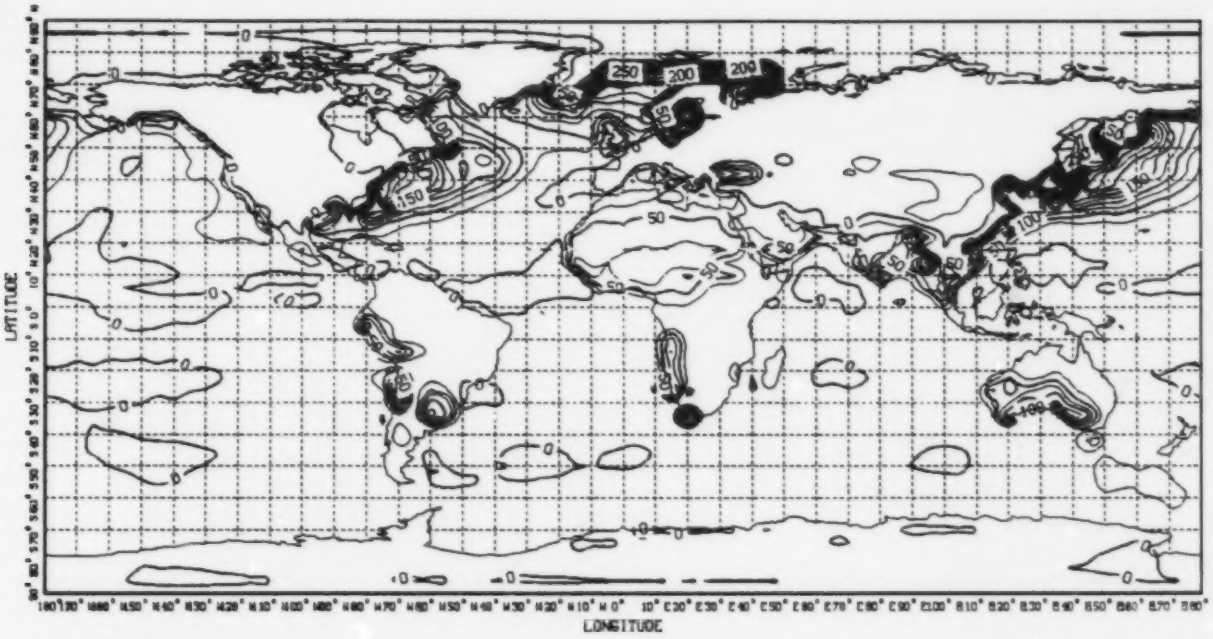

JAPAN (MRI) JULY SENSIBLE HEAT (W/M**2)

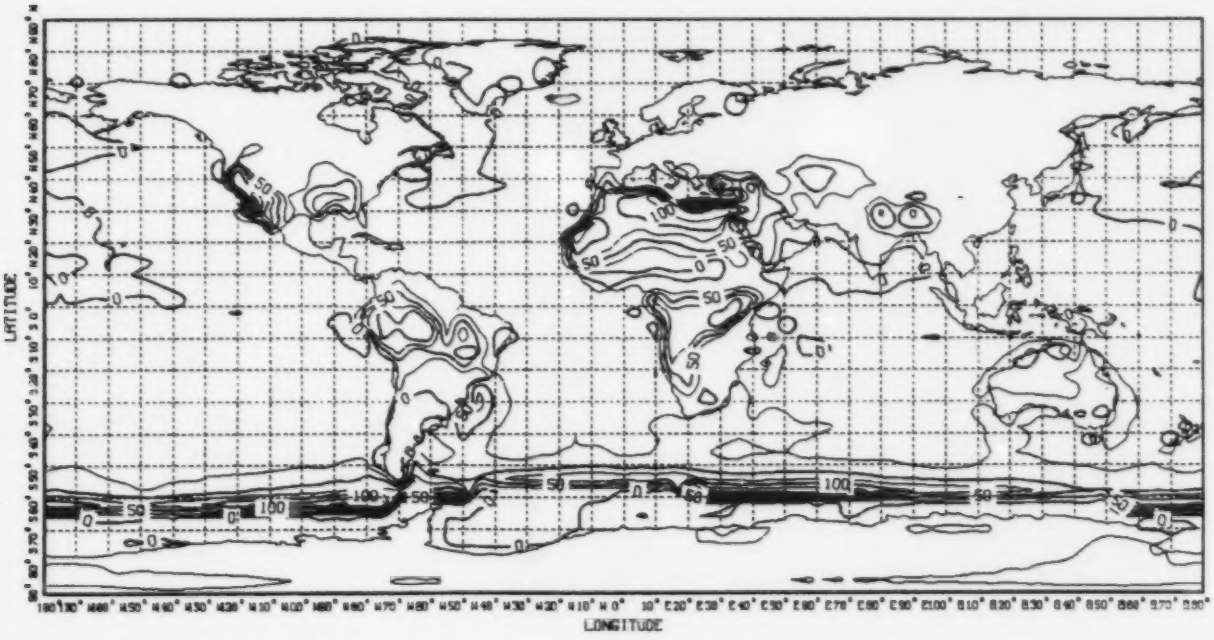

Figure 105

ECMWF JANUARY SENSIBLE HEAT (W/M**2)

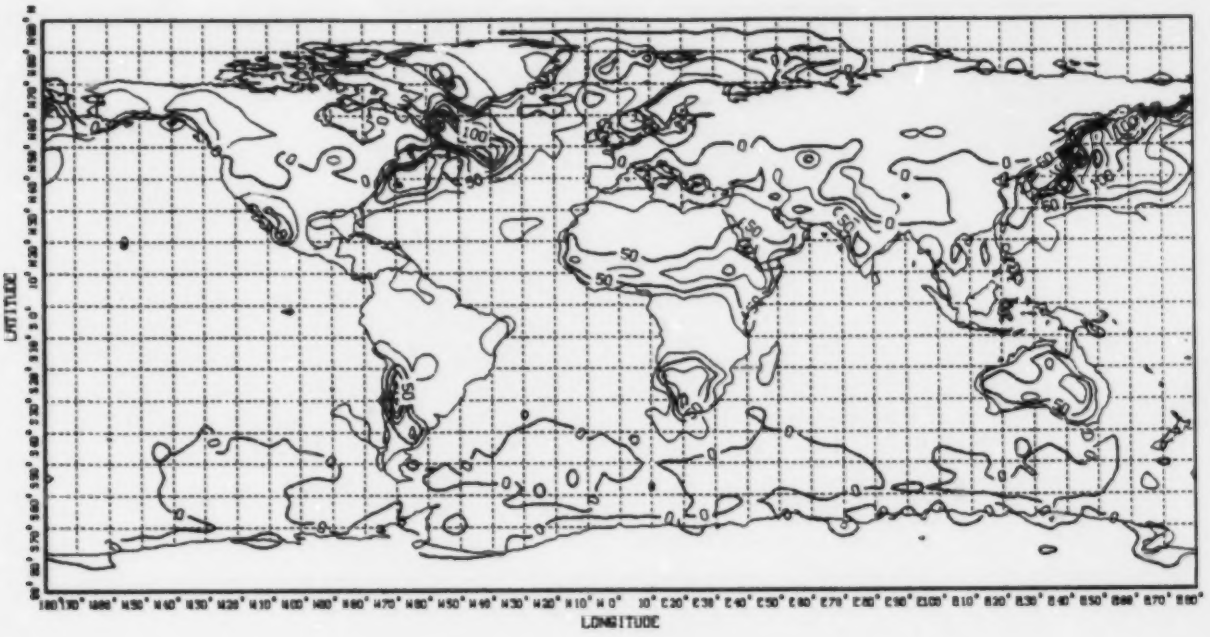

ECMWF JUNE SENSIBLE HEAT (W/M**2)

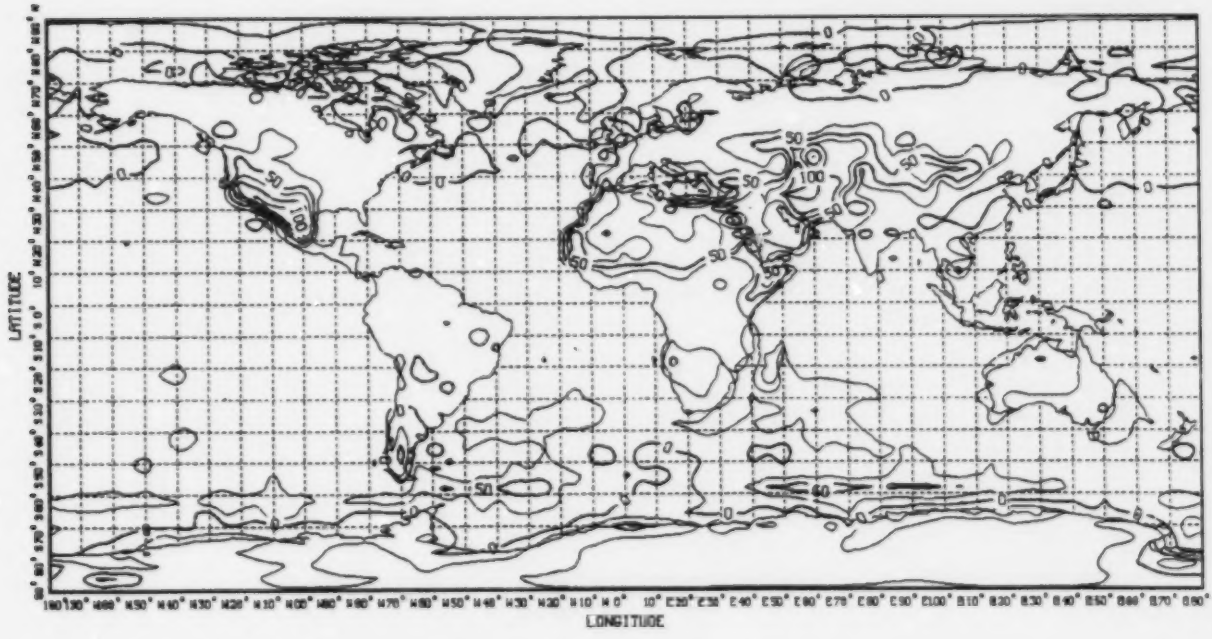

Figure 106

FRANCE (CNRM) WINTER SENSIBLE HEAT (W/M**2)

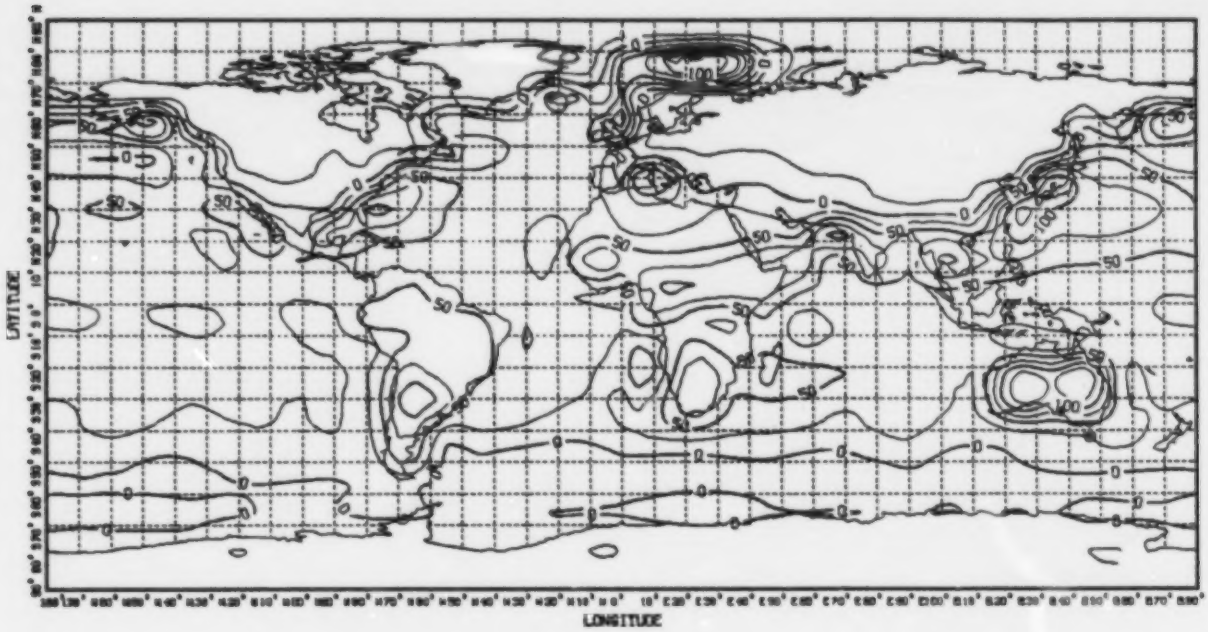

FRANCE (CNRM) SUMMER SENSIBLE HEAT (W/M**2)

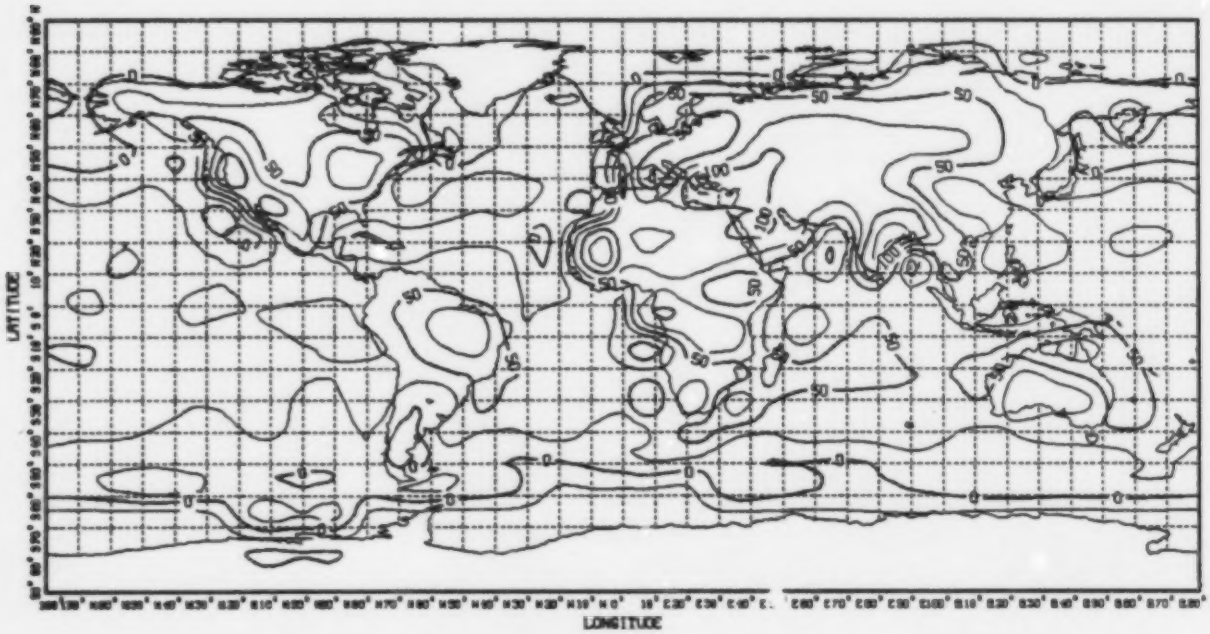

Figure 107

F R G (HAMBURG U) JANUARY SENSIBLE HEAT (W/M**2)

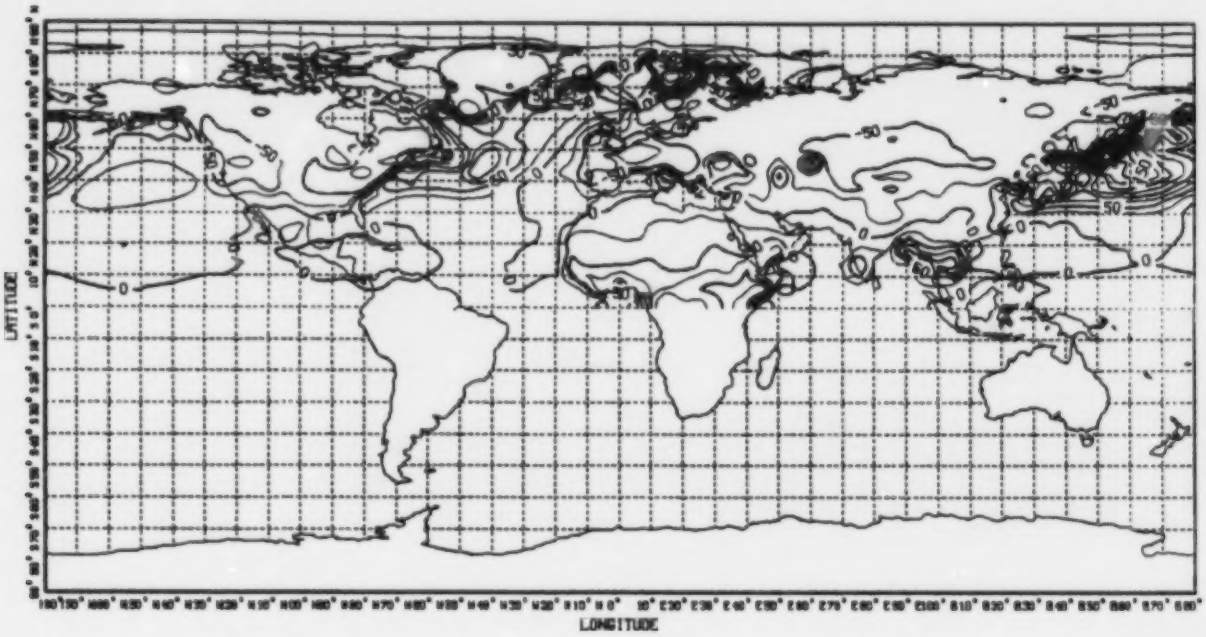

Figure 108

HAN AND LEE JANUARY U SURFACE STRESS .001*(N/M**2)

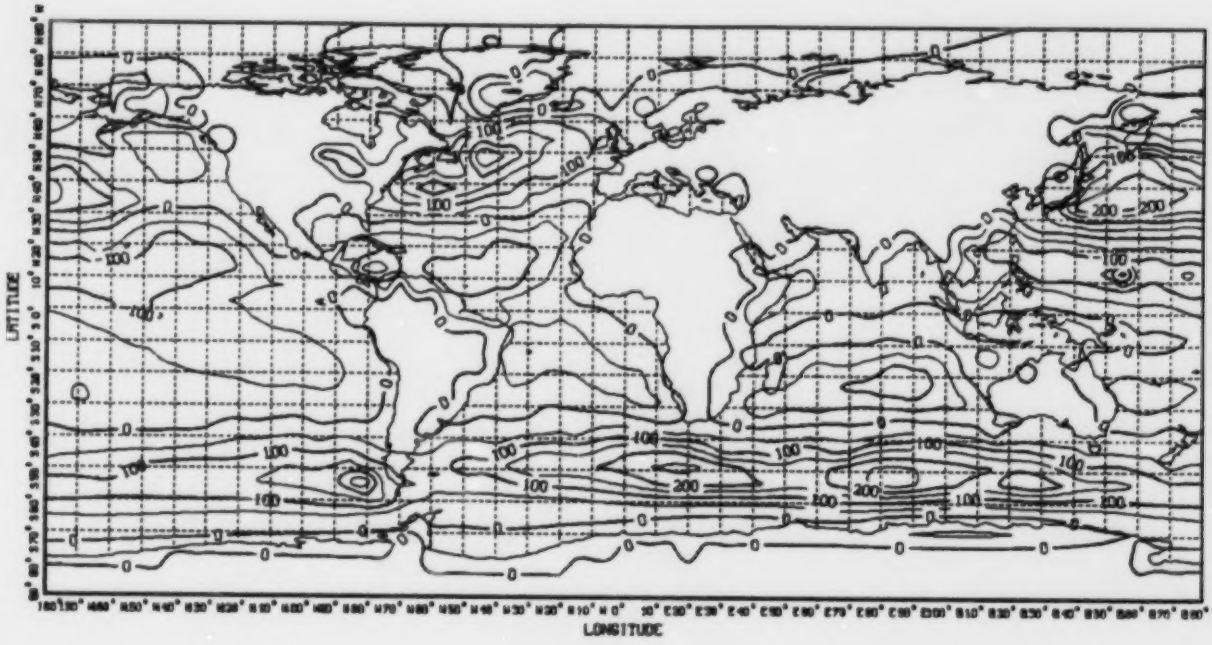

HAN AND LEE JULY U SURFACE STRESS .001*(N/M**2)

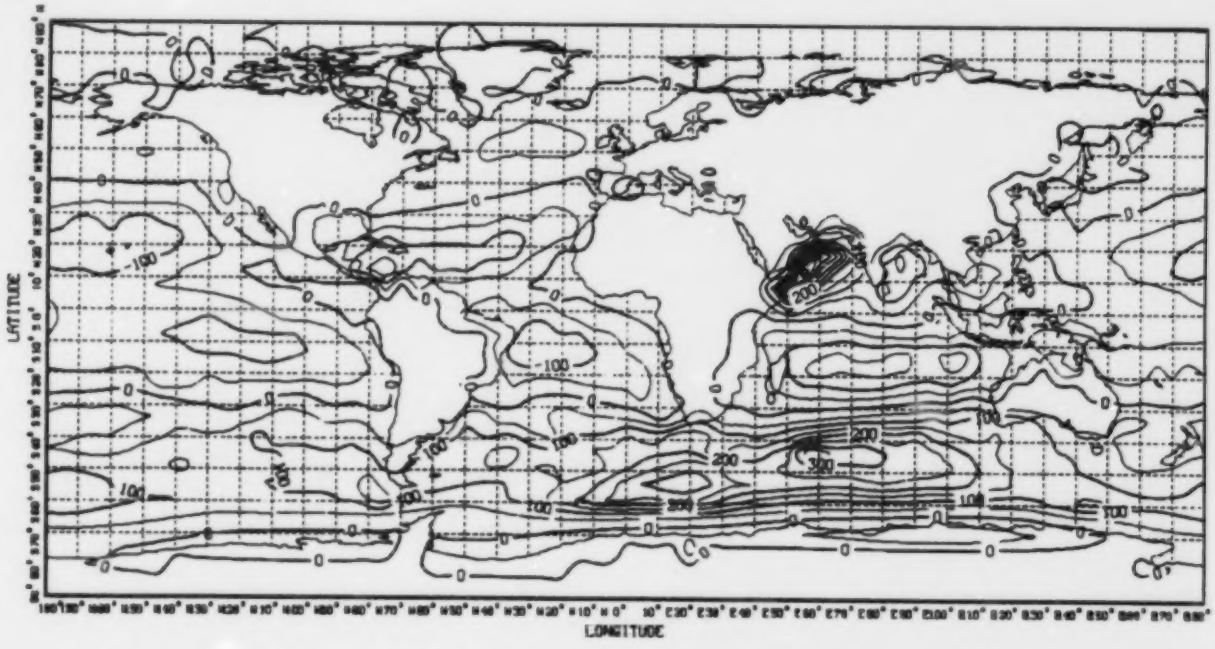

Figure 109

CANADA (CCC) WINTER U SURFACE STRESS .001*(N/M**2)

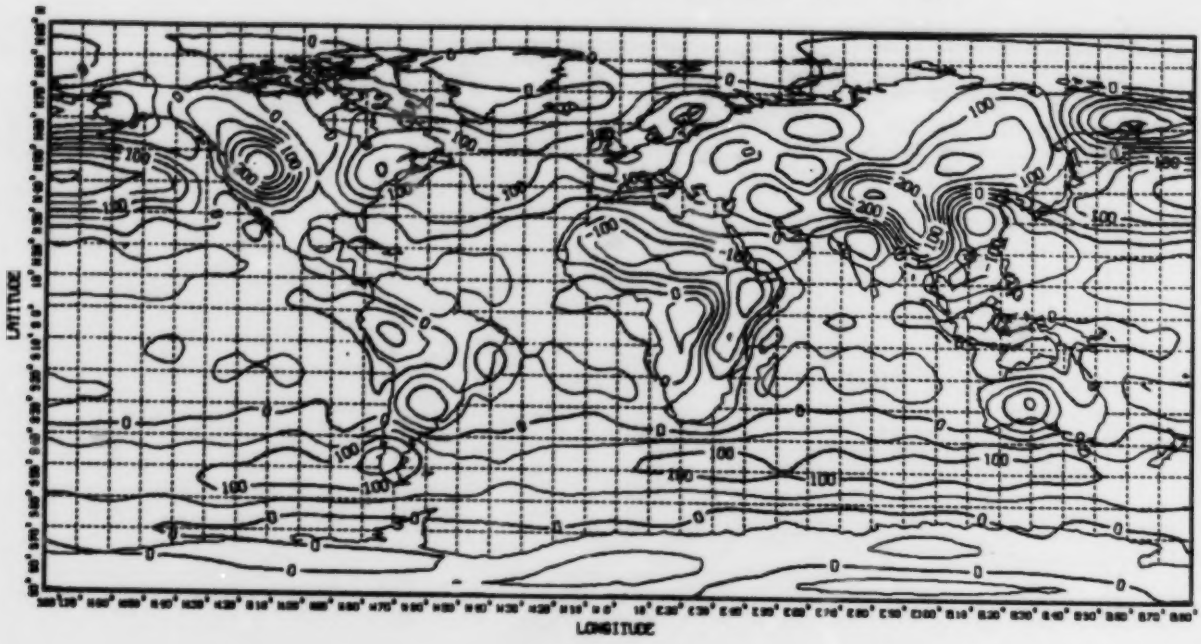

CANADA (CCC) SUMMER U SURFACE STRESS .001*(N/M**2)

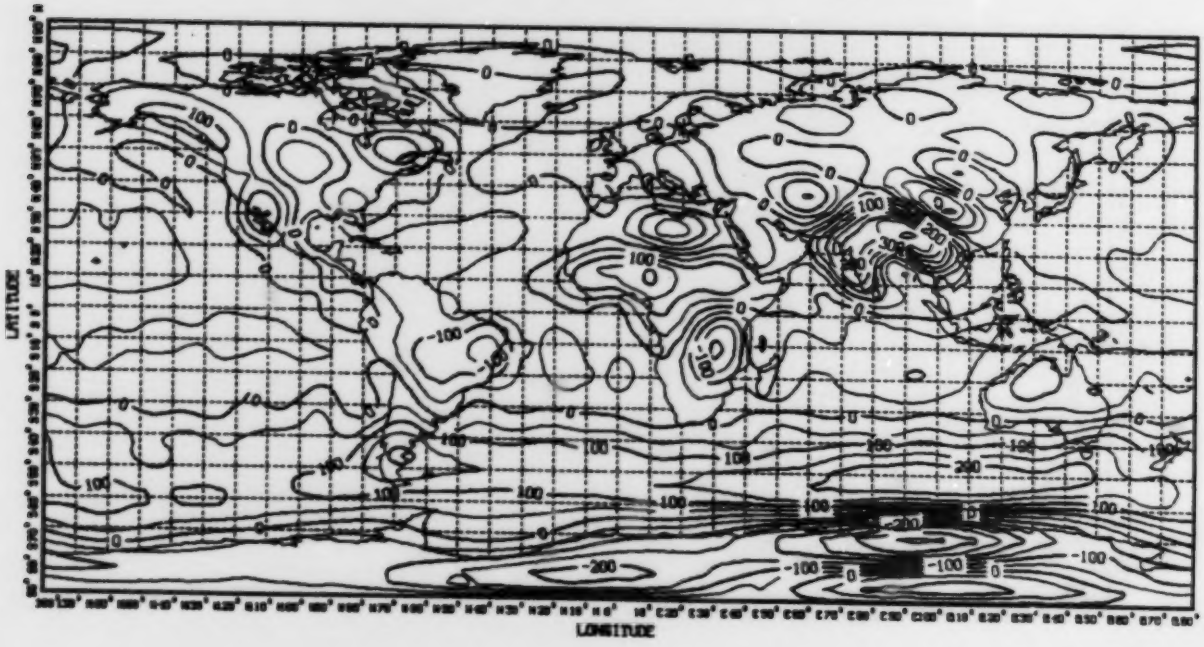

Figure 110

ENGLAND (BMO) WINTER U SURFACE STRESS .001*(N/M**2)

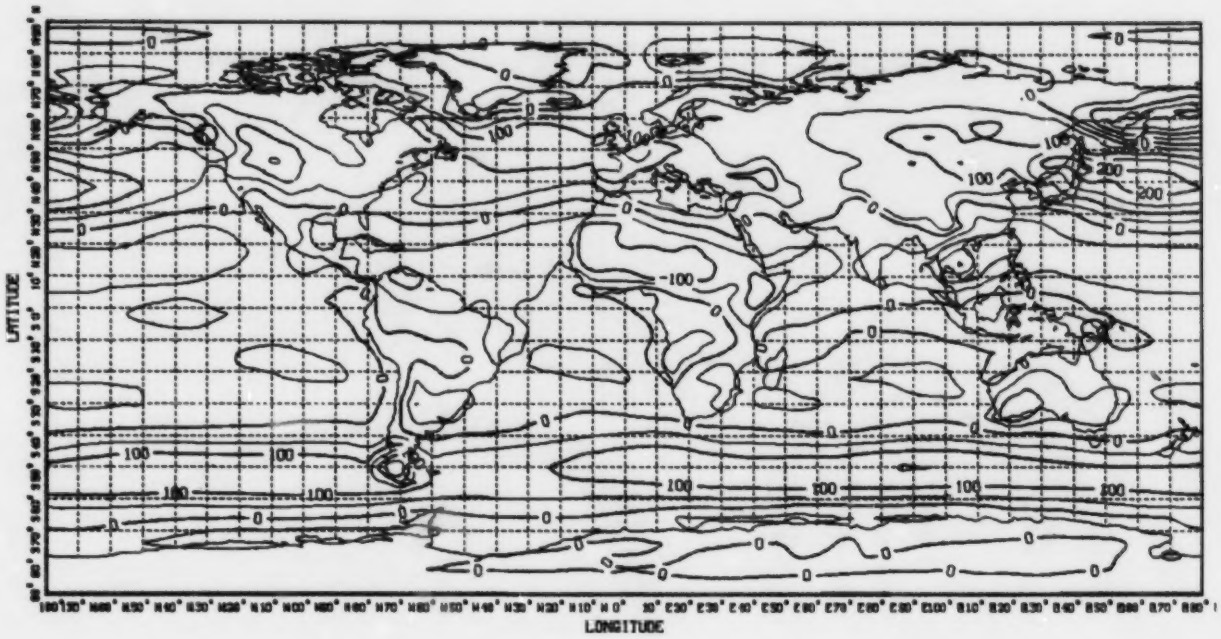

ENGLAND (BMO) SUMMER U SURFACE STRESS .001*(N/M**2)

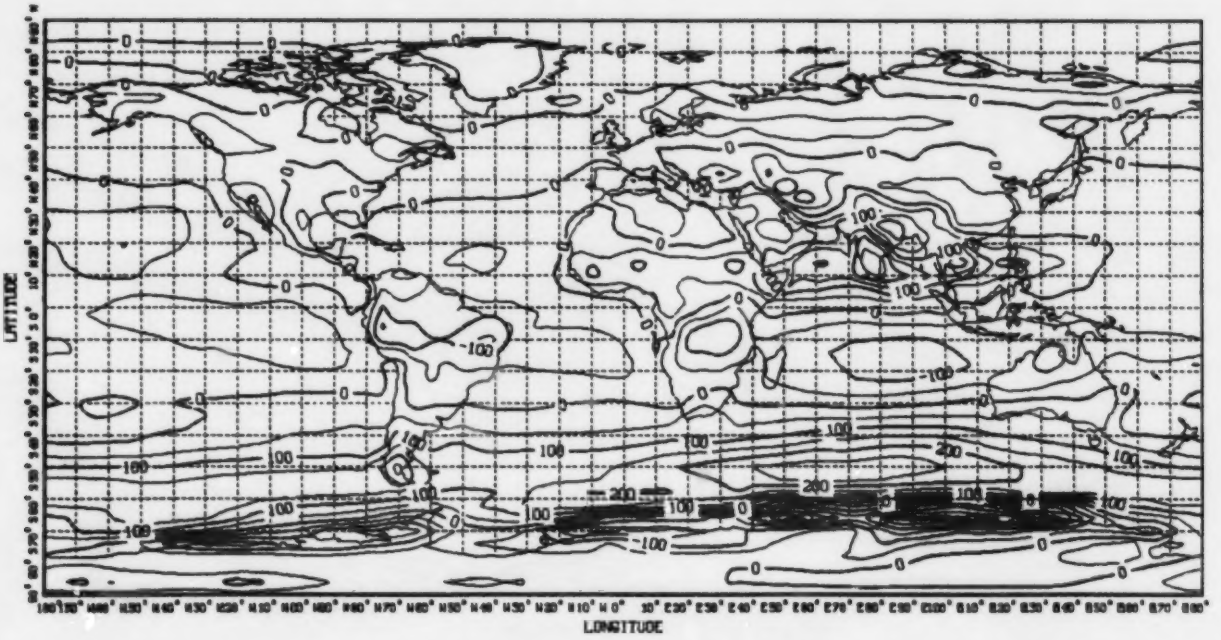

Figure 111

AUSTRALIA (BMRC) JANUARY U SURFACE STRESS .001×(N/M××2)

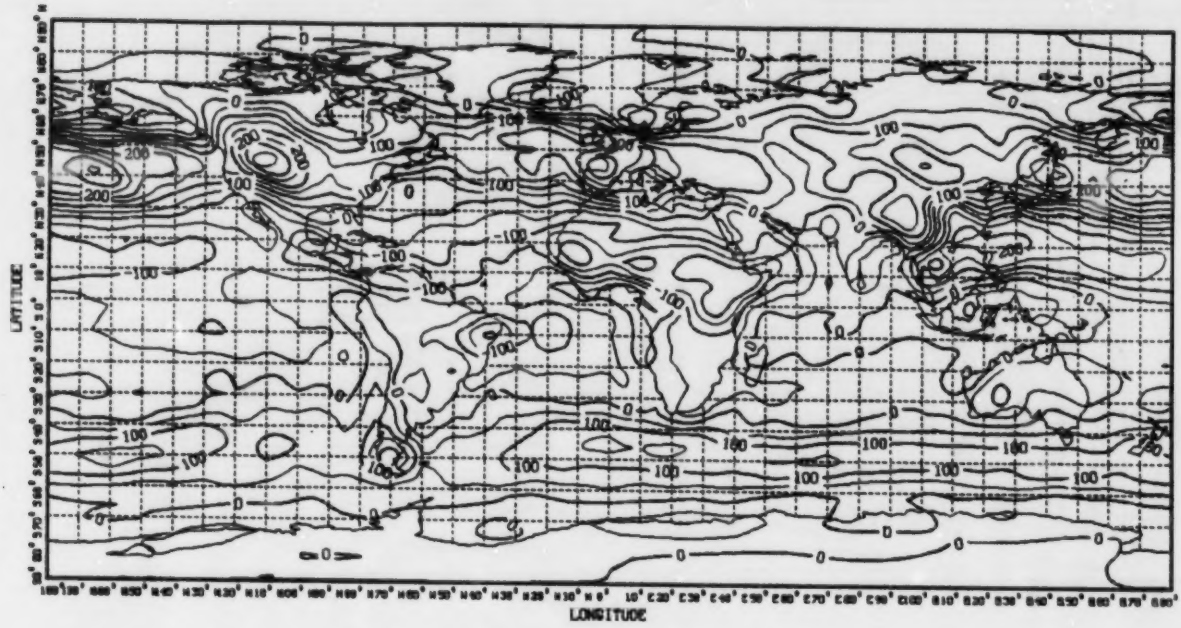

AUSTRALIA (BMRC) JULY U SURFACE STRESS .001×(N/M××2)

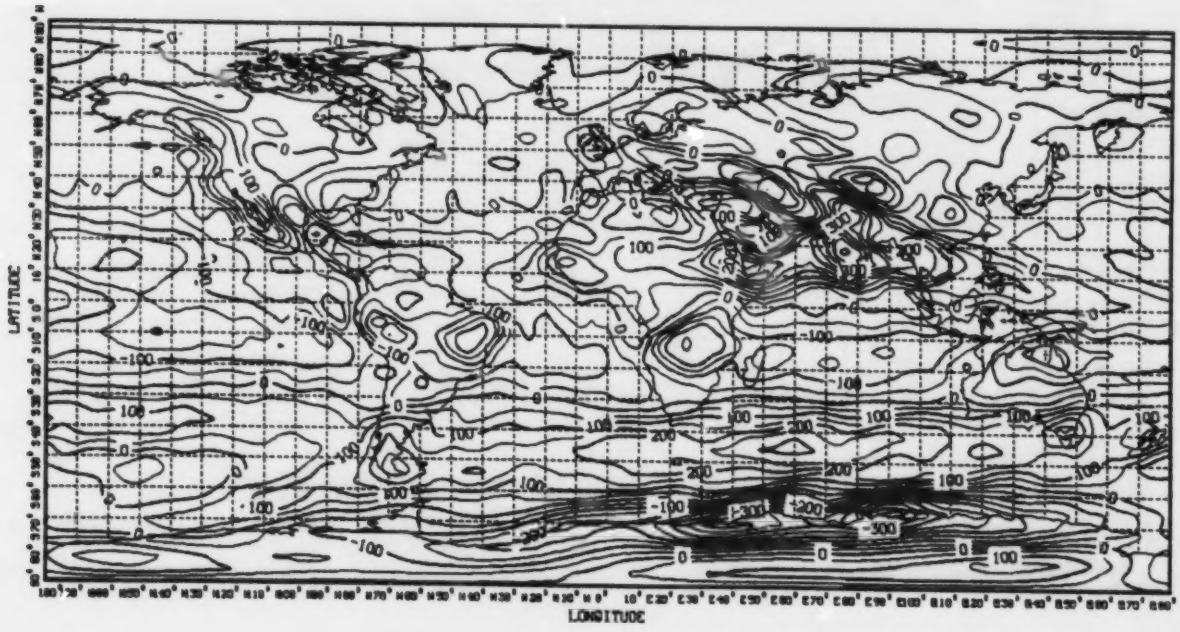

Figure 112

U S A (COLA!) JANUARY U SURFACE STRESS .001*(N/M**2)

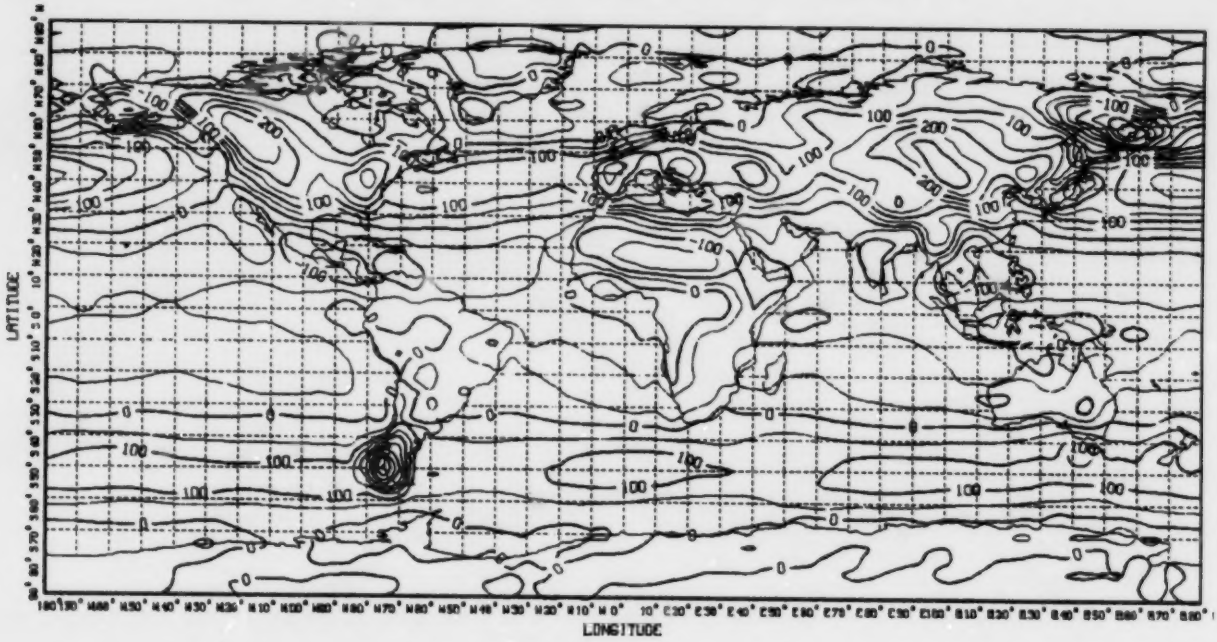

U S A (COLA!) JULY U SURFACE STRESS .001*(N/M**2)

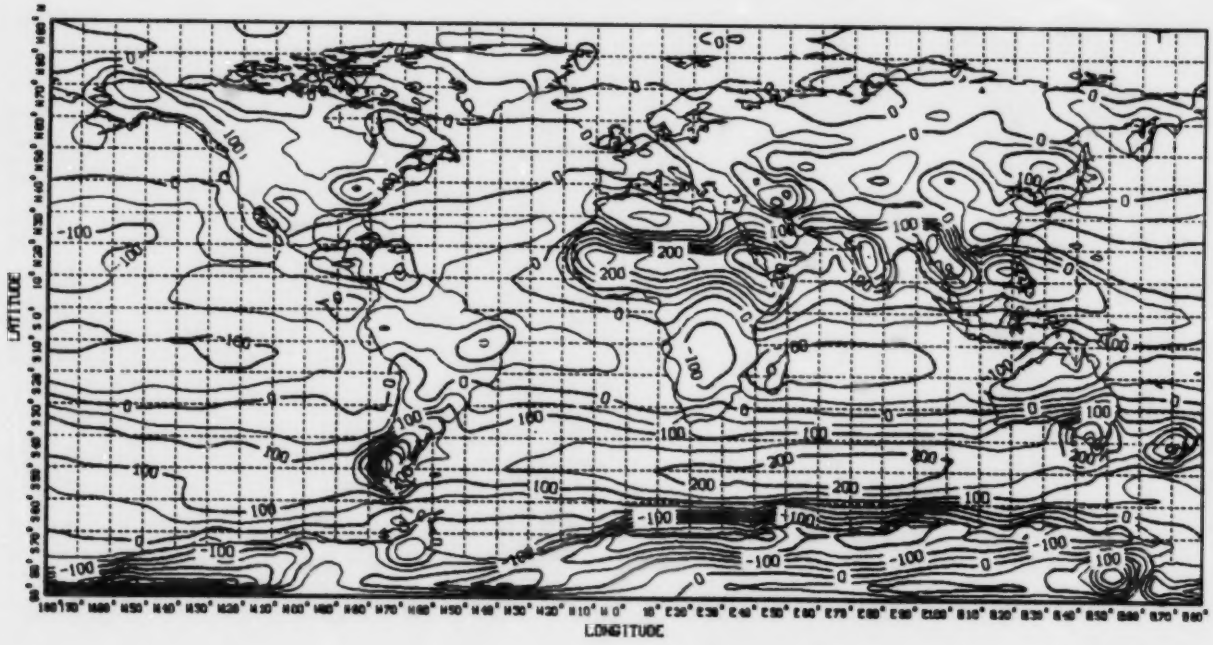

Figure 113

U S A (GFDL) JANUARY U SURFACE STRESS .001×(N/M××2)

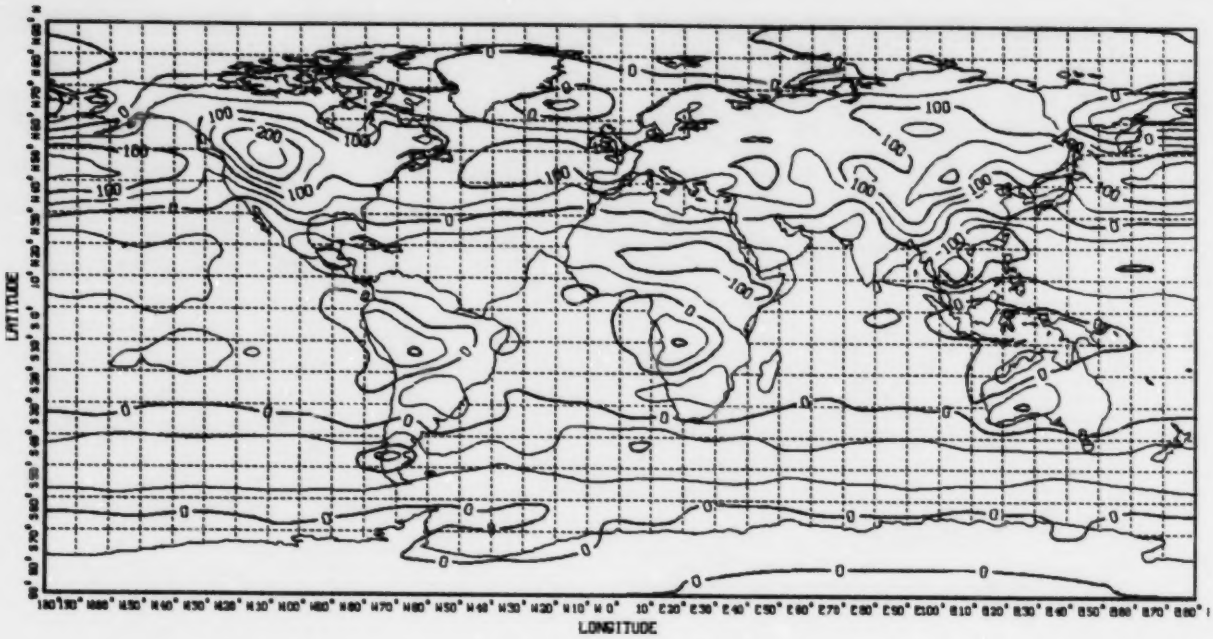

U S A (GFDL) JULY U SURFACE STRESS .001×(N/M××2)

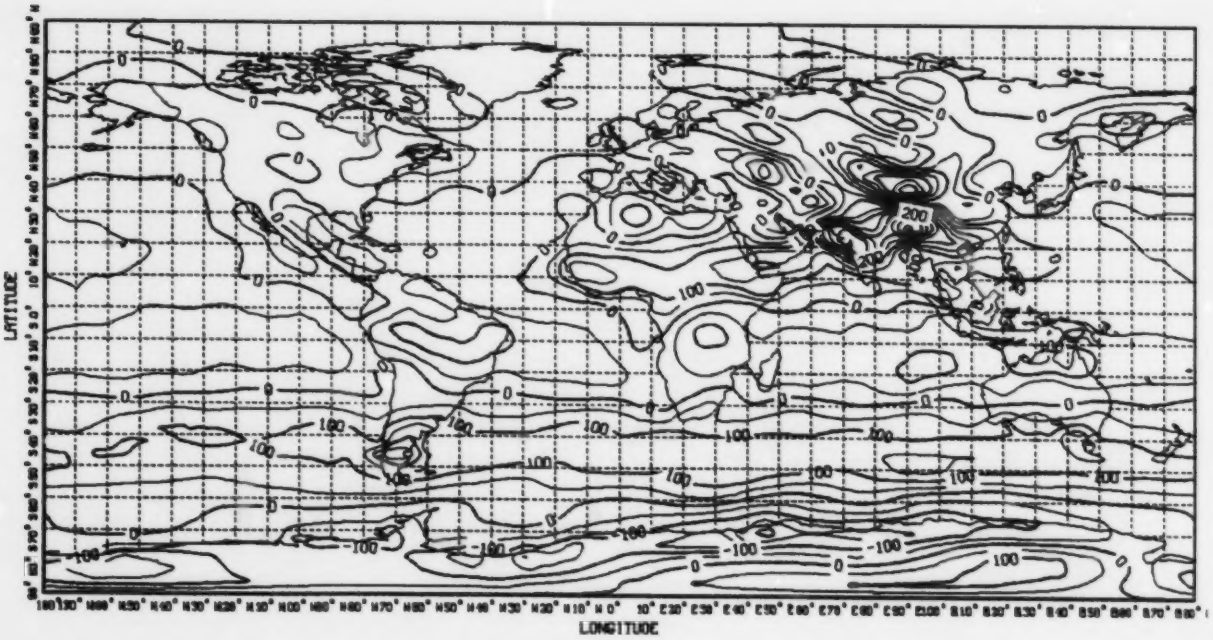

Figure 114

U S A (GISS) WINTER U SURFACE STRESS .001×(N/M××2)

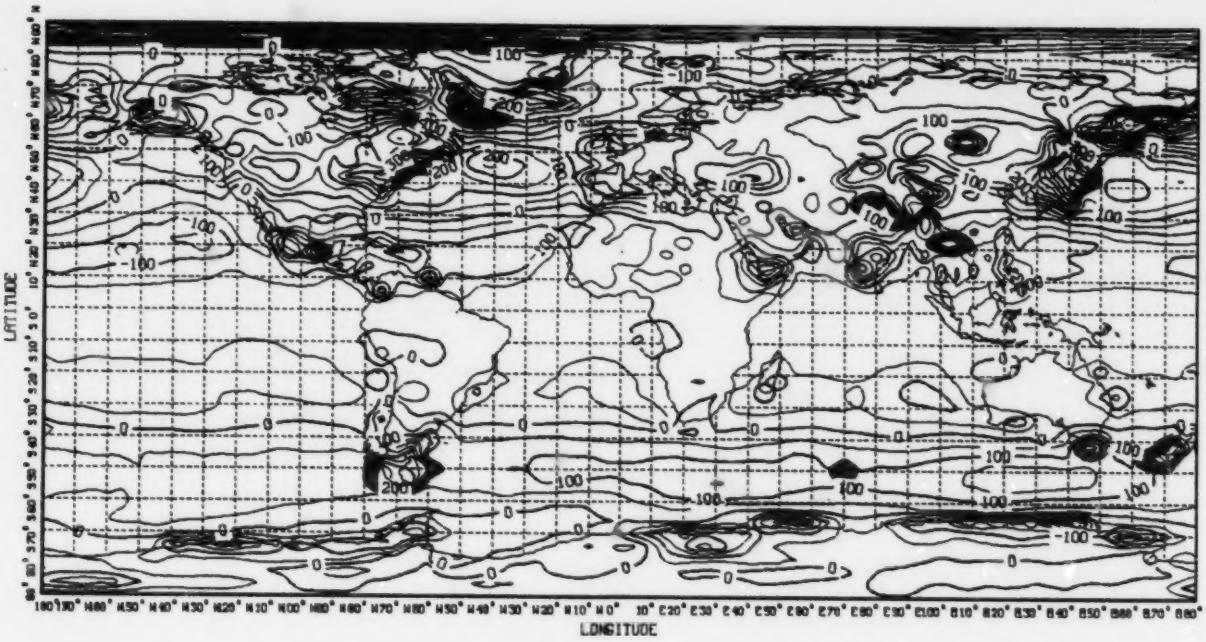

U S A (GISS) SUMMER U SURFACE STRESS .001×(N/M××2)

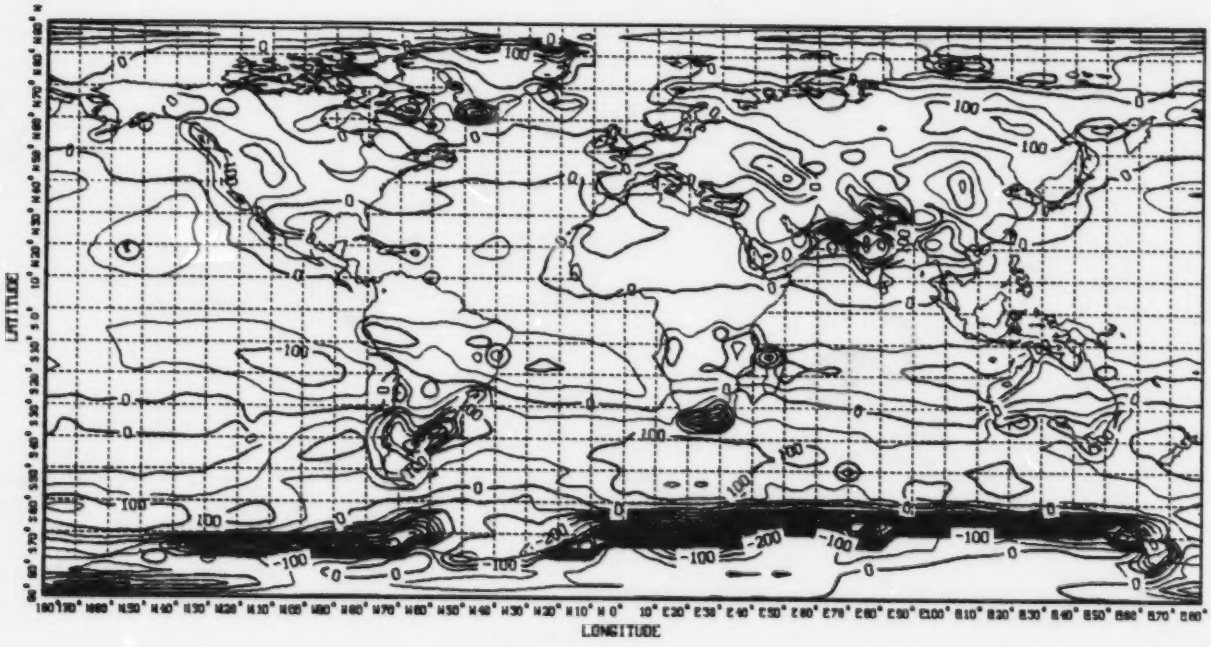

Figure 115

U S A (NCAR) JANUARY U SURFACE STRESS .001×(N/M××2)

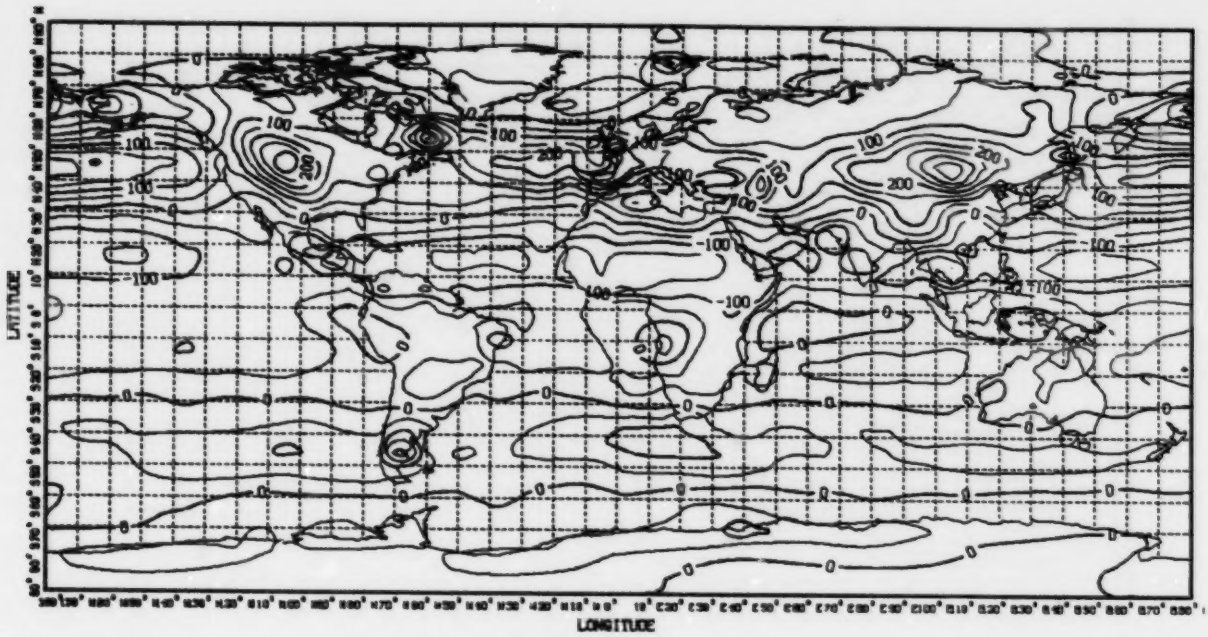

U S A (NCAR) JULY U SURFACE STRESS .001×(N/M××2)

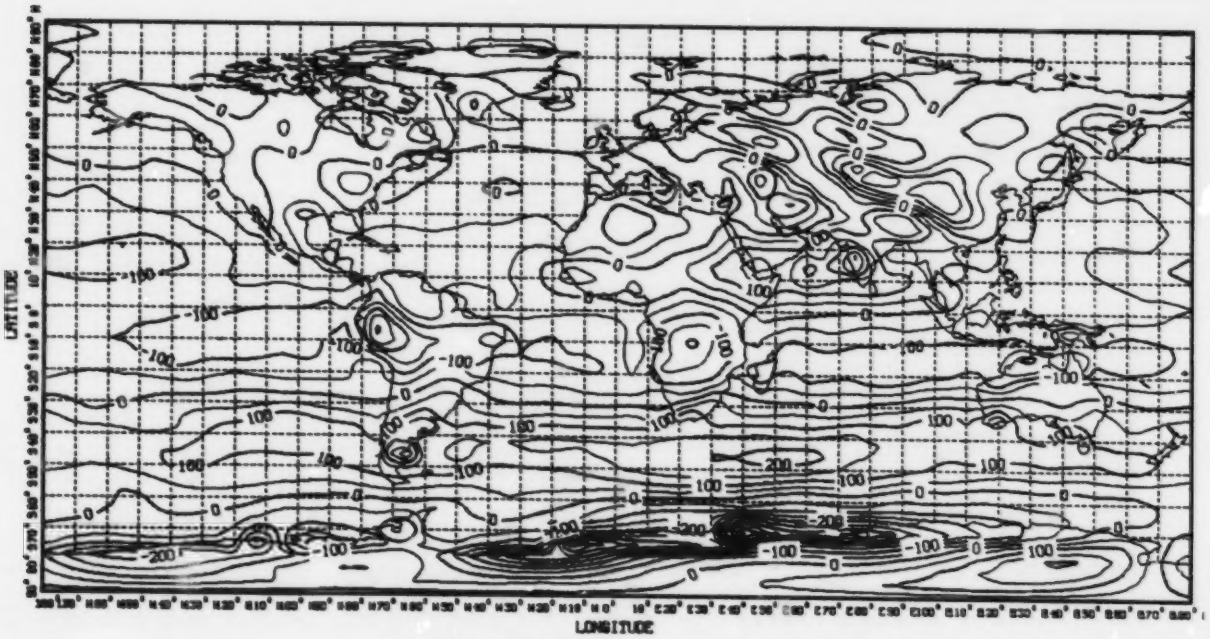

Figure 116

U S A (OSU) JANUARY U SURFACE STRESS .001*(N/M**2)

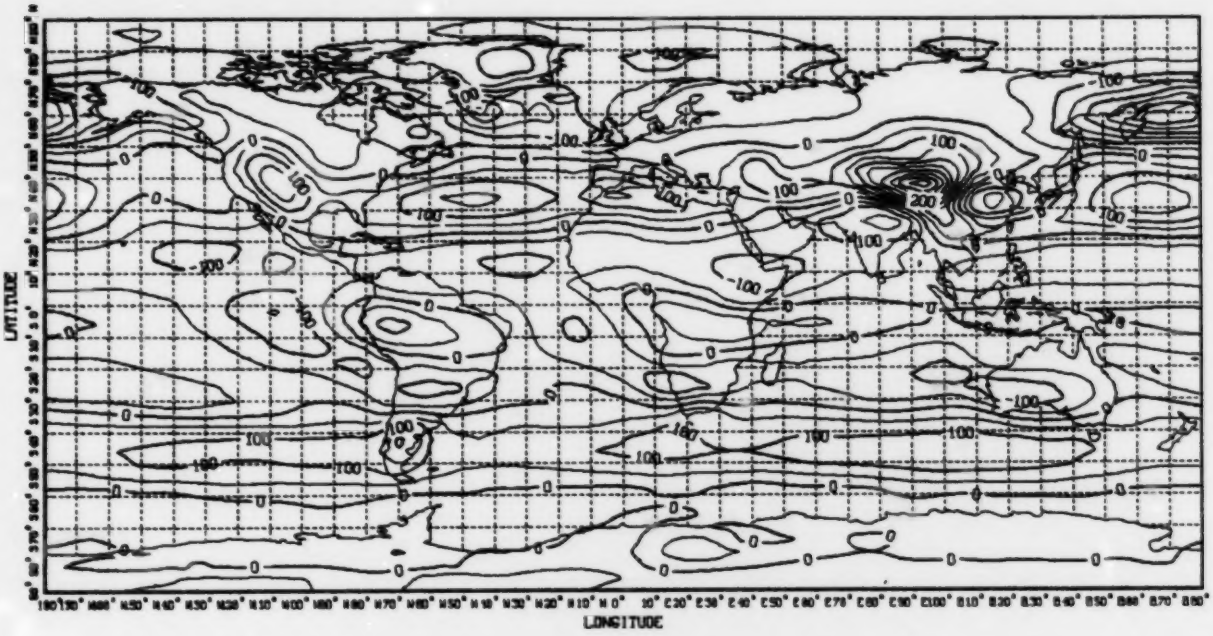

U S A (OSU) JULY U SURFACE STRESS .001*(N/M**2)

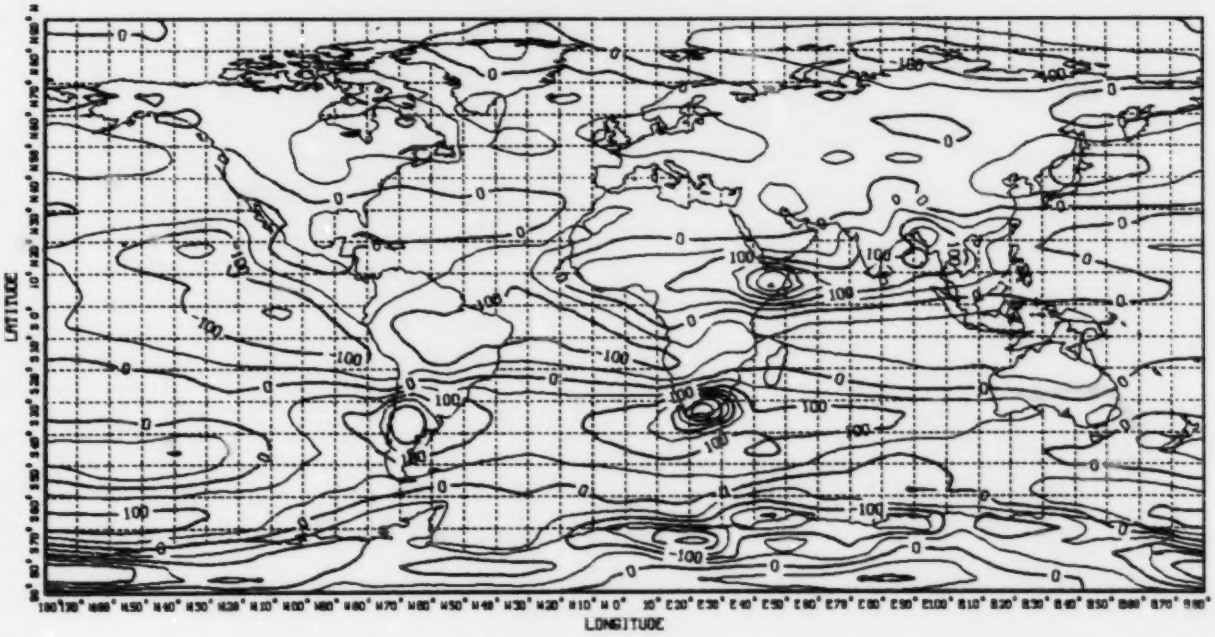

Figure 117

JAPAN (MRI) JANUARY U SURFACE STRESS .001×(N/M××2)

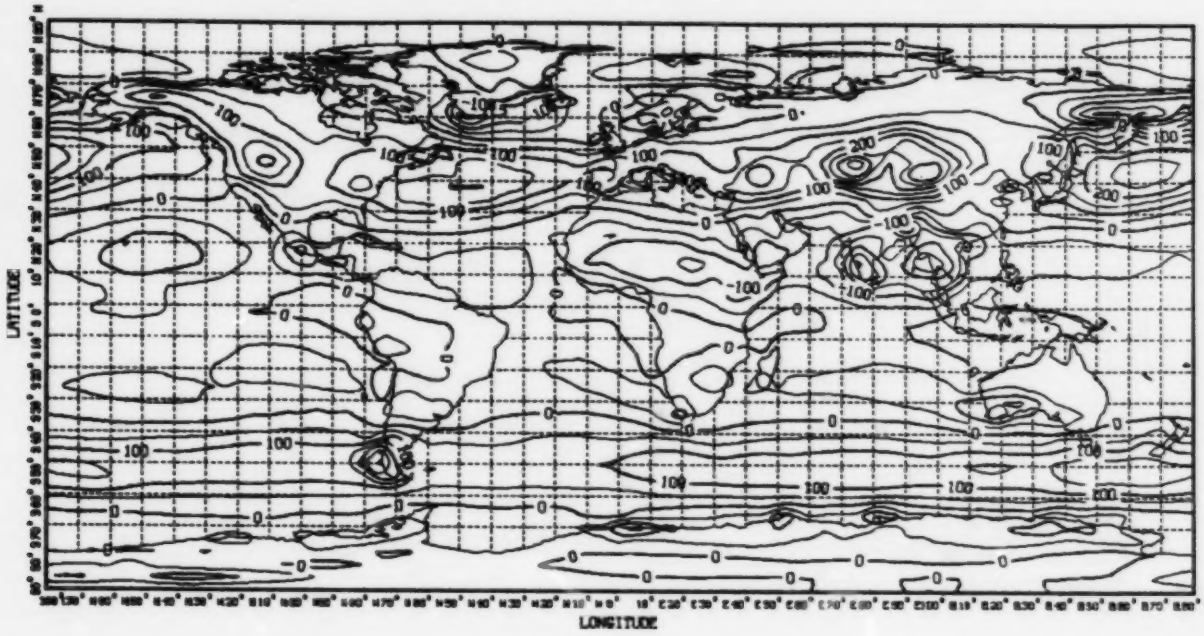

JAPAN (MRI) JULY U SURFACE STRESS .001×(N/M××2)

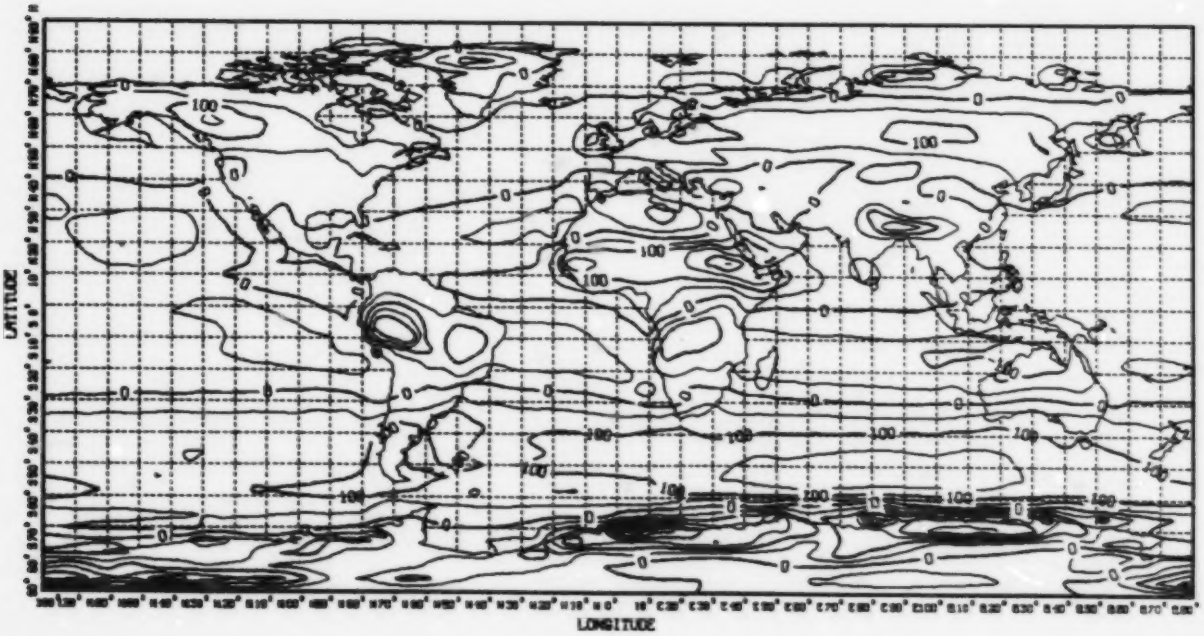

Figure 118

ECMWF JANUARY U SURFACE STRESS .001*(N/M**2)

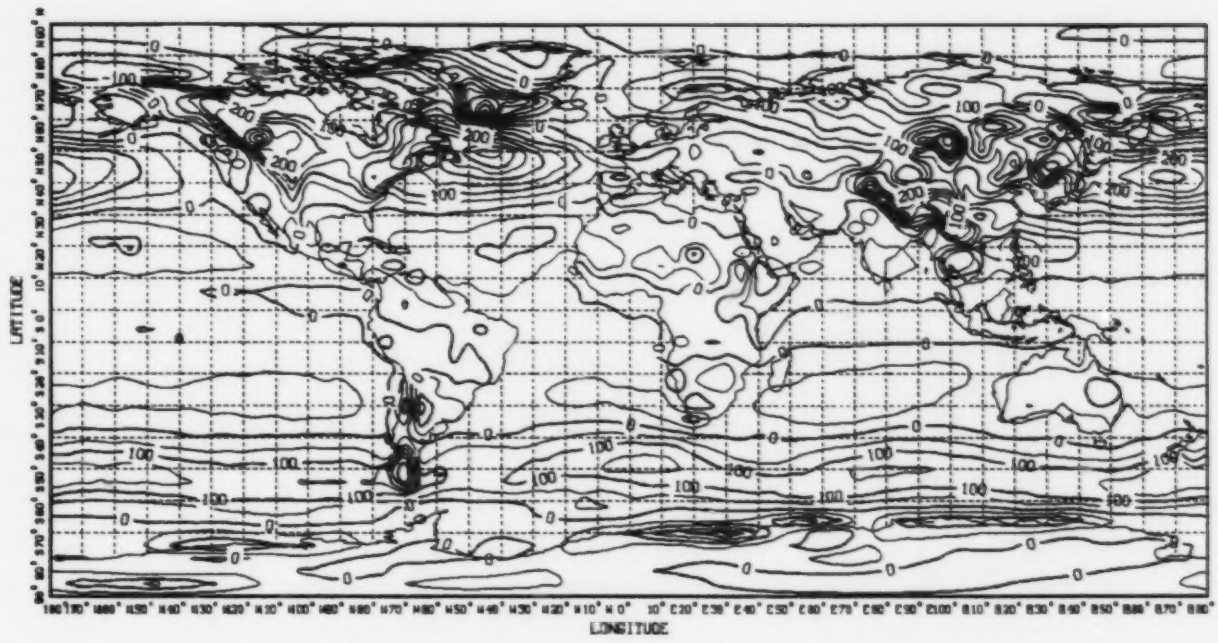

ECMWF JUNE U SURFACE STRESS .001*(N/M**2)

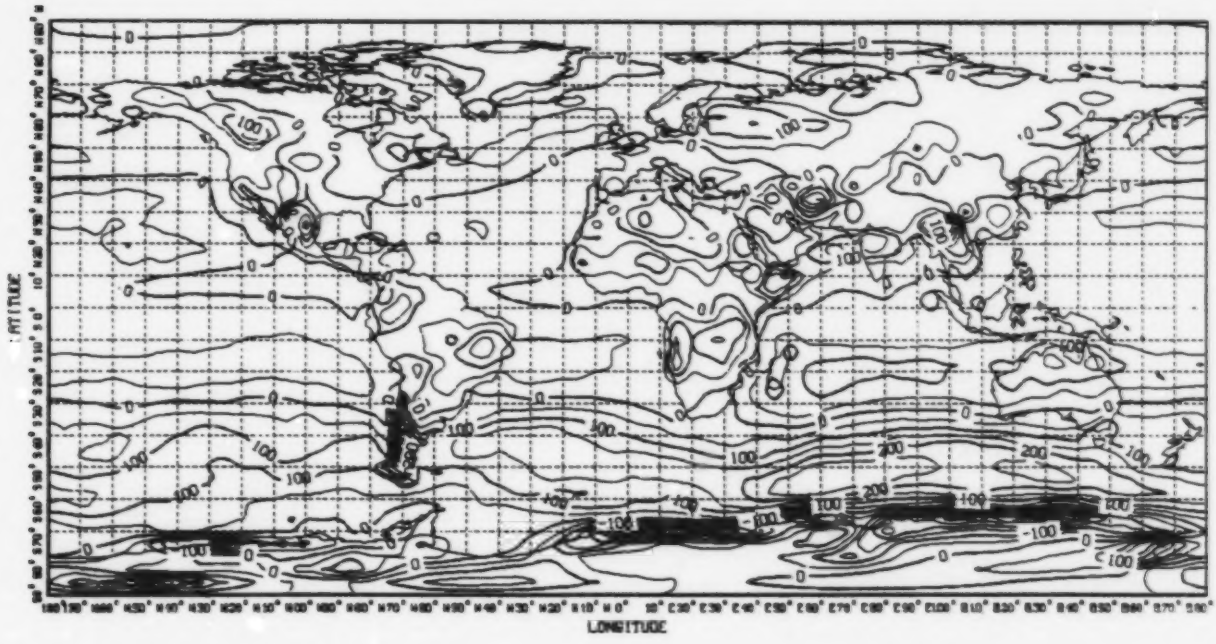

Figure 119

F R G (HAMBURG U) JANUARY U SURFACE STRESS .001*(N/M**2)

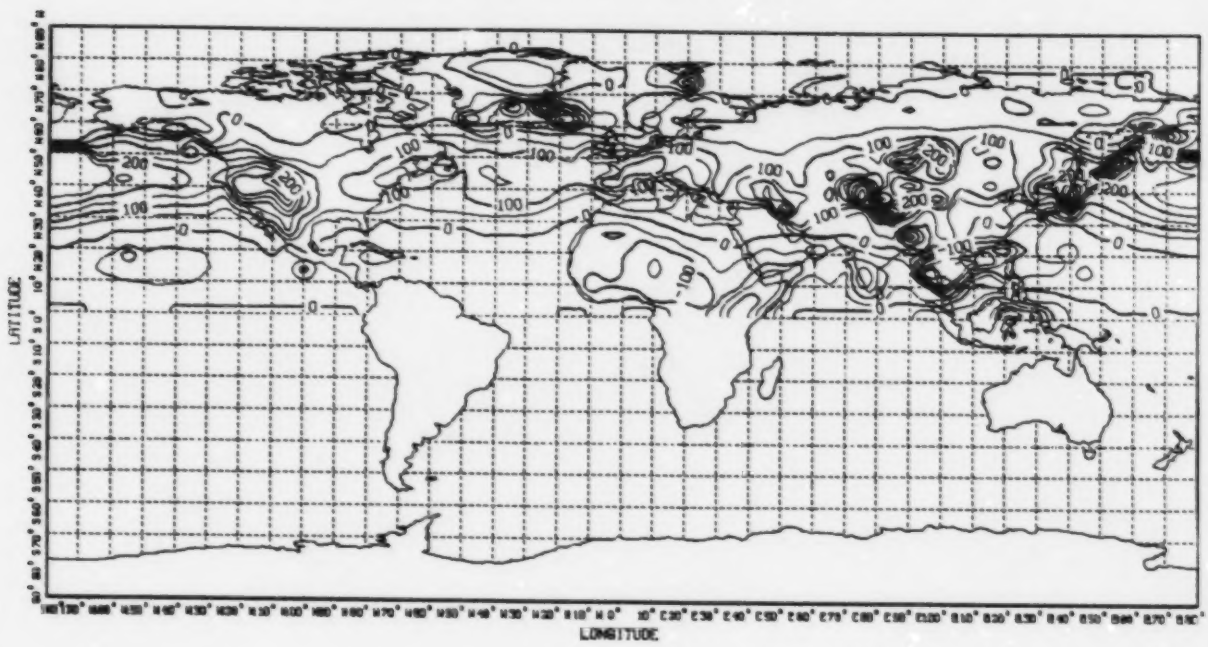

Figure 120

HAN AND LEE JANUARY V SURFACE STRESS .001*(N/M**2)

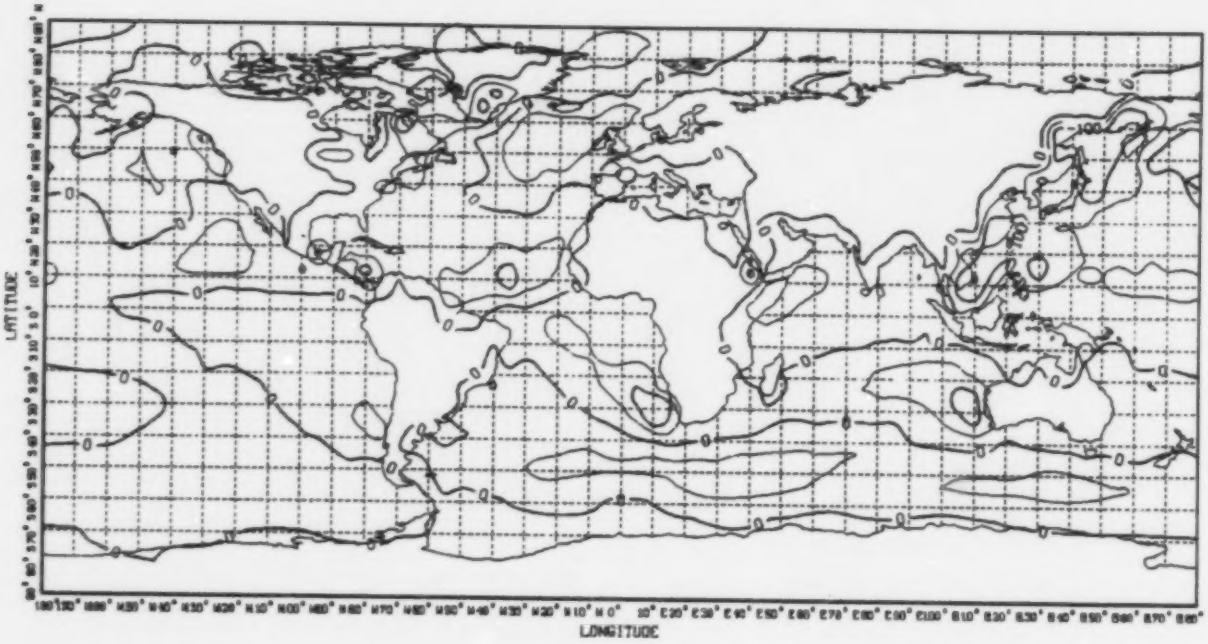

HAN AND LEE JULY V SURFACE STRESS .001*(N/M**2)

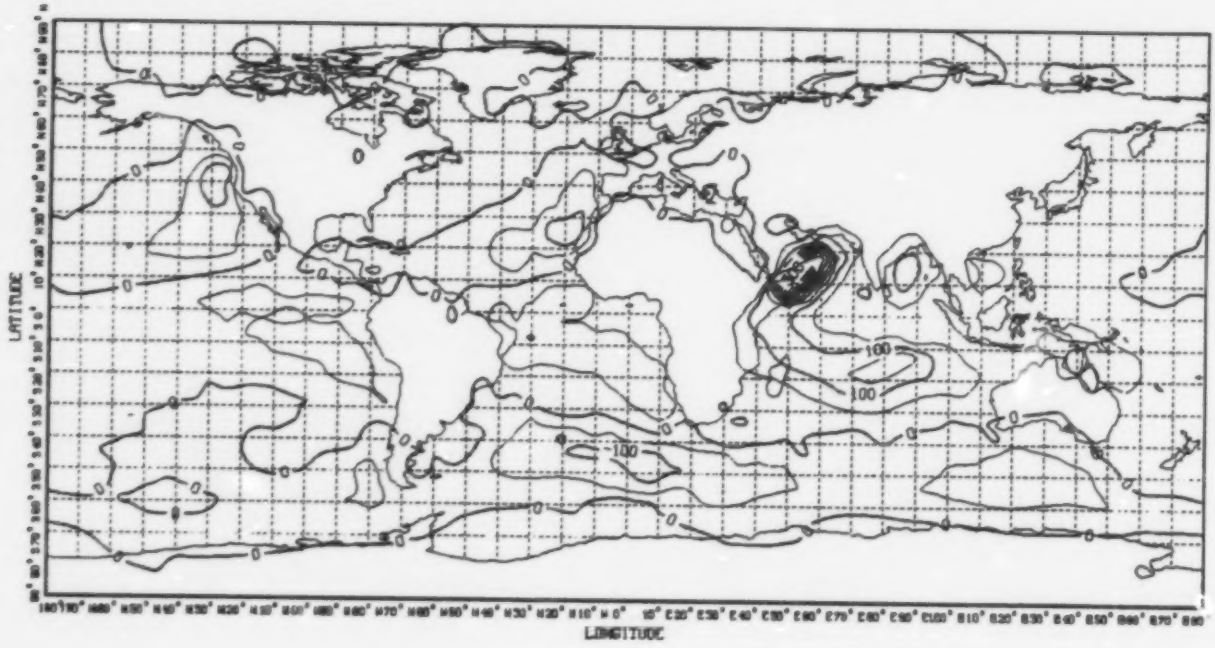

Figure 121

CANADA (CCC) WINTER V SURFACE STRESS .001*(N/M**2)

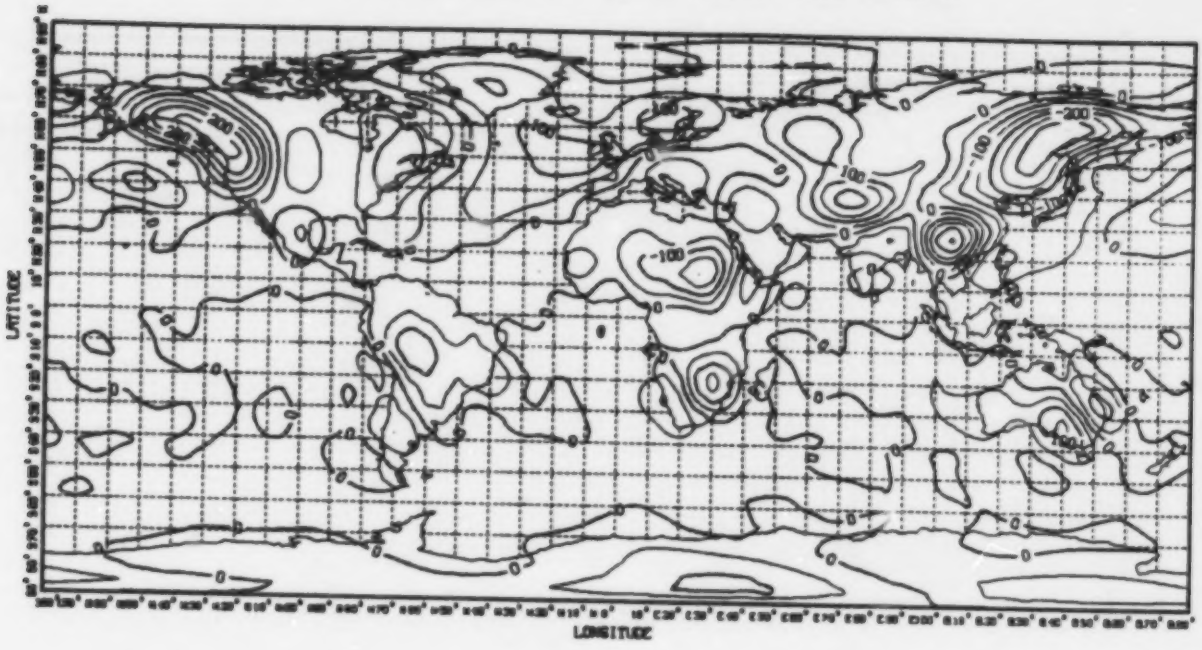

CANADA (CCC) SUMMER V SURFACE STRESS .001*(N/M**2)

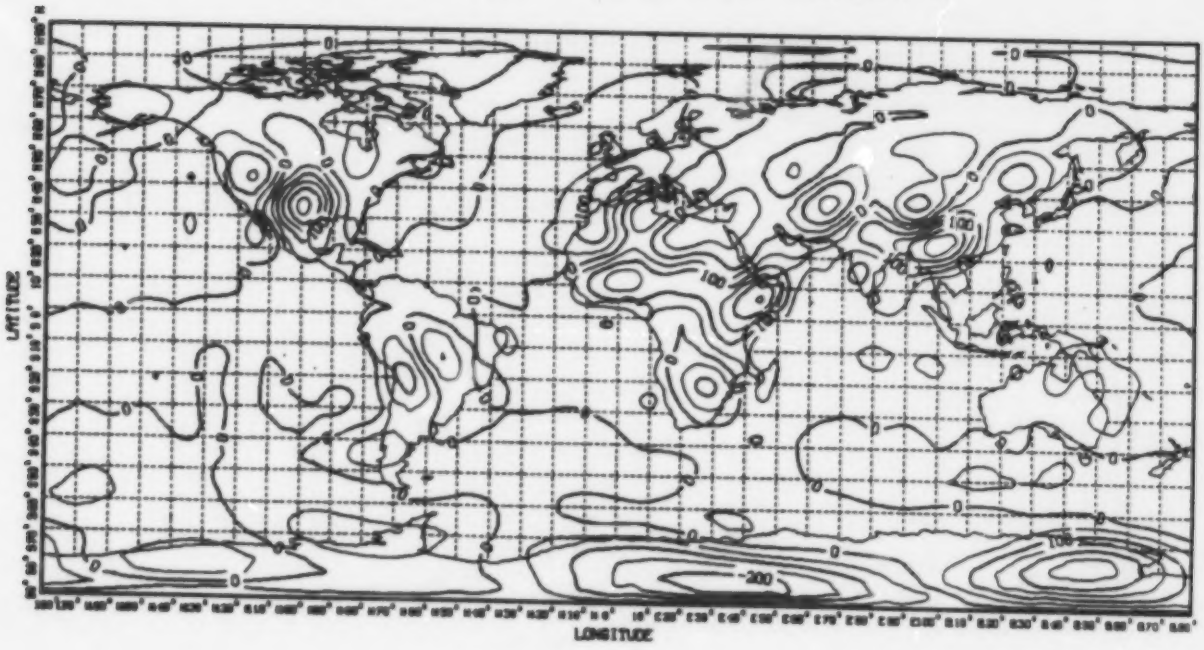

Figure 122

ENGLAND (BMO) WINTER V SURFACE STRESS .001×(N/M××2)

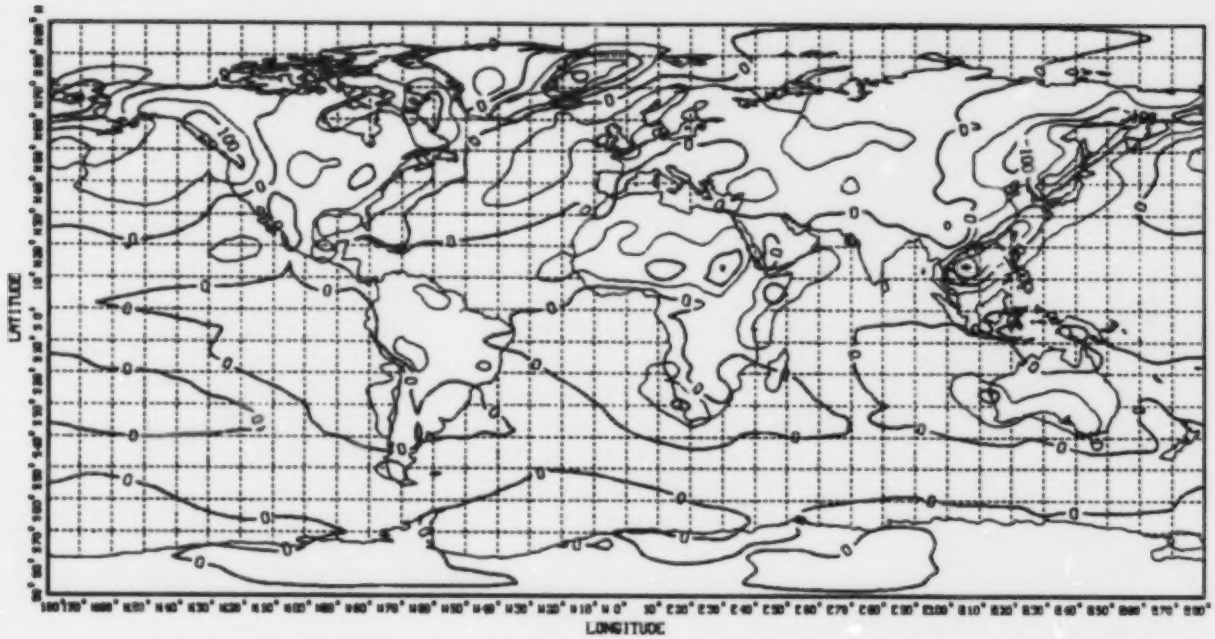

ENGLAND (BMO) SUMMER V SURFACE STRESS .001×(N/M××2)

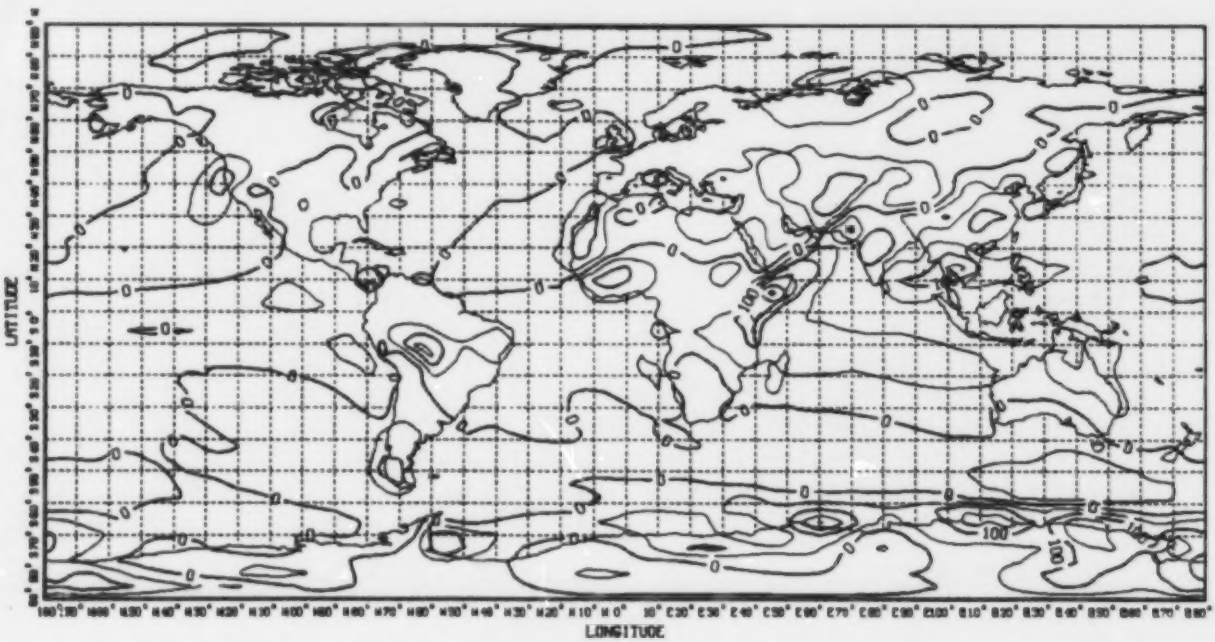

Figure 123

AUSTRALIA (BMRC) JANUARY V SURFACE STRESS .001×(N/M××2)

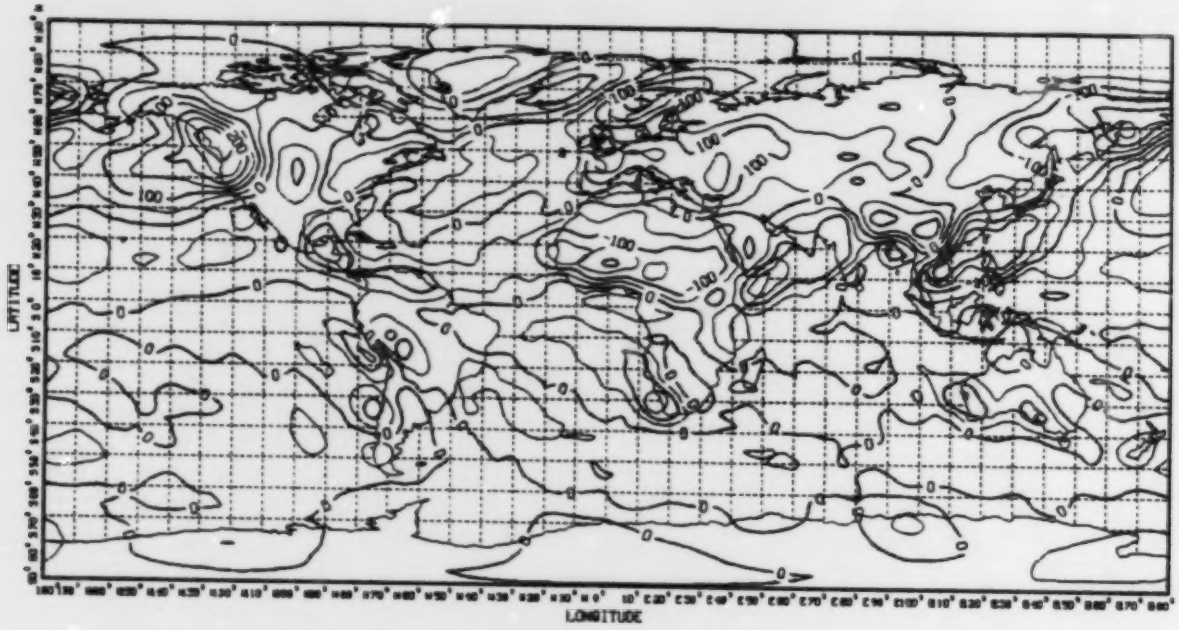

AUSTRALIA (BMRC) JULY V SURFACE STRESS .001×(N/M××2)

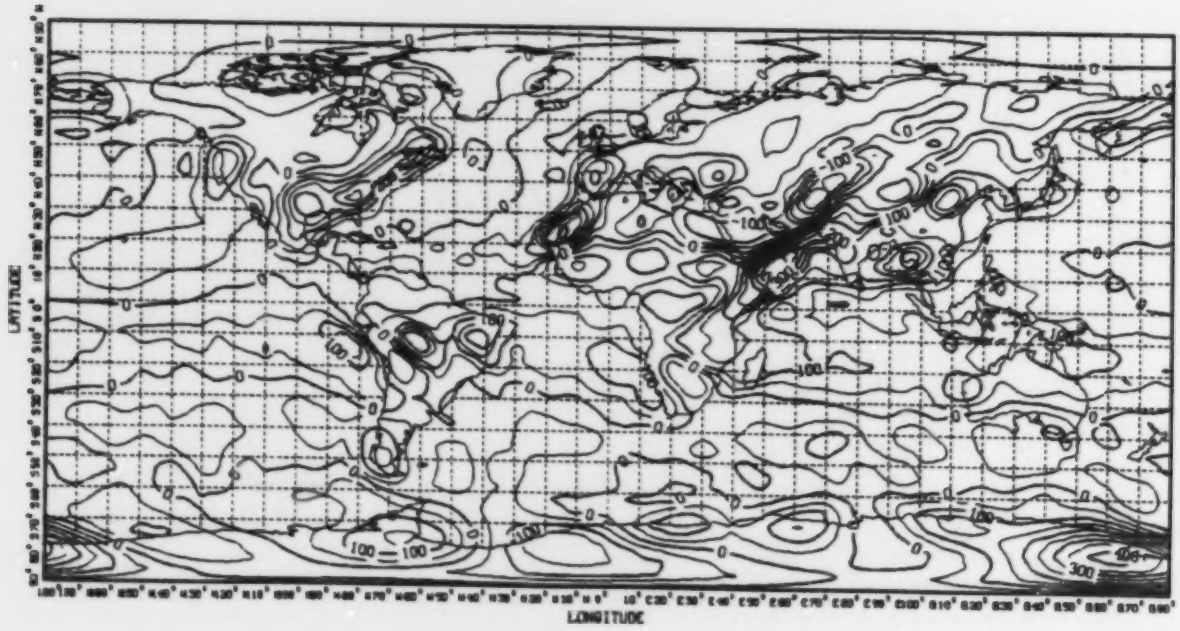

Figure 124

U S A (COLAI) JANUARY V SURFACE STRESS .001*(N/M**2)

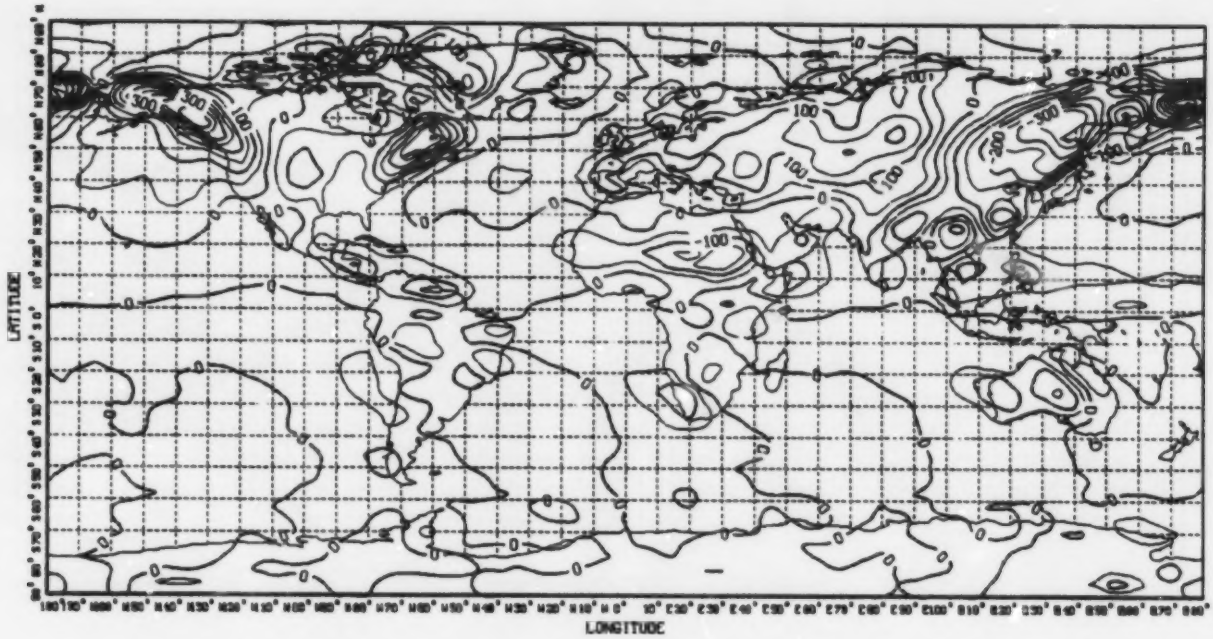

U S A (COLAI) JULY V SURFACE STRESS .001*(N/M**2)

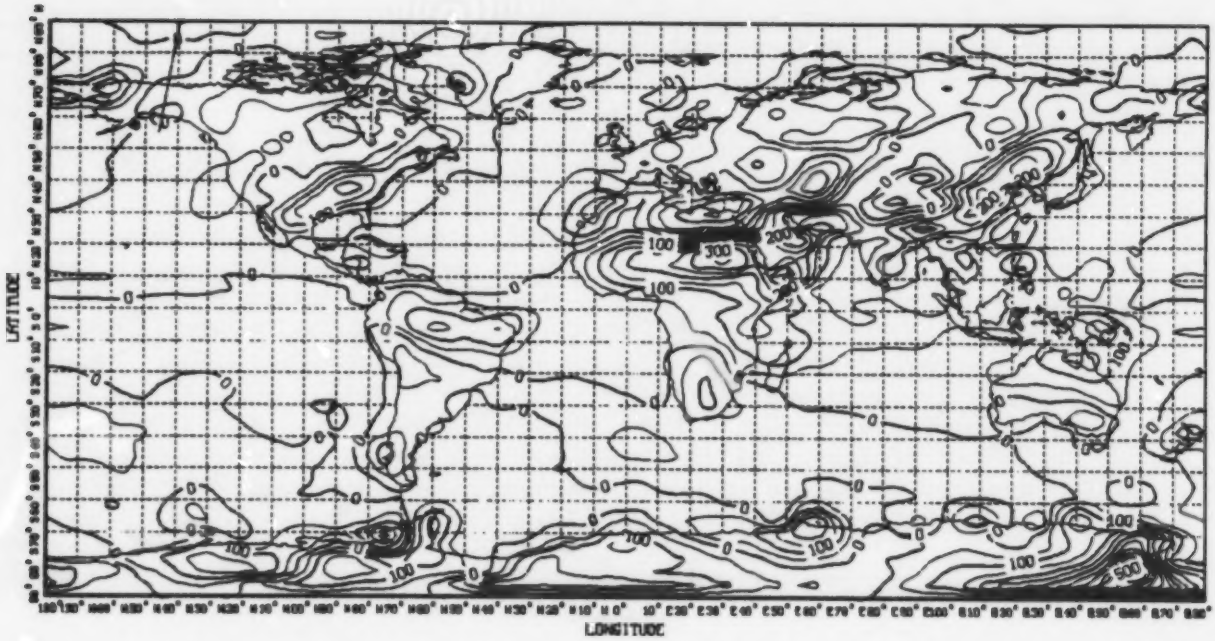

Figure 125

U S A (GFDL) JANUARY V SURFACE STRESS .001×(N/M××2)

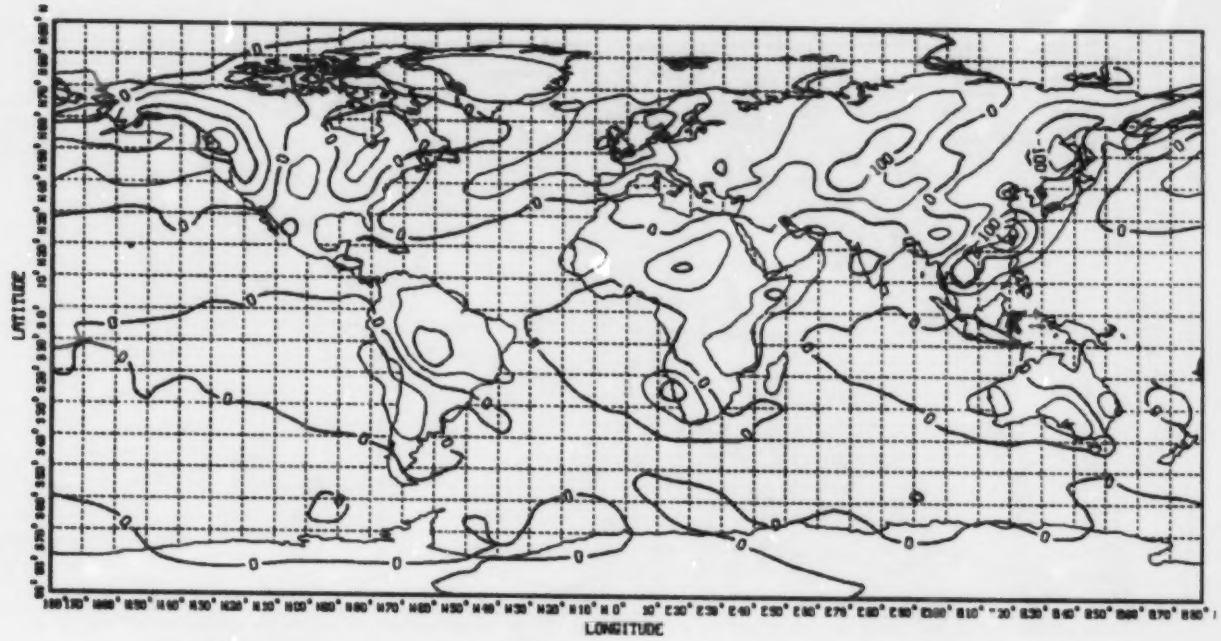

U S A (GFDL) JULY V SURFACE STRESS .001×(N/M××2)

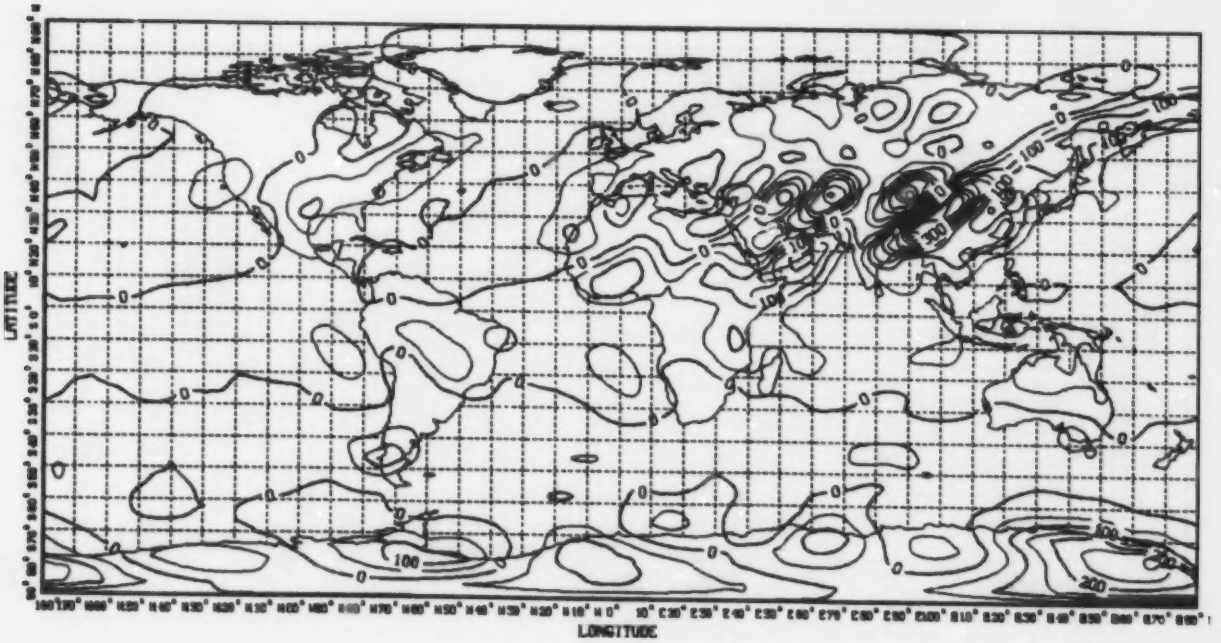

Figure 126

U S A (GISS) WINTER V SURFACE STRESS .001*(N/M**2)

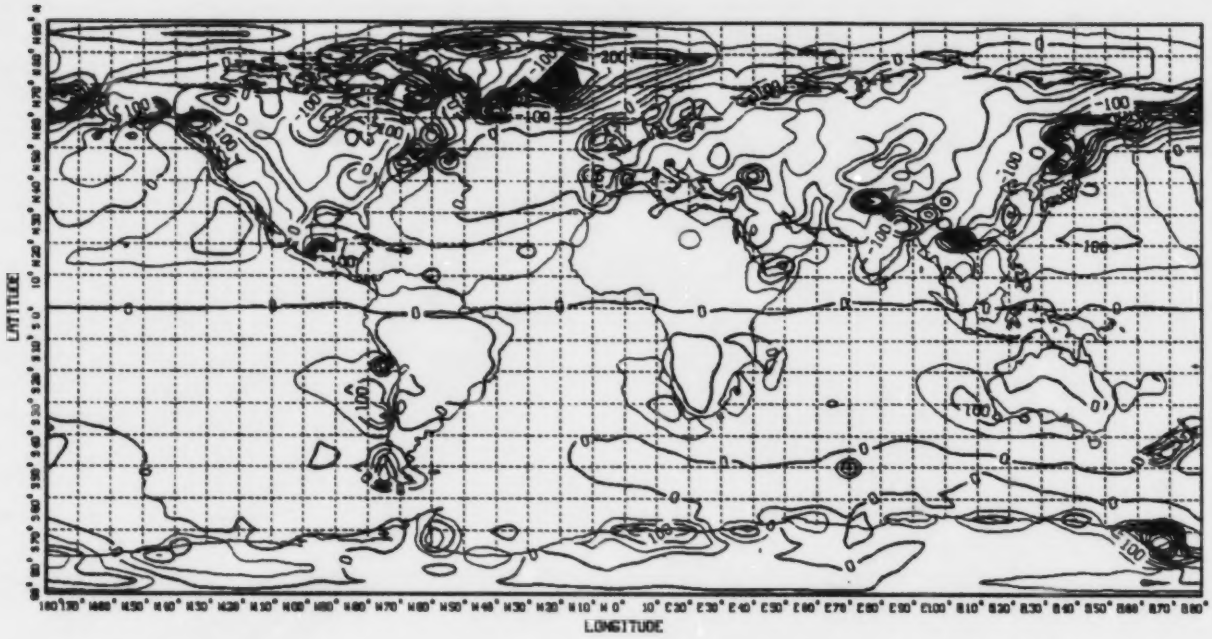

U S A (GISS) SUMMER V SURFACE STRESS .001*(N/M**2)

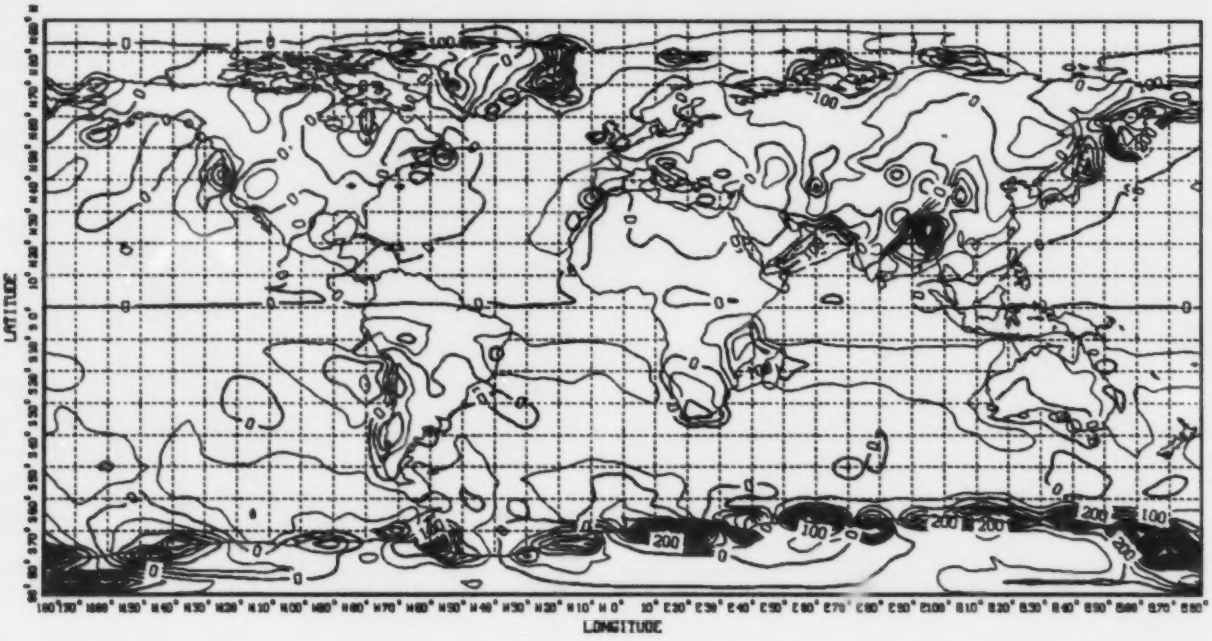

Figure 127

U S A (NCAR) JANUARY V SURFACE STRESS .001×(N/M××2)

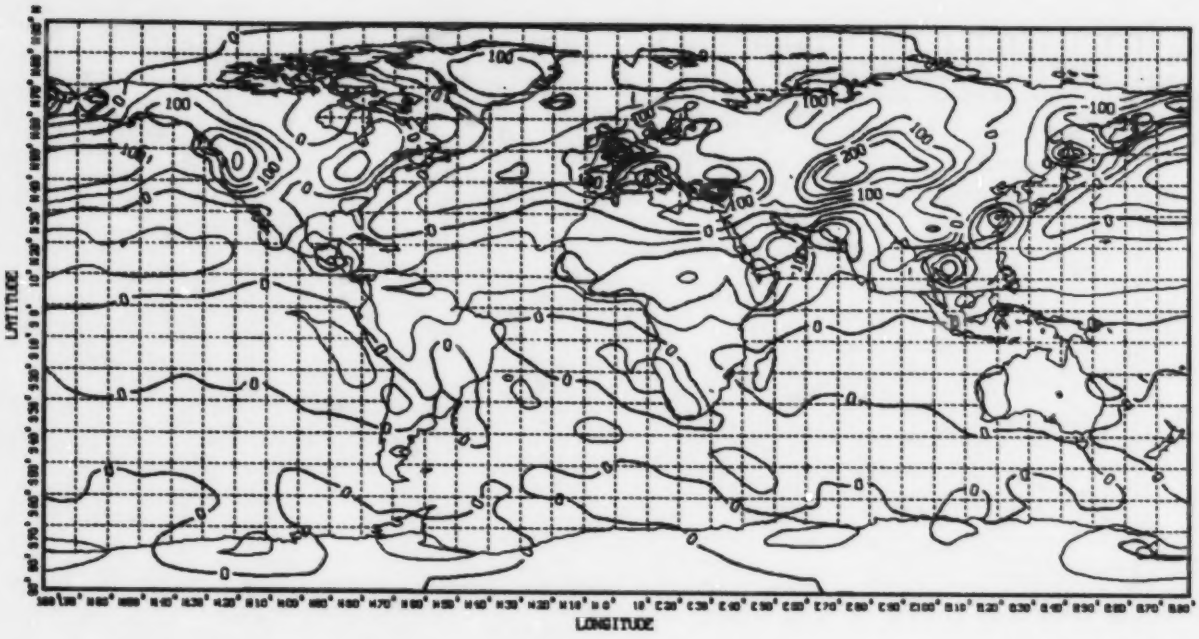

U S A (NCAR) JULY V SURFACE STRESS .001×(N/M××2)

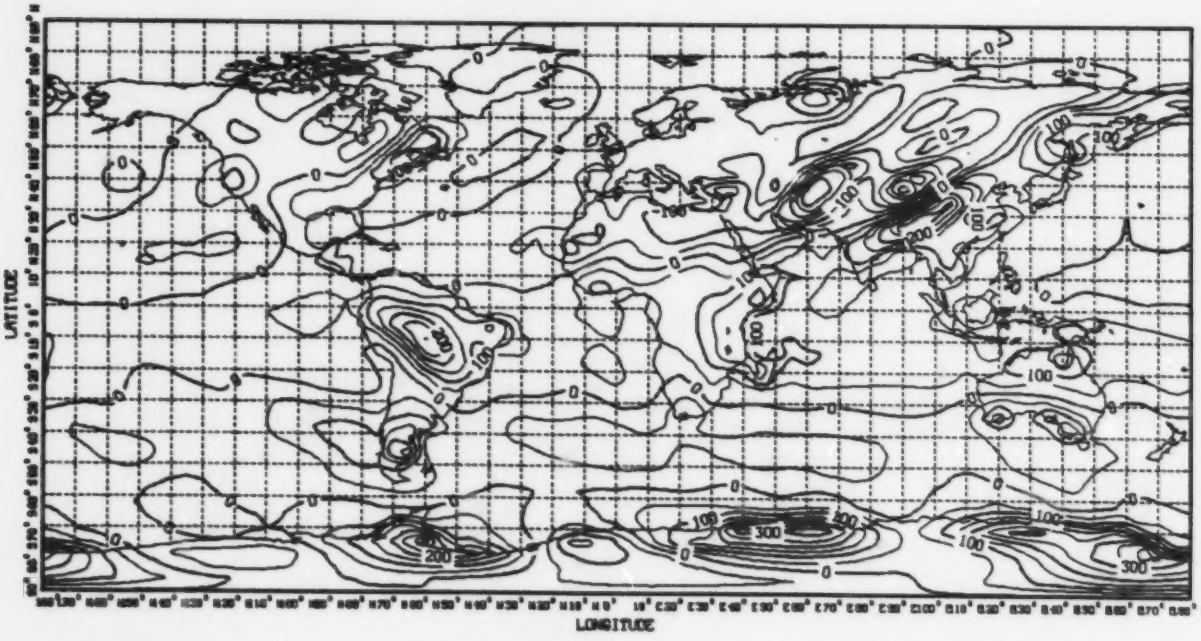

Figure 128

U S A (OSU) JANUARY V SURFACE STRESS .001×(N/M××2)

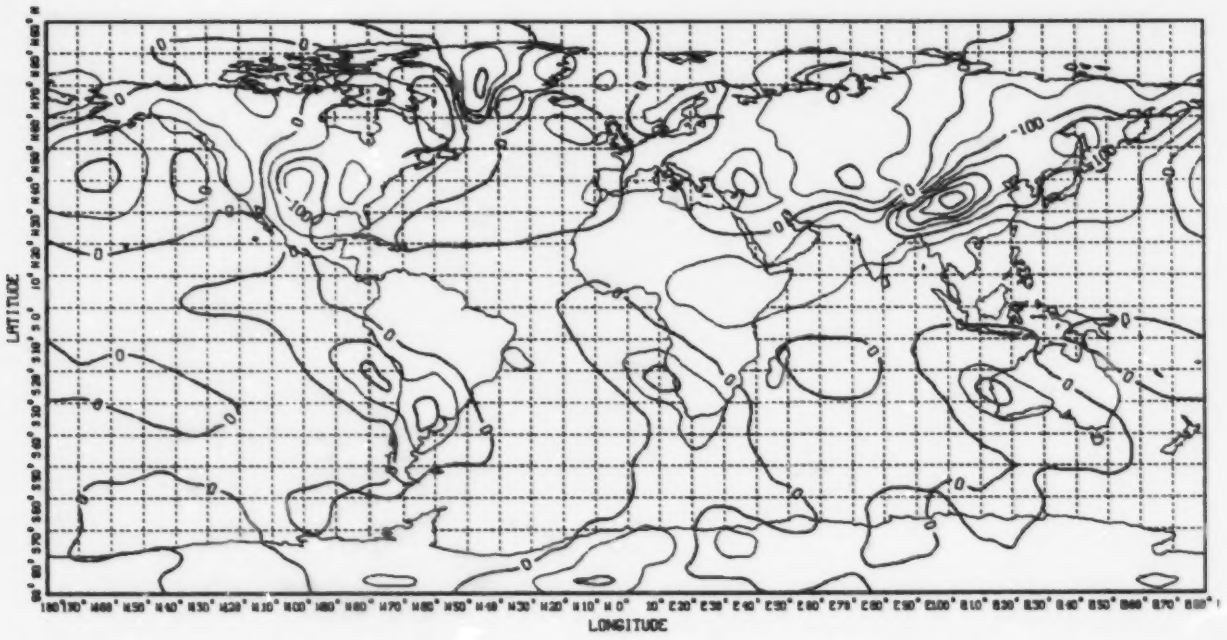

U S A (OSU) JULY V SURFACE STRESS .001×(N/M××2)

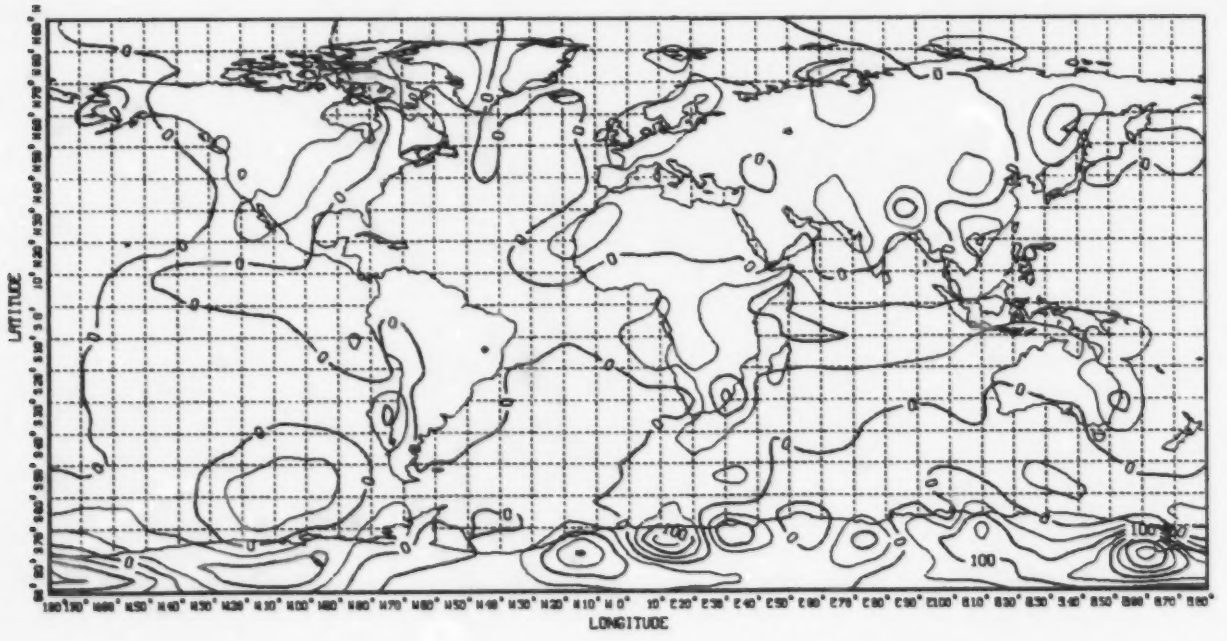

Figure 129

JAPAN (MRI) JANUARY V SURFACE STRESS .001*(N/M**2)

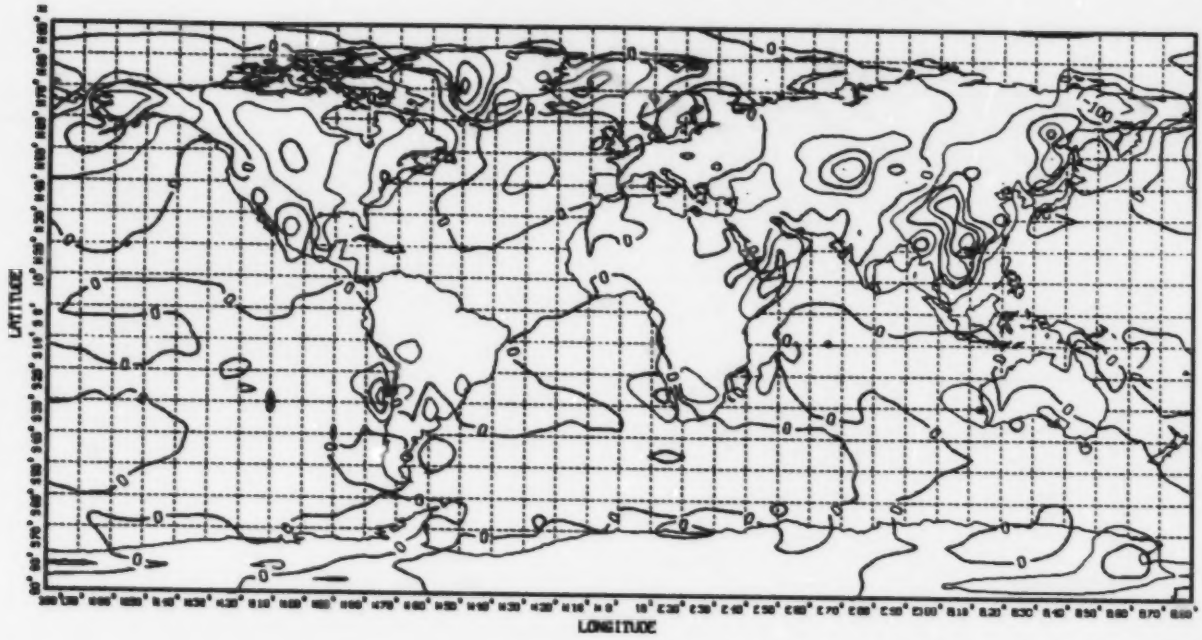

JAPAN (MRI) JULY V SURFACE STRESS .001*(N/M**2)

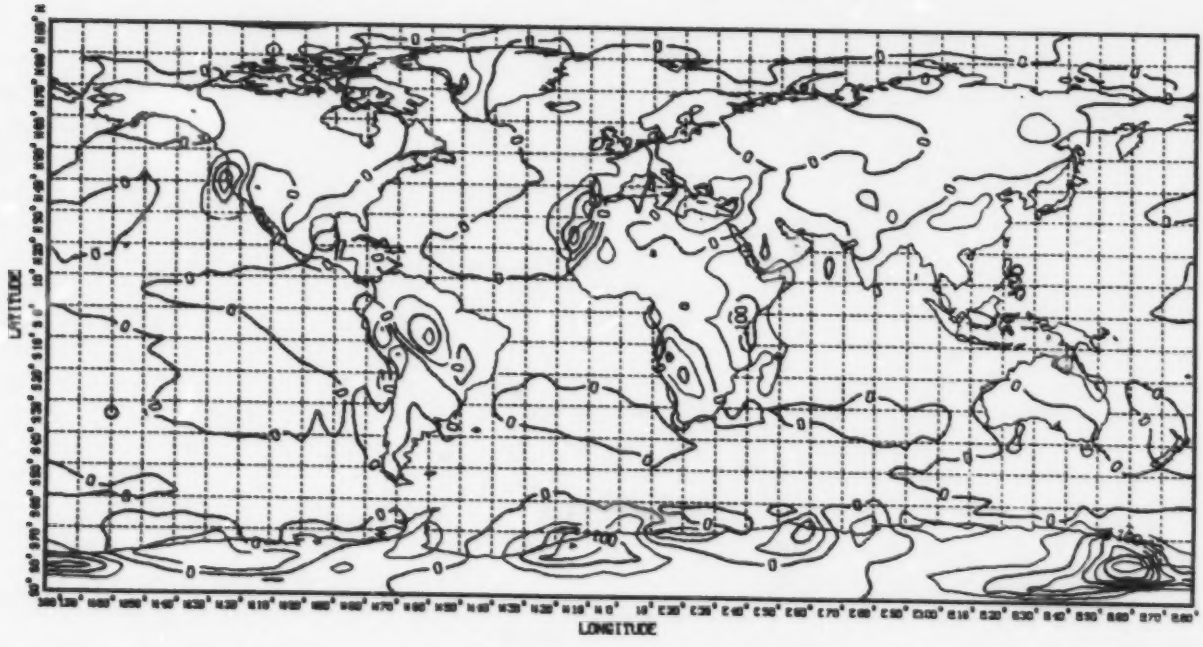

Figure 130

ECMWF JANUARY V SURFACE STRESS .001*(N/M**2)

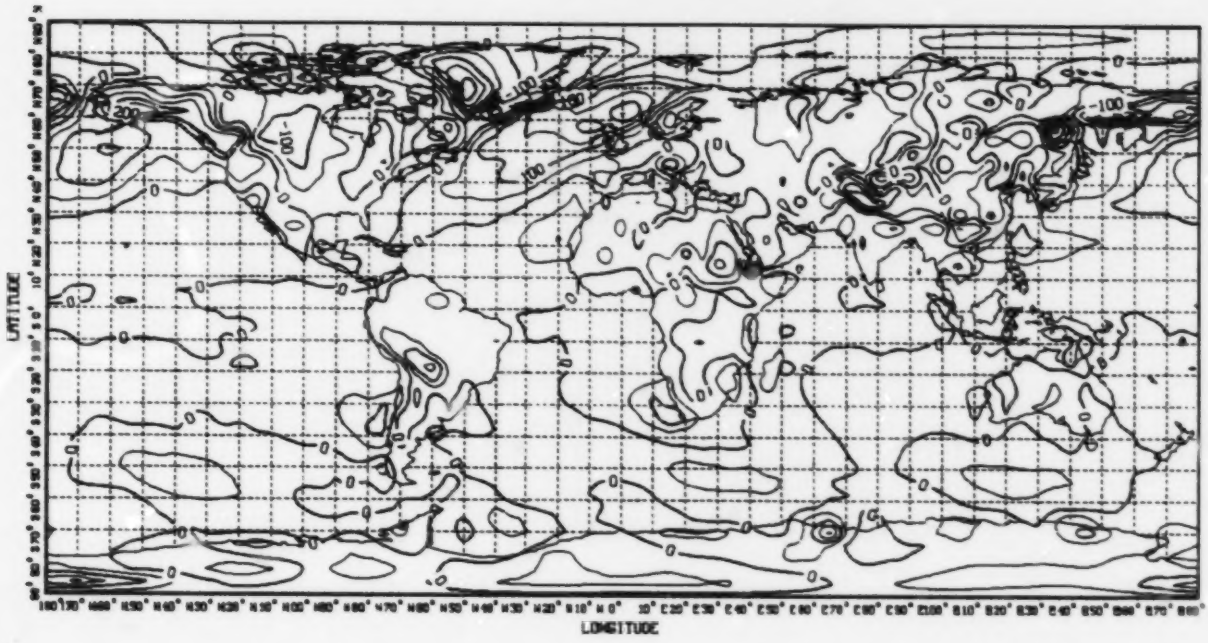

ECMWF JUNE V SURFACE STRESS .001*(N/M**2)

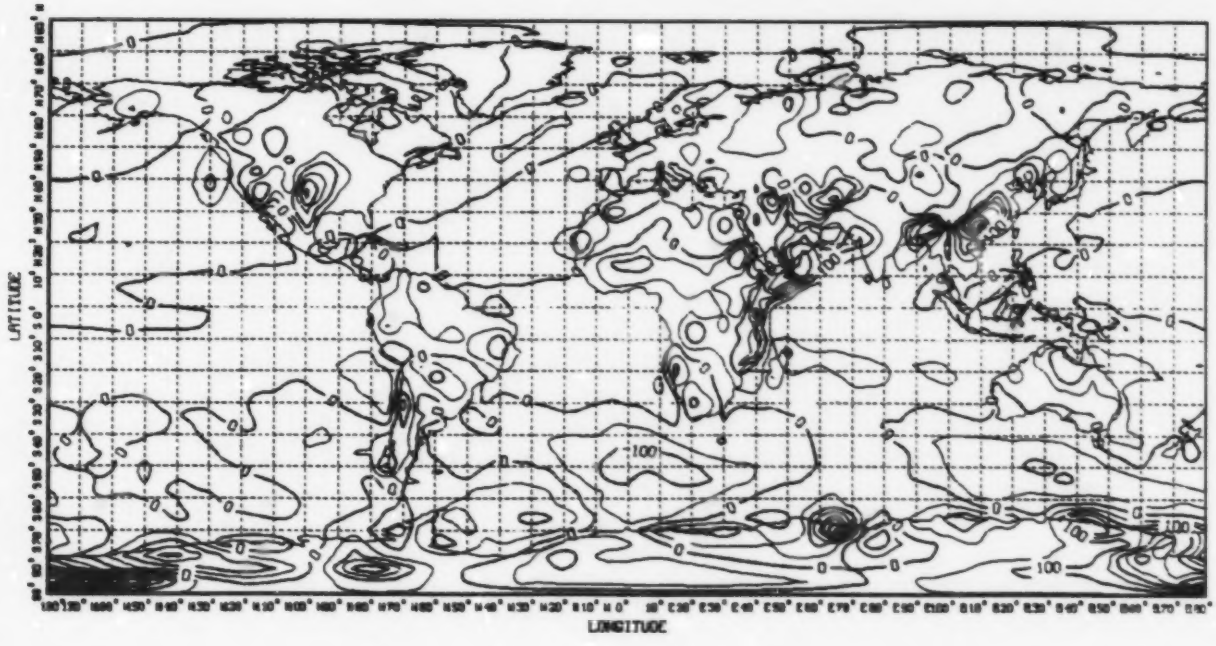

Figure 131

F R G (HAMBURG U) JANUARY V SURFACE STRESS .001*(N/M**2)

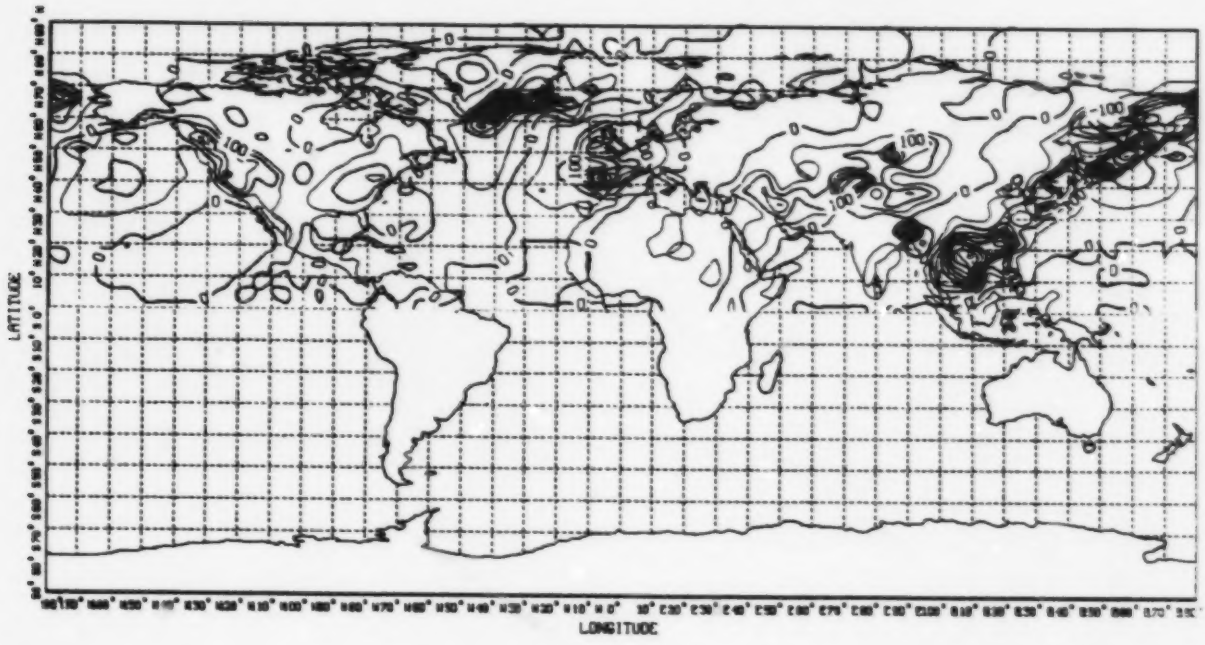

Figure 132

OBS JANUARY PRECIPITATION-EVAPORATION (MM/DAY)

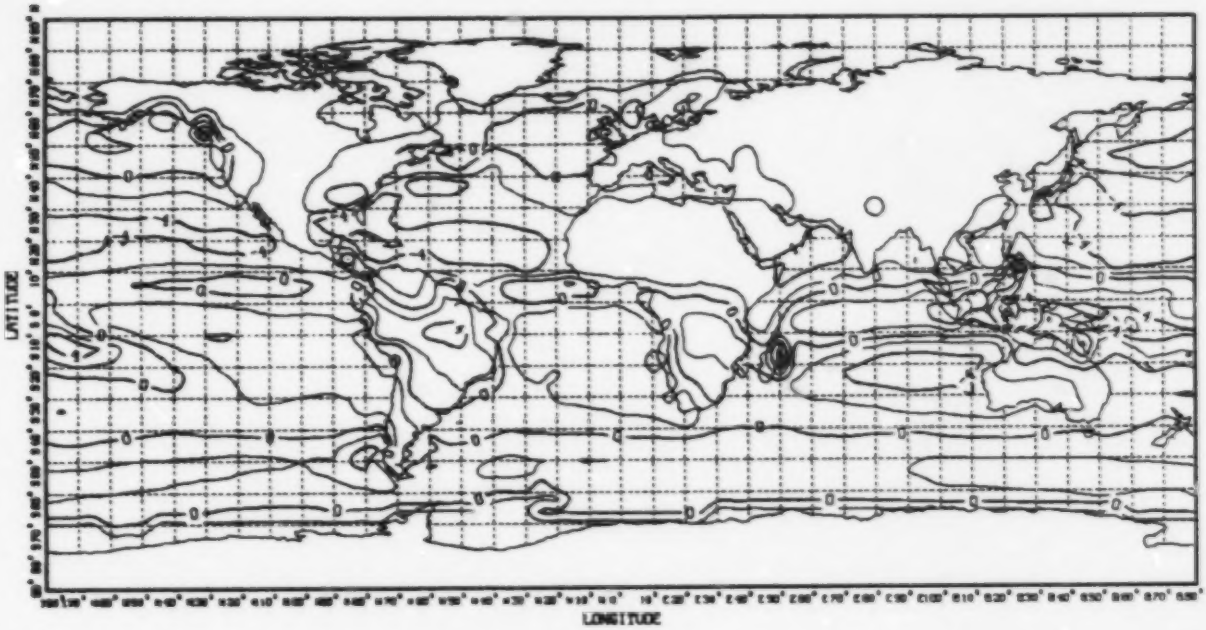

OBS JULY PRECIPITATION-EVAPORATION (MM/DAY)

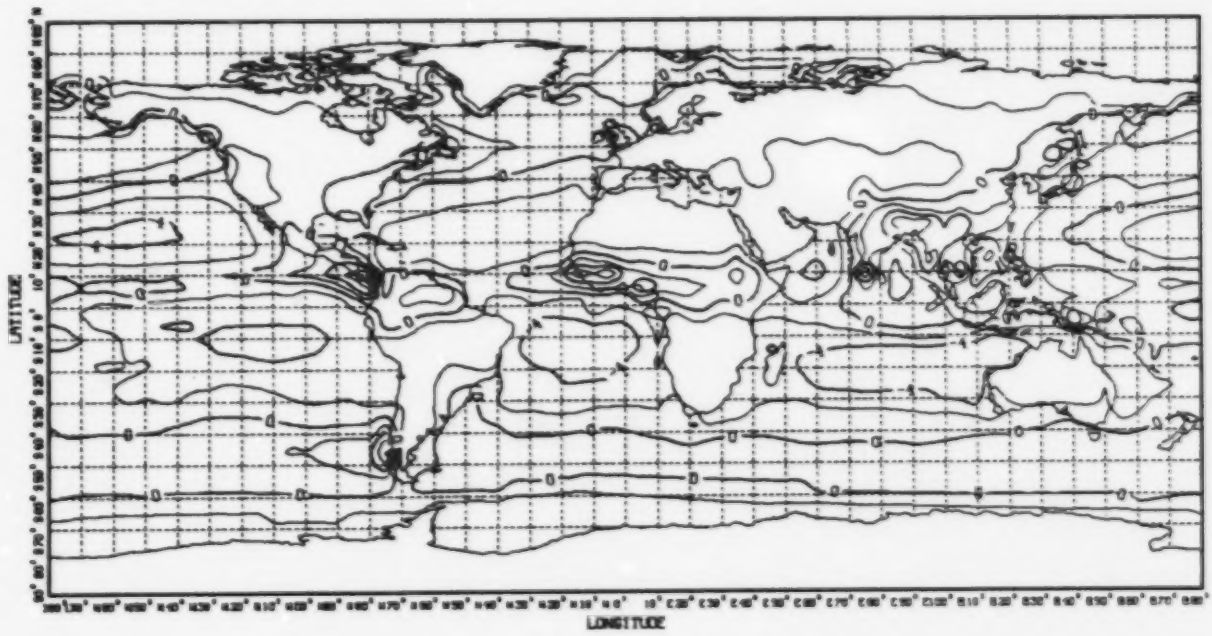

Figure 133

CANADA (CCC) JANUARY PRECIPITATION-EVAPORATION (MM/DAY)

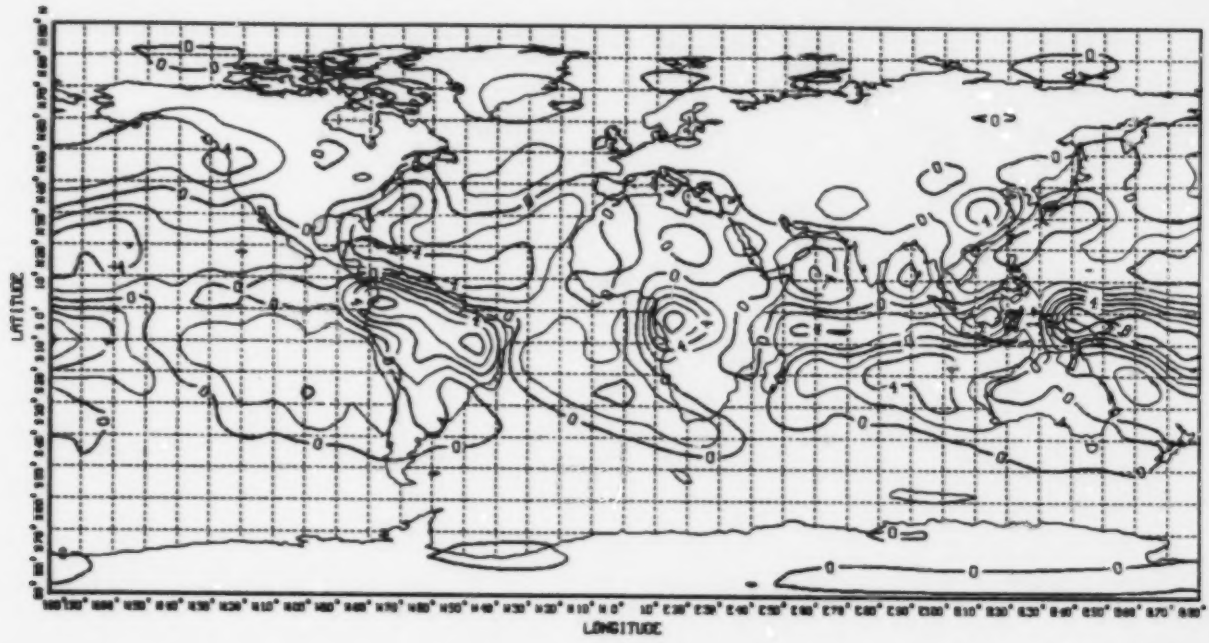

CANADA (CCC) JULY PRECIPITATION-EVAPORATION (MM/DAY)

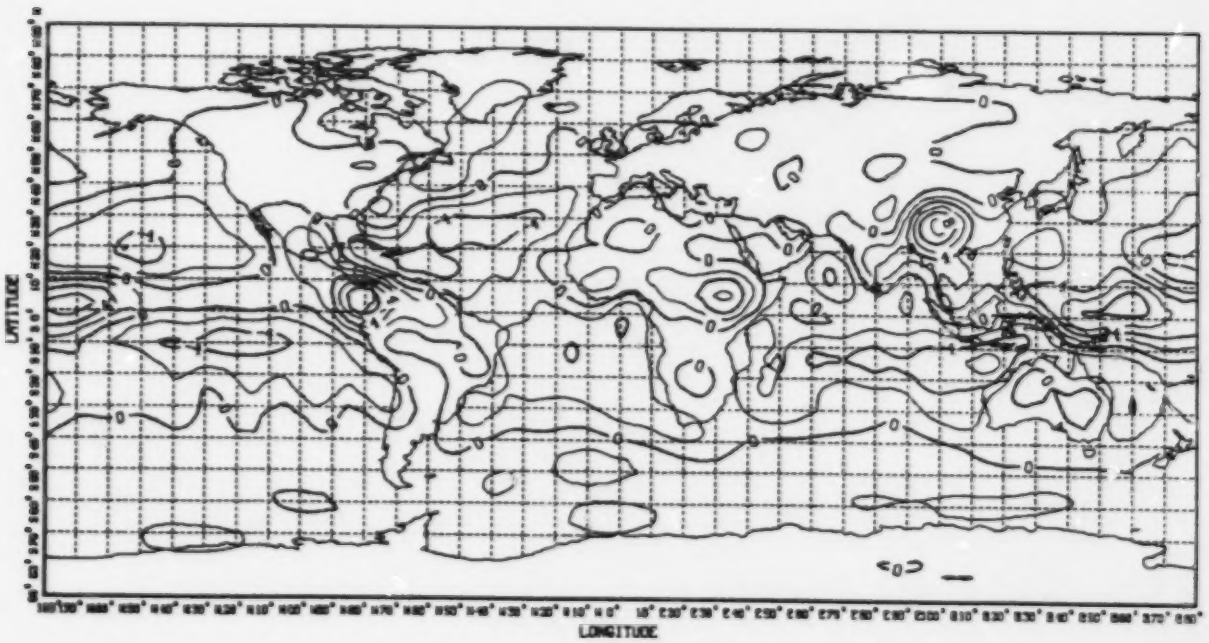

Figure 134

ENGLAND (BMO) JANUARY PRECIPITATION-EVAPORATION (MM/DAY)

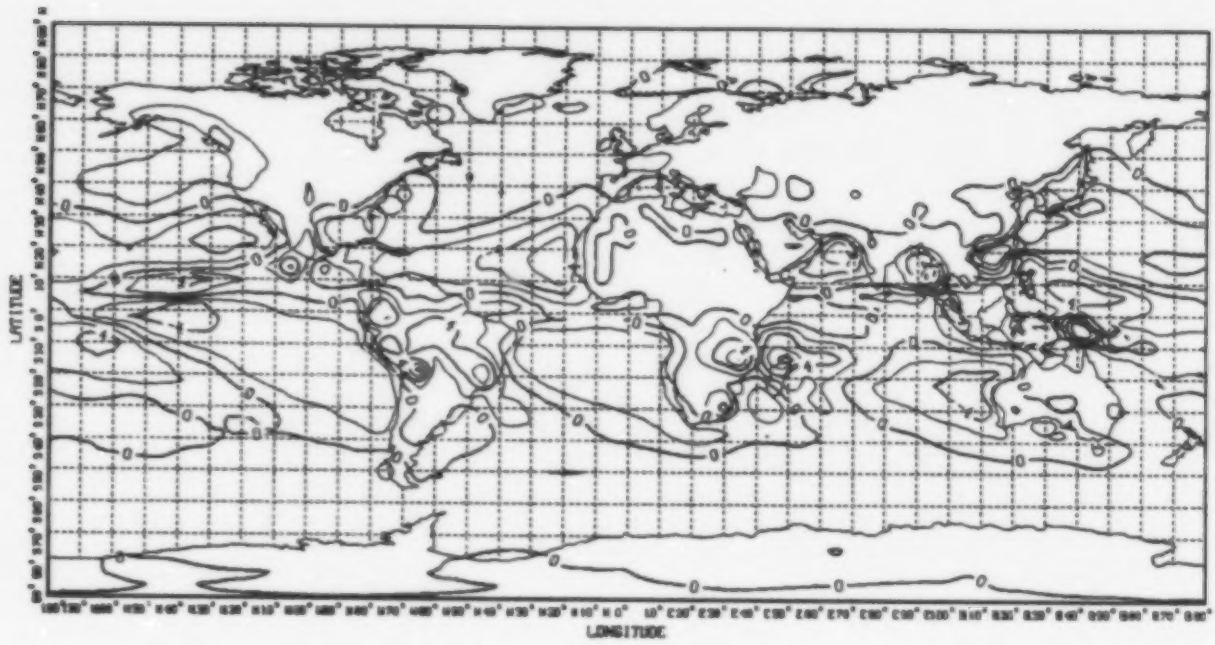

ENGLAND (BMO) JULY PRECIPITATION-EVAPORATION (MM/DAY)

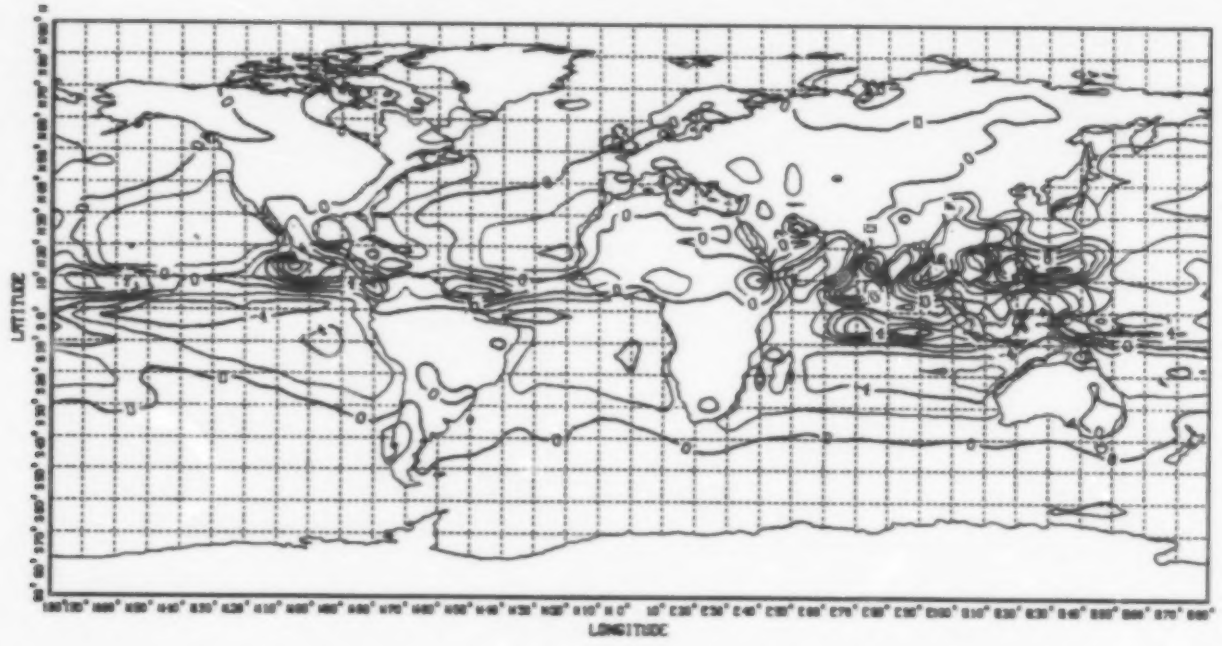

Figure 135

AUSTRALIA (BMRC) JANUARY PRECIP-EVAP (MM/DAY)

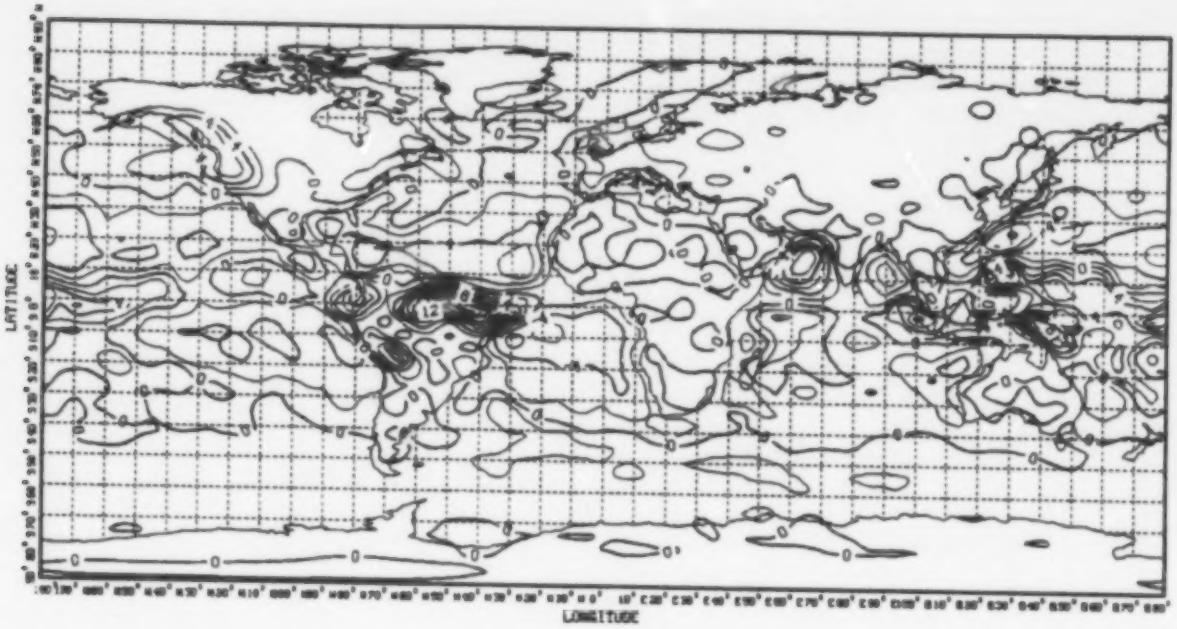

AUSTRALIA (BMRC) JULY PRECIP-EVAP (MM/DAY)

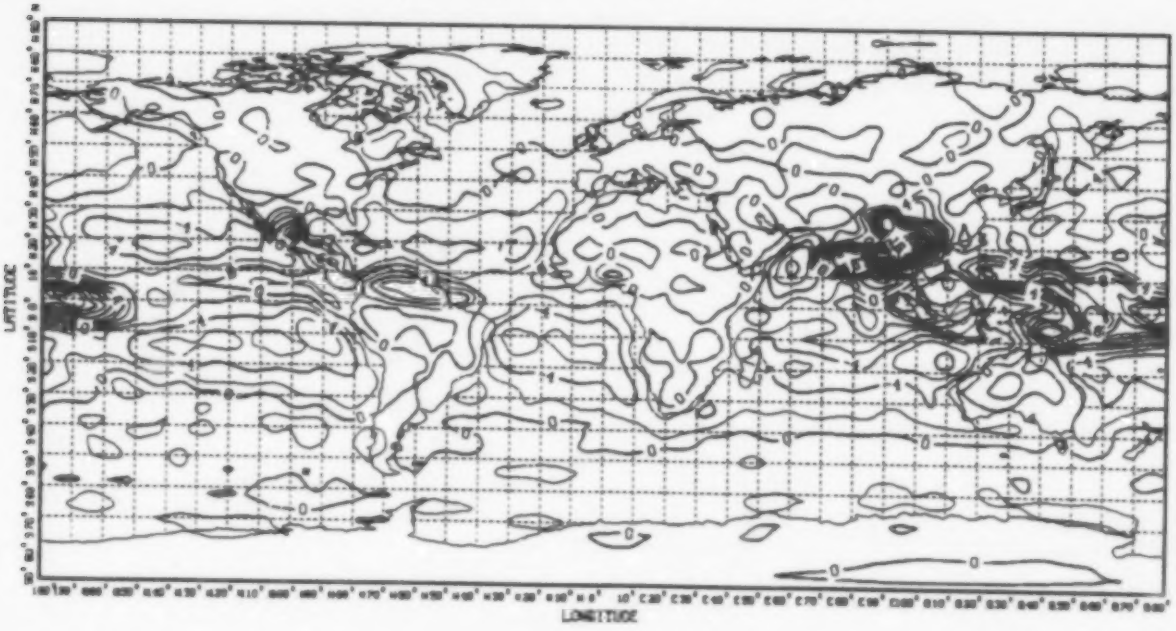

Figure 136

U S A (COLA!) JANUARY PRECIPITATION-EVAPORATION (MM/DAY)

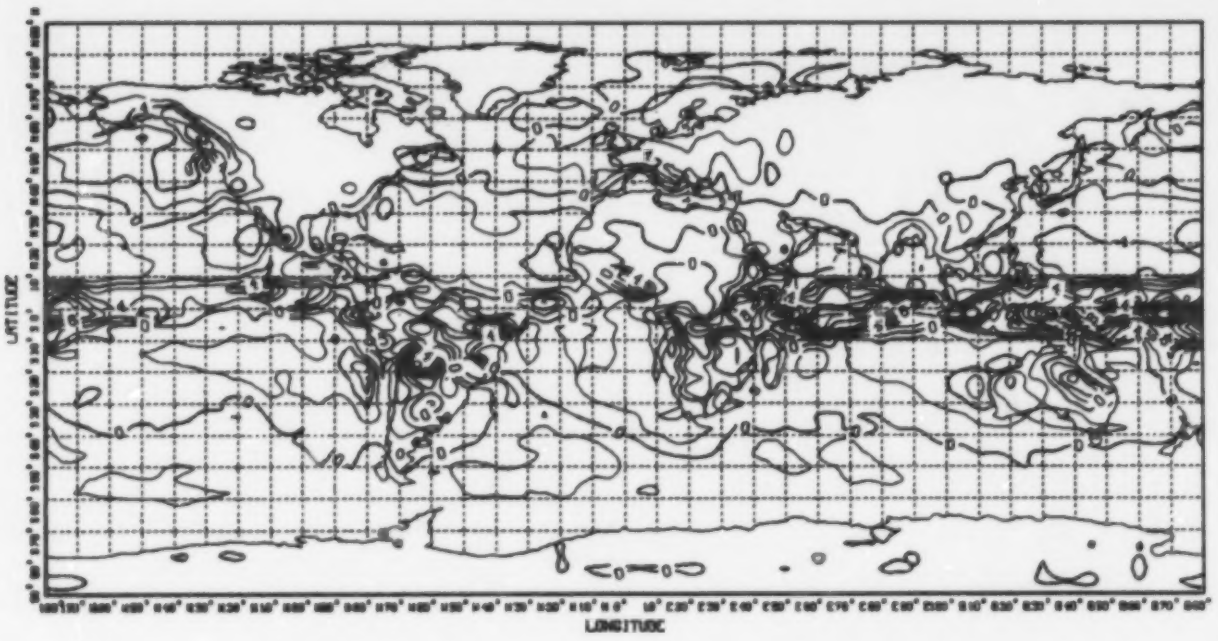

U S A (COLA!) JULY PRECIPITATION-EVAPORATION (MM/DAY)

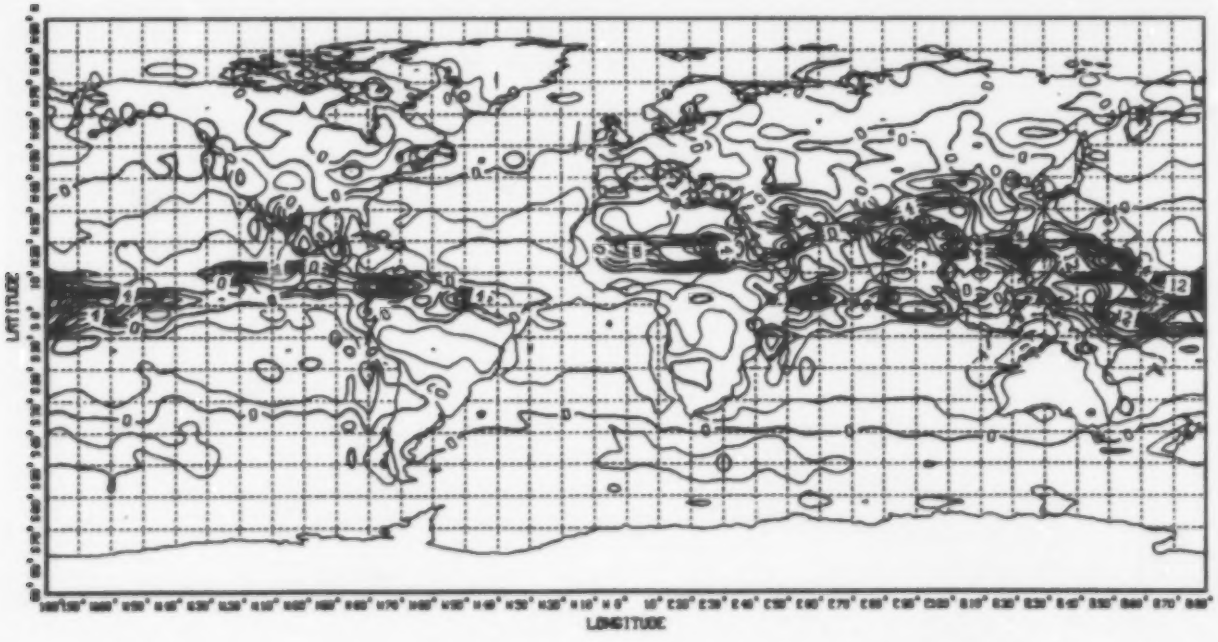

Figure 137

U S A (GFDL) JANUARY PRECIPITATION-EVAPORATION (MM/DAY)

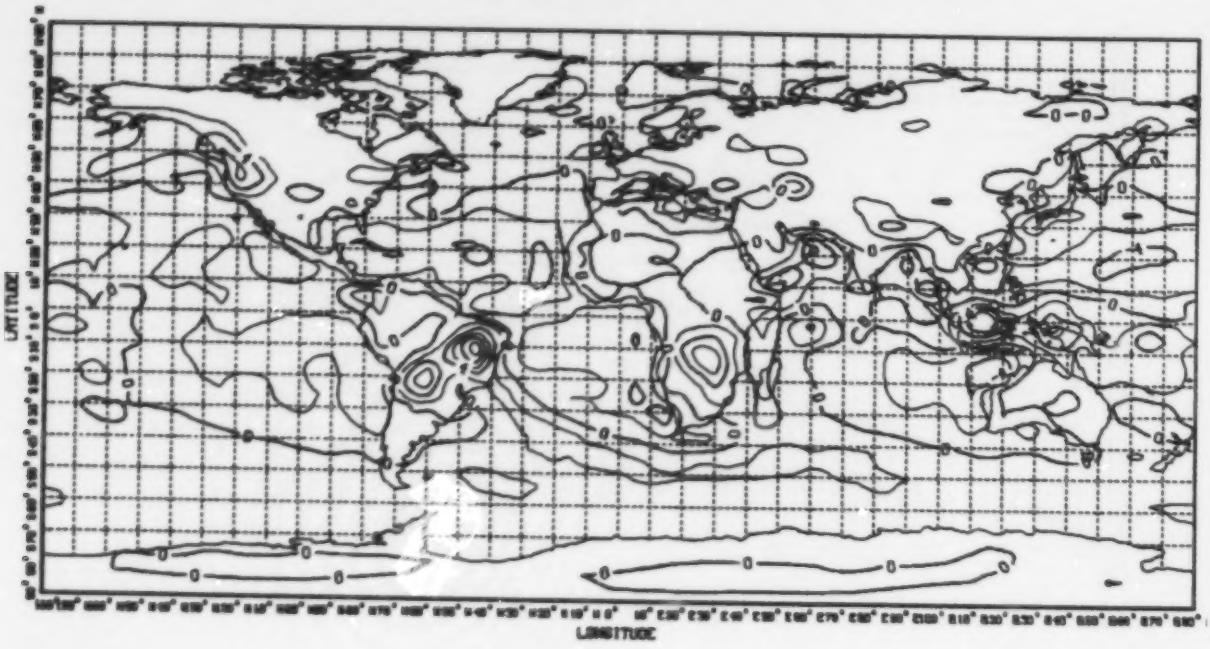

U S A (GFDL) JULY PRECIPITATION-EVAPORATION (MM/DAY)

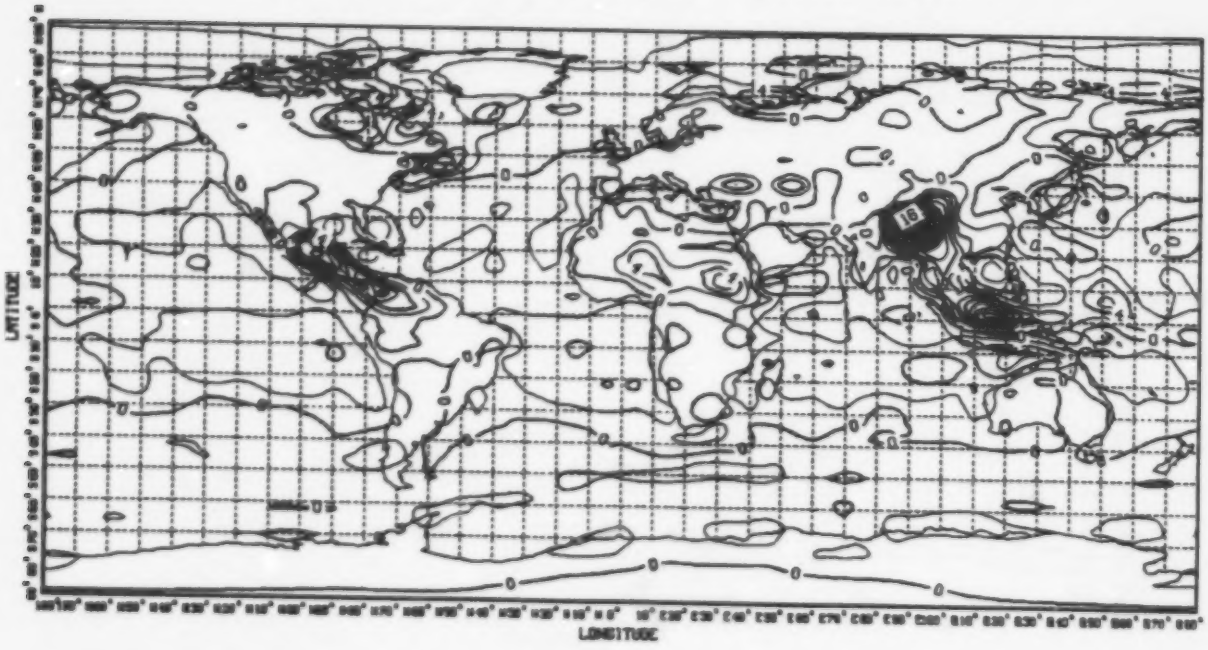

Figure 138

U S A (GISS) JANUARY PRECIPITATION-EVAPORATION (MM/DAY)

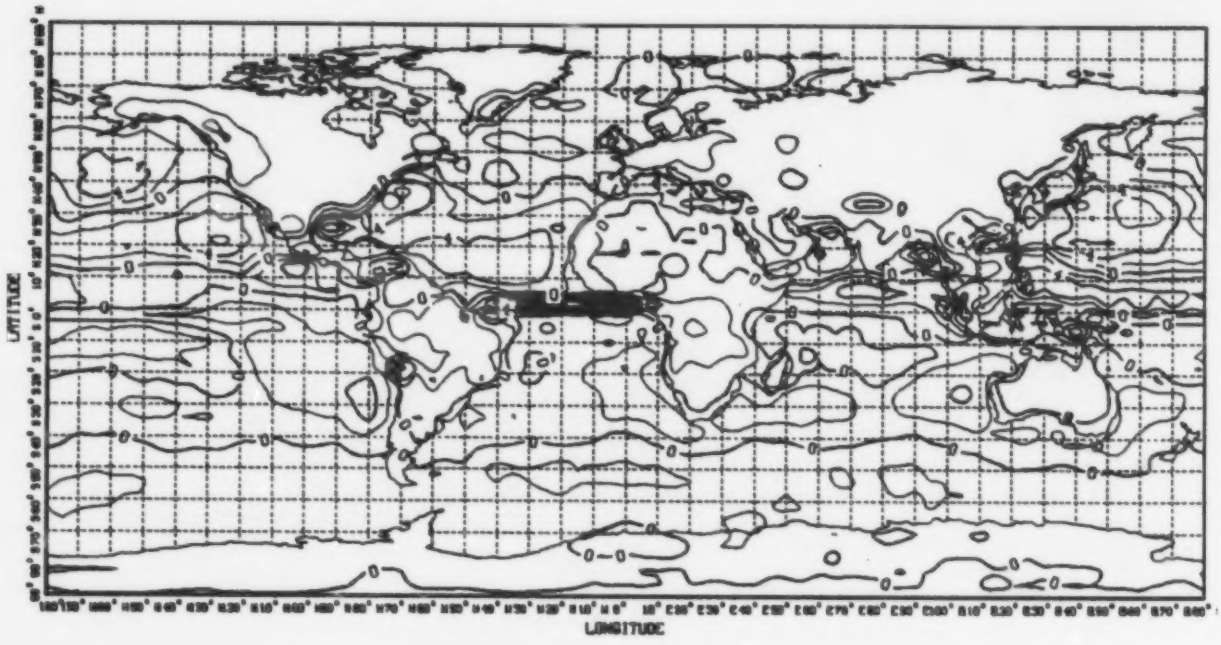

U S A (GISS) JULY PRECIPITATION-EVAPORATION (MM/DAY)

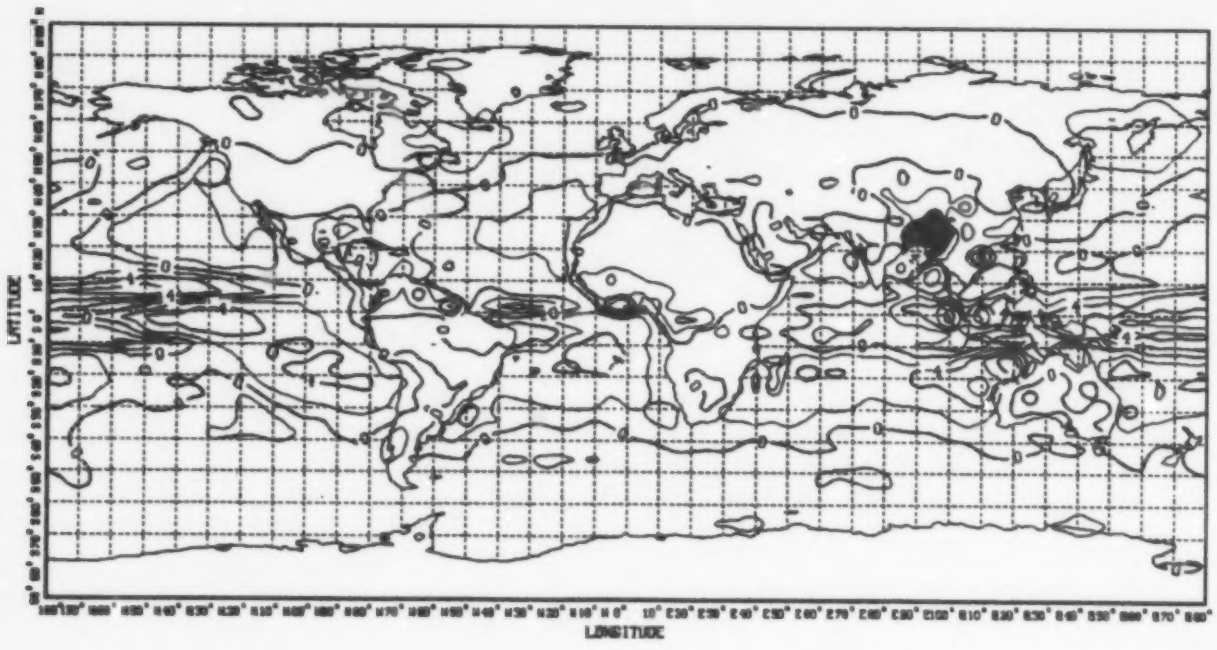

Figure 139

U S A (NCAR) JANUARY PRECIPITATION-EVAPORATION (MM/DAY)

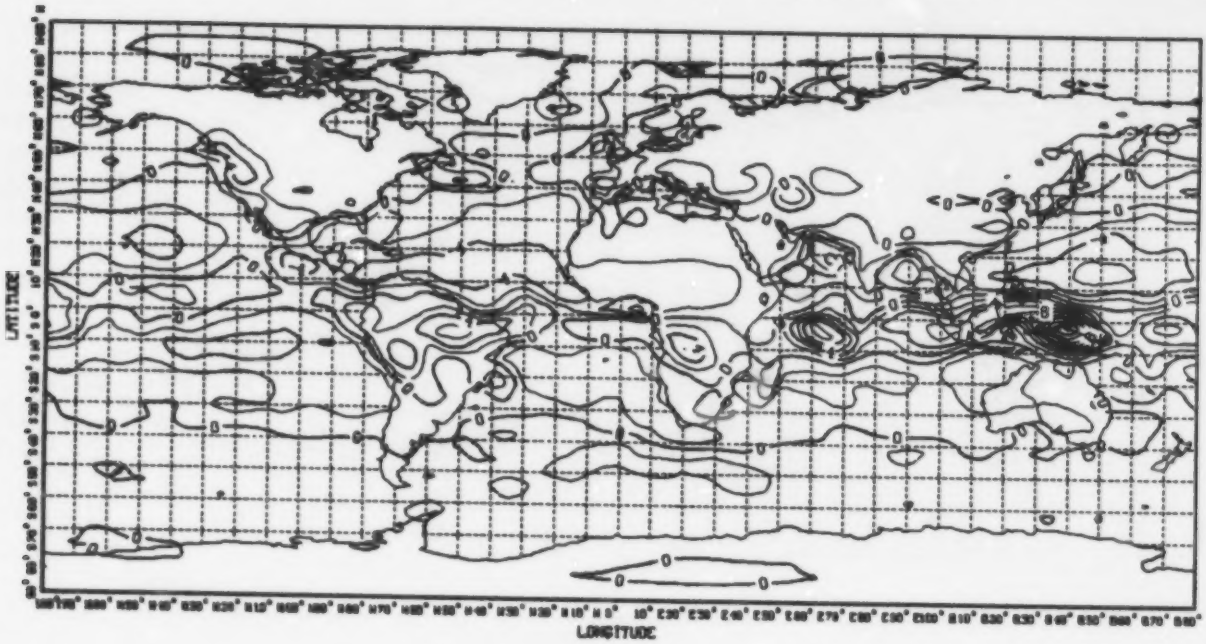

U S A (NCAR) JULY PRECIPITATION-EVAPORATION (MM/DAY)

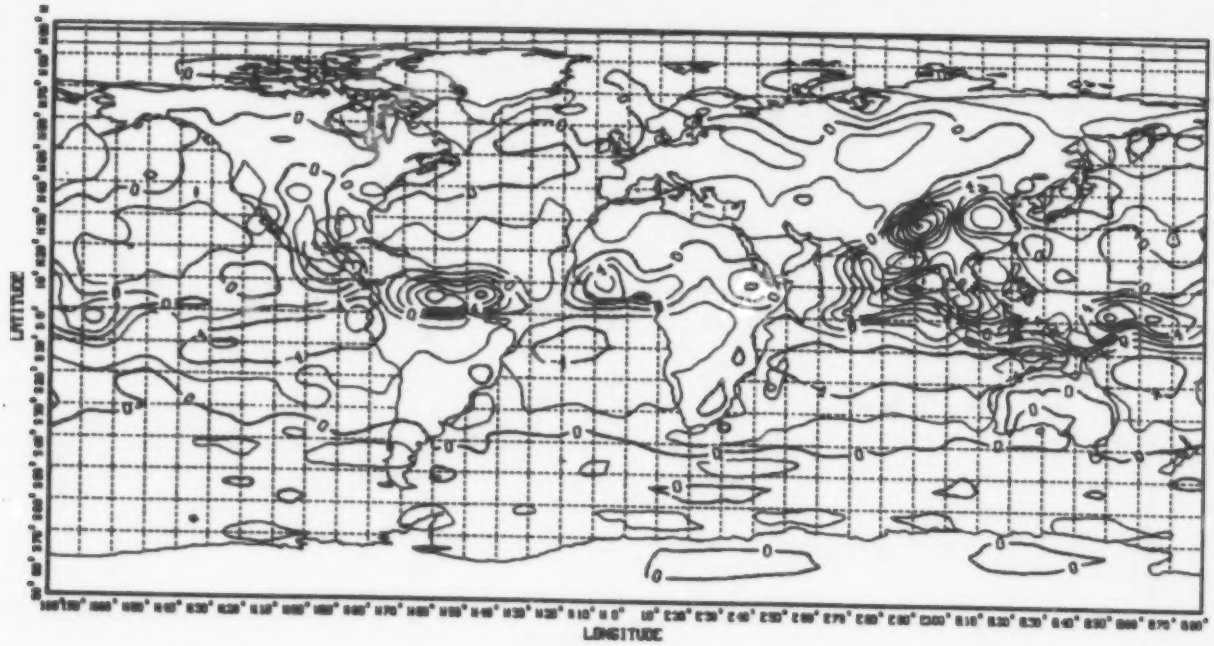

Figure 140

U S A (OSU) JANUARY PRECIPITATION-EVAPORATION (MM/DAY)

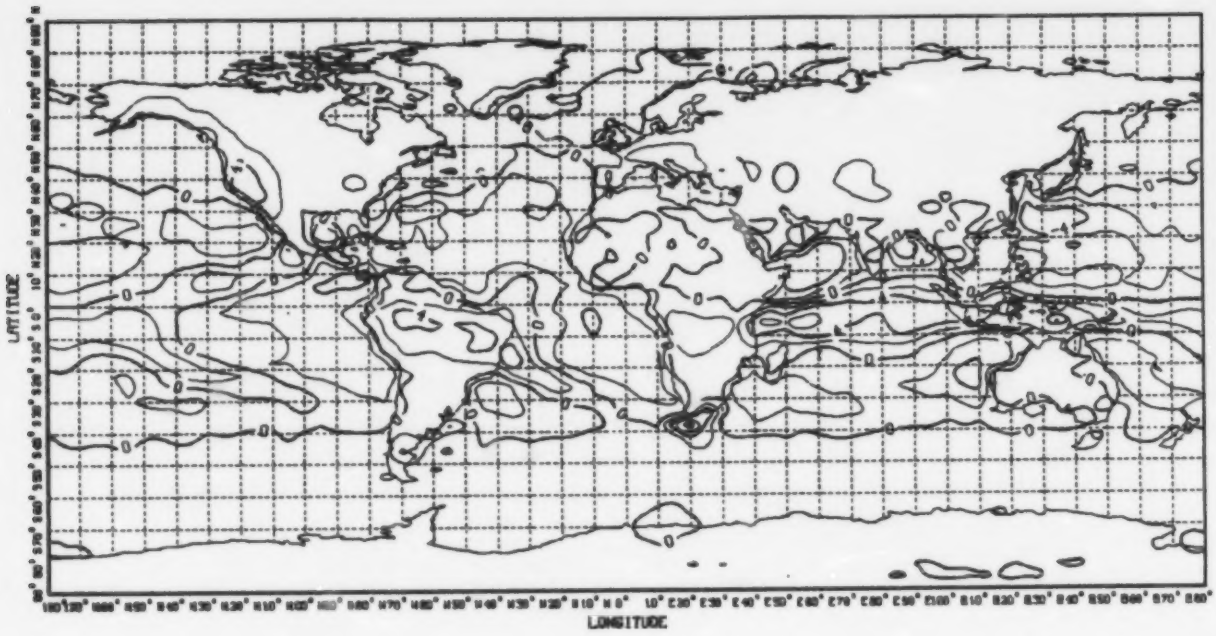

U S A (OSU) JULY PRECIPITATION-EVAPORATION (MM/DAY)

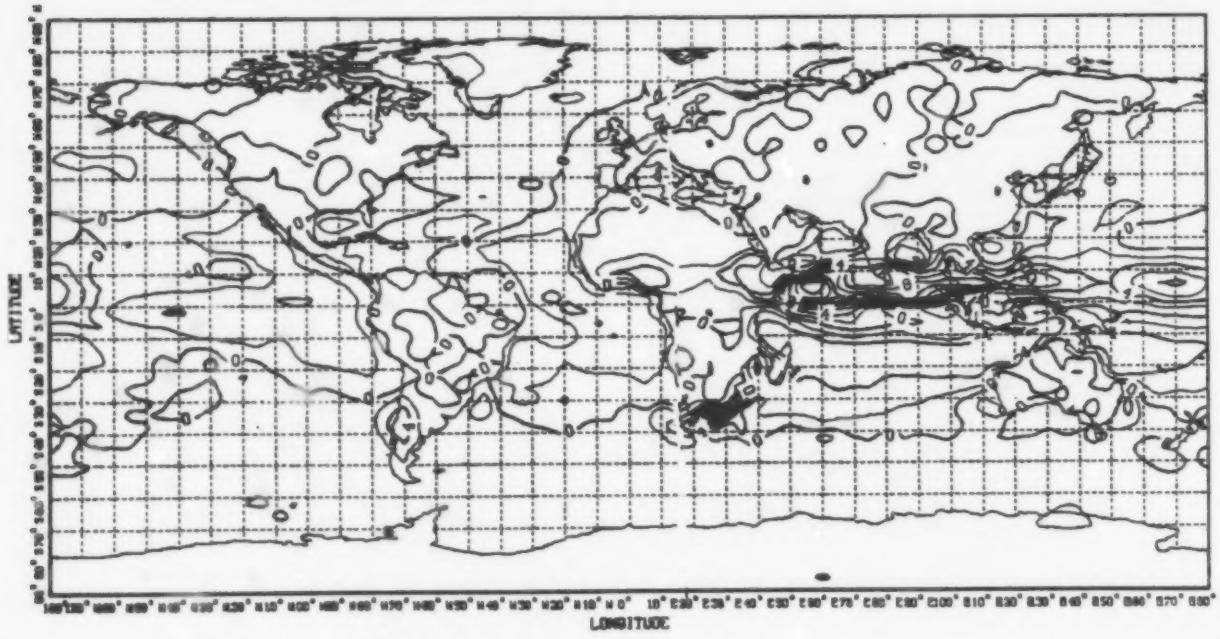

Figure 141

JAPAN (MRI) JANUARY PRECIPITATION-EVAPORATION (MM/DAY)

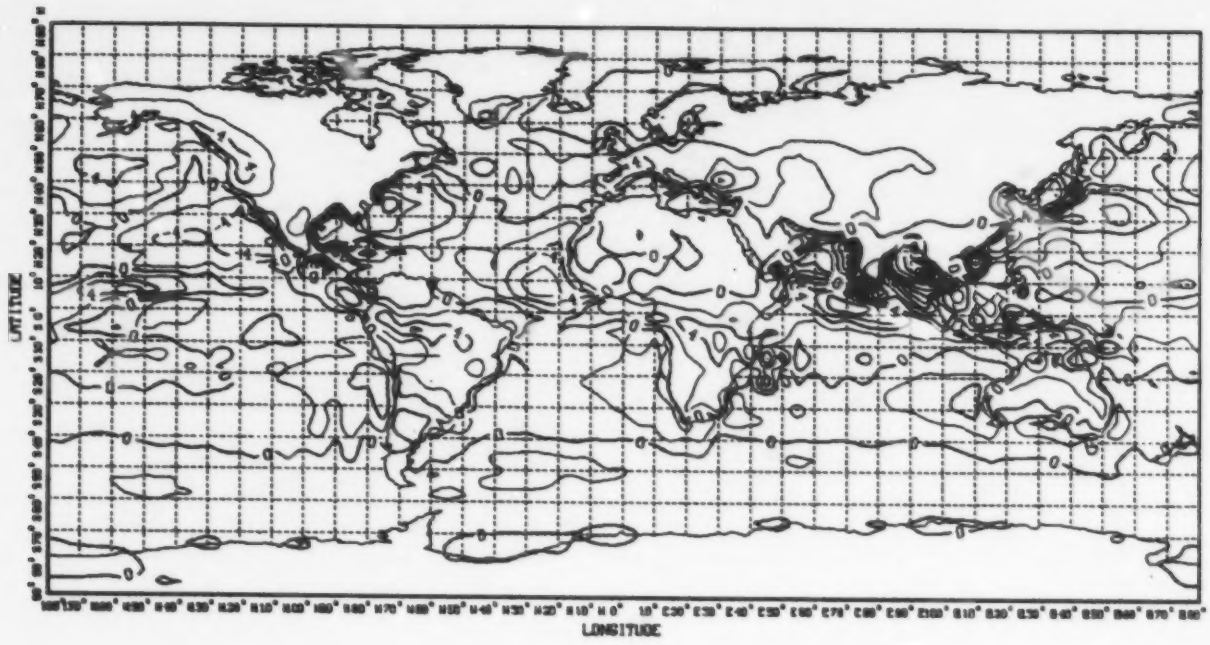

JAPAN (MRI) JULY PRECIPITATION-EVAPORATION (MM/DAY)

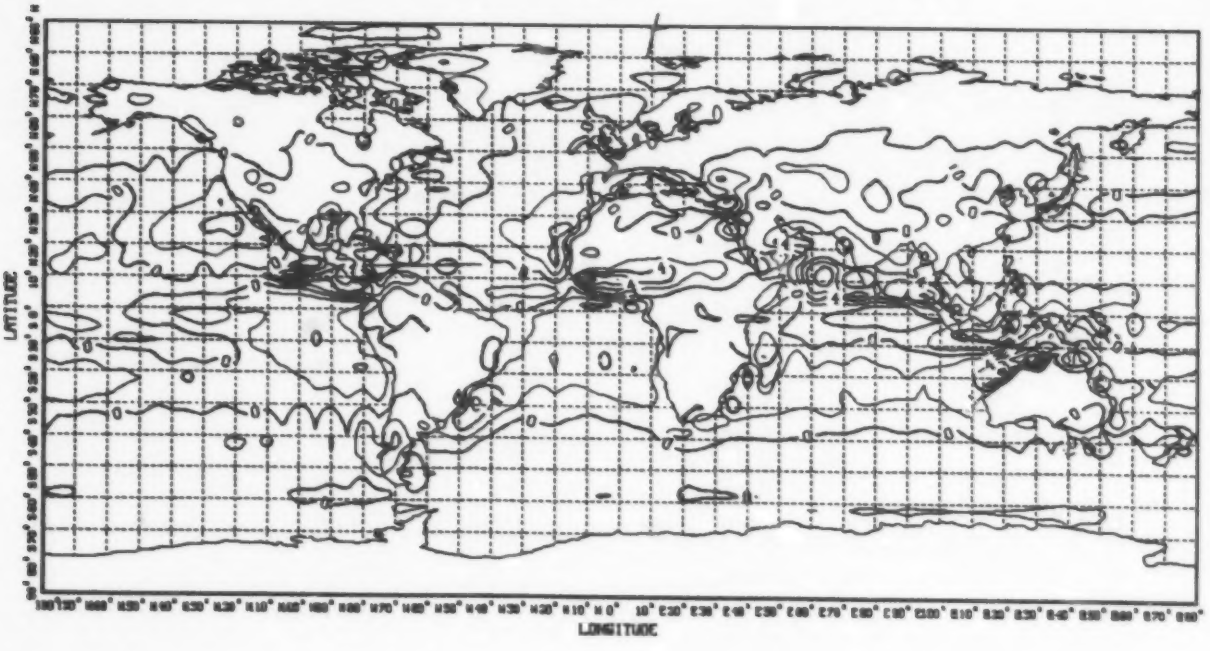

Figure 142

ECMWF JANUARY PRECIPITATION-EVAPORATION (MM/DAY)

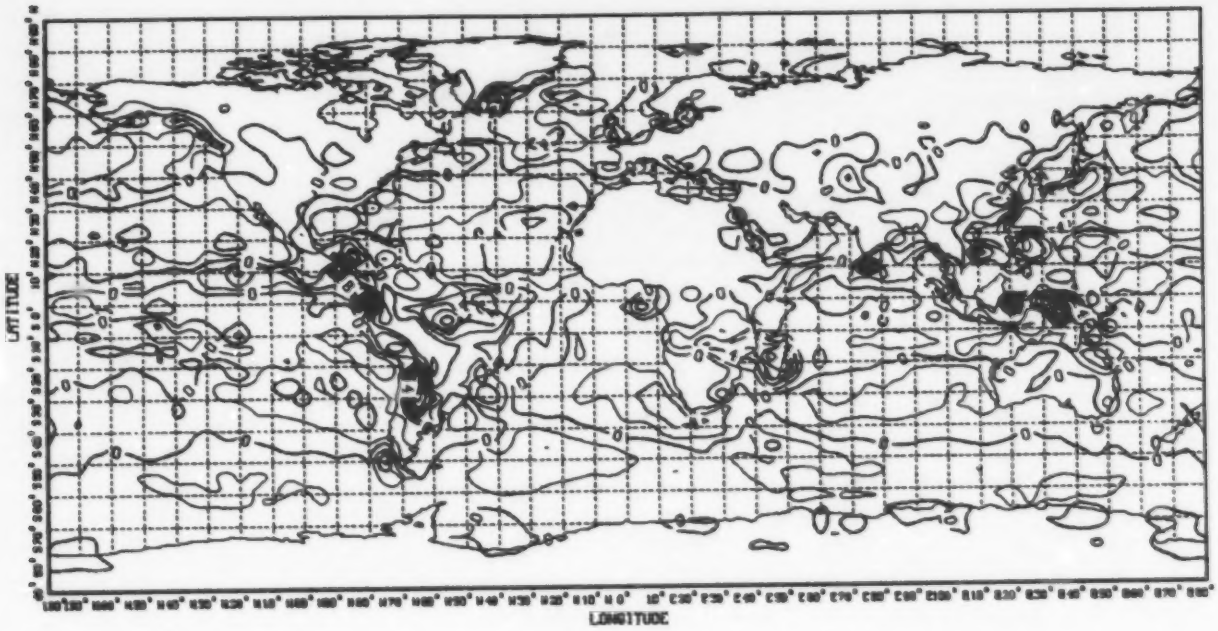

ECMWF JUNE PRECIPITATION-EVAPORATION (MM/DAY)

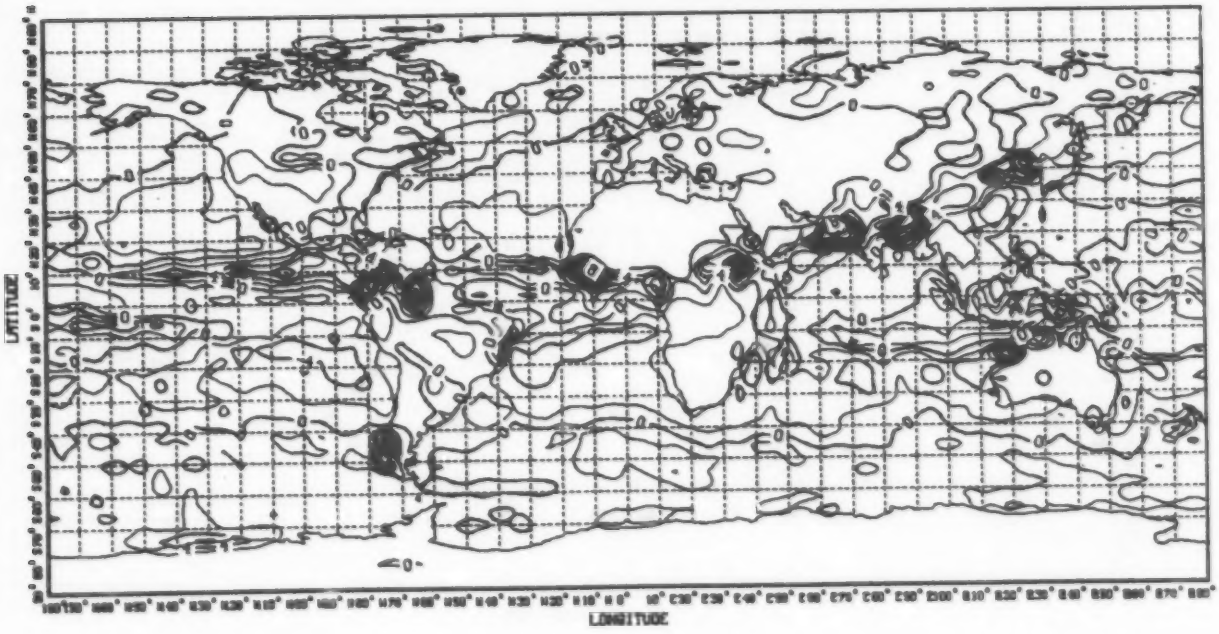

Figure 143

FRANCE (CNRM) JANUARY PRECIPITATION-EVAPORATION (MM/DAY)

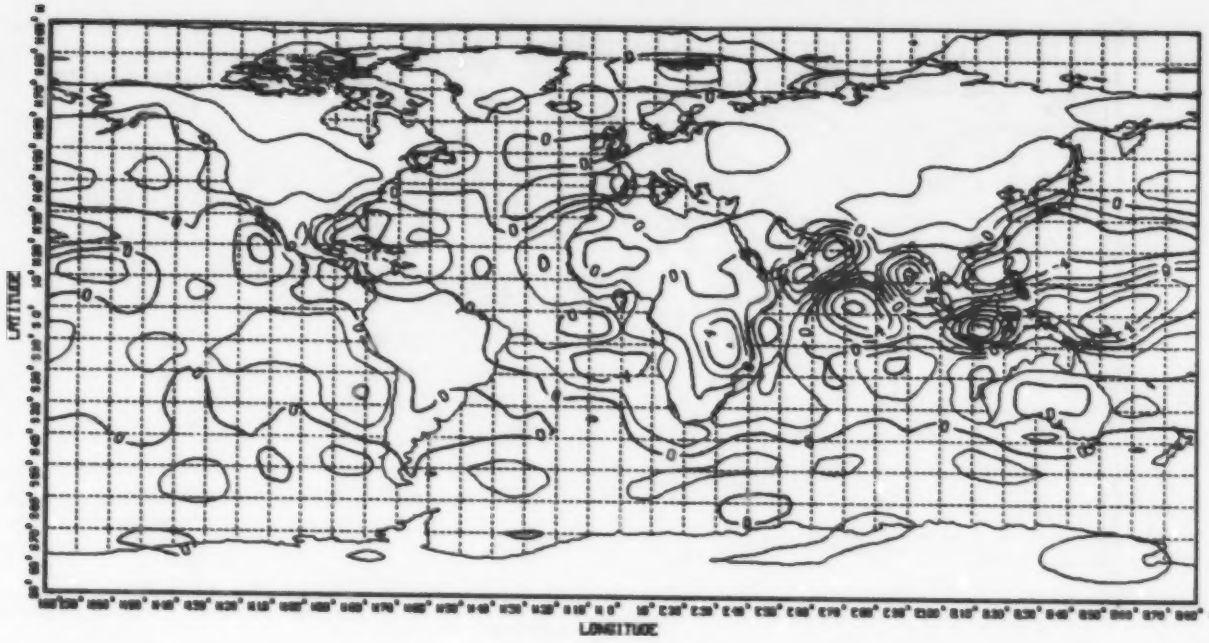

FRANCE (CNRM) JULY PRECIPITATION-EVAPORATION (MM/DAY)

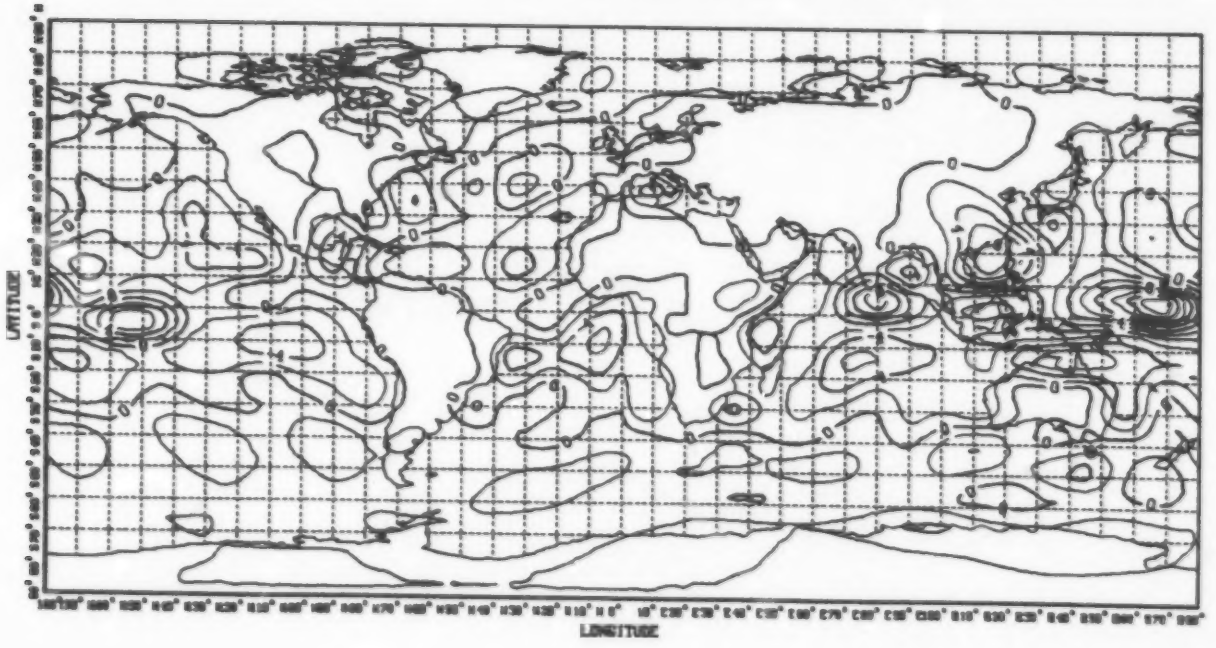

Figure 144

F R G (UHAM) JANUARY PRECIPITATION-EVAPORATION (MM/DAY)

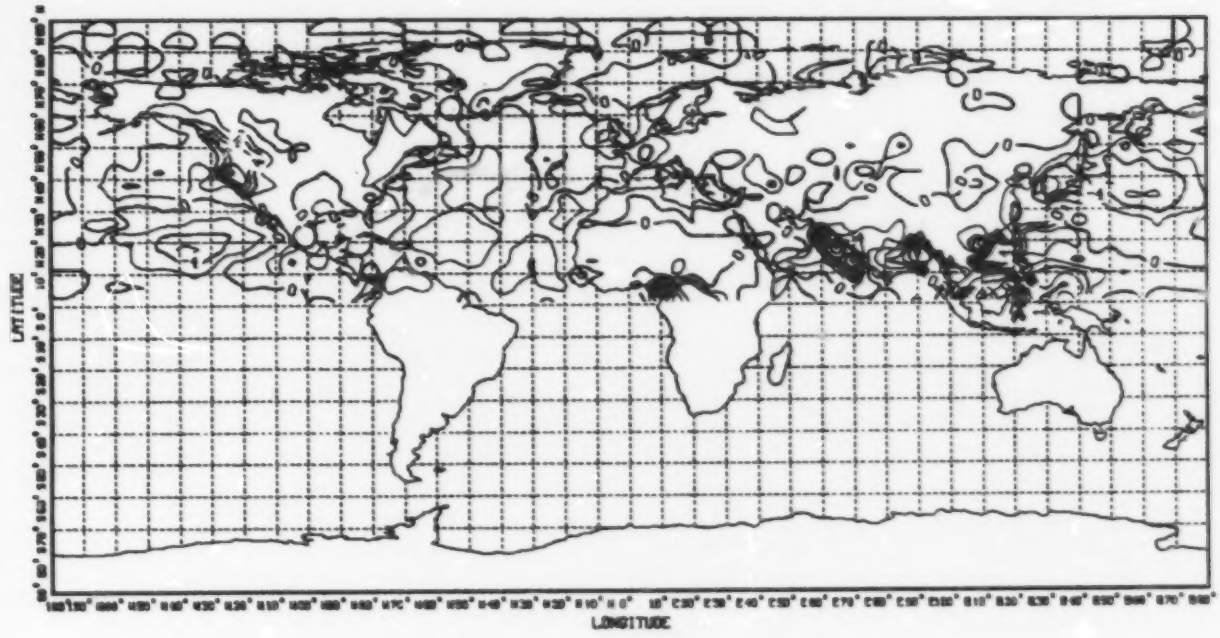

Figure 145

MÖLLER WINTER PRECIPITATION (MM/DAY)

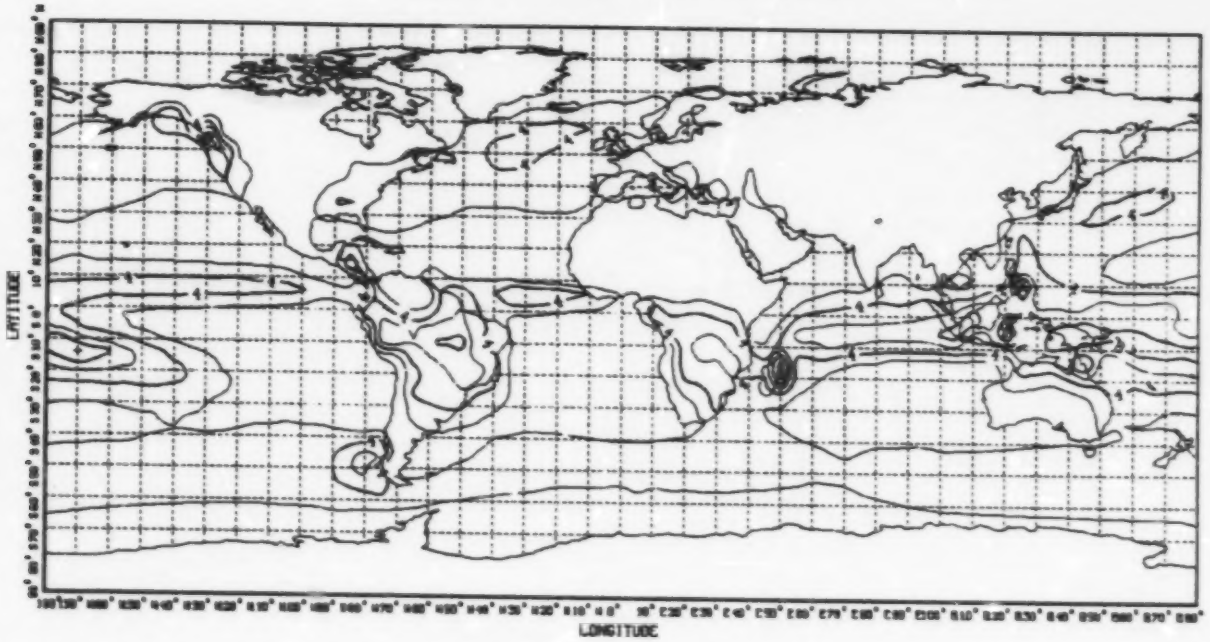

MÖLLER SUMMER PRECIPITATION (MM/DAY)

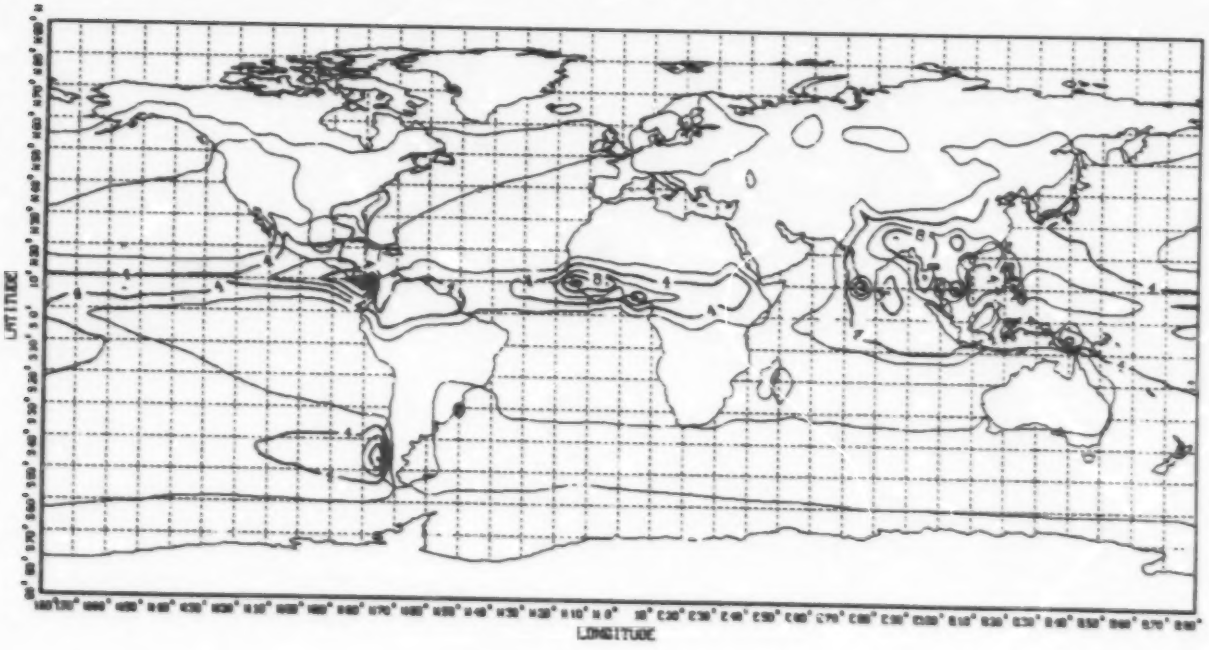

Figure 146

CANADA (CCC) WINTER PRECIPITATION (MM/DAY)

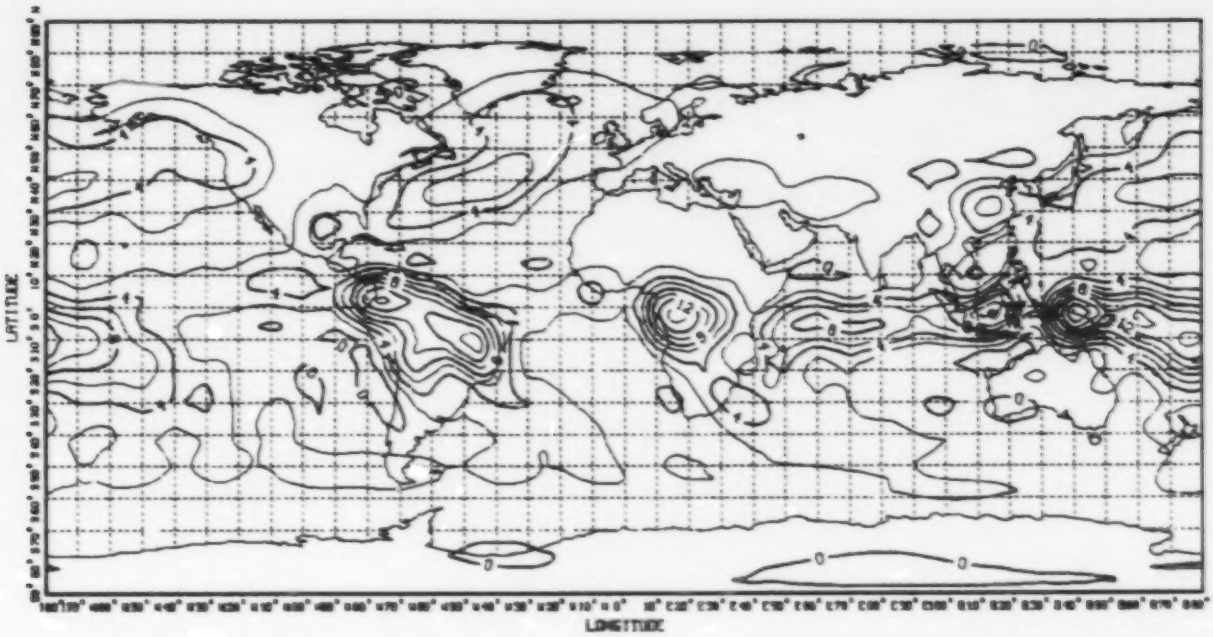

CANADA (CCC) SUMMER PRECIPITATION (MM/DAY)

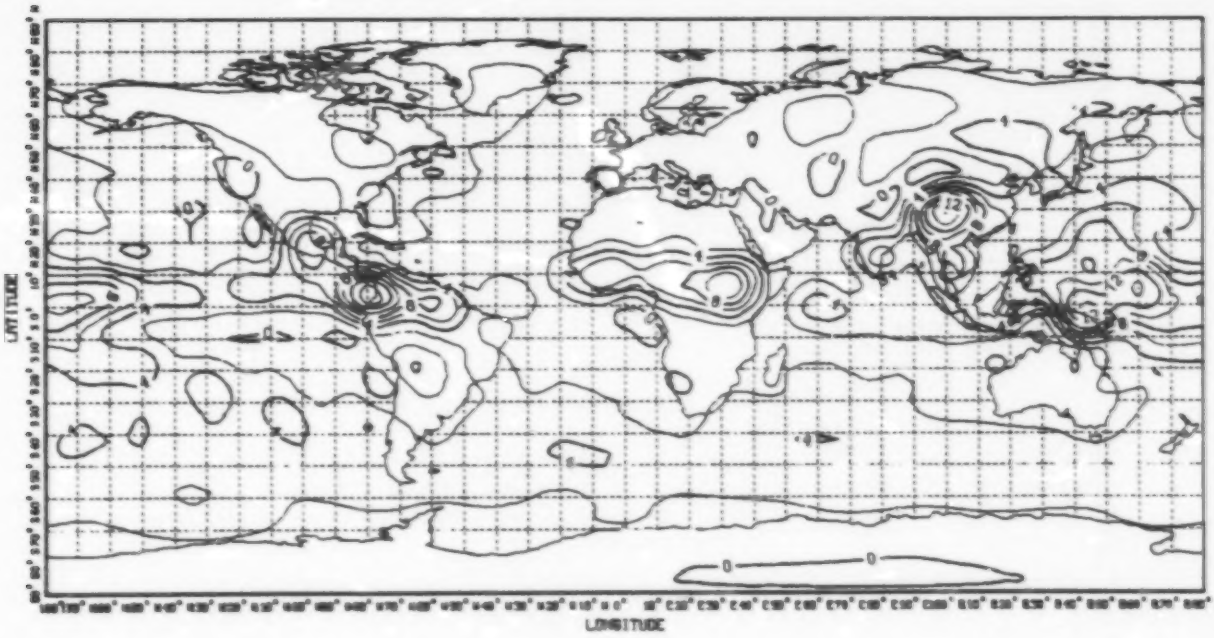

Figure 147

ENGLAND (BMO) WINTER PRECIPITAION (MM/DAY)

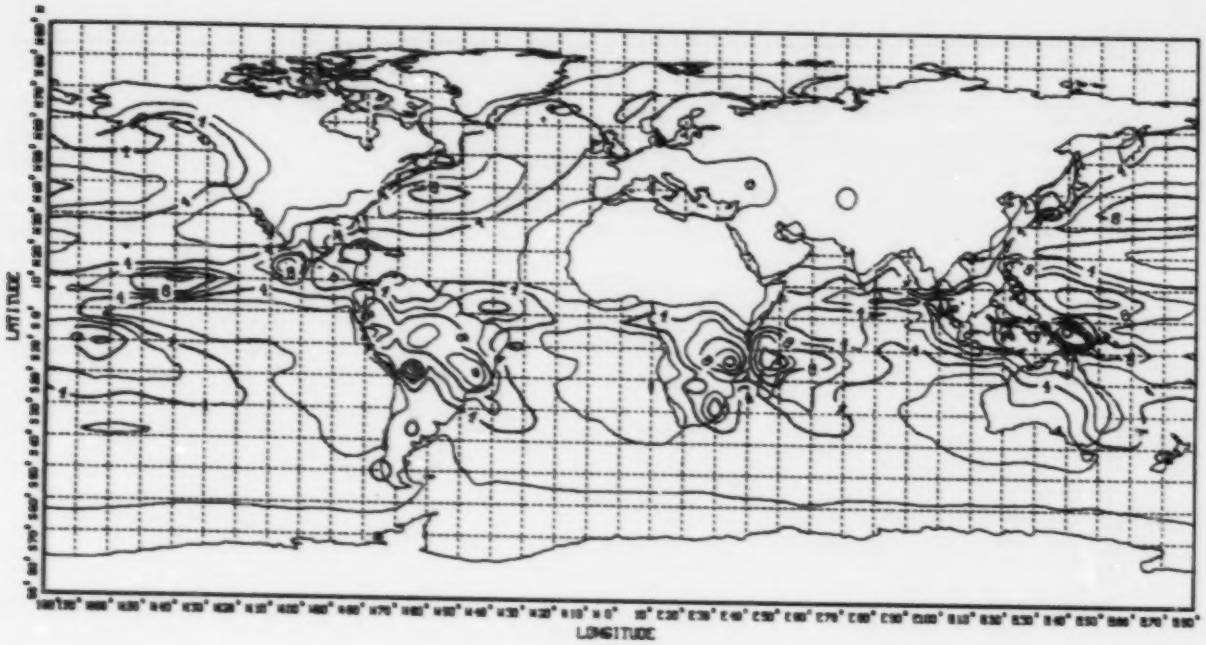

ENGLAND (BMO) SUMMER PRECIPITATION (MM/DAY)

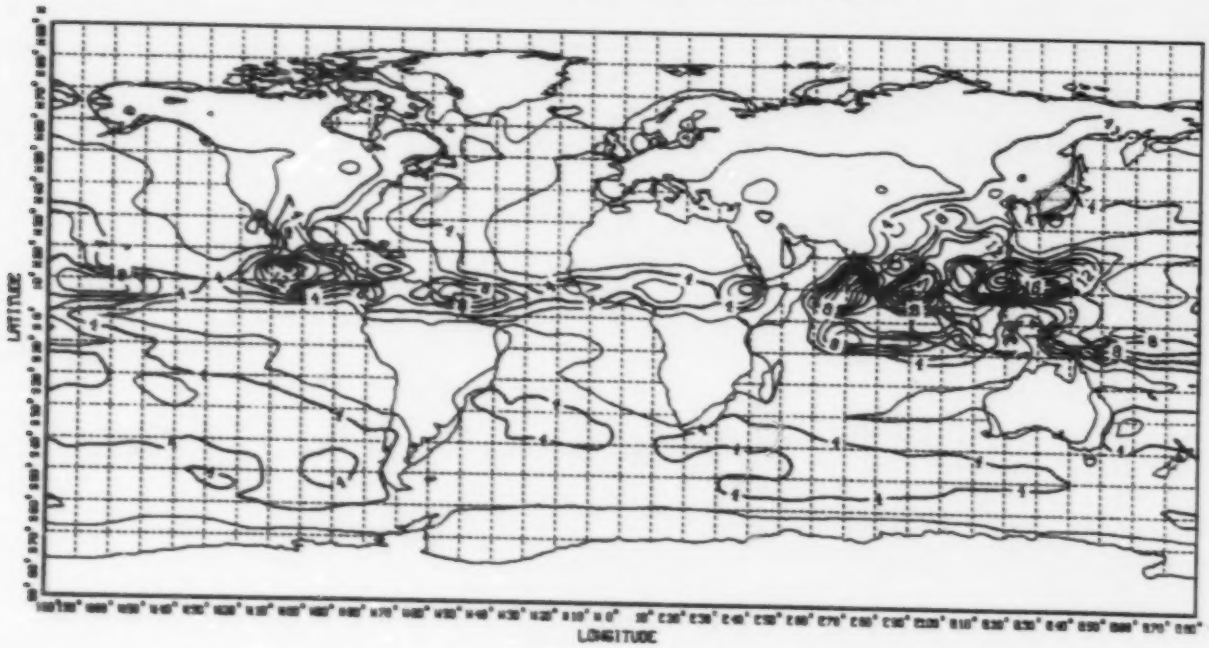

Figure 148

AUSTRALIA (BMRC) JANUARY PRECIPITATION (MM/DAY)

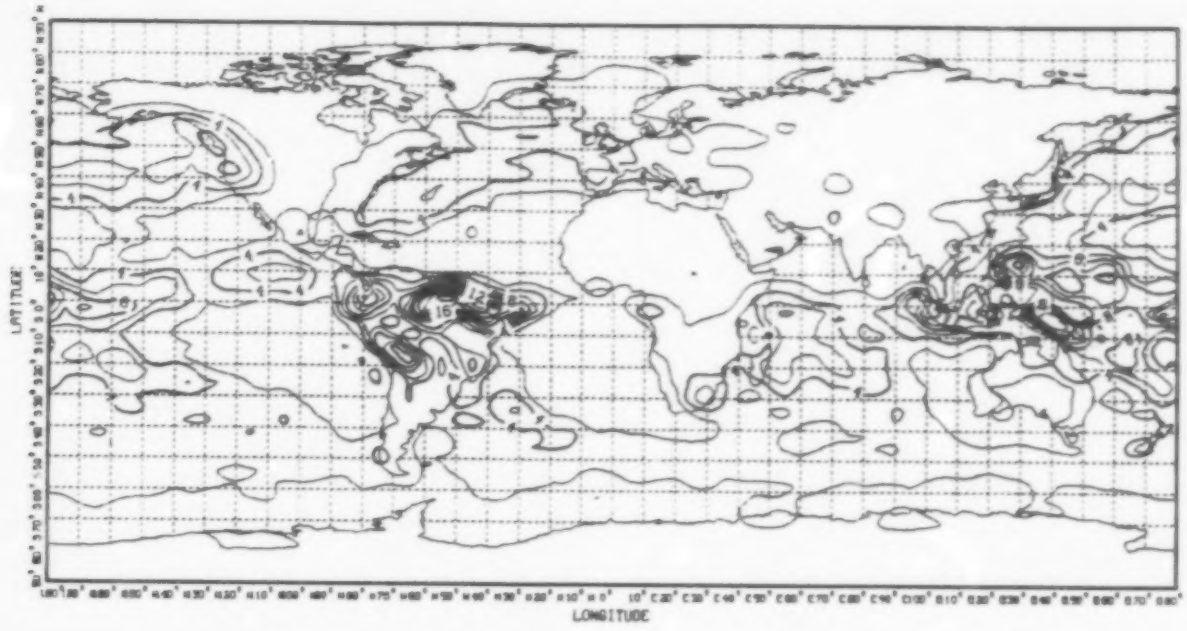

AUSTRALIA (BMRC) JULY PRECIPITATION (MM/DAY)

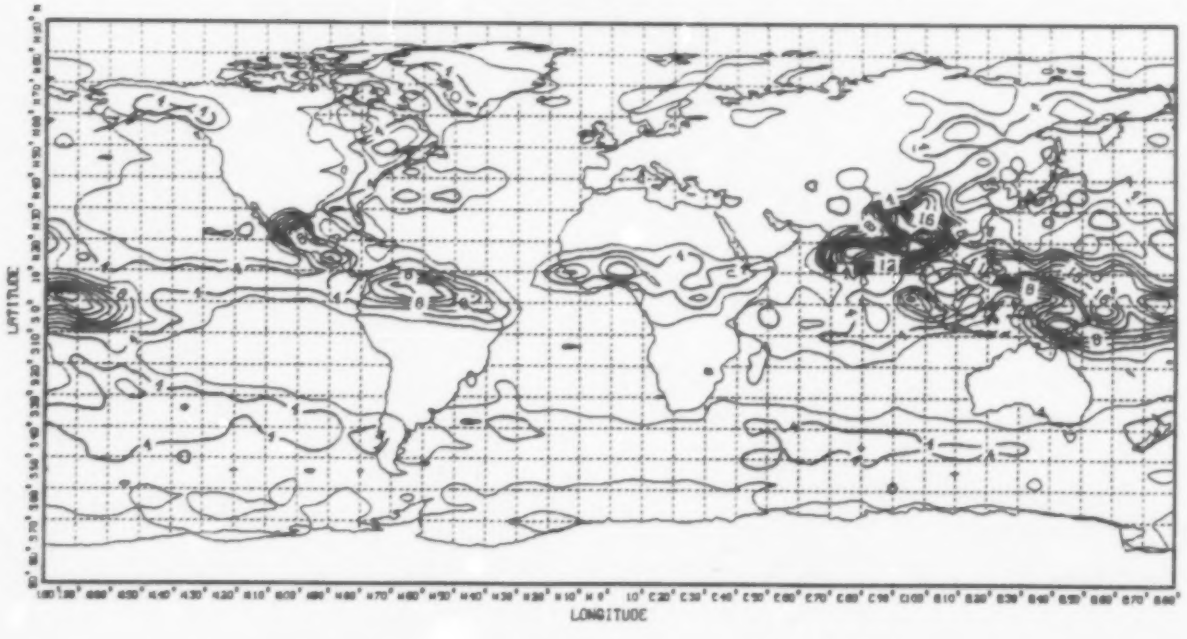

Figure 149

U S A (COLA!) JANUARY PRECIPITATION (MM/DAY)

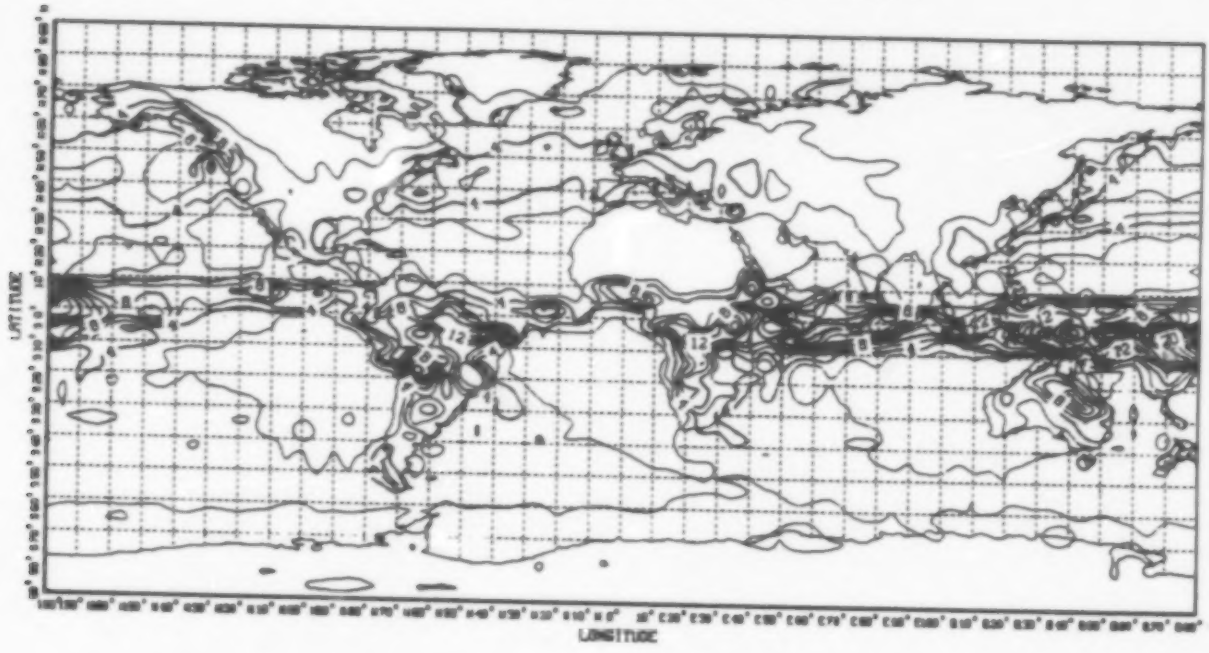

U S A (COLA!) JULY PRECIPITATION (MM/DAY)

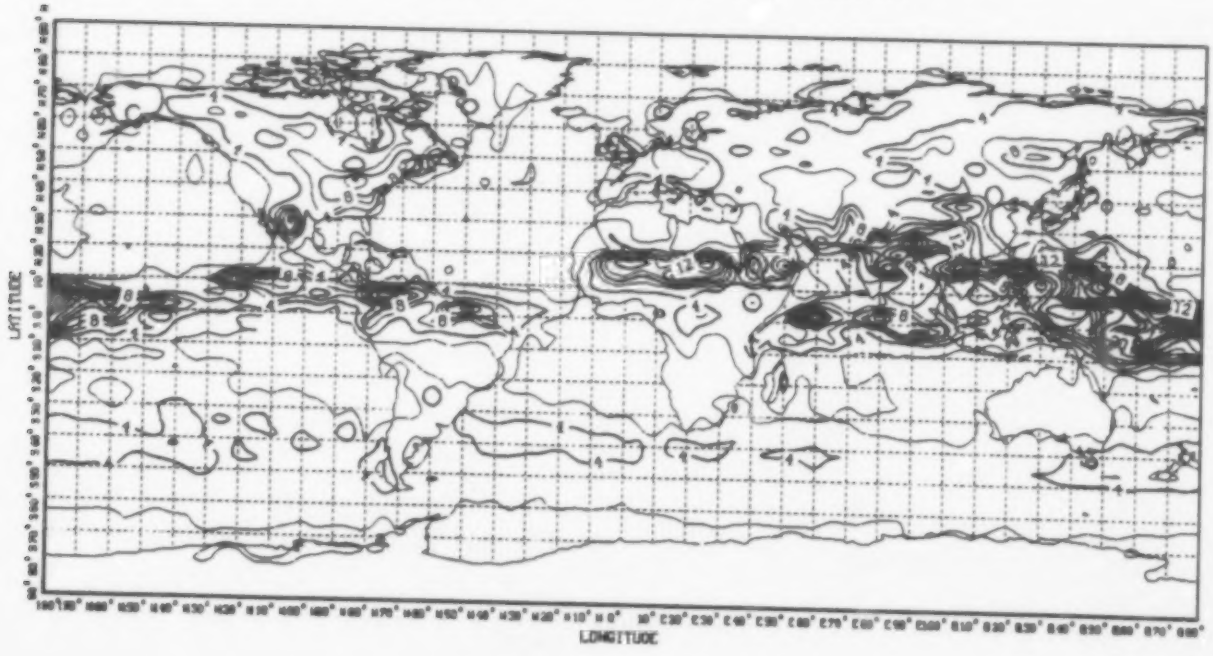

Figure 150

U S A (GFDL) JANUARY PRECIPITATION (MM/DAY)

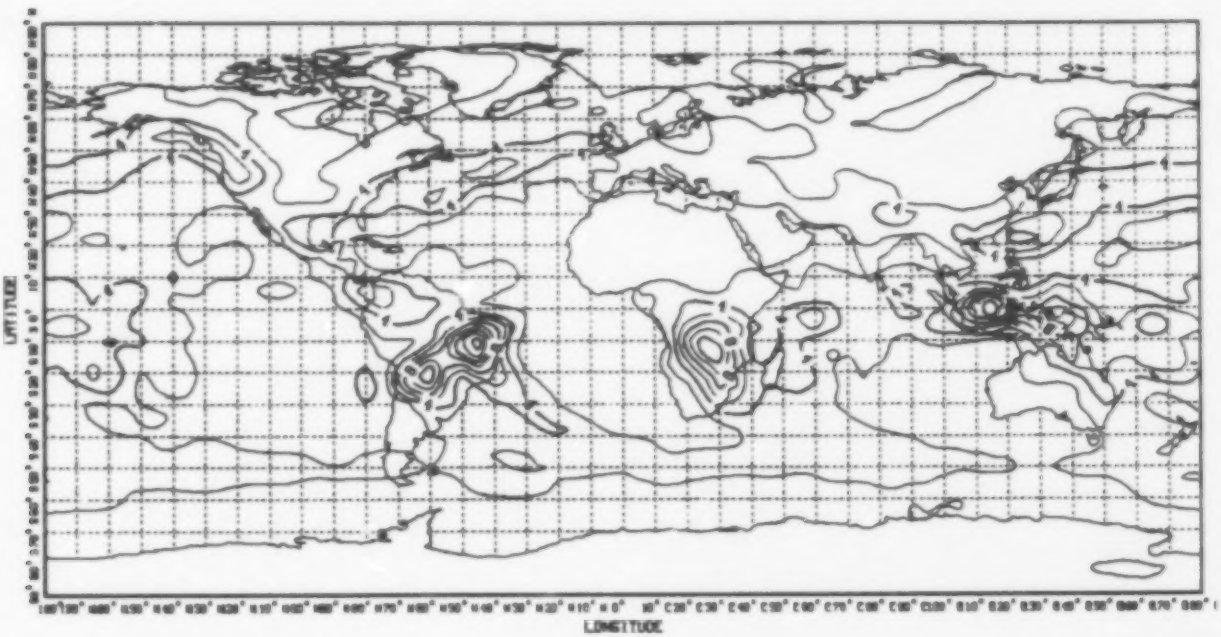

U S A (GFDL) JULY PRECIPITATION (MM/DAY)

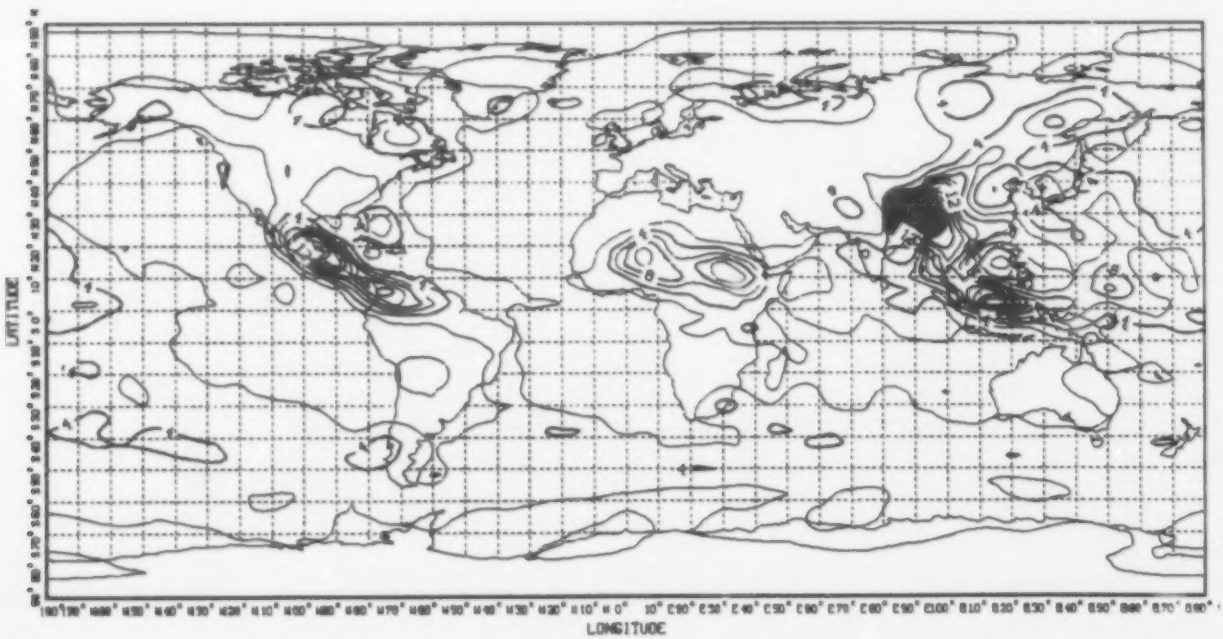

Figure 151

U S A (GISS) WINTER PRECIPITATION (MM/DAY)

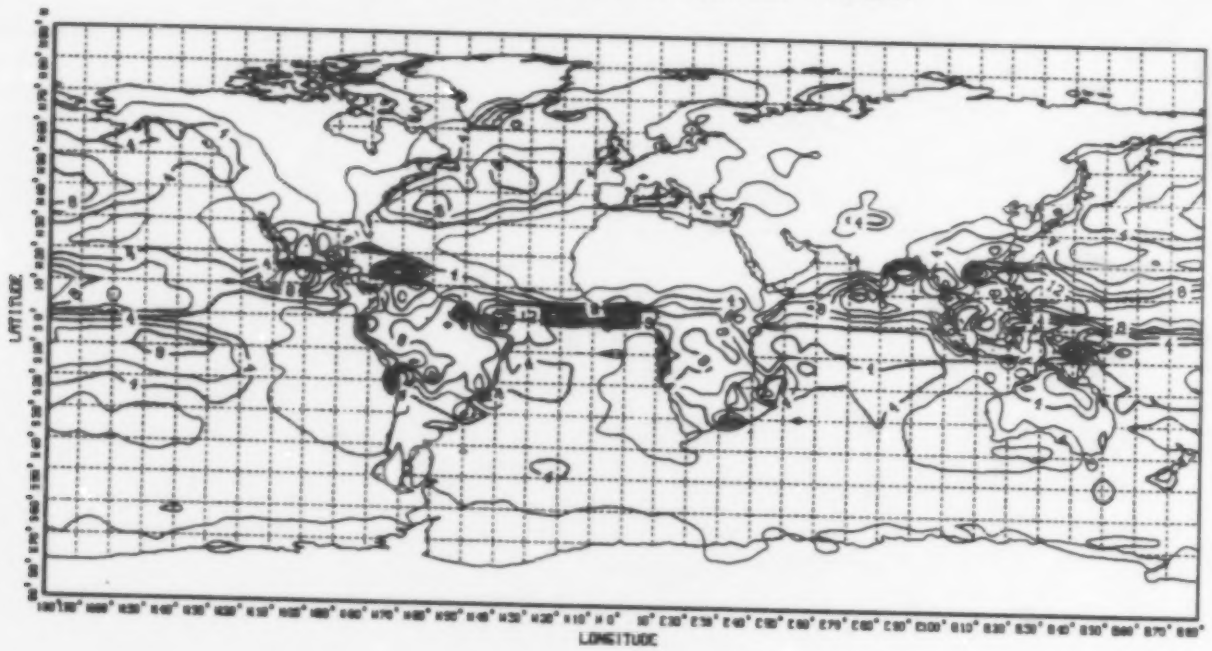

U S A (GISS) SUMMER PRECIPITATION (MM/DAY)

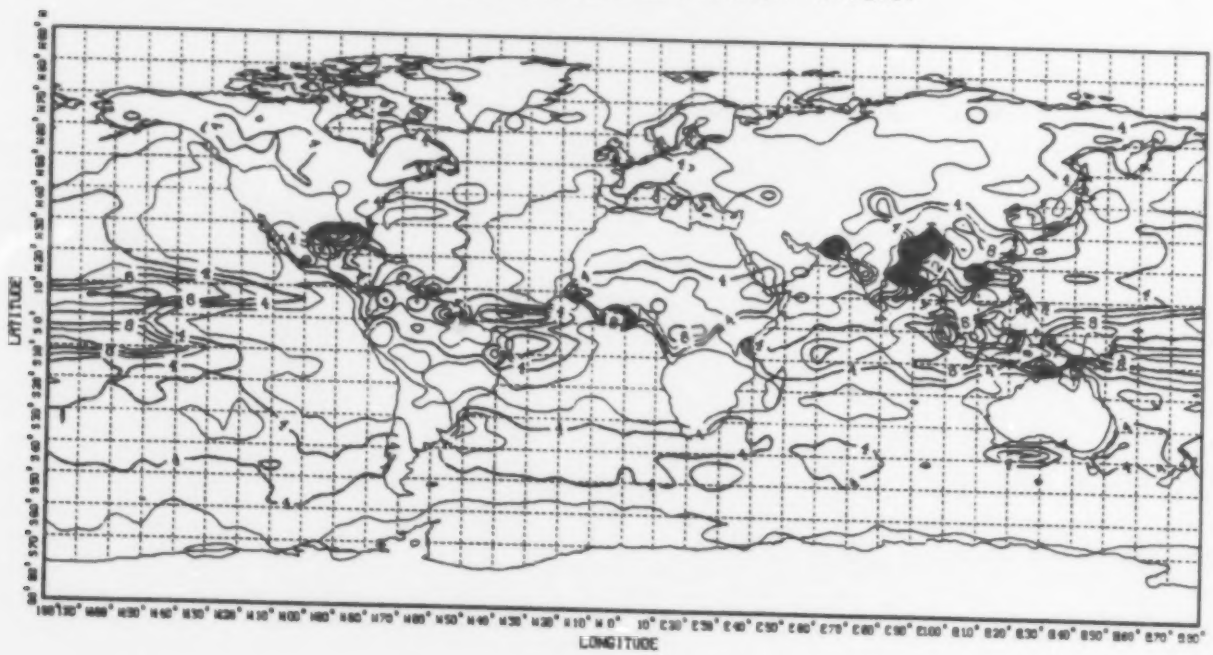

Figure 152

U S A (NCAR) JANUARY PRECIPITATION (MM/DAY)

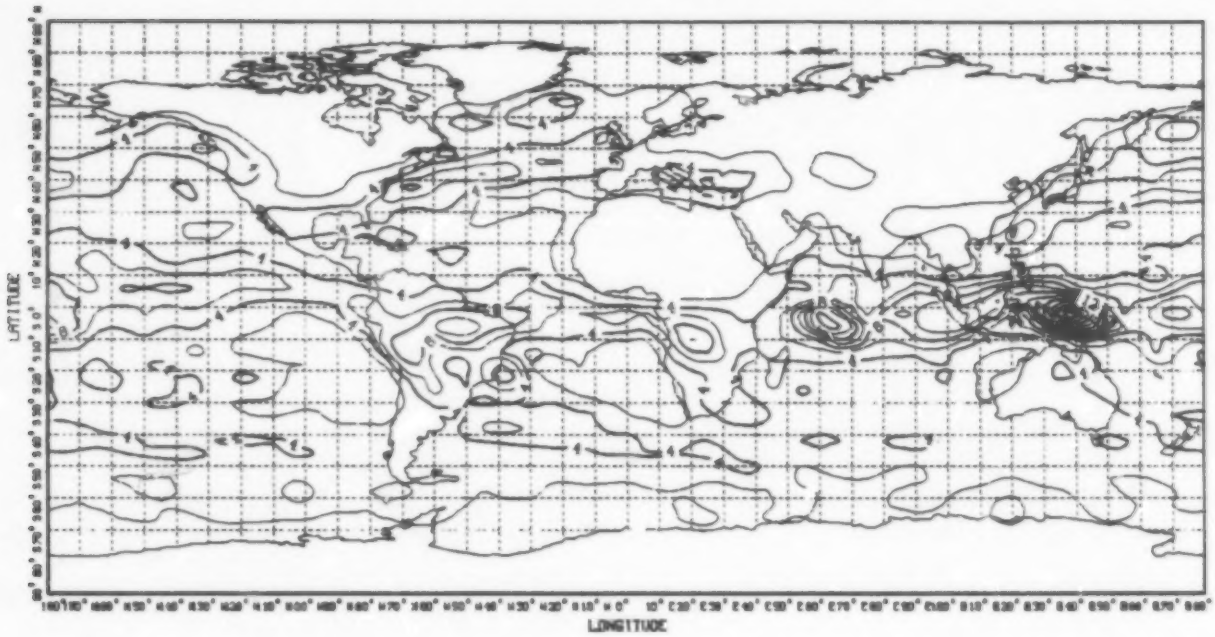

U S A (NCAR) JULY PRECIPITATION (MM/DAY)

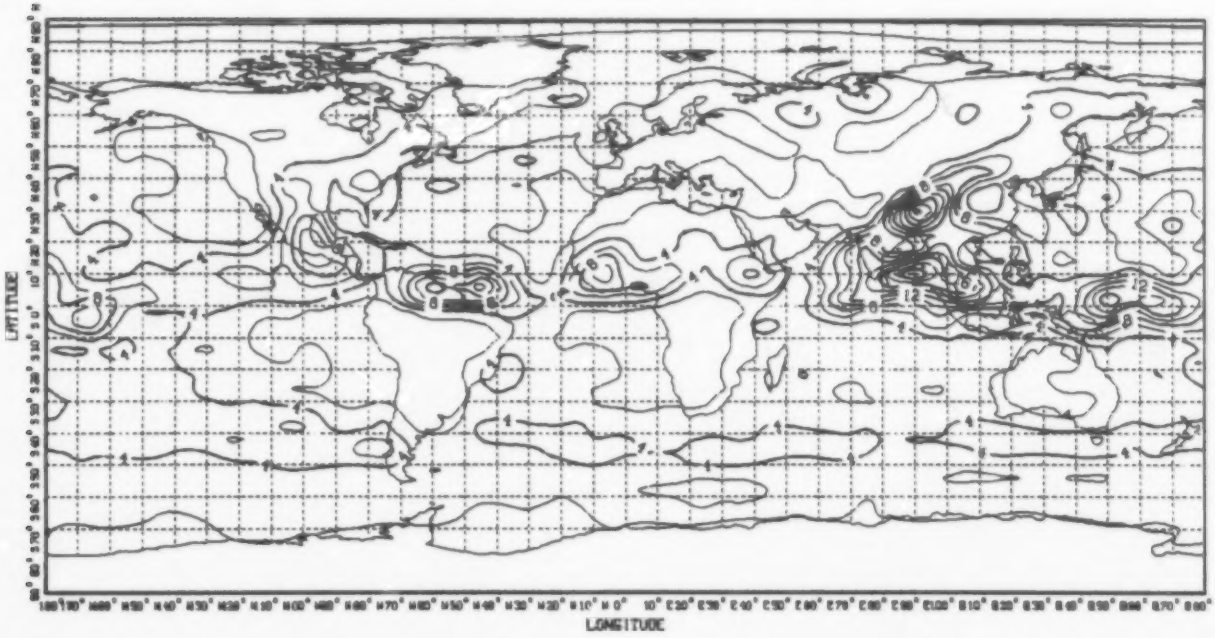

Figure 153

U S A (OSU) JANUARY PRECIPITATION (MM/DAY)

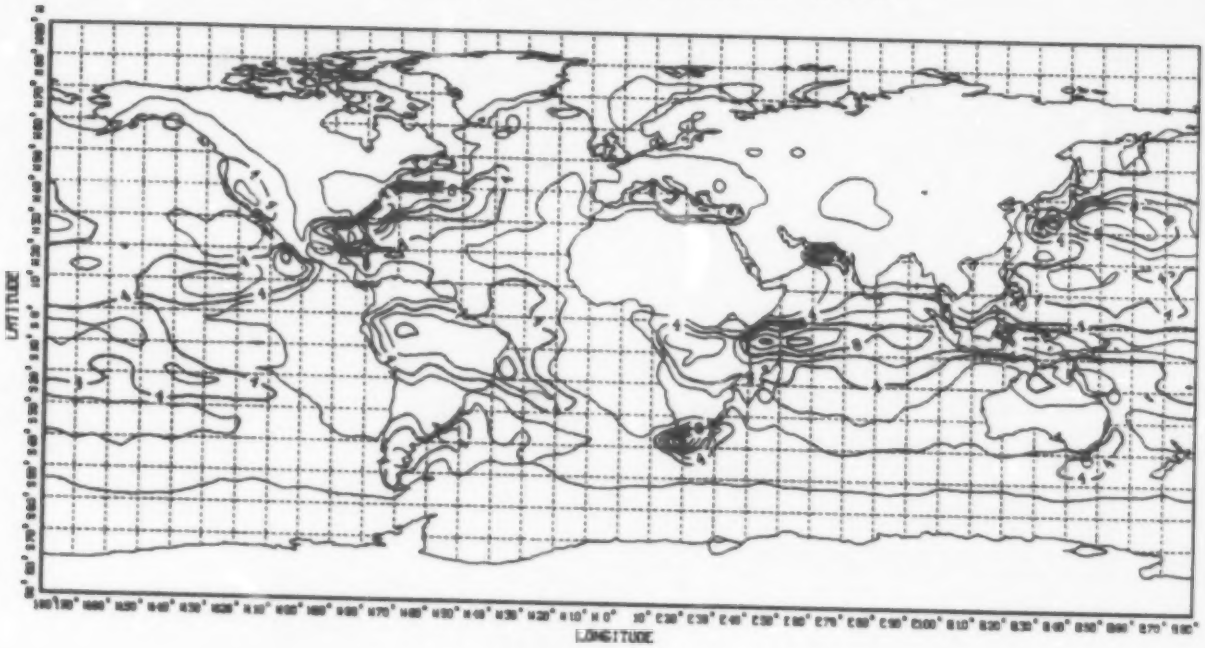

U S A (OSU) JULY PRECIPITATION (MM/DAY)

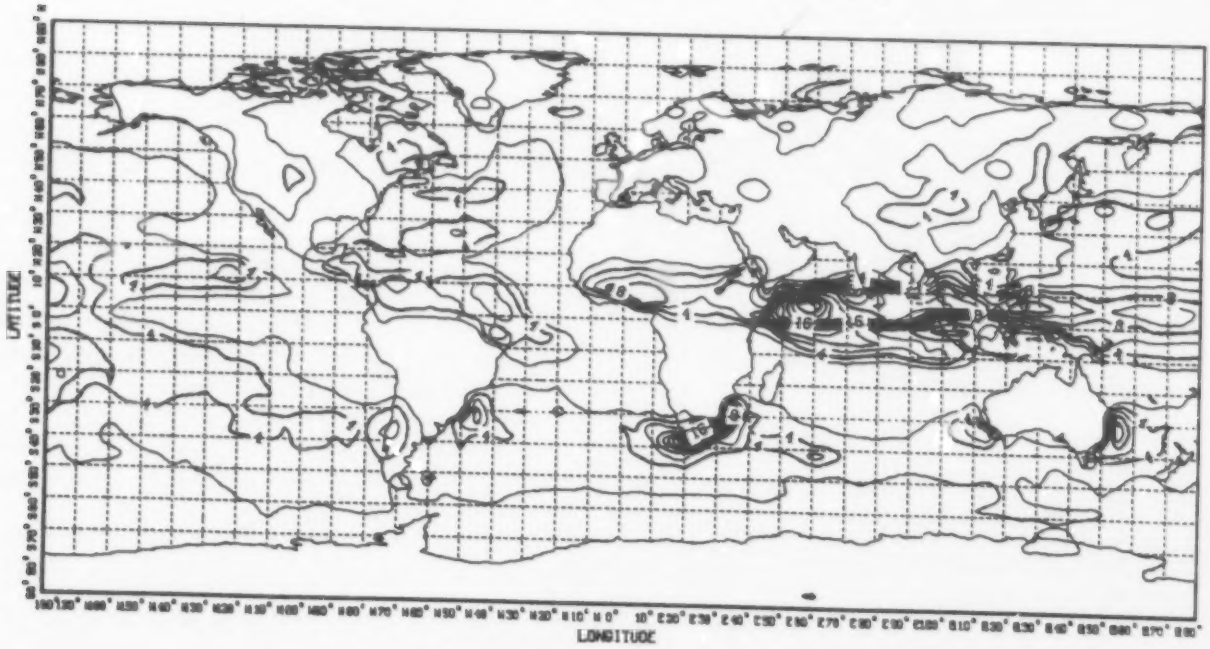

Figure 154

JAPAN (MRI) JANUARY PRECIPITATION (MM/DAY)

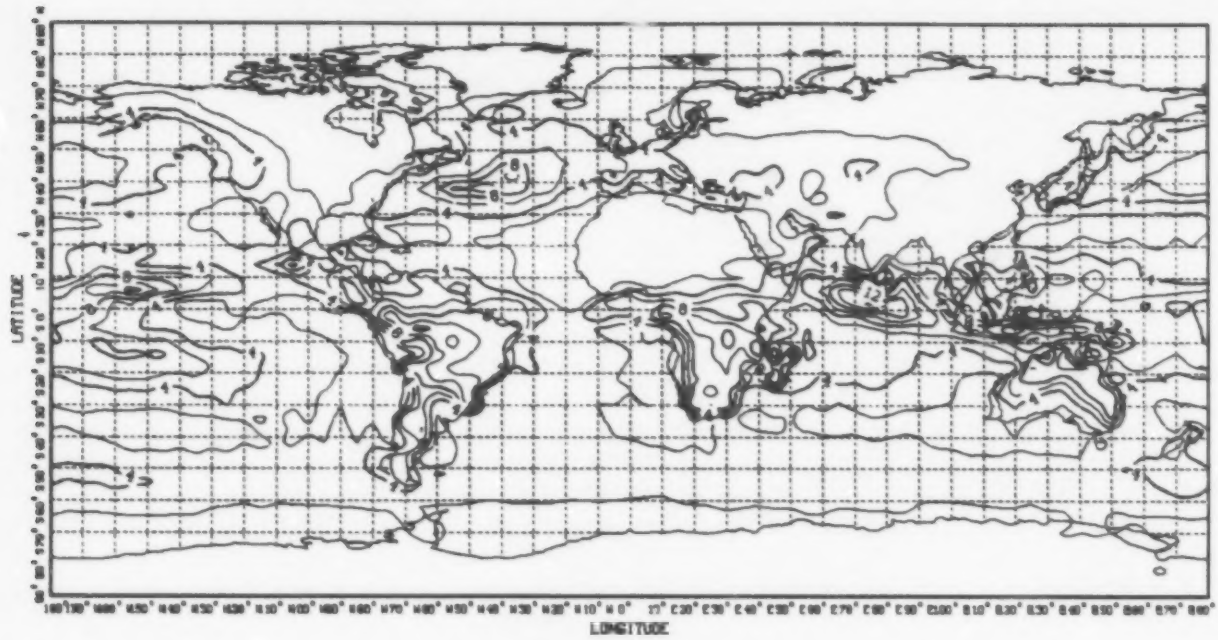

JAPAN (MRI) JULY PRECIPITATION (MM/DAY)

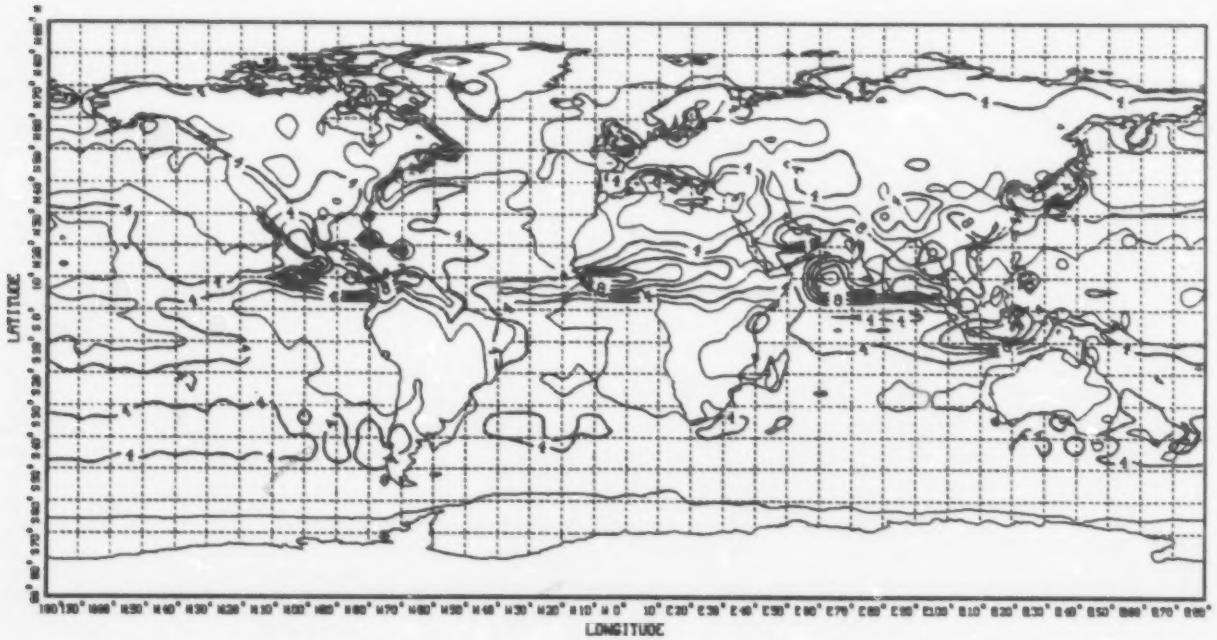

Figure 155

ECMWF JANUARY PRECIPITATION (MM/DAY)

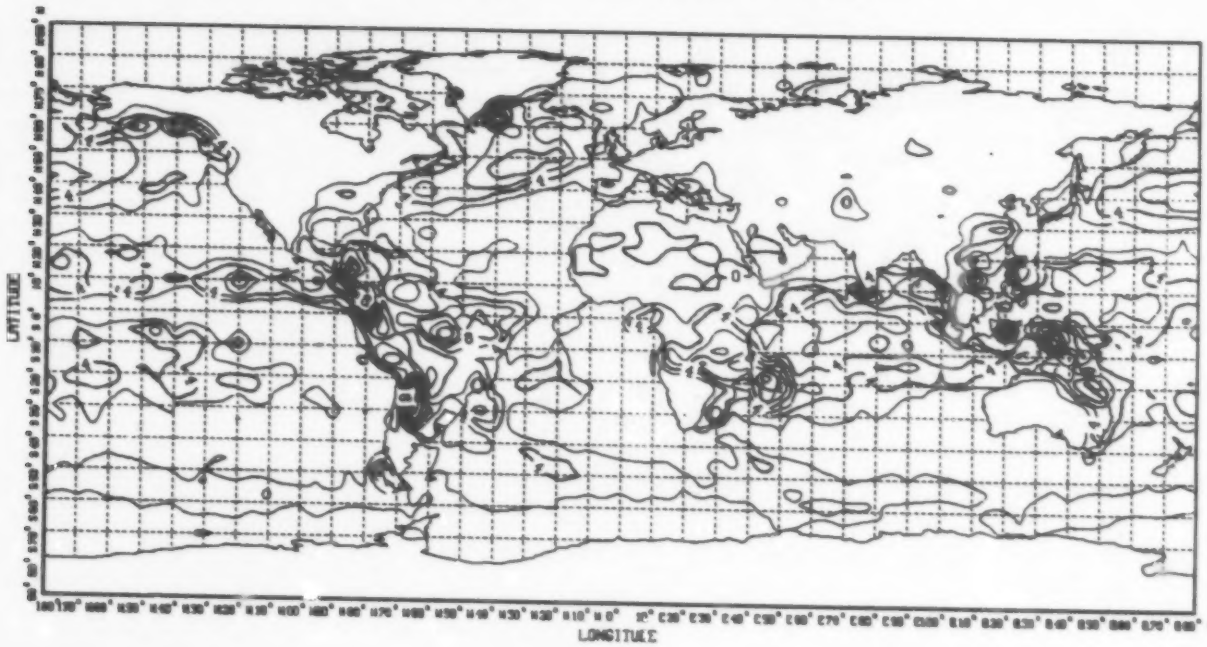

ECMWF JUNE PRECIPITATION (MM/DAY)

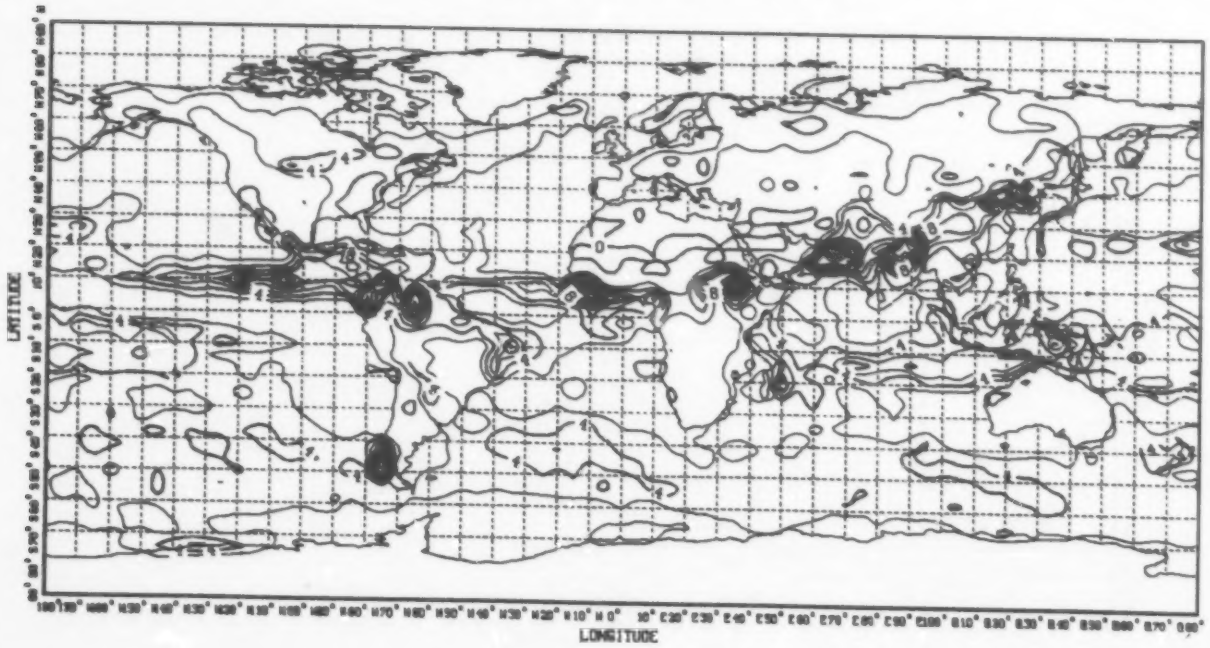

Figure 156

FRANCE (CNRM) WINTER PRECIPITATION (MM/DAY)

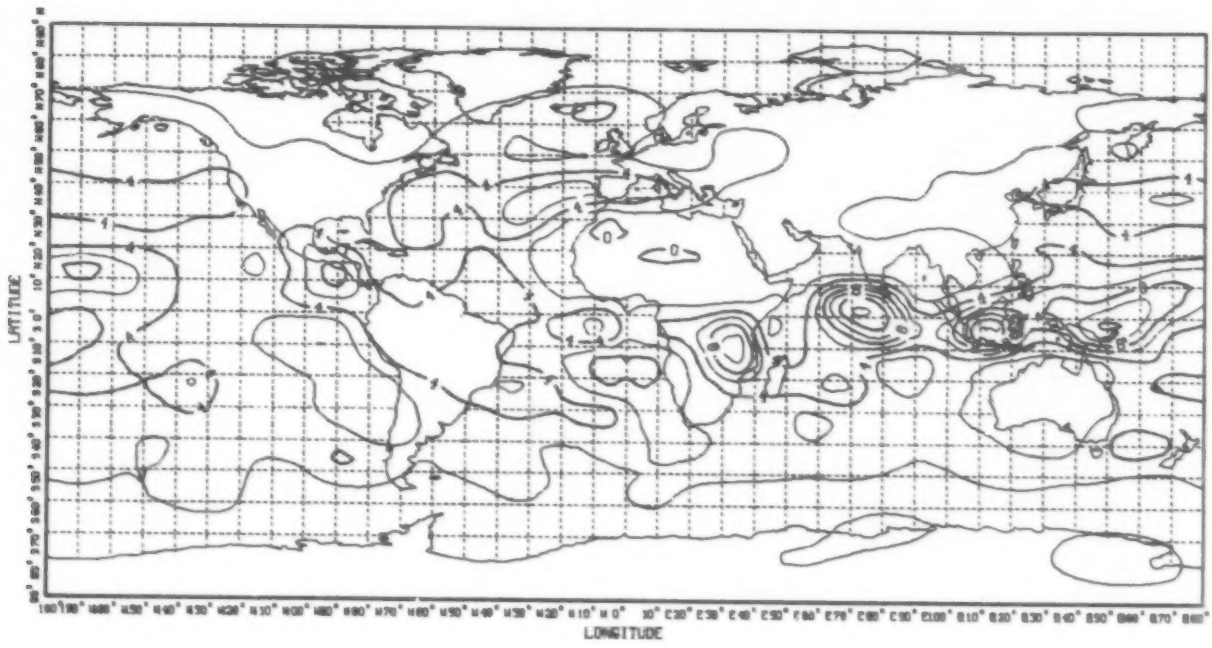

FRANCE (CNRM) SUMMER PRECIPITATION (MM/DAY)

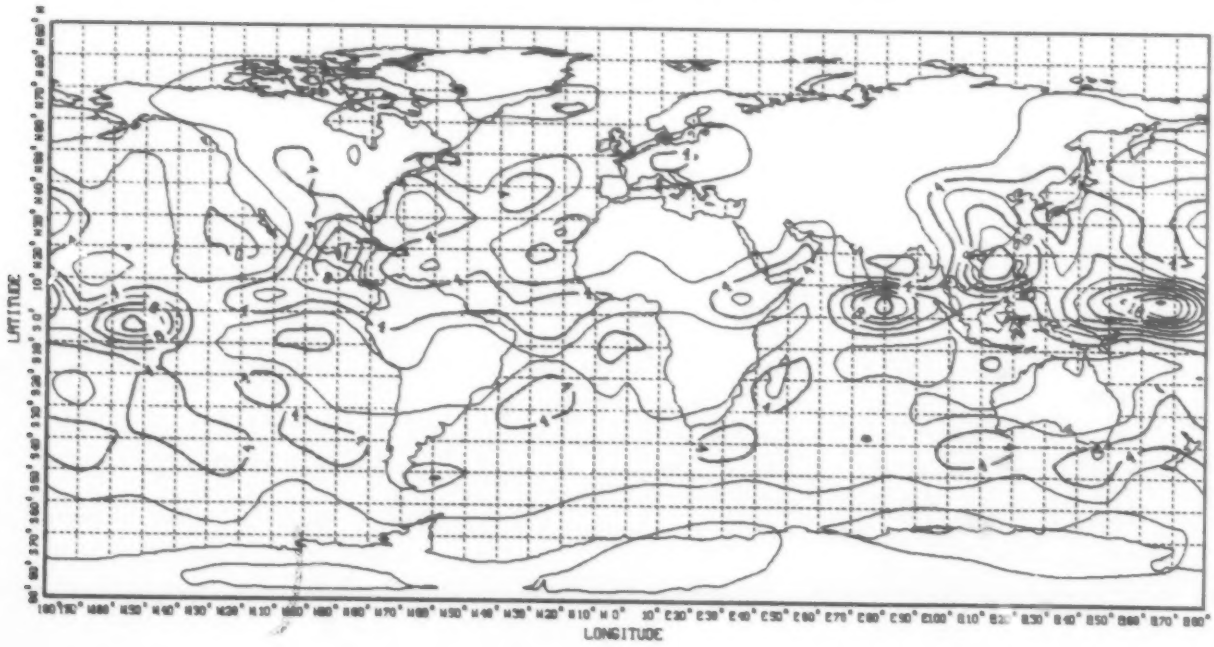

Figure 157

F R G (HAMBURG U) JANUARY PRECIPITATION (MM/DAY)

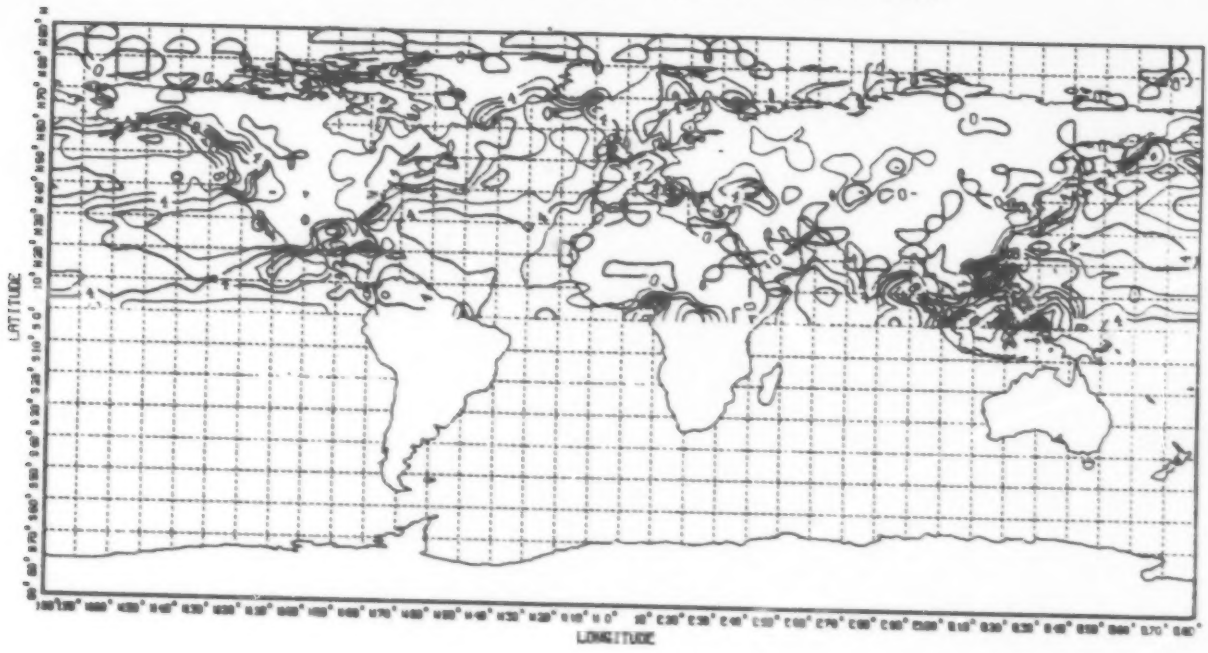

Figure 158